Program

LUNAR AND PLANETARY INSTITUTE

Enceladus and the Icy Moons of Saturn

July 26–29, 2016 • Boulder, Colorado

Institutional Support

Universities Space Research Association (USRA)
Lunar and Planetary Institute (LPI)

Local Organizing Committee

Larry Esposito, *University of Colorado*
Carly Howett, *Southwest Research Institute*
Laura Bloom, *University of Colorado*

Science Organizing Committee

Paul Schenk, *Lunar and Planetary Institute*
Bonnie Buratti, *Jet Propulsion Laboratory*
Roger Clark, *Planetary Science Institute*
Tilmann Denk, *Freie Universität Berlin*
Athena Coustenis, *Observatoire de Meudon*
Dale Cruikshank, *NASA Ames Research Center*
Candice Hansen, *Planetary Science Institute*
Matthew Hedman, *University of Idaho*
Amanda Hendrix, *Planetary Science Institute*
Carly Howett, *Southwest Research Institute*
Simon Kattenhorn, *ConocoPhillips Petroleum*
Sascha Kempf, *University of Colorado*
Luciano Iess, *University of Rome*
William McKinnon, *Washington University*
Jeffrey Moore, *NASA Ames Research Center*
Francis Nimmo, *University of California at Santa Cruz*
Robert Pappalardo, *Jet Propulsion Laboratory*
Wesley Patterson, *Applied Physics Laboratory*
Laurence Soderblom, *U.S. Geological Survey, Flagstaff*
John Spencer, *Southwest Research Institute*
Federico Tosi, *Istituto Nazionale di Astrofisica*
Anne Verbiscer, *University of Virginia*
J. Hunter Waite, *Southwest Research Institute*
Robert West, *Jet Propulsion Laboratory*

Lunar and Planetary Institute 3600 Bay Area Boulevard Houston TX 77058-1113

Abstracts for this conference are available via the conference website at

www.hou.usra.edu/meetings/enceladus2016/

Abstracts can be cited as

Author A. B. and Author C. D. (2016) Title of abstract. In *Enceladus and the Icy Moons of Saturn,* Abstract #XXXX. LPI Contribution No. 1927, Lunar and Planetary Institute, Houston.

Guide to Sessions

Tuesday, July 26, 2016

8:30 a.m.	Boulderado Ballroom	Origins and Evolution: Past and Future
10:45 a.m.	Boulderado Ballroom	Interiors and Geophysics
1:30 p.m.	Boulderado Ballroom	Geology and Tectonics 101
3:40 p.m.	Boulderado Ballroom	Geology and Tectonics 102

Wednesday, July 27, 2016

9:00 a.m.	Boulderado Ballroom	Ages and Cratering
10:20 a.m.	Boulderado Ballroom	Surface Composition and Properties
1:30 p.m.	Boulderado Ballroom	Plumes 101: Plumbing and Dynamics
4:45 p.m.	Boulderado Ballroom	Poster Session

Thursday, July 28, 2016

9:00 a.m.	Boulderado Ballroom	Plumes 102: Variability in Space and Time
2:00 p.m.	Boulderado Ballroom	Interactions: Moon-Moon-Rings-Saturn
4:35 p.m.	Boulderado Ballroom	Small Fry in the Saturn System

Friday, July 29, 2016

9:00 a.m.	Boulderado Ballroom	Astrobiology and the Future

Hotel Boulderado

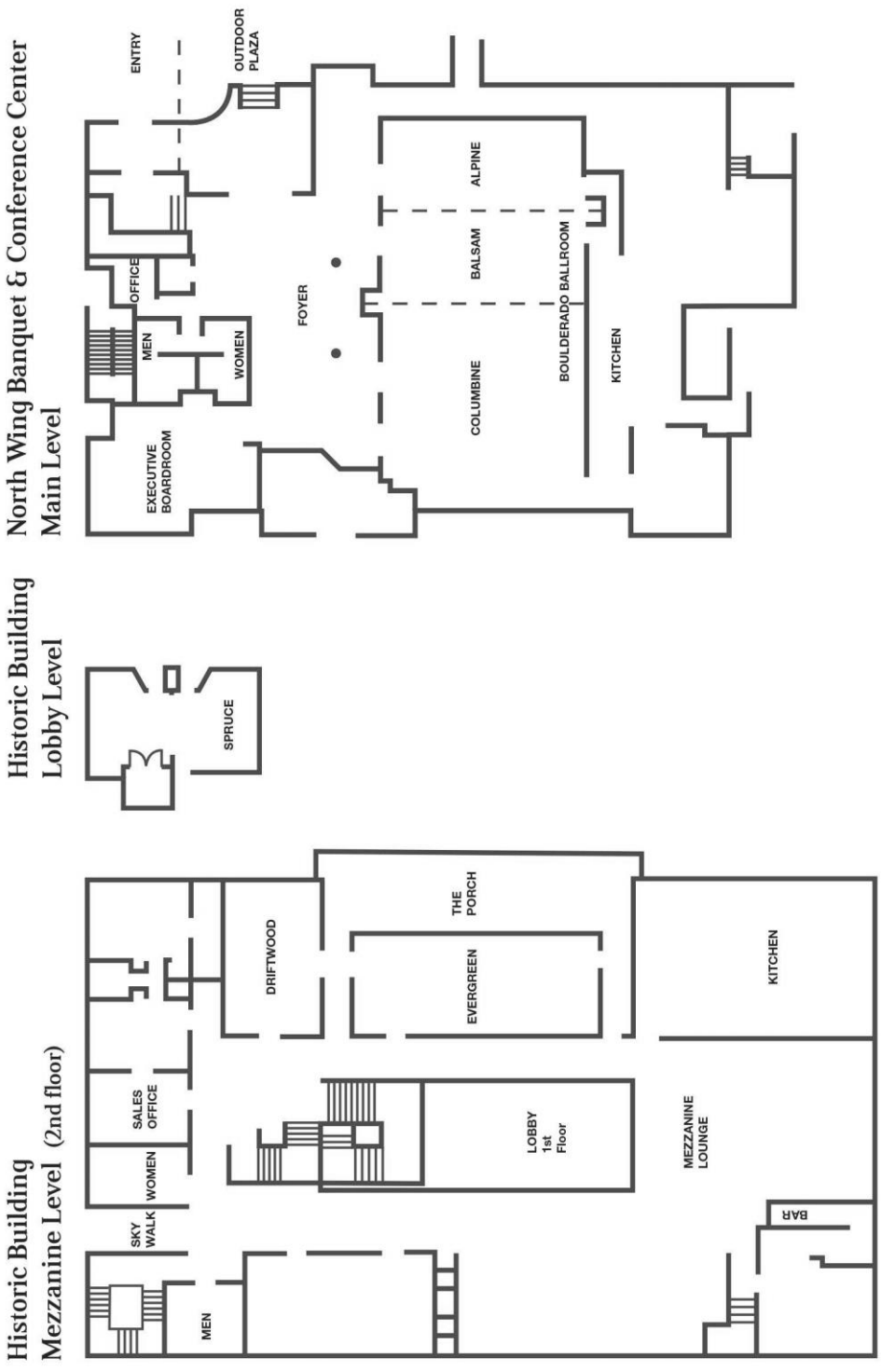

Program

Tuesday, July 26, 2016
ORIGINS AND EVOLUTION: PAST AND FUTURE
8:30 a.m. Boulderado Ballroom

Chairs: **Paul Schenk**
Rick Binzel

8:30 a.m. Schenk P. M. * Binzel R. P.
Introductory Comments

8:40 a.m. Dougherty M. K. * Buratti B. J. Seidelmann P. K. Spencer J. R.
The History of the Enceladus Discovery **[#3033]**
This work describes the history leading to the discovery of water vapour plumes at Enceladus.

9:00 a.m. Lunine J. I. * Tobie G. Mitri G. Tosi F. Coustenis A.
Future Exploration of Enceladus and Saturn's Icy Moons **[#3023]**
The future exploration of Enceladus, beyond Cassini, has already been charted in a number of recent proposals.

9:20 a.m. Castillo-Rogez J. C. * Hemingway D. McKinnon W. B. Schubert G. Tobie G.
Review: Origin and Evolution of Saturn's Midsize Icy Moons **[#3083]**
We review advances in midsize satellite research spurred over the past decade by the exploration of the saturnian satellite system by the Cassini-Huygens mission.

9:40 a.m. McKinnon W. B. * Waite J. H. Jr. Mousis O. Lunine J. I. Zolotov M. Yu.
Composition of Enceladus: Origin and Evolution **[#3011]**
Cassini data for Enceladus strongly imply the existence of an internal ocean in contact with a rock core that may be undergoing hydrothermal activity. But can such activity be sustained after 4.5 GY, or is Enceladus much younger than we thought?

10:00 a.m. Salmon J. * Canup R. M.
Accretion of Saturn's Ice-Rich Moons from Massive Rings **[#3060]**
We investigate the formation of Mimas, Enceladus, and Tethys as accumulation of material from primordial massive ice-rich rings around Saturn. We then determine whether these satellites may have acquired their rock during an LHB-type event.

10:15 a.m. DISCUSSION

10:30 a.m. Break

Tuesday, July 26, 2016
INTERIORS AND GEOPHYSICS
10:45 a.m. Boulderado Ballroom

Chairs: **William McKinnon**
Julien Salmon

10:45 a.m. Hemingway D. J. * Iess L. Tajeddine R. Tobie G.
Interior of Enceladus **[#3051]**
Cassini-based measurements of the gravity field and physical libration amplitude have confirmed that Enceladus is differentiated, with a global subsurface liquid ocean lying between a rocky core and an icy shell that is thinnest at the south pole.

11:05 a.m. Nimmo F. * Barr-Mlinar A. McKinnon W. B. Behounkova M.
Geophysics and Tidal-Thermal Evolution of Enceladus **[#3028]**
Enceladus presents two major geophysical puzzles: how does a global ocean survive?; and how is the present-day high heat flux explained? I will discuss potential answers to these questions.

11:25 a.m. Tiscareno M. S. *
Orbits and Rotation States of Enceladus and Other Moons of Saturn **[#3009]**
The orbits and rotation states of Saturn's moons yield information about their interiors and history. In particular, we'll discuss the inference from Enceladus' rotation state that its subsurface ocean must be global.

11:40 a.m. Hay H. * Matsuyama I.
Modelling Ocean Dissipation in a Variable Thickness Ocean on Enceladus **[#3054]**
Ocean dissipation in an ocean of variable thickness is modelled for Enceladus. A tidal dissipation code is modified to investigate how dissipation differs between the thick southern ocean and the thinner northern ocean.

11:55 a.m. DISCUSSION

12:10 p.m. Lunch

Tuesday, July 26, 2016
GEOLOGY AND TECTONICS 101
1:30 p.m. Boulderado Ballroom

Chairs: **Paul Byrne**
Emily Martin

1:30 p.m. Patterson G. W. * Collins G. C. Helfenstein P. Kattenhorn S. A.
Pappalardo R. T. Schenk P.
The Geological History and Tectonics of Enceladus **[#3059]**
The geological history of Enceladus is remarkably complex for a body with a radius of ~250 km. Understanding that history requires integrating a substantial body of work into a self-consistent picture of the surface evolution of this unusual moon.

1:50 p.m. Collins G. C. * Patterson G. W. Pappalardo R. T. Kattenhorn S. A.
Early Tectonic History of Enceladus from Global Geologic Mapping **[#3057]**
We examine the earliest evidence for tectonics exposed on Enceladus' surface through mapping of the cratered plains.

2:05 p.m. Patthoff D. A. * Pappalardo R. T. Maue A. Martin E. S. Chilton H. T. Thomas P. C.
Ridges of Enceladus: Preserving Ancient and Recent Tectonics Beyond the South Polar Terrain **[#3034]**
We explore the diverse array of Enceladus's ridges outside of the south polar terrain.

2:20 p.m. Bland M. T. * McKinnon W. B.
Folding and Faulting on Enceladus: Constraints on Geophysical Evolution **[#3041]**
Folding and Faulting / Both occur on the surface / Clues to a moons past.

2:35 p.m. Rhoden A. R. *
Reexamining the Role of Tidal Stress in Enceladus' Tectonic History **[#3081]**
Developing a self-consistent model for an ocean-bearing Enceladus is challenging due to recent analyses of heat, stress, and global tectonics.

2:50 p.m. Tajeddine R. * Soderlund K. M. Thomas P. C. Helfenstein P. Hedman M. M.
Burns J. A. Schenk P. M.
True Polar Wander of Enceladus from Topographic Data **[#3027]**
We built the shape of Enceladus as degree 16 in spherical harmonics using Cassini ISS data. We show evidence of true polar wander on Enceladus by reporting the discovery of sets of basins that could represent a paleo-equator and paleo-poles.

3:05 p.m. DISCUSSION

3:20 p.m. Break

Tuesday, July 26, 2016
GEOLOGY AND TECTONICS 102
3:40 p.m. Boulderado Ballroom

Chairs: **Donald Patthoff**
Alyssa Rhoden

3:40 p.m. Schenk P. * Moore J. M. White O. Byrne P.
"Not so Boring as We Were Led to Believe!": Geology of Saturn's Other Midsize Icy Moons **[#3045]**
Cassini mapping of Saturns' other moons, Mimas, Tethys, Dione, Rhea, and Iapetus is complete to 250–400 m/pixel, and, with color and spectroscopy into IR, reveal worlds of surprising diversity and complexity, and planetary processes previously unknown.

4:00 p.m. White O. L. * Schenk P. M. Bellagamba A. W. Grimm A. M. Dombard A. J.
Crater Relaxation Across Rhea, Iapetus, Dione, and Tethys, and Relation to Past Heat Flow **[#3006]**
We have measured crater morphologies on four saturnian satellites, and used relaxation simulations to determine the heat flow experienced by a selection of the craters. Dione and Tethys display more complex thermal histories than Rhea and Iapetus.

4:15 p.m. Byrne P. K. * Schenk P. M. McGovern P. J. Collins G. C.
Hemispheric-Scale Rift Zones on Rhea, Tethys, and Dione **[#3020]**
Moons of Saturn are / Different sizes but crack'd / In similar ways.

4:30 p.m. Martin E. S. * Patthoff D. A. Watters T. R.
History of Tectonic Disruption on Enceladus, Dione, and Rhea **[#3035]**
We use a comparative planetalogical approach to enhancing our understanding of Enceladus's tectonic history by exploring Dione and Rhea where tectonic activity ceased before terrains were tectonically resurfaced.

4:45 p.m. Stickle A. M. * Roberts J. H.
Modeling an Exogenic Origin for the Equatorial Ridge on Iapetus **[#3048]**
A ridge soars above / Iapetus's surface / Did debris form it?

5:00 p.m. Neveu M. * Rhoden A. R.
Why is Enceladus Active Whereas Mimas is Not? **[#3071]**
Wet Enceladus / Inactive Mimas / Are tides the answer?

5:15 p.m. DISCUSSION

Wednesday, July 27, 2016
AGES AND CRATERING
9:00 a.m. Boulderado Ballroom

Chair: Michael Bland

9:00 a.m. Kirchoff M. R. * Bierhaus E. B. Dones L. Robbins S. J. Singer K. N. Wagner R. J. Zahnle K. J.
Cratering Histories in the Saturnian System **[#3056]**
We review new insights into the cratering histories of the mid-sized saturnian satellites provided by Cassini.

9:20 a.m. Bierhaus E. B. * Dones L. Robbins S. J.
The Unusual Role of Secondaries in the Evolution of Crater Populations on Enceladus, and Consequences for Age Estimation **[#3065]**
Enceladus may occupy a unique place among the saturnian satellites in terms of the accumulation of primary and secondary craters. We discuss the physical reasons for this situation and the consequences for deriving surface ages using craters.

9:35 a.m. Kinczyk M. J. * Patterson G. W. Collins G. C. Pappalardo R. T. Becker T. L.
Impact Crater Distributions for Geological Terrains on Enceladus **[#3068]**
Global crater density measurements for geologic terrains on Enceladus are compared.

9:50 a.m. DISCUSSION

10:05 a.m. Break

Wednesday, July 27, 2016
SURFACE COMPOSITION AND PROPERTIES
10:20 a.m. Boulderado Ballroom

Chair: John Spencer

10:20 a.m. Hendrix A. R. * Clark R. N. Cruikshank D. P. Buratti B. J. Howell C. J. A. Scipioni F.
Surface Composition of Icy Moons **[#3072]**
We present an overview of results covering the surface compositions of the mid-sized moons of Saturn.

10:40 a.m. Scipioni F. * Schenk P. Clark R. Tosi F. Combe J.-Ph. Dalle Ore C. M.
Spectral Analysis of Enceladus's Surface **[#3013]**
We show maps of the variation of the depth of the main water ice absorption bands, obtained by analysing VIMS-IR data, and we compare the results with the predicted plumes deposits.

10:55 a.m. Verbiscer A. J. * Helfenstein P. Buratti B. J. Royer E. M.
Optical Remote Sensing and Surface Properties of Saturn's Icy Moons **[#3043]**
We review the scattering properties of particles on the surfaces of Saturn's icy moons at multiple wavelengths from the far ultraviolet to the near-infrared.

11:15 a.m. Buratti B. J. * Brown R. H. Clark R. N. Baines K. H. Nicholson P. D. Mosher J. A.
Photometry of Icy Moons over Many Wavelengths from Cassini VIMS **[#3010]**
The multi-wavelength capabilities of the Cassini Visual Infrared Mapping Spectrometer (VIMS), coupled with a more than decade-long tour of the icy moons, has enabled a full photometric analysis of the moons.

11:30 a.m. DISCUSSION

11:45 a.m. Lunch

Wednesday, July 27, 2016
PLUMES 101: PLUMBING AND DYNAMICS
1:30 p.m. Boulderado Ballroom

Chairs: **Joseph Spitale**
Edwin Kite

1:30 p.m. Glein C. R. * Zolotov M. Y. Vance S. D. Shock E. L. Postberg F.
The Geochemistry of Enceladus' Ocean Toward the End of the Cassini Mission **[#3042]**
We present an overview on the current understanding of the geochemistry of Enceladus' ocean.

1:50 p.m. Postberg F. * Coates A. J. Clark R. N. Dalle Ore C. Hansen C. J. Hedman M. M. Scipioni F. Waite J. H. Jr.
Plume and Surface Composition of Enceladus **[#3008]**
The versatile instrumentation of Cassini allows for many compositional perspectives on Enceladus' plume and surface composition. We try to combine these different aspects to one comprehensive picture but also discuss divergent views and open issues.

2:10 p.m. Spencer J. R. * Howett C. J. A. Verbiscer A. J. Hurford T. A. Gorius N. J. P. Pearl J. C. Segura M.
Observations of Active Thermal Emission from Enceladus by the Cassini Composite Infrared Spectrometer **[#3052]**
Cassini's Composite Infrared Spectrometer (CIRS) provides unique information on the heat flow, temperatures, and spatial distribution of endogenic thermal emission from Enceladus' active south polar region.

2:25 p.m. Goguen J. D. * Buratti B. J. Cassini VIMS Team
Cassini VIMS Spectra of the Thermal Emission from the Hottest Spots Along Enceladus South Pole Fissures **[#3064]**
We present an overview of the VIMS measurements of the hottest fissure thermal emission and put these data within the context of the larger picture of these ocean world fissure eruption characteristics as reported from other instruments.

2:40 p.m. Wood S. E. *
The Effects of Temperature-Dependent Thermal Properties, Cohesion, and Crystallinity on Model-Predicted Temperatures of Icy Regolith on Saturn's Moons **[#3084]**
The effective thermal conductivity of icy regolith depends strongly on temperature and crystallinity, which has significant consequences for interpretation and predictions of surface and subsurface temperatures.

2:55 p.m. Gorius N. * Spencer J. Howett C. Albright S. Jennings D. Hurford T. Romani P. Segura M. Verbiscer A.
High Resolution Observations of Enceladus' South Pole Using Cassini/CIRS **[#3086]**
We will present our results from E18 and E21 during which Cassini/CIRS was configured to record variations of the thermal emission at high spatial resolution.

3:10 p.m. DISCUSSION

3:25 p.m. Break

3:40 p.m. Goldstein D. B. * Hedman M. Manga M. Perry M. Porco C. Schmidt J. Teolis B.
Plume Vents and Dynamics: A Chapter Preview **[#3047]**
The chapter on plume vents and dynamics will examine the observations of the plume and surface vent region and explore the mechanisms which lead from the subsurface vapor and particulate source to the observed properties.

4:00 p.m. Dzhanoev A. R. * Schmidt J. Spahn F.
Kinetic Processes in the Enceladus Vents **[#3075]**
We study the possibility of dust aggregation and fragmentation processes when icy grains are transported to space by water vapor streams in the subsurface vents of Saturn's active moon Enceladus.

4:15 p.m. Bouquet A. * Brockwell T. Waite J. H. Chocron S. Teolis B. Perryman R. S. Walker J.
Modeling the H_2 Production in the Cassini Ion and Neutral Mass Spectrometer at Enceladus: Effect of Ice Grains Impacts in Low Velocity Flybys and Implication for the Identification of Native H_2 in the Plumes **[#3014]**
H_2 in the plumes of Enceladus would be a smoking gun for hydrothermal activity in its ocean but the data is ambivalent, as ice grains impact produce H_2 in the instrument. We present our methods to disentangle this artifact from native H_2.

4:30 p.m. DISCUSSION

Wednesday, July 27, 2016
POSTER SESSION
4:45 p.m. Boulderado Ballroom

Yin A. Pappalardo R. T.
A Global Tectonic Map and Tectonic History of Enceladus **[#3026]**
The trailing edge and south polar terrains were created by unidirectional flow with complex interior deformation, whereas the leading edge terrain was formed by fragmentation of the ancient Cratered Terrain through ductile strike-slip shearing.

Roatsch Th. Kersten E. Matz K.-D. Scholten F. Wagner R. Porco C. C.
Cartography of the Medium-Sized Saturnian Satellites Based on Cassini-ISS Images **[#3032]**
The stated objective of the ISS is to obtain global coverage for all medium-sized icy satellites with a resolution better than 1 km/pixel. This goal was achieved with image sequences obtained during close flybys and additional lower-res images.

Schenk P.
Global Color and Cartographic Mapping of Saturn's Midsize Icy Moons **[#3053]**
Map in color, its so much better.

Denk T. Roatsch T. Matz K. D.
Imaging Observation Planning for Dione, Rhea, Iapetus, and Phoebe in the Cassini Primary Mission **[#3076]**
Basic concepts of the Cassini ISS observations in the prime mission, planned by DLR and Freie Universität Berlin, are described. In addition, some details of the used tools and of the targeted flybys at Phoebe and Iapetus are given.

Clark C. S. Clark P. E. Stooke P. J.
Constant-Scale Natural Boundary Global Maps of Enceladus **[#3070]**
Enceladus tiger stripes in context!

Stephan K. Wagner R. Jaumann R. Clark R. N. Cruikshank D. P. Dalle Ore C. Brown R. H.
Giese B. Roatsch T. Filacchione G. Matson D. Baines K. Krupp N. Cappaccioni F.
Buratti B. J. Nicholson P. D.
Spectral and Geological Properties of Tethys **[#3030]**
We present the spectral and geological properties of Tethys derived from Cassini VIMS and ISS data.

Leonard E. J. Yin A. Pappalardo R. T.
Constraining the Viscosity of Enceladus's Ice Shell Through the Crater Islands **[#3036]**
The apparent rigid block rotation of crater "islands" on the leading hemisphere of Enceladus may constrain the ice shell viscosity at the time of the rotation.

Rhoden A. R. Henning W. Hurford T. A. Bland M. Collins G. Tajeddine R.
Implications of Tidal Stresses on Global Ocean Models of Mid-Sized Icy Moons **[#3082]**
We calculate tidal stresses in ocean-bearing models of Mimas, Enceladus, Dione, and Rhea to determine whether oceans are compatible with their geologic records.

Buratti B. J.
Enceladus and Europa: Very Early Hints of Activity **[#3021]**
Observations of Enceladus prior to the Cassini mission suggested cryovolcanism almost a century before its discovery.

Parekh R. Vijayan S. Sivaraman B.
Landslide Phenomena on Saturn's Icy Moon: Rhea **[#3055]**
Here in given abstract author has tried to find the possible mechanism for the formation of landslides on icy bodies like Rhea by studying the existing condition of crater and its morphology.

Denk T. Spencer J. R. Roatsch T. Schmedemann N. Galuba G. G.
Saturnian Moon Iapetus — Global Albedo Enigma and Cassini ISS Observations **[#3063]**
The global albedo dichotomy of Iapetus, known since almost 340 years, is now eventually explained by runaway global thermal migration of water ice, triggered by the deposition of dark material on the leading hemisphere.

Aftabi P.
The Brittle-Ductile Tectonics of Ice Shell on Europa from Pole to Pole **[#3005]**
In this paper mapped the icy shell of Europa from pole to pole.

Royer E. M. Hendrix A. R.
Far-Ultraviolet Photometric Modeling of the Icy Satellites of Saturn **[#3024]**
We present here an analysis of ultraviolet disk-integrated phase curves of the five inner moons of Saturn: Mimas, Enceladus, Tethys, Dione, and Rhea.

Hendrix A. R. Hansen C. J. Esposito L. W. Royer E. Cassidy T. Shemansky D. E. Holsclaw G.
Enceladus and the Other Moons of Saturn as Observed by Cassini UVIS **[#3079]**
We present highlights of UVIS studies of the surfaces of the moons of Saturn, with a focus on Enceladus.

Desai R. T. Coates A. J. Cowee M. M. Jones G. H. Gary S. P. Wei H. Regoli L. Volwerk M.
Negative Pickup Ions at Icy Moons: Rhea and Europa **[#3069]**
In this study we analyse the negatively charged pickup ions observed at Rhea and Europa to better understand what they are telling us about their source environments.

Becker T. M. Retherford K. D. Roth L. Saur J. McGrath M. A.
Far-UV Spectral and Spatial Albedo Comparisons Between Enceladus and Europa **[#3044]**
We aim to understand the observed FUV spectral differences between Europa and Enceladus, including the lack of a water absorption edge at ~165 nm in the Europa spectra that is present at Enceladus, as well as the overall lower FUV albedo of Europa.

Kochemasov G. G.
Tectonic Dichotomy of Icy Satellites of Saturn **[#3016]**
Saturnian icy satellites are tectonically dichotomous and have different color of their halves. This feature is common of celestial bodies moving in keplerian elliptical orbits and thus warped by inertia-gravity waves. Wave1 produces two hemispheres.

Gilliam A. E. Lerman A.
Formation Mechanisms of Channels on Titan **[#3058]**
We examine different fluvial features on Titan and evaluate the possibilities of channel formation by dissolution of ice by a concentrated solution of ammonium sulfate and by mechanical erosion by flow of liquid ammonia and liquid ethane.

Struck J.-T.
Titan and Enceladus Relationship-Titan as Planet and Enceladus Water Related to Titan **[#3001]**
Titan has a diameter of 3200 miles larger than Mercury at 3032 miles, so Titan could be called a planet. Gravitation from Titan and Saturn can be seen as pressuring the moon Enceladus. Enceledus' water or emissions could be seen as linked to Titan.

Dougherty A. Chumsky R. Morris D.
Freezing of Methanol-Water Mixtures at High Pressure in a Subsurface Ocean **[#3039]**
Impurities in a subsurface ocean on Enceladus would change the freezing temperature, and are relevant to any successful thermal model for generating plumes. We measure the liquidus and eutectic temperatures for methanol-water solutions.

Takahagi W. Shibuya T. Takano Y. Seo K. Adachi K. Fujishima K. Tomita M. Takai K.
Abiotic Peptide Synthesis Under Enceladus Alkaline Hydrothermal Condition **[#3050]**
Assuming abiotic amino acids existing in the Enceladus alkaline seawater, we hypothesized that water-rock interaction may contribute to condensation of localized amino acids leading to a peptide formation.

Guzman M. McKay C. P. Hurley D. Lorenz R. Gold R.
Modeling of Low Altitude Dynamics of Grains in Enceladus Jets **[#3040]**
The particulate mass in the Enceladus plume is of particular interest to astrobiologists. At low altitude, >99% of the grains are salt-rich by mass. Modeling of the salt-rich grains is the subject of this research.

Perov N. I.
Any Small Bodies Near the Enceladus Orbit **[#3002]**
In the frame of the restricted circular three body problem dust matter motion is considered near the Enceladus orbit. For the given model undiscovered bodies with negligible mass may move along closed trajectories in the system Saturn-Enceladus.

Poppe A. R.
Interplanetary Dust Flux to Saturn's Icy Satellites: A Potential Surface Contaminant Source? **[#3015]**
We examine the possibility of interplanetary dust grain fluxes to Saturn's icy satellites as a possible source of surface composition contamination (i.e., "dark material"). We compare to previous dynamical investigations of Phoebe dust at Saturn.

Thursday, July 28, 2016
PLUMES 102: VARIABILITY IN SPACE AND TIME
9:00 a.m. Boulderado Ballroom

Chairs: **Alexis Bouquet**
Sascha Kempf

9:00 a.m. Ingersoll A. P. * Ewald S. P.
Decadal Timescale Variability of the Enceladus Plumes Inferred from Cassini Images **[#3003]**
The mass of the Enceladus plumes decreased by a factor of two from 2005 to 2015. Launch velocity is less at apocenter, greater at pericenter. The decadal trend in plume mass is likely related to an 11-year cycle in orbital eccentricity.

9:15 a.m. Hurley D. M. * Perry M. E.
Local Enhancements in the Enceladus Plume **[#3012]**
Spatial and temporal variability in the Enceladus plume is investigated by comparing Cassini INMS data to model output, identifying regions requiring local enhancements in the plume source to reproduce observations, providing constraints on jets.

9:30 a.m. Dhingra D. * Hedman M. M.
Variations in the Spectral Properties of Encealdus' Plume in Time and Space **[#3018]**
Near-Infrared spectra of Enceladus' plume vary with both time and space and can provide new insights into conditions beneath the moon's surface.

9:45 a.m. Kite E. S. * Rubin A. M.
Sustained Eruptions on Enceladus Explained by Turbulent Dissipation in Tiger Stripes **[#3004]**
The sustainability of conduits linking Enceladus' ocean and surface is not understood. A model of tiger stripes as tidally-flexed slots that puncture the ice shell explains the eruption phase-curve and the long-term sustainability of the eruptions.

10:00 a.m. Hansen C. J. * Esposito L. Portyankina G. Aye K.-M. Hendrix A.
The Role of Enceladus' Gas Jets in Diurnal Variability of Particle Flux **[#3066]**
A new occultation of epsilon Orionis by Enceladus' plume reveals supersonic gas jets as playing a key role in diurnal variability of the particle flux.

10:15 a.m. Spitale J. N. * Hurford T. A. Rhoden A. R. Hedman M. M.
Observing Surface-Level Eruptive Variability at Enceladus' South Pole **[#3080]**
Enceladus experiences curtain- and discrete-style eruptions. Each style may have a different response to tidal stress. Assessing variability at the local level is in progress. Three jets may have been captured turning on in Cassini observations.

10:30 a.m. DISCUSSION

10:45 a.m. Break

11:00 a.m. Hurford T. A. * Spitale J. N. Rhoden A. R. Hedman M. M.
Linking Tidal Volcanic Activity to Subsurface Volatile Sources on Enceladus **[#3038]**
Tides stress surface cracks / Tap volatile reservoirs / Affects eruptions.

11:15 a.m. Portyankina G. * Esposito L. W. Hansen C. J. Aye K.-M.
Comparing UVIS Occultations of the Sun and Stars via Jet Modeling **[#3067]**
We use DSMC model of water vapor jets to compare occultation observations of Enceladus jets by UVIS conducted between 2005 and 2016 and detect variability in the relative strengths of the detected jets.

11:30 a.m. Roberts J. H. * Stickle A. M.
Impact Heating and the South Polar Thermal Anomaly on Enceladus **[#3022]**
Tidal heat pattern / Impact breaks the symmetry / Locally thin ice.

11:45 a.m. Crary F. J. *
Small-Scale Structure of Plasma Withing the Enceladus Plume: Cassini Observations on the E7, E17 and E18 Encounters **[#3046]**
Cassini CAPS data show small scale plasma structures (<17 km) within the Enceladus plume. Combined with RPWS/LP measurements, incorrect identifications due to time aliasing have been removed and structures at ~0.4 km resolution have been revealed.

12:00 p.m. Perry M. E. * Teolis B. D. Hurley D. M. Waite J. H. McNutt R. L.
The Velocity of Water Molecules in the Enceladus Plumes **[#3074]**
The Cassini INMS directly measures the velocity of water vapor emitted from Enceladus and finds both dense, Mach-4 jets with a distribution that peaks at 1 km/s, and a slower, wider distribution.

12:15 p.m. DISCUSSION

12:30 p.m. Lunch

Thursday, July 28, 2016
INTERACTIONS: MOON-MOON-RINGS-SATURN
2:00 p.m. Boulderado Ballroom

Chairs: **Frank Postberg**
Amanda Hendrix

2:00 p.m. Kempf S. * Hill T. Krupp N. Horanyi M. Schmidt J. Smith T. Srama R.
Saturn's Diffuse E Ring and Its Connection with Enceladus **[#3062]**
Saturn's E ring is the second largest planetary ring in the solar system. We now know that the Enceladus plume is the main source for the E ring particles and that many ring features can be explained by the dynamics of the plume particle ejection.

2:20 p.m. Teolis B. D. * Tokar R. L.
Icy Moon Atmospheres/Exospheres from Magnetospheric Interactions **[#3073]**
The icy moon atmospheres/exospheres from magnetospheric interactions chapter will explore the exospheric physics of Saturn's icy satellites, the observations by the Cassini spacecraft, and the new understanding revealed by these data.

2:40 p.m. Howett C. J. A. * Hendrix A. R. Paranicas C. Spencer J. R. Schenk P. M. Verbiscer A. J.
Ring/Magnetosphere Interactions with Satellite Surfaces **[#3007]**
The surface of each of Saturn's icy satellites are affected by their interactions with both Saturn's ring and magnetosphere. How the surfaces are modified will be discussed.

3:00 p.m. Nordheim T. A. * Hand K. P. Paranicas C. Howett C. J. A. Hendrix A. R.
Jones G. H. Coates A. J.
The Near-Surface Electron Radiation Environment of Saturn's Moon Mimas **[#3078]**
We have modeled the effect of energetic electron bombardment across the surface of Saturn's moon Mimas. Our results are discussed in the context of previously reported Cassini remote sensing observations of this moon.

3:15 p.m. Schaible M. J. * Johnson R. E. Zhigilei L. V.
Radiative Sintering of Ice Grain Regoliths: Formation of the PacMan Anomalies on the Icy Saturnian Moons **[#3037]**
The PacMan anomalies on Mimas and Tethys can be explained through grain sintering due to high energy electron irradiation. The sintering models developed can be used to provide an additional constraint on the regolith grain size and porosity.

3:30 p.m. DISCUSSION

3:45 p.m. Break

4:00 p.m. Smith H. T. * Crary F. Dougherty M. Perry M. Roussos E. Simon S. Tokar R.
Enceladus and Its Influence on Saturn's Magnetosphere **[#3049]**
Enceladus is the primary source of particles in Saturn's magnetosphere. We present an overview of the current understanding of Enceladus' impact on Saturn's magnetosphere with respect to neutral and charged particles, magnetic fields and dynamics.

4:20 p.m. Sivaraman B. * Pavithraa S. Lo J. I. Raja Sekhar B. N. Cheng B. M. Mason N. J.
Using Hartley Band to Detect the Ozone Precursor on Icy Satellites **[#3025]**
We propose using the Hartley band in identifying the ozone precursor molecule on the icy satellites based on a series of experiments carried out on simple ozone precursor ice analogs.

Thursday, July 28, 2016
SMALL FRY IN THE SATURN SYSTEM
4:35 p.m. Boulderado Ballroom

Chair: Matthew Tiscareno

4:35 p.m. Denk T. * Mottola S. Bottke W. F. Hamilton D. P.
Phoebe and Saturn's Captured Outer Moons **[#3061]**
The abstract, the talk and the related book chapter give an overview on what we know about the irregular moons of Saturn and the Phoebe ring. A main focus lies on the Cassini imaging observation campaign to determine basic physical properties.

4:55 p.m. Thomas P. C. * Tiscareno M. S. Helfenstein P.
Systematics of the Inner Small Satellites of Saturn **[#3019]**
The inner small satellites of Saturn have distinctive morphologies dependent upon their dynamical position.

5:15 p.m. DISCUSSION

Friday, July 29, 2016
ASTROBIOLOGY AND THE FUTURE
9:00 a.m. Boulderado Ballroom

Chairs: **Christopher Glein**
Amanda Stockton

9:00 a.m. McKay C. *
Astrobiology of Enceladus

9:20 a.m. Duca Z. Tan G. Cantrell T. Van Enige M. Dorn M. Cato M. Putman P. Kim J. Mathies R. A. Stockton A. *
Development of an Extraterrestrial Organic Analyzer (EOA) for Highly Sensitive Organic Detection on a Kinetic Penetrator **[#3087]**
We show the development of an EOA for future planetary impact penetrator missions. EOA can survive a 50,000 g impact, making it the only current optical instrument with this capability.

9:35 a.m. Fujishima K. * Dziomba S. Takahagi W. Shibuya T. Takano Y. Guerrouache M. Carbonnier B. Takai K. Rothschild L. Yano H.
A Fly-Through Mission Strategy Targeting Peptide as a Signature of Chemical Evolution and Possible Life in Enceladus Plumes **[#3085]**
We present a combination of two latest and unpublished experiments that enable us to realize in situ life signature detection and chemical evolution for deep habitats of the "Ocean World.".

9:50 a.m. Kowalski J. * Schüller K. Zimmermann A.
Towards Simulation-Based Mission Support for Subsurface Exploration of the Icy Moons **[#3077]**
Advanced subsurface mission scenarios for the icy moons suggest to deploy a robotic probe. In our contribution, we will present an integrated computational model for a probe migrating through ice, as well as its ambient cryospheric state.

10:05 a.m. Break

10:20 a.m. Baader F. * Dachwald B. Espe C. Feldmann M. Francke G. Förstner R.
Testing of a Miniaturized Subsurface Icecraft for an Enceladus Lander Mission Under Enceladus-Like Conditions **[#3029]**
The German project "Enceladus Explorer - Environmental Experimental Testing" is conducting research to evaluate technology for an Enceladus lander mission. The concept of an advanced melting probe will be evaluated in simulated Enceladus environment.

10:35 a.m. Dachwald B. * Kowalski J. Baader F. Espe C. Feldmann M. Francke G. Plescher E.
Enceladus Explorer: Next Steps in the Development and Testing of a Steerable Subsurface Ice Probe for Autonomous Operation **[#3031]**
Within Enceladus Explorer, the technology for a lander is developed and tested. The steerable subsurface ice probe was used in 2013 in Antarctica to get a clean subglacial sample and is now redesigned for testing in a more Enceladus-like environment.

10:50 a.m. Laine P. E. *
Life on Icy Worlds? Emergence vs. Panspermia **[#3017]**
The icy moons present some of the promising examples of extended habitable locations in our solar system. How do they fit in to our knowledge about the origin of life? Where are the challenges for models for the origin life on the icy moons?

11:05 a.m. ASTROBIOLOGY DISCUSSION

11:35 a.m. ENCELADUS ROUND TABLE

Notes

THE BRITTLE-DUCTILE TECTONICS OF ICE SHELL ON EUROPA FROM POLE TO POLE

P.Aftabi*(Pedram.Aftabi@gmail.com)

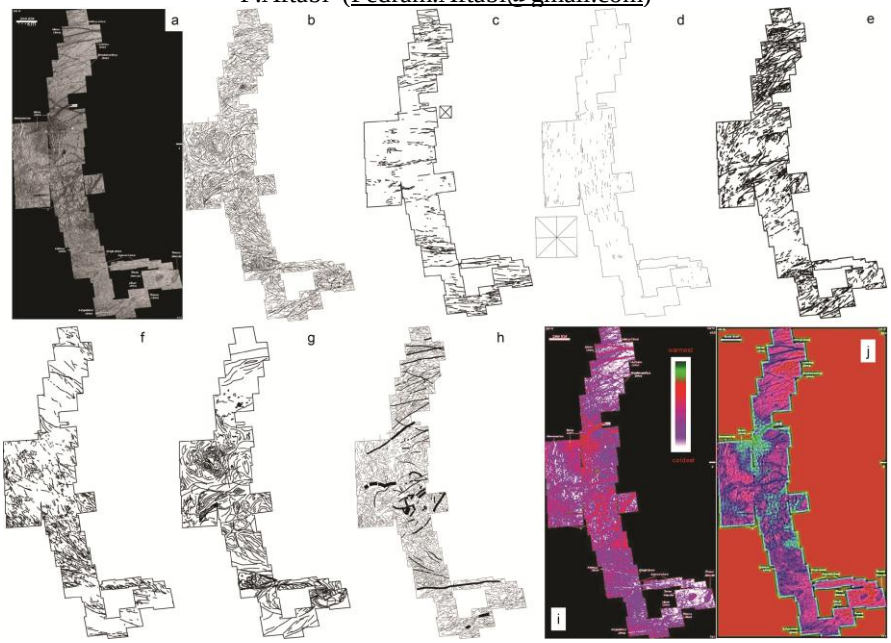

The fractures-faults are common in salt and ice sheets which spread or moving by tidal and weather effects on Earth [10, 11, and 12].Milazzo. et al [1] and the Galileo SSI team at University of Arizona prepared Fig-a of this paper which used for structural analysis by author. This coverage is from 62^0 N to 73^0 S latitude, 160^0 W to 246^0 W longitude (Fig a).Another near strip published by Greenberg[13]. The process of mosaicing these images is described in Becker *et al.* [4] and Milazzo *et al.* [5]&[1] .This strip of Europa shows many different types of structures. This global view is necessary to understand the local processes shaping Europa[1]. Some of the faults-fractures related to pure and simple shear globally in this moon and some of the fractures generated by impact craters on the icy surface and their related diapirs and chaos. Some of the faults-fractures generated by injection of warm ice and water circulations through the icy ridges and bands (Figi, j). Because of this non-synchronous planetary rotation, the directions and magnitudes of the tidal stresses experienced at any particular location are expected to gradually change in a systematic manner [6, 7].Therefore tidal movements operated on the kinematics and reactivation of faults-fractures on this moon. Europa's icy crust may be migrating eastwards over time with respect to its rocky core and possible liquid interior, due to tidal forces exerted by Jupiter [9]. Europa's dominant surface morphology changes from double ridges (Fig h here)at the north pole to chaos and diapirs(Fig g here)[3] and dissected terrain near the equator to strike slip faults [2,17].I here classified different fractures-faults related to shear and upwelling of ice diapirs ice ridges and crater(Fig g).The faults-fractures and ridges classified as geographic indications(see Fig b to j).The structures distinguished as open and closed fractures and faults(see Figs a to h).Some of the faults-fractures in Europa are strike slip[17]or may be normal , thrust faults,transtension and tranpression faults. These geographic structures classified as E-W(Figc),NS(Figd),NW-SE(Figf),NE-SW(Fige)fractures and faults, conjugate fractures-faults(Figj),concentric fractures-faults related to chaotic features craters and diapirs(Fig g).The ice diapirs are in two types warm ice diapirs(Fig i- red areas and green areas in Figj- see also Fig16 in ref[18]and[19]) produced injection as ridges but the oldest diapirs (pink areas of fig j)are related to the old craters which recognized by different types of concentric fractures. Some of the circular to sub circular features were mapped, including pits, uplifts, spots and chaos in small locations of Europa before[14].Topographic data reveals that most pits are ~100 m deep to ~500 m[14].This range of pit depths fits numerical simulations [15,16]but some of the circular features are as diapirs[17] with overhangs deeps similar to pits(exps by author). After impact ,the warm ice diapirs and injected water beneath the thin freeze ice of the surface start to rise and generated concentric faults and radial joints (Fig g,i,j).New circulations in the warm ice in the recent time generated ridges (dark pink in Figi and black areas of Fig h).Some of the ridges are younger than the craters but some of them are old .The ice diapirs can not pierce the overburden of the same material and remained below the icy crust(pink areas inFigj). But every time the reactivation of diapir generated fractures and faults in the concentric form(Fig g).The variety of structural features shown in the fig a to j base on the mosaic (Figa) enables us to get a global view of the Ice tectonics in the Europa moon. Some of the fractures are younger than craters and chaotic features. Some of the fractures-faults are Syn- diapirism, and some of them are post diapirism.The faults- fractures system on the surface of Europa may be active and most be considering for future missions to the Europa. The reactivation of faults generated by movements in the warm ice and water flow just beneath the brittle icy thin crust. The morphology of faults-fractures related to upwelling of ice or molten ice or cold water and also simple and pure shear processes serve as probes into the interiors of Europa. Brine mobilization during lithospheric heating on Europa [20] can be flow through the strike slip faults, ridges and fractures or can be injected to the chaos and diapirs. These data (see Figs) are available on request for use in mapping and modeling of geological feature in future works by author. The maps here have been used to investigate the properties of the icy outer layers and in some cases the thermal histories and thermal diapirs. The mapping problems on Europa described by author in another subscription in LPI as print only abstract. For other pictures of Europa see www.NASA.Gov[21]. To see better please use zoom in object.

References: [1]Milazzo,A.S. et al and the Galileo SSI team. Planetary Image Research Laboratory, LPL, University of Arizona, MEDIUM RESOLUTION IMAGING OF EUROPA: A VIEW FROM POLE TO POLE. Generated Fig a for LPI used for mapping here. [2] Tufts, B.R., 1999, *Icarus.* [3] Greenberg R., et al. (1999, submitted) Icarus. [4] Becker, T. et al., (1998) *LPSC XXIX*, 1892-1893. [5] Milazzo, M. et al., (1998) *LPSC XXIX*, 1833-1834. [6] Helfenstein, P. and E. Parmentier, Icarus, 61, 175-184, 1985. [7]Greenberg, R. et al., Icarus, 135, 64-78, 1998. [9] Greenberg, R. and S. Weidenschilling, Icarus, 58, 186-196, 1984.[10]Aftabi,In prepertion,Joints in the salt diapirs and salt-ice sheets,5pp.[11]Aftabi,p.,In prep.,Geologic map of Qum Kuh, in scale 1:25000.[12]Aftabi,P.,9th VEXAG meeting and International workshop,2pp.[13]Greenberg,R.,2005,Europa the ocean moon, springer,380pp.[14]Singer,K.N. et al.,2010, 41st LPSC,pdf2195,2pp. [15] Han L. and Showman A.P. (2005) *GRL* L20201. [16] Showman A.P. and L. Han (2005) *Icarus 177*, 425-437.[17]Greeley ,R.etal.,2000,Journal of Geophysical Research,V.105,N.9,pp559-578.[18] Collins,G &Nimmo,F., Chaotic Terrain on Europa,20pp on web.[19] Collins G. C.,et al.,2000, J. Geophys. Res., 105, 1709–1716.[20] Head J. W. and Pappalardo R. T. ,1999, J. Geophys. Res., 104, 27143–27155. [21] www.NASA.Gov.

TESTING OF A MINIATURIZED SUBSURFACE ICECRAFT FOR AN ENCELADUS LANDER MISSION UNDER ENCELADUS-LIKE CONDITIONS. F. Baader[1], B. Dachwald[1], C. Espe[1], M. Feldmann[1], G. Francke[1], R. Förstner[2], [1]Faculty of Aerospace Engineering, FH Aachen University of Applied Sciences, Hohenstaufenallee 6, 52064 Aachen, Germany, fabian.baader@fh-aachen.de, [2]Institute for Space Technology and Space Applications, Bundeswehr University Munich, Werner-Heisenberg-Weg 39, 85579 Neubiberg, Germany

Introduction: The prospects of liquid water at Enceladus' South Polar Terrain make it an interesting target for future missions [1]. The German Enceladus Explorer (EnEx) initiative is focused on the evaluation of the technology for a potential lander mission with the deployment of a subsurface melting probe. EnEx is funded and managed by the DLR Space Administration and comprises several German universities with separate sub-projects. The probe shall autonomously navigate through the ice to a location where a water sample can be taken and analyzed in situ [2]. At FH Aachen University for Applied Sciences, the EnEx-nExT (Enceladus Explorer – Environmental Experimental Testing) project team is conducting research about the suitability of combined drilling and melting probes like the IceMole [3] for extraterrestrial application on Enceladus**.**

Previous Related Research at FH Aachen: Several prototypes of melting probes were designed at FH Aachen since 2009. Field tests on glaciers in the Swiss Alps, on Iceland, and in Antarctica revealed several advantages with respect to conventional drilling/melting methods. These include maneuverability in ice (including upwards cruise), penetration of sediment layers, contamination-free melting, large depths and recoverability. The last development step (the "EnEx-IceMole") was utilized successfully at Blood Falls/Antarctica to access a sub-surface water reservoir and recover a sample.

Experiments in near-Enceladus environment: All testing so far was done on terrestrial glaciers. Since ice temperatures and pressures differ significantly on Earth and Enceladus, EnEx-nExT undertakes further investigations regarding a potential deployment on Enceladus. First of all, effects due to lower ice temperatures include increased shear strength of ice, a higher required energy input and a reduced cruise speed, and thus decreased efficiency. An optimization of the screw geometry also has to be considered. Secondly, an ambient pressure below the triple point of water results in sublimation of ice instead of melting. The resulting effects include a heavily increased phase transition enthalpy, an unknown expanding gas flow around the probe and potential re-freezing of molecules inside the melt channel. The impact of a much smaller gravity on Enceladus is assumed to be insignificant for melting operation and therefore neglected (since the concept uses a screw to guarantee ice contact, no gravitational force is necessary).

Experimental Setup: The investigation of melting behavior takes place in a vacuum chamber at pressures below 6 mbar. An ice body (V_{ice}=160 l, d ≈ 0.4 m; h ≈ 1.3 m) will be cooled down to 90-100 K. It contains 64 temperature sensors to identify the 3D temperature field around the probe. The ice is continuously cooled to simulate an infinite ice mass. A miniaturized IceMole probe (8 x 8 x 40 cm, P_{heat} ≈ 5.5 kW) is currently in its design phase and will be available in summer 2016. The probe is equipped with sensors to measure force and torque of the screw, heating power and distribution, pressure sensors along the side (for ambient pressure measurement) and visual/IR-cameras at the back (to examine the melt channel over time). The simulation chamber is equipped with a high speed camera and an infrared camera to observe the ejected gas and particles.

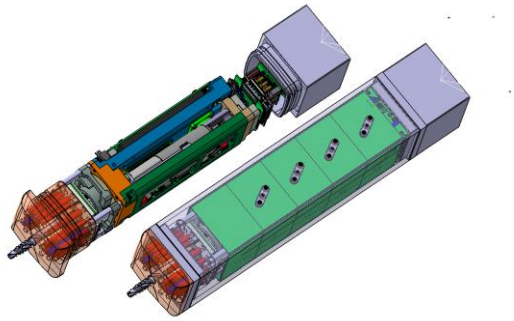

Experiment Objectives: EnEx-nExT is aiming towards a better understanding of melting power requirements, melting efficiency and melting speed for combined melting and drilling probes. Before a lander mission to sample water on Enceladus or other icy moons, there must be a solid understanding of the sublimation/melting process. Melt channel geometry is interesting as well, since a closing melt channel would result in a pressure increase inside the ice block and a transition from sublimation to melting. This could lead to less energy consumption and faster melting speed.

References: [1] Konstantinidis K. et al. (2015), *Acta Astronaut., 106*, 63–89. [2] Kowalski J. et al. (2016), *Cold Reg. Sci. Technol., 123*, 53-70. [3] Dachwald B. et al. (2014), *Ann. Glaciol., 55(65)*, 14-22.

FAR-UV SPECTRAL AND SPATIAL ALBEDO COMPARISONS BETWEEN ENCELADUS AND EUROPA. T. M. Becker[1], K. D. Retherford[1], L. Roth[2,1], J. Saur[3], M. A. McGrath[4], [1]Southwest Research Institute, San Antonio, TX, tbecker@swri.edu, krethereford@swri.edu; [2]School of Electrical Engineering, Spade and Plasma Physics, Sweden, lorenzr@kth.se; [3]Institute of Geophysics and Meteorology, University of Cologne, Germany, saur@geo.uni-koeln.de; [4]SETI Institute, Mountain View, CA, mmcgrath@seti.org

Introduction: Observations of Saturn's satellite Enceladus and Jupiter's satellite Europa have revealed these two icy worlds to be currently geologically active. The apparently young (relatively reduced in craters) surfaces of these moons show some spectral similarities, including FUV-dark patches that appear bright at visible wavelengths, generally low UV reflectance, and some hemispheric dichotomy; however, there remain significant differences between the two moons [1, 2]. One of the most interesting differences is the lack of a strong H_2O absorption ledge between 165-190 nm in Europa spectra that is clearly detectable for Enceladus [1, 3] and the overall lower FUV albedo observed across Europa. Additionally, previous comparisons between the two satellites revealed that the visible coherent backscatter component of the opposition surge observed on Enceladus is broader and weaker than observed on Europa, possibly indicating differences in the general roughness of the two surfaces [4].

The Cassini mission has provided an unprecedented look at the surface of Enecladus, revealing small amounts of NH_3 and possibly tholins distributed globally across the H_2O outer layer [1, 3]. IR/UV asymmetries across the surface consistent with fall-out from plume material emanating from the tiger stripes at the south pole [5]. These observations link the surface material with Enceladus' interior, which enables the exciting prospect of understanding the sub-surface ocean through analyses of the moon's surface.

Questions of Interest: A natural question then arises for Europa; if Europa is also a geologically active, icy world, then why is its surface so different from that of Enceladus? Are the differences exogenic, resulting from the strong Jovian magnetosphere or implantation from the Io torus rather than the E ring material for Enceladus, or endogenic, indicative of different interiors? The differences may be attributed to the various mechanisms for resurfacing; the Enceladus plumes appear to be a consistent source of global surface material, whereas the plumes on Europa currently appear to be stochastic [6] with a more localized impact. Perhaps geological activity associated with the observed darker linea across Europa dominate the resurfacing of the satellite, and these processes result in different material reaching the surface. The contrasting surface compositions may have important implications for the internal structure, crustal thickness, and composition of the sub-surface oceans of the two satellites.

Current Work: In order to address why the surfaces of Europa and Enceladus are different and the inherent implications of those variations, we must expand upon our understanding of the surface of Europa. We will present an on-going analysis of an extensive data set of FUV observations of Europa, spaning from 1999 – 2015. The data were obtained using the G140L mode of the STIS instrument on the Hubble Space Telescope. We analyze the spectral and spatial albedo properties across Europa. Our analysis utilizies high-resolution solar spectra to accurately map the surface albedo. We also account for the expected Lyman-α IPM for each observation.

In our analysis we explore latitudinal variations in the albedo, spectral trends with phase angle, and whether the UV albedo is consistently inverted from the visible (i.e. are all FUV-dark regions bright in the visible?). Accurate mapping of the spectral and spatial albedo is also necessary for distinguishing and constraining any atmospheric emissions. As a result, previous studies of the albedo on Enceladus may then be used in placing stronger constraints on a possible tenuous Enceladus atmosphere. We compare the UV spectra of the two satellites and explore possible compositional disparities responsible for the differences in absorption features and reflectance. Additionally, we analyze the phase-angle dependence of the Europa spectra from the HST data and compare with the published Enceladus results.

We will present the new spatial and spectral albedo maps and UV spectral light curve analyses of Europa with an emphasis on comparing these data sets with the substantial knowledge of Enceladus obtained through Cassini observations. We explore the implications of the differences and similarities between the two icy worlds.

References: [1] Hendrix, A. R. et al. (2010) *Icarus 206,* 608-617. [2] Carlson, R. W., et al. (2009) *Europa (book),* 283. [3] Zastrow, M. et al. (2012) *Icarus 220*, 29-35. [4] Verbiscer, A. J. et al. (2005) *Icarus 173*, 66-83. [5] Schenk, P. et al. (2011) *EPSC-DPS* 1358. [6] Roth, L., et al. (2014) *Science 343,* 171-174.

The unusual role of secondaries in the evolution of crater populations on Enceladus, and consequences for age estimation. E. B. Bierhaus[1] , L. Dones[2], and S. Robbins[2], [1]Lockheed Martin, [2]Southwest Research Institute.

Introduction: The ongoing (but sadly near final) Cassini image library of the icy Saturnian satellites provides many new pages of history in this rich, complex, and compelling system of satellites, rings, and giant planet. As with history in general, questions of timing are fundamental to our understanding of the evolution of these fascinating objects. A technique to constrain, and under optimum circumstances and knowledge even define, ages and sequences of events is to examine impact crater populations – cataloguing their sizes, locations and spatial densities is a chronometer that can mark relative and absolute ages.

We are in the process of measuring crater populations on the Saturnian satellites [1] and developing a high-fidelity model [2] of the accumulation of primary and secondary craters for the mid-sized Saturnian satellites, with the ultimate goal of using the crater populations to constrain timing and ages of events in the Saturnian system. Here we report on progress of this work, with attention to interesting consequences for Enceladus, including the young terrains.

Complex outcomes from simple inputs: Earlier [3] we demonstrated that the simple variation of impact speed (v_i), surface gravity (g), and escape velocities (v_{esc}) between the satellites can result in observably different crater populations, even if they all are exposed to the same impacting population. Another important parameter is v_{min}, the minimum speed necessary to form a secondary (see [3]), which dictates the presence and proximity of secondaries relative to their parent primary crater.

Enceladus lives in a special combination of these parameters compared with the mid-sized Saturnian satellites, and in contrast to the Galilean satellites. Enceladus has an effective escape velocity (velocity to reach the Hill Sphere) of ~209 m/s; if v_{min} for icy surfaces is ~150 m/s, then there is only a ~60 m/s window of ejection speeds that results in secondaries. This narrow window affects not only the total population of secondaries, it also affects the resulting imprint of the secondary size-frequency distribution (SFD), i.e. the secondary SFD is somewhat truncated at smaller sizes because the smaller ejecta fragments are typically ejected at higher velocities, and thus escape.

Adjacent secondaries depend on g and v_{min}. On the Moon, Mars, and on the Galilean satellites there is a classic progression of features beyond the rim of large impact craters: first there is the continuous ejecta blanket, which beyond roughly 1 crater radius transitions to a dense annulus, the adjacent secondary crater population.

In contrast, there are only a few possible examples of such "classic" behavior around large craters on the mid-sized Saturnian satellites, and none on Enceladus. While large craters have continuous ejecta blankets, and some (presumably young) craters have rays, the presence of a dense annulus of adjacent secondaries is subtle at best, or in many cases, simply absent.

This is likely due to the interplay between v_{min} and the distance that corresponds to that velocity. On high-g bodies v_{min} can get ejecta fragments only so far, meaning secondaries that form close to their parent primaries – i.e. adjacent secondaries – are possible. However, as g decreases, v_{min} results in greater distances. At some point, as g gets small enough, and because secondaries cannot form at velocities less than v_{min}, adjacent secondaries in the traditional sense will disappear altogether. (In the extreme case that the escape velocity becomes less than v_{min}, then secondaries may not form at all, which may be the case on Mimas.)

The fragments that form the adjacent secondaries on higher-g bodies are also the largest secondaries made by a primary impact. In the case of Enceladus, these large secondaries are globally distributed across the satellite.

Consequences for age estimates on Enceladus: Enceladus will have secondaries, but only secondaries from fragments moving in a narrow velocity range, and these fragments tend to be the largest. Because of the relatively low surface gravity, these large fragments, rather than making a dense, adjacent annulus of secondaries, will contribute to the global background of randomly distributed craters.

We are examining two consequences: (1) the evolution of the crater SFD over time could be uniquely diagnostic on Enceladus because of the narrow velocity range of secondaries that form, and (2) we can use the entire surface area of Enceladus to constrain the ages of lightly cratered terrains – this is because young terrains accumulate direct primaries, as well as secondaries from anywhere else on the satellite.

We will present the details of our calculations at the meeting.

References: [1] Robbins S.J. et al. (2015) *LPSC XXXXVI*, Abstract #1832. [2] Bierhaus E.B. et al. (2015), DPS #47, id 508.01. [3] Bierhaus E.B. et al. (2012) Icarus, v. 218, 602-621.

FOLDING AND FAULTING ON ENCELADUS: CONTRAINTS ON GEOPHYSICAL EVOLUTION. M. T. Bland[1] and W. B. McKinnon[2], [1]USGS, Astrogeology Science Center, Flagstaff, AZ (mbland@usgs.gov), [2]Department of Earth and Planetary Sciences, Washington University in Saint Louis, St. Louis, MO.

Introduction: Much of Enceladus' surface has been modified by tectonic deformation [1]. As on many icy satellites (e.g., Ganymede, Europa, Tethys), much of this deformation is extensional in origin [e.g., 2]. However, Enceladus also exhibits numerous features that appear to have formed through surface contraction. These features include kilometer-high ridges (dorsa) and long-wavelength folds in the equatorial region (Fig. 1) [3], thrust belts at the margins of the south polar terrain [4], and putative small-scale folds between the tiger stripe fractures [5,6]. Here we compare the morphology and topography of these features to numerical simulations of tectonic deformation to gain greater insight into the geophysical evolution of Enceladus.

Numerical Results: Finite element simulations of lithospheric shortening reproduce both fold-dominated and fault-dominated deformation (and in some cases, a mixture of the two) depending on the conditions assumed. Warmer effective temperatures (T_s) (e.g., beneath an insulating regolith) and higher heat flows (F) favor folding (Fig. 1 and [6]). Colder temperatures and lower heat fluxes favor fault-like deformation (Fig. 2).

Application to Enceladus and Comparison to Europa: Enceladus' equatorial long-wavelength folds are consistent with warm effective surface temperatures and high heat fluxes during their formation (Fig 1). However nearby ridges (Fig 1) that likely formed by faulting [3], and older extensional deformation [2] indicate a complex geologic history in the region (Fig 1). Thrust belts at high latitudes are consistent with deformation of the colder lithosphere there. The funiscular terrain between the tiger stripes requires extremely high heat flow, low thermal conductivity, and warm effective temperatures, if it forms via folding [6]. These inference inform the geophysical process that have occurred on the satellite.

Surface temperature is the dominant influence on whether folding or faulting occurs, and on the amplitude of deformation. Enceladus' colder temperatures relative to Europa explain why contractional features are common on the former, but are sparse on the latter. Heat flux plays a secondary role.

Acknowledgments: This work is supported by NASA SSW (NNH15AZ80I).

References: [1] Crow-Willard, E.N. and Pappalardo, R.T. 2015, *JGR* 120. [2] Bland, M. T. et al., 2007, *Icarus* 192, 92-105. [3] Patthoff, D. A. et al. 2015, *LPSC 46*, #2870. [4] Yin, A. and Pappalardo, R. T., 2015, *Icarus* 260, 409-439. [5] Barr, A. C. and Preuss, L.J. 2010, *Icarus* 208, 499-503. [6] Bland, M. T., et al. 2015, *Icarus* 260, 232-245.

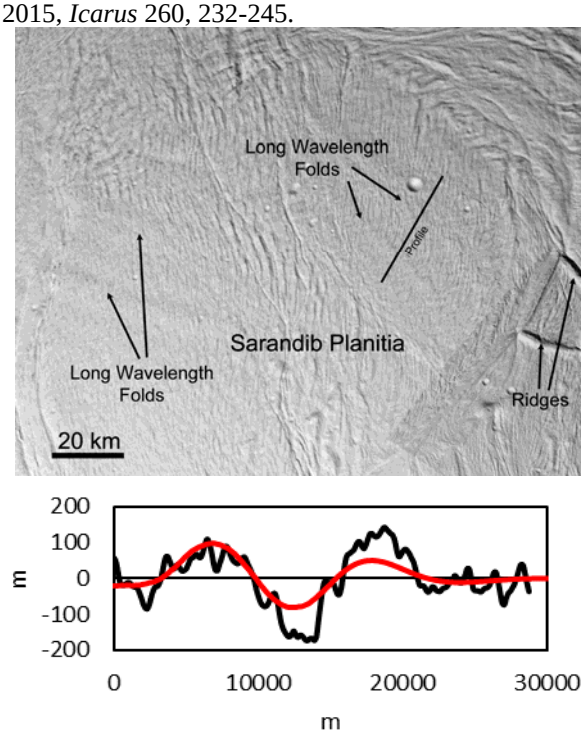

Figure 1: (Top) A portion of Enceladus' trailing hemisphere showing long-wavelength folds and discrete ridges in Sarandib Planitia. The deformation superposes older extension deformation. (Bottom) Comparison of fold topography (black - location of profile noted above) and a simulation of lithospheric shortening assuming T_s=120 K and F=300 mW m^{-2} (red). Assuming a lower thermal conductivity would decrease the required heat flux.

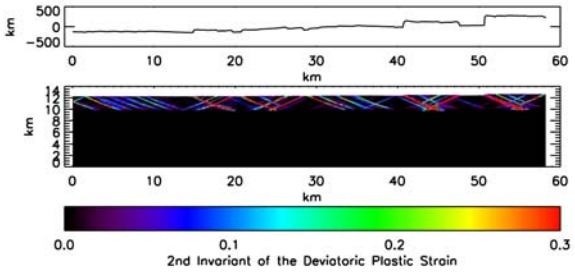

Figure 2: Simulation of lithospheric shortening (black box) showing the development of linear fault-like zones (colored regions). The surface (top panel) is deformed by a series of scarps rather than folds. The simulation used a T_s= 70 K and F=200 mW m^{-2}.

Modeling the H_2 production in the Cassini Ion and Neutral Mass Spectrometer at Enceladus: Effect of Ice Grains Impacts in Low Velocity Flybys and Implication for the Identification of Native H_2 in the Plumes.

A. Bouquet[1,2] , T. Brockwell[2], J.H. Waite[2,1], S. Chocron[2], B. Teolis[2], R. S. Perryman[2], J. Walker[2]
[1]University of Texas at San Antonio, Department of Physics and Astronomy, TX 78249 [2]Southwest Research Institute, San Antonio, TX 78228
email contact: alexis.bouquet@swri.org

Introduction: The data from the Cassini-Ion and Neutral Mass Spectrometer (INMS) at Enceladus' plumes shows presence of H_2 in important quantities (15% for low speed flybys). H_2 can be considered as a "smoking gun" for the suspected hydrothermal activity in Enceladus' ocean ([1][2]) as it is ultravolatile and would need to be the result of an ongoing production. However, while results for low velocity (7.5 km/s) are consistent with regard to the abundance of H_2, high velocity flyby show a higher quantity, up to 40%. This is attributed to the presence of ice grains in the plumes [3]: their impacts on the walls of the titanium antechamber of INMS expose/project fresh titanium that will react with water to form hydrogen. The large number of small ice grains arriving during a single integration period of INMS creates a background signal in addition of large grains causing punctual spikes. This process poses the question of how much of the detected hydrogen is native and how much is an artifact.

Models: A surface chemistry model of the INMS has been developed in order to determine how much H_2 is produced from the expected ice grains distribution for each flyby (given by Cassini CAPS data [4]). This model considers adsorption and chemisorption effects to follow the evolution of surface and gas phase species in the antechamber. [5]

CTH Simulations of impacts on an titanium surface [6] have shown that above 16 km/s (as is the case for flyby E5) the impact produces titanium vapor, while at the velocities of the slow flybys, the titanium stays in the form of solid fragments. Multiple CTH simulations of low velocity impact have provided the total amount of fragments created by impacts of ice grains of all sizes.

In order to translate antechamber population into simulated counts given by the INMS, a revised sensitivity model [7], including entry/escape of plumes species through other pathways in the instrument, has been combined to the antechamber model.

Results: As shown in Figure 1, taking only ice grains into account (no H_2 coming from the plumes) the quantity of H_2 produced just by the grains is obviously excessive, pointing to an excess of titanium. The excess can however be explained by the uncertainty on the ice grains population.

Even with an excessive ice grains population, it takes time to accumulate enough titanium to produce a noticeable H_2 signal. The shape of the H_2 background signal is therefore expected to differ from the shape of the H_2 signal from the plumes (if there is one). The two major spikes in the graph are attributed to ~2 microns ice grains.

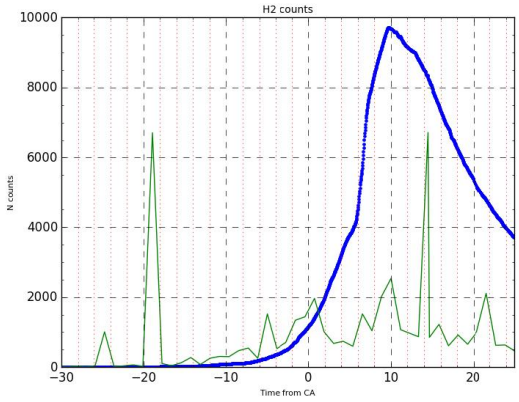

Figure 1: Comparison of H_2 counts per integration period from the simulation (blue) and from E18 slow flyby data (green). Time is given is seconds relative to closest approach.

Way forward: We will first adjust the ice grains total to the residual H_2 signal after plume crossing (since it only depends on total titanium from impacts) and from there adjust the quantity of H_2 in the plumes to match the total of counts from plumes crossing. Application to other slow flybys E14 and E17 will be needed to consolidate the final value of H_2 quantity.

References:

[1] Hsu et al., 2015, *Nature*, *519*(7542), 207-210.

[2] Bouquet et al., 2015 *Geophysical Research Letters*,*42*(5), 1334-1339.

[3] Waite, J.H. et al.,(2009) Nature*, 460(7254):p 487-490.*

[4]Dong et al., 2015 *Journal of Geophysical Research: Space Physics*, *120*(2), 915-937.

[5] Brockwell et al.,2014 Workshop on the Habitability of Icy Worlds, held 5-7 February, 2014 in Pasadena, California. LPI Contribution No. 1774, p.4022

[6] Walker et al., 2015, *Procedia Engineering*, *103*, 628-635.

[7] Teolis et al., 2015, *Space Science Reviews*, 190 (1-4), 47-84.

ENCELADUS AND EUROPA: VERY EARLY HINTS OF ACTIVITY. B. J. Buratti[1], [1]Jet Propulsion Laboratory, California Institute of Technology, Pasadena, CA 91109; bonnie.buratti@jpl.nasa.gov.

Introduction: Even before the first hint of activity on Enceladus, the measurement of unit albedo by the two *Voyager* spacecraft, this mysterious moon was giving up some of its secrets. Observations by P. Lowell and E. C. Slipher in 1913-1914 showed a 0.3 magnitude increase in the brightness of Enceladus at western elongation (the trailing side) when the subobserver latitude was -32º, which is near the southmost observation possible from Earth. Similarly, in 1972-73, O. Franz and R. Millis observed a brightening of 0.3 magnitudes at western elongation when the subobserver latitude was -30º [1]. These time periods both correspond to the maximum visibility of the active region of Enceladus, the "Tiger Stripes."

***Voyager* observations of Enceladus**: The measurement of an accurate size by the *Voyagers* enabled the determination of the albedo of Enceladus: a staggering number near unity [2]. Almost immediately there was speculation that an albedo this high could only mean ongoing activity on its surface, possibly due to volcanoes or geysers. Prior to the *Cassini* mission, statements were made such as "the E-ring is continuously replenished by volcanic eruptions on Enceladus" [3], the first mention of active volcanos on the moon. What appeared to be coating by the E-ring of the other main inner moons of Saturn added to the evidence for ongoing activity [4,5]. Thus, decades prior to the discovery of cryovolcanism on Enceladus, observers noted evidence for it and were making predictions of its existence.

Europa: Well-known is the claim by A. Cook of the *Voyager* imaging team that a large solar phase angle image of Europa showed forward-scattered radiation from a plume. The work was never published, and other investigators were unable to identify the plume. Less well known is the observation of a thermal event on Europa. Observing Europa at NASA's Infrared Telescope Facility (IRTF) on Mauna Kea, Hawaii, Bill Sinton and James Tittemore reported the following thermal anomaly: "There is only one definite measurement at M [filter] on 23 April 1981, made at the IRTF. It seems that this measurement, which yields a fourfold increase in the observed flux over any other M measurement, is unassailable. The data acquisition system prints the telescope position encoders, and these values are in good agreement with computed offsets from other Galilean satellites and their encoder readings. Thus, there seems no possibility of misidentification. A total of 25 pairs of integrations were made that were mutually consistent. Filter positions and the amplifier gains are encoded, and there seems no possibility of error in these parameters." [6]. Observations of plume activity on Europa by the *Hubble Space Telescope* over 30 years later [7], and the subsequent failure to observe the plumes since this detection, imply that the activity on Europa is sporadic.

The importance of continued ground-based and Earth-orbiting observations: Spacecraft observations present data from a moment in time, while ground-based or Earth-orbiting observations provide synoptic coverage of activity which, at least in the case of Europa, may be sporadic. The *Galileo* spacecraft failed to capture any observations of ongoing activity on Europa, but there are at least two reliable observations of it from *HST* and IRTF. It is thus essential to continue ground-based studies. In the case of Enceladus, it is important to devise methods of observing the heat flux and evolution of its plume activity after the *Cassini* mission ends in 2017.

References: [1] Franz, O. and Millis, R. (1975). *Icarus* **24,** 433. [2] Buratti, B. J. and Veverka, J. (1984). *Icarus* **58**, 254-264. [3] Pang, K. et al. (1984). *J.G.R.* **89**, 9459-9470. [4] Buratti, B. J., Mosher, J. A., Johnson, T. V. (1990). *Icarus* **87**, 339-357. [5] Verbiscer, A. et al. (2007). *Science* **315**, 815-817. [6] Tittemore, W. C., Sinton, W. (1989) *Icarus* **77**, 82-97. [7] Roth, L. et al. (2014). *Science* **343**, 171-174

Acknowledgments: This research was carried out at the Jet Propulsion Laboratory, California Institute of Technology under contract to the National Aeronautics and Space Administration.

PHOTOMETRY OF ICY MOONS OVER MANY WAVELENGTHS FROM CASSINI VIMS. B J. Buratti[1], R. H. Brown[2], R. N. Clark[3], K. H. Baines[1], P. D. Nicholosn[4], J. A. Mosher[1]. [1]Jet Proplusion Laboratory, Callifornia Institute of Technology, Pasadena, CA 91109, bonnie.buratti@jpl.nasa.gov; [2]University of Arizona, Tucson, AZ; [3]Planetary Science Institute, Tucson, AZ; [4]Cornell University, Ithaca, NY.

Introduction: The Visual Infrared Mapping Spectrometer (VIMS) instrument on the Cassini Spacecraft possesses an unprecented range in wavelength, spanning nearly the entire solar spectrum. Investigation of photometric properties as a function of wavelength offers new insights on the physical properties of icy moons, and it provides tests of various models. Coupled with a planetary tour lasting more than a decade, this wide range of wavelengths has opened by a number of new areas of study. Among them are investigations of the directional scattering properties of icy moons spanning a full range of viewing geometries; accurate measurements of the bolometric Bond albedo, and maps of that parameter; and more accurate charterizations of physical parameters such as roughness, particle size and regolith porosity based on wavelengths for which the confounding factor of multiple scattering is not important.

Phase curves: Ground-based observations of the icy moons of Saturn are restricted to solar phase angles less than 6°, and *Voyager* observations provided a handful of visible measurements at larger solar phase angles [1]. *Cassini* VIMS observations enabled the measurement of phase curves over a full excursion of densely spaced phase angles, which have been used to compute bolometric Bond albedos [2]. Observations at small solar phase angles over a full range of wavelengths exhibit intriguing behavior that shows a drastic change at longer wavelengths. This change may be due to decreased importance of small particles at larger wavelengths or to the disappearance of multiple scattering. Phase angle measurements at very large angles have been used to characterize the plumes of Enceladus and to search for activity on Tethys and Dione by seeking forward scattered radiation [3, 4].

Macroscopic roughness: Another tool that can be used to probe the physical nature of the surfaces of icy moons is modeling of rough facets, which range from clumps of particles to mountains and craters. Larger wavelengths where the albedo of water ice is low are particularly effective for understanding roughness because multiple scattering, which partly illuminates primary shadows cast by rough features, is minimal, and the roughess models are more robust. Models fit to the low-albedo hemipshere of Iapetus reveal the surface to be much smoother than is typical for an icy moon, suggesting infilling of features by a dusty deposit [5]. An analysis of the various terrains of Enceladus shows that the plains north of the "tiger stripes" are fairly smooth, and that the stripes themselves are only slightly more rough, suggesting in-filling of craters with plume particles throughout the entire south polar region of Enceladus.

Maps of bolometric Bond albedo: The Bond albedo is the product of the geometric albedo times the phase integral. The wide wavelength range of VIMS offers the opportunity to directly measure the bolometric Bond albedo of icy moons, an important parameter for undertstanding the energy balance on a planetary surface and for doing thermal modeling.. With both albedo maps and phase integrals over the entire solar spectrum, a map of the bolometric Bond albedo is possible. The figure below shows such a map for Phoebe created from VIMS data.

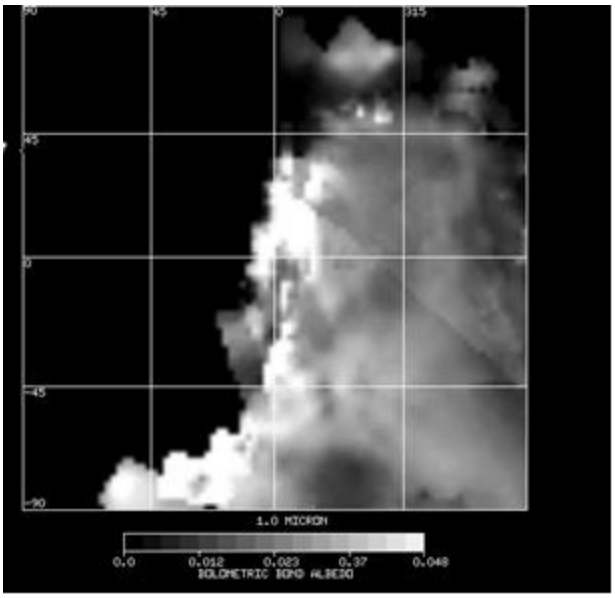

References: [1] Buratti, B. J. and Veverka, J. (1984). *Icarus* **5**8, 254-264. [2] Pitman, K. M., Buratti, B. J., and Mosher, J. A. (2010). *Icarus* **206**, 537-560. [3] Hedman, M. et al. (2013). *Nature* **500**, 182-184. [4] Buratti, B. J. et al. (2011). Icarus 214, 534-540. [5] Lee, J. S., Buratti, B. J., Hicks, M. D., Mosher, J. A. (2010). *Icarus* **206**, 623-630. [6] Buratti, B. J., Dalba, P. A., Hicks, M. D., Chang, J. (2014). *LPS* **XLV**, Abstract # 1777.

Acknowledgments: This research was carried out at the Jet Propulsion Laboratory, California Institute of Technology under contract to the National Aeronautics and Space Administration.

HEMISPHERIC-SCALE RIFT ZONES ON RHEA, TETHYS, AND DIONE

P. K. Byrne[1], P. M. Schenk[2], P. J. McGovern[2], and G. C. Collins[3]

[1]Planetary Research Group, Department of Marine, Earth, and Atmospheric Sciences, North Carolina State University, Raleigh, NC 27695 (paul.byrne@ncsu.edu), [2]Lunar and Planetary Institute, Universities Space Research Association, Houston, TX 77058, [3]Department of Physics and Astronomy, Wheaton College, Norton, MA 02766.

Introduction: Rhea, Tethys, and Dione are among the largest moons of Saturn. Each exhibits substantial extensional tectonic deformation in the form of rift zones ("chasmata"). Numerous mechanisms have been proposed to account for the stresses responsible for the surface deformation of icy satellites, including changes in volume due to phase changes within a satellite and solid-state convection, polar wander, diurnal tides, non-synchronous rotation, and tidal recession [1–8]. We show the map patterns of the chasmata (and impact features) on Rhea, Tethys, and Dione in **Fig. 1**.

Rhea: Galunlati and Yamsi Chasmata are both located close to the center of Rhea's trailing hemisphere (**Fig. 1a**), and trend approximately north–south. Galunlati is the longer of two, extending for ~1,500 km and subtending 113° of arc. Both systems vary in width along their course, from ~40–90 km, and are characterized by normal fault segments that display minor local variations in strike, relay ramps, and numerous stepover regions tens of kilometers long.

Tethys: Tectonic deformation on this moon is dominated by Ithaca Chasma, which ranges from high northern latitudes in the moon's trailing hemisphere, across the prime meridian, to high southern latitudes at the perimeter of the leading hemisphere (**Fig. 1b**). Although at 1,400 km it is shorter than the chasmata on Rhea, Ithaca Chasma subtends a longer arc (151°), and is between 70 km and 110 km in width. Ithaca Chasma hosts more individual fault segments than either chasma on Rhea, but is similarly oriented ~north–south along much of its course.

Dione: Rifting on this moon displays the greatest structural complexity of the three bodies we survey. Numerous chasmata populate the center of Dione's trailing hemisphere, with several following again ~north–south-oriented trends (notably Palatine, Eurotas, and Padua Chasmata) (**Fig. 1c**). Collectively, these rifts extend ~1,300 km, subtend 133° of arc, and vary 40–130 km in width. The cumulative number of fault segments on Dione is considerably greater than that of Rhea or Tethys.

Discussion: Despite differences in size, density, internal structure, impact cratering history, and dynamical environment, fundamental similarities exist in the style and distribution of large-scale extensional deformation on the icy satellites we investigate. Rifting is concentrated within or at the borders of each moon's trailing hemisphere, shows a preference for ~north–south-oriented strikes, and shows a systematic increase in complexity from Rhea, to Tethys, to Dione.

Sections of each moon's chasma or chasmata appear to lie along substantial portions of great circles (green lines in **Fig. 1a–c**), indicating that the rifting process(es) operated over considerable distances along lines of constant bearing (in spherical geometry). Further, tidally induced stresses alone tend to result in degree-two distributions in strain, in contrast to the hemispherical dichotomy in the localization of strain observed on these three Saturnian icy satellites (and on Rhea and Tethys in particular). Hemispherical differences in ice shell thickness, for example, may account for this "degree-one" dichotomy. Thus these large-scale rifts may have formed under a scenario in which tidal processes contributed at most a secondary component of stress, with Rhea representing the least, and Dione the most advanced stage of deformation.

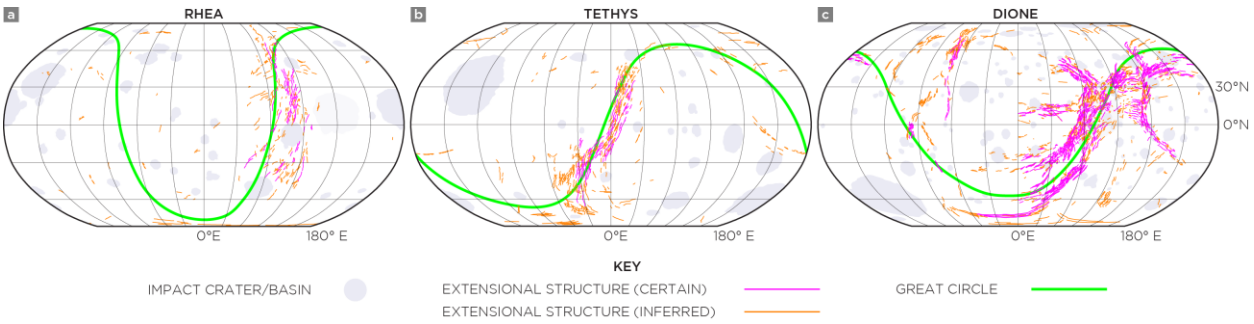

[1] Hillier, J. and Squyres, S. W. (1991) *JGR*, *96*, 15,665–15,674. [2] Czechowski, L. and Leliwa-Kopystyńskia, J. (2002) *Adv. Space Res*., *29*, 751–756. [3] Nimmo, F. (2004) *JGR*, *109*, E01003. [4] Nimmo, F. and Matsuyama, I. (2007) *GRL*, *34*, L19203. [5] Matsuyama, I., and Nimmo, F. (2008) *Icarus*, *195*, 459–473. [6] Nimmo, F. and Manga, M. (2009) in *Europa*, Pappalardo, R. T. et al. (eds.) Univ. Arizona Press, pp. 381–404. [7] Patthoff, D. A. et al. (2012) *LPS*, *43*, Abstract 2527. [8] Martin, E. S. and Kattenhorn, S. A. (2014) *LPS*, *45*, Abstract 1083.

REVIEW: ORIGIN AND EVOLUTION OF SATURN'S MIDSIZE ICY MOONS. J. C. Castillo-Rogez[1], D. Hemingway[2,3], W. B. McKinnon[4], G. Schubert[5], and G. Tobie[6], [1]Jet Propulsion Laboratory, California Institute of Technology (Julie.C.Castillo@jpl.nasa.gov), [2]Miller Institute for Basic Research in Science and [3]Department of Earth and Planetary Science, University of California Berkeley, [4]Department of Earth and Planetary Sciences, Washington University in Saint Louis, [5]University of California Los Angeles, [6]Laboratoire de Planetologie and Geodynamique de Nantes, Universite de Nantes, France.

Introduction: We review advances in midsize satellite research spurred over the past decade by the exploration of the Saturnian satellite system by the *Cassini-Huygens* mission. This presentation covers Mimas, Tethys, Enceladus, Dione, Rhea, and Iapetus. Enceladus' interior and evolution is addressed at length in other presentations (e.g., [1]) but is included here for the sake of comparative planetology.

Observational Constraints: *Cassini-Huygens* observations have yielded refined GM and mean radii for all the midsize satellites. Triaxial were obtained with uncertainties of a few kilometers [2], insufficient in most case to constrain interior structures. Iapetus exhibits a highly non-hydrostatic, fossile shape witness of an early period of faster rotation [3, 4]. Degree-two gravity harmonics were inferred from radioscience observations at Enceladus [5] and Rhea [6] and in both cases revealed departures from hydrostatic equilibrium that have been ascribed to core shape anomalies [6, 7]. Determination of Mimas' librations may also be associated with an irregular core or the presence of a deep liquid layer [8]. The temporary occurrence of a deep ocean was suggested for Tethys based on morphological observations [9]. While deep oceans have been predicted in these objects [10], definitive observational evidence is lacking, with the exception of Enceladus.

Questions Raised by Midsize Satellite Physical Properties: The lack of pattern in the physical properties of Saturn's midsize satellites is a major mystery. Satellite densities range from 0.98 g/cm^3 at Tethys and up to 1.61 g/cm^3 at Enceladus. Iapetus' separation distance of ~50 Saturn's radii with respect to the inner satellites likely points to variations in accretional environments across the Saturnian system. These observations have led to the introduction of novel origin scenarios for the moons: e.g., ablation [11] and formation from the tidal interaction of Saturn and its rings [12]. The diversity in physical properties and geological evolution observed across the satellite system offers a laboratory for testing fundamental physical processes: response to tidal stressing, feedback between dynamical and geophysical evolution, onset of convection, etc. The midsize satellites also offer context for comprehending the peculiar evolutionary path followed by Enceladus. Considered in the broader context of icy moons observed across the outer Solar system, these bodies help test the boundaries of ocean worlds.

Drivers of Geophysical Evolution: Geophysical modeling can help address these questions. The heat budget available to the midsize satellites depends in part on their accretional environment that determined the formation timeframe and timescale and in turn the amount of radioisotopes. Internal evolution depends on the balance between heat produced for radioiosotopes and tidal heating and heat loss via conduction and convection. Depending on their heat budget some of the satellites may have undergone partial melting of their volatile phase leading to serpentinization. While some of the midsize satellites display geological evidence for endogenic activity, these features are generally not associated with variations in composition. This potentially sheds light on the extent of chemical evolution and the modalities of material and heat transfer in these objects.

Many unconstrained or not yet explored parameters and processes complicate internal modeling: remnant porosity can bear significant impact on material thermophysical properties; mechanisms driving tidal dissipation in mixtures are not well understood; evolution through resonances adds further complexity; etc.

The presentation will explore these questions and present big picture findings gathered from comparisons across the Saturnian satellite system and with the Uranian system.

References: [1] Hemingway D. et al. (2016) This conference. [2] Thomas P. C. (2010) *Icarus* 208, 395-401. [3] Castillo-Rogez J. C. et al. (2007) *Icarus* 190, 179-202. [4] Miroslav K. et al. (2015) *Icarus* 252, 454-465. [5] Iess L. et al. (2014) *Science* 344, 78-80. [6] Tortora P. et al. (2016) *Icarus* 264, 264-273. [7] McKinnon W. B. (2013) *J. Geophys. Res.* 118, 1775-1788. [8] Tajeddine R. et al. (2014) *Science* 346, 322-324. [9] Chen E. M. A. and F. Nimmo (2008) *Geophys. Res. Lett.* 35, L19203. [10] Hussmann H. et al. (2006) *Icarus* 185, 258-273. [11] Mosqueira I. et al. (2009) *Icarus* 207, 448-460. [12] Charnoz S. et al. (2010) *Icarus* 210, 635-643.

Acknowledgement: *Part of this work is being conducted at the Jet Propulsion Laboratory, California Institute of Technology, under contract to NASA. Government sponsorship acknowledged.*

CONSTANT-SCALE NATURAL BOUNDARY GLOBAL MAPS OF ENCELADUS. C.S. Clark[1], P.E. Clark[2] and P.J. Stooke[3], [1]Chuck Clark architect, Atlanta, GA (rightbasicbuilding@gmail.com), [2]Jet Propulsion Laboratory, California Institute of Technology, Pasadena, CA, [3]University of Western Ontario, London, Ontario, Canada.

Introduction: Icy satellites present cartographic challenges unadressable with standard projections—such as showing Enceladan tiger stripes in global context. Yet this can be done with constant-scale natural boundary methods [CSNB], which transform the surface of any essentially globular object to 2-D in a way that not only preserves relative proportions and logical adjacencies, but also composes the map from natural considerations. Projection preselection is unnecessary; instead, one selects a critical boundary, which defines the map shape [1]. Algebraic shortcuts may be unavailable, but CSNB is digitizable [2].

Method: We deconstructed tidal flexure into component forces and persistent strain regimes, noting that inflection zones at 45˚ latitudes limit both polar regions, and an active south pole pairs dichotomically with a quiescent north pole. The quiescent terrain, extending narrowly along the Saturnian axis, separates leading- and trailing-hemisphere compression regimes. Scientific intuition identified a boundary of opportunity, cutting 270˚ along the quiescent meridian from 45˚S to 45˚S, north-pole centered [3]. We then hand-plotted a CSNB world map grid, using Renaissance-era rules of perspective, via steps shown in [1]. To facilitate graphic overlays [4], we pushed the central region (45˚S–90˚S) to conform to equal azimuth projection.

Results: The map shows proportionally accurate spatial relationships between polar and equatorial terrains—a better picture that may beget better understandings.

There are other ways to show these relationships, such as transverse cylindrical or Eisenlohr projections, but transverse cylindrical is severely distorted away from the projection axis while the CSNB map is not, and the Eisenlohr, with a cut of only 180˚ [7], greatly reduces the midmap polar region relative to the lobes while the CSNB map does not.

We have also produced 270˚-cut maps of Enceladus from other aspects—rotating the north-centered cut in 45˚ increments [5]; and flipping the cut to traverse the south pole, thereby featuring quiescent terrain for comprehensive crater assessment [6].

The LPS-47 map (see Figure) contains imperfections: the north-pole curve is not quite smooth, and, more seriously because of greatest shape distortion, the curve at the cusp is not tangent to the vertical. We have corrected these imperfections [6].

References: [1] Clark P.E., Clark C. (2013) "Constant-Scale Natural Boundary Mapping to Reveal Global and Cosmic Processes," *SpringerBrief*. [2] Kirk R.L. (2007) personal communication. [3] Clark C.S., Clark P.E. (2015) *LPS 46*, Abs. #1389 & E-Poster. [4] Ibid. (2016) *LPS 47*, Abs. #1044 & E-Poster. [5] Ibid. (2016) *LPS 47*, Abs. #2520 & E-poster. [6] Clark C.S. (2016) rightbasicbuilding.com, posted 11 May. [7] Snyder J.P. (1989) *USGS* Prof. Paper #1453, p. 184. [8] Mosaic: PIA18434 NASA/JPL-Caltech/SSI/ LPI.

Figure: Tiger stripes in context (leading hemisphere in left lobe; trailing hemisphere in right lobe) [5] [8]

EARLY TECTONIC HISTORY OF ENCELADUS FROM GLOBAL GEOLOGIC MAPPING. G. C. Collins[1], G. W. Patterson[2], R. T. Pappalardo[3], and S. A. Kattenhorn[4], [1]Wheaton College, Norton, Massachusetts, USA, gcollins@wheatoncollege.edu, [2]Applied Physics Lab, Laurel, Maryland, [2]Jet Propulsion Lab, Pasadena, California, [4]University of Alaska, Anchorage, Alaska.

Introduction: With the completion of the controlled USGS basemap of Enceladus [1], we are embarking on global geologic mapping of the surface. One of the main goals of the geologic map effort is to provide a better understanding of the global history of Enceladus through the sequence of features recorded on its surface. Much attention has been paid in the literature to current and very recent activity on Enceladus, but here we look from the other end and ask the question: what occurred at the beginning of observable geologic history on Enceladus?

Cratered plains: The most ancient terrain unit on Enceladus forms a band from the sub-Saturn hemisphere, over the north pole, to the anti-Saturn hemisphere, and has been referred to by various authors as "cratered terrain" or "cratered plains" [2-5]. It has also been recognized that this unit may be subdivided into a rougher, more heavily cratered unit, and a more sparsely cratered, subdued unit [2,3,5]. *Kirchoff & Schenk* [6] showed that the equatorial cratered plains are more lightly cratered than the mid- and high- latitude cratered plains, but that the transition appears to be gradual. They pointed out that viscous relaxation or plume burial could help to account for this difference in crater density, though the amount of plume material needed may be unrealistic [7] and the level of viscous relaxation requires remarkably high heat flows under an insulating regolith [7].

Indeed, it is difficult to draw a sharp dividing line between the rougher and more subdued cratered plains. Many potential unit boundaries in our geologic map are sharply defined by a prominent tectonic structure, but the resurfacing that has affected the cratered plains does not display such a boundary. Is this because the ancient tectonic structures have been erased, or because the resurfacing was a fundamentally diffusive process? Answering this question requires careful examination of the oldest tectonic structures.

Structures in the cratered plains: The cratered plains host a few types of tectonic structures, and are crosscut by several other types. The structures within the cratered plains would fit into the classification scheme of *Nahm & Kattenhorn* [8] as troughs and chasma. At the scale of our mapping effort, there appears to be a continuous morphological progression from wide chasma, to chasma, to narrow chasma, to troughs, to pit chains. It is likely that all of these tectonic features are extensional in origin [e.g. 8], and occupy a spectrum between graben, dilational normal faults, and mode I tension cracks. These features are found throughout the cratered plains, and crosscut most craters, so they record the most recent tectonic deformation of the unit.

There are also subdued ridges and troughs in the cratered plains (*Fig. 1*) that are wider than most of the recent tectonic features in the unit, and underlie most of the craters in the unit. These subdued tectonic features appear to be more densely populated in the equatorial areas (rigorous analysis of this statement is in progress), which is also where crater density is lower [6]. This would imply that the crater erasure process was correlated with localized tectonic activity (perhaps in concert with viscous relaxation) in the distant past, since burial or relaxation of preexisting craters in the equatorial areas would have also affected these structures. At the meeting we will present our latest mapping, classification, and analysis of these structures and the implications for the early history of Enceladus.

References: [1] Becker T. L. et al., *LPSC 47*, #2342, 2016; [2] Smith B. A. et al., *Science*, *215*, 504-537, 1982; [3] Porco C. C. et al., *Science*, *311*, 1393-1401, 2006; [4] Spencer J. R. et al., *Saturn from Cassini-Huygens*, 2009; [5] Crow-Willard E. N. and R. T. Pappalardo, *JGR*, *120,* 928-950, 2015; [6] Kirchoff, M. R., and P. Schenk, *Icarus*, *202*, 656-668, 2009; [7] Bland, M. T. et al., *GRL*, *39*, L17204, 2012; [8] Nahm, A. L., and S. A. Kattenhorn, *Icarus*, *258*, 67-81, 2015.

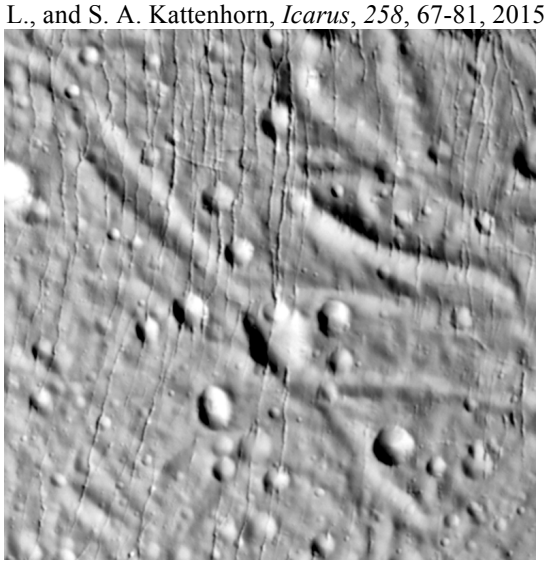

Figure 1. In the equatorial cratered plains, troughs and pit chains run N-S, cutting across most craters, while subdued ridges and troughs underlie most craters. Image is 30 km across.

Small-scale structure of plasma withing the Enceladus plume: *Cassini* observations on the E7, E17 and E18 encounters. F. J. Crary[1], [1]Laboratory for Atmospheric and Space Physics, University of Colorado, Boulder, 3665 Discovery Drive, Boulder, CO 80303, frank.crary@lasp.colorado.edu.

Introduction: During several Cassini encounters with Saturn's satellite, Enceladus, the spacecraft passed through the plume of water vapor and dust south of the satellite with a spacecraft orientation which allowed the Cassini Plasma Spectrometer (CAPS) to observe ions and nanograin dust particles associated with the plume. During three of these encounters, E7 (November 2, 2009), E17 (March 27, 2012) and E18 (April 14, 2012), the trajectories were very similar and parallel to the equatorial plane (i.e. little north-south velocity, so that the spacecraft moved perpendicular to the rotation axis of Enceladus.)

Previous analysis, using data from the CAPS ion mass spectrometer (IMS) and electron spectrometer (ELS), identified cold ions at rest with respect to Enceladus [1], negative water group and water cluster ions [2], and both positively and negatively charged dust particles in the 0.5 to 2 nm (1000 to 20,000 AMU) size range [3,4].

Observations from the third CAPS sensor, the ion beam spectrometer (IBS), which operates at twice the time resolution IMS and ELS and at 1.4% rather than 18% energy resolution, showed that the plume is highly structured, down to the 17 km along track limit of the instrument's sampling [5]. In many cases, consecutive spectra are significantly different, indicating both structure on smaller scales and the danger of time-aliasing in the CAPS/IBS measurements.

These observations show distinct regions of cold, dense ions, resembling a collisional ionosphere. These regions are intermixed with a broad background of warmer, non-thermal ions, possibly resulting from charge exchange between magnetospheric ions and plume neutrals. The data also suggest an ion drift velocity away from Saturn and in the direction of the upstream flow.

The above conclusions are only robust if the spectra are not aliases over the 2-second resolution of the instrument. To control for this, we have also analyzed the RPWS/LP data in the sensor's constant-voltage mode. In this mode, and during the Enceladus plume crossings, current at a fixed probe bias voltage is sampled at 20 Hz (425-m along track.) The measured current is a function of electron density and temperature, as well as ion composition. It can not be unique converted into any one of these parameters. However these data may be used to identify periods when conditions are stable for 1-2 seconds, allowing CAPS/IBS measurements to be used without fear of time aliasing. In addition, the RPWS/LP data indicate times when the plasma conditions are highly variable (i.e. plume or jet structures on kilometer to sub-kilometer scales.) The nature of this variability can not be specified, but the location of these structures can be mapped relative to the jet sources.

References: [1] Tokar et al., 2009, Cassini detection of Enceladus' cold water-group plume ionosphere, Geophysical Research Letters, Vol. 36, L13203, doi:10.1029/2009GL038923 [2] Coates et al., 2010, Negative ions in the Enceladus plume, Icarus 206, 618-622 [3] Jones et al., Fine jet structure of electrically charged grains in Enceladus' plume Geophysical Research Letters, Vol. 36, L16204, doi:10.1029/2009GL038284 [4] Hill et al., 2012, Charged nanograins in the Enceladus plume, Journal of Geophysical Research, Vol. 117, A05209, 2012JGRA.11705209H [5] Crary et al., Ions in the Enceladus plume: Cassini/CAPS ion measurements at high energy resolution, SM32B-04, presented at the 2012 American Geophyiscal Union Fall meering.

ENCELADUS EXPLORER: NEXT STEPS IN THE DEVELOPMENT AND TESTING OF A STEERABLE SUBSURFACE ICE PROBE FOR AUTONOMOUS OPERATION.

B. Dachwald[1], J. Kowalski[2], F. Baader[1], C. Espe[1], M. Feldmann[1], G. Francke[1], E. Plescher[1],
[1]Faculty of Aerospace Engineering, FH Aachen University of Applied Sciences, Hohenstaufenallee 6, 52064 Aachen, Germany, dachwald@fh-aachen.de, [2]Aachen Institute for Advanced Study in Computational Engineering Science, RWTH Aachen University, Germany

Introduction: Direct access to subsurface liquid material for in-situ analysis at Enceladus' South Polar Terrain is very difficult and requires advanced access technology with a high level of cleanliness, robustness, and autonomy. A new technological approach has been developed as part of the collaborative research project / initiative "Enceladus Explorer" (EnEx) [1]. Within EnEx, the required technology for a potential Enceladus lander mission [2] is developed, evaluated, and tested, with a strong focus on a steerable subsurface ice probe. The EnEx probe shall autonomously navigate through the ice and find a location where a liquid water sample can be taken and analyzed in situ. EnEx is funded and managed by the DLR Space Administration and comprises several German universities.

The Enceladus Explorer Project (2012–2015): Several prototypes of a steerable subsurface ice probe, called IceMole, were developed and tested at FH Aachen since 2009. The IceMole design is based on the novel concept of combining melting and mechanical feed – using an ice screw at the tip of the melting head [3]. It can change melting direction by differential heating of the melting head and optional side-wall heaters. The first two prototypes were successfully tested between 2010 and 2012 on glaciers in Switzerland and Iceland. They demonstrated downward, horizontal and upward melting, as well as curve driving and dirt layer penetration. Within the EnEx project, a more advanced probe, called EnEx-IceMole (Fig. 1), was developed between 2012 and 2015. It provides concepts for obstacle avoidance, target detection, and navigation in ice. This probe was successfully tested on Canada Glacier (Fig. 2) and Taylor Glacier, Antarctica, in 2013 and 2014, respectively [1]. During the 2014 deployment, it was used in international collaboration with the US-American NSF-funded MIDGE (Minimally Invasive Direct Glacial Exploration) project for clean access into Blood Falls, a unique aquatic subsurface environment, with subsequent return of a clean subglacial brine sample to the surface. Since Blood Falls is categorized as an ASPA (Antarctic Specially Protected Area), we had to pay particular attention to clean protocols for the sampling of subglacial materials for biogeochemical analysis.

The Enceladus Explorer Initiative (2015+): After the successful Antarctic deployment of the EnEx-IceMole, EnEx was continued in the form of a more flexibly organized initiative with sub-projects focused on key research and development areas. The sub-project at FH Aachen is called EnEx-nExT (Environmental Experimental Testing). Since the EnEx-IceMole was quite large (15 x 15 x 200 cm) and heavy (60 kg), a much smaller (8 x 8 x 40 cm) and lightweight (< 5 kg) probe is currently developed within EnEx-nExT. In the next two years, this smaller probe will be tested in a vacuum chamber under simulated space conditions (pressure < 6 mbar, temperature < 100 K) to prove the applicability of combined drilling and melting probes under more Enceladus-like environmental conditions. More detailed information about these experiments will be given in a separate conference contribution. Within the sub-project EnEx-DiMIce (Directional Melting in Ice), the complex melting behavior of such probes is modeled and simulated at RWTH Aachen University. Information about these computational models will be given as part of a separate conference contribution.

Figure 1: EnEx-IceMole (with hull removed)

Figure 2: EnEx-IceMole deployment during Antarctic field test

Acknowledgements: The project is supported by the Federal Ministry of Economics and Technology, Germany, on the basis of a decision by the German Bundestag (FKZ: 50NA 1503)

References: [1] Kowalski J. et al. (2016), *Cold Reg. Sci. Technol., 123,* 53-70. [2] Konstantinidis K. et al. (2015), *Acta Astronaut., 106*, 63–89. [3] Dachwald B. et al. (2014), *Ann. Glaciol., 55(65)*, 14-22.

PHOEBE AND SATURN'S CAPTURED OUTER MOONS. T. Denk[1], S. Mottola[2], W.F. Bottke[3], and D.P. Hamilton[4], [1]Freie Universität Berlin, Germany (Tilmann.Denk@gmx.de), [2]DLR (German Aerospace Center), Berlin, Germany, [3]SwRI, Boulder, CO, [4]University of Maryland, College Park, MD.

Introduction: The giant planets of our solar system are known to host far more than 100 outer moons which orbit at distances of many million kilometers on eccentric and inclined paths. Similarly to Jupiter Trojans, Centaurs, or Kuiper belt objects, the "irregulars" constitute another distinct group of small objects residing in the outer solar system.

Around Saturn, 38 irregular satellites have been discovered so far (compared to 24 regular moons), 29 of which on retrograde orbits. Their sizes lie between 4 km and 40 km (with the exception of Phoebe: 213 km), the apparent magnitudes as seen from Earth are $\gtrsim 20$ mag (Phoebe: 16.4 mag). Their distances to Saturn range from $7.6 \cdot 10^6$ to $33 \cdot 10^6$ km, the orbit excentricities from 0.11 to 0.54, and the inclinations from 34° to 47° (prograde moons) and from 145° to almost 180° (retrograde moons; these ranges correspond to inclination supplemental angles i' between ~0° and 35°, with $i' = 90° - |90° - i|$). While orbital parameters and in parts sizes, albedos, and colors of these objects were measured from ground-based observations, most other fundamental physical parameters remained unknown.

Tab. 1: 24 rotational periods of irregular moons from Cassini ISS data, in hours. Left column: moons in orbits with $i' < 27°$; right: $i' > 27°$. *Italic*: prograde moons. Less reliable periods are marked with '*'.

Hati	5.42	*Siarnaq*	*10.188*
Mundilfari	6.74	Narvi	10.21
Loge	6.94*	*Tarvos*	*10.69*
Skoll	7.26	Skathi	11.45
Kari	7.70	Hyrrokkin	12.76
Suttungr	7.82*	*Ijiraq*	*13.03*
Bergelmir	8.13	*Albiorix*	*13.32*
Phoebe	9.27	Bestla	14.624
Ymir	11.922	*Bebhionn*	*16.4*
Greip	12.79*	*Paaliaq*	*18.75*
Thrymr	35 or >45*	*Kiviuq*	*22*
		Erriapus	*28.0*
		Tarqeq	*60-90**

Cassini imaging observation campaign: Particularly during the second half of the Cassini mission at Saturn, a campaign to study the outer moons was performed with the goal of investigating basic physical properties through disk-integrated photometric lightcurves with the ISS camera [1]. Doing such a research from a spacecraft offers *numerous* advantages like a large phase angle range, long continuous observation times, almost no straylight and weather issues, and many more. As of summer 2016, 25 outer Saturnian moons have been investigated with the ISS.

Rotational periods: *Tab. 1* shows results for 24 moons. For 19 satellites, rotation periods were measured to an accuracy better than 1%. For 5 objects, the results are less reliable and require improvement. The shortest period (5.4 h) is not even close to the spin barrier observed for asteroids (2.3 h). Minimum ratios of the equatorial axes $(a/b)_{min}$ of the bodies have also been determined. For at least 5 objects, $(a/b)_{min} > 1.4$.

Patterns: Two general trends from lower to higher phase angles are observed: an increase in the number of lightcurve extrema, and an increase in the lightcurve amplitudes. While the amount of "2max/2min" lightcurves is ~85% for low-phase ($\lesssim 45°$) observations, the number of "3max/3min" lightcurves increases to ~50% for mid-phase (~45° to ~90°) and even to ~2/3 for high phase angle ($\gtrsim 90°$) observations. Also, most low-phase observations show amplitudes $\lesssim 0.5$ mag, while most lightcurves taken at mid- and high phase exhibit amplitudes $\gtrsim 0.5$ mag.

An unexpected correlation between orbit inclination supplemental angles and rotational periods was found. All 13 known objects with $i' \gtrsim 27°$ have rotational periods > 10 h, while most measured moons with a lower i' have shorter periods < 8.2 h (see *Tab. 1*).

Pole directions and shapes: Pole directions and convex shape models were calculated for three objects so far. Two of them show 3max/3min lightcurves even at low phase, and their shapes show triangular equatorial sections. Some objects have been found to be very elongated, which suggests a contact binary nature.

Phoebe: The by far largest outer moon of Saturn has been observed from Earth, Voyager 2, and Cassini. During the targeted flyby on 11 June 2004, Cassini came as close as 2070 km to Phoebe, and images with a resolution down to 13 m/pxl were obtained [2]. Several physical and photometric parameters, surface composition, and the crater-size distribution could be determined. Albedo, topographic, and cartographic maps were also compiled from these data.

Phoebe dust ring: A very faint dust ring, discovered in 2009, extends from ~$6 \cdot 10^6$ to ~$16 \cdot 10^6$ km from Saturn [3]. It is very likely produced by Phoebe and other retrograde irregular moons, and plays an important role in shaping the global asymmetry of the thermally driven albedo dichotomy on Iapetus [4].

Origin: The origin of the irregular satellites is still debated. In the Nice model, comet capture via three body interactions, followed by intense collisional evolution among the irregulars, is a viable option [5].

References: [1] Denk T. (2013) Participating Scientist prop., NASA Prop. No. 13-CDAPS13_2-0049. [2] Porco, C.C. *et al.* (2005) *Science* **307**, 1237-1242. [3] Hamilton, D.P. *et al.* (2015) *Nature* **522**, 185-187. [4] Spencer, J., Denk, T. (2010) *Science* **327**, 432-435. [5] Bottke, W.F. *et al.* (2010) *AJ* **139**, 994-1014.

IMAGING OBSERVATION PLANNING FOR DIONE, RHEA, IAPETUS, AND PHOEBE IN THE CASSINI PRIMARY MISSION. T. Denk[1], Th. Roatsch[2], and K.-D. Matz[2], [1]Freie Universität Berlin, Germany (Tilmann.Denk@gmx.de), [2]DLR (German Aerospace Center), Berlin, Germany.

Introduction: Adviced by the ISS team in 2000, team members Steve Squyres, Peter Thomas (Cornell Univ.), and Gerhard Neukum (DLR Berlin) agreed to split the upcoming planning task for Cassini Imaging (ISS) observations of the mid-sized icy moons between the two groups. (Excluded were observations for orbit dynamic purposes and optical navigation.) Since this time, Mimas, Enceladus, Tethys, and Hyperion became "Cornell moons", while Dione, Rhea, Iapetus, and Phoebe are the "DLR moons" for ISS. This discrimination is not considered strict, and mutual support between the two groups worked extremely well throughout the mission. The Cornell group is also responsible for ISS observation planning of the small inner moons, and the DLR/FU Berlin groups later took over the ISS observations of the irregular moons.

Prime mission concept: For the icy mid-sized moons (and to a lesser degree for distant Iapetus), the observations were subdivided into the following six categories: (A) Targeted flyby observations; (B) Regional mapping, geodesy, regional color; (C) Limb topography; (D) global multi-color; (E) Spectrophotometry; (F) miscellaneous (like pre-SOI, photo opps, zero phase, or eclipse imaging).

The targeted flybys (there was one for each "DLR moon" in the prime mission) were treated most important. As a general scheme, the agreement was to stay $\geq$ 2 min at each location ("footprint") to allow VIMS to take data at the same field-of-view as the ISS Narrow Angle Camera (ISS-NAC). In the meantime, ISS took 3 or 4 color images (Uv3, green (Grn), infrared-1 (Ir1) and/or Ir3) in 2x2 binning (summation) mode, followed by a full-resolution image in the clear filter.

REGMAP: Second most important was regional mapping which followed the same scheme.

REGGEOD: The purpose of these is stereo imaging; they can be combined with regional mapping or other "geodesy" observations.

Limb topography: Except for Iapetus LIMBTOPOs, these observations were usually not planned separately because all global and many regional images contain the limb and are thus useful here.

For global multi-color observations (GLOCOLs) which were taken at spatial resolutions so that the full disk of the moon roughly fills the field-of-view of the NAC, a consistent filter scheme was developed. Uv3, Grn, Ir1, and Ir3 ("N04" filter sets) were used jointly with the Bl1 (blue), Red, Ir2, and Ir4 broadband filters (N08) plus the 3x3 polarizer filters (P0,P60,P120) x (Grn,Uv3,Mt2) (NP09 filter set). Mt2 (methane-2) is the filter with the longest wavelength useable with the three polarizer filters. As a maximum, up to 24 different color filters (N24) plus NP09 were used with the NAC for satellite multi-color imaging.

The spectrophotometry task had four variables to deal with: sub-spacecraft (sub-S/C) location, distance to the moon, phase angle, and position of the illuminated side (left, right, top, bottom). Since control of all four was not practical, we chose to observe five of the mid-sized moons (Mimas to Rhea) mainly during equatorial orbits at sub-S/C longitudes of 22°W, 94°W, 166°W, 238°W, and 310°W, while the lit side was pointing towards bottom right (north up). The phase angles of the available data range from almost zero to 168°. The request naming scheme contains the sub-S/C longitude and the phase angle. For example, a Dione observation at 310°W and 64° phase angle in orbit 15 is named 015DI_310W064PH.

Tools: Critical tools used for planning are pdt ("pointing design tool", from JPL), ISSPT ("ISS planning tool", from the Imaging team), and ckView ("cKernel Viewer", from DLR). Pdt computes the command files required to control the S/C's attitude for general poining and detailed mosaics. With ISSPT, the camera command files ("IOIs") are built. CkView is extremely valuable and capable to visualize the pointings created with pdt. It is also used for many other missions like Dawn, Rosetta, or JUICE.

Phoebe 000PH: The sole targeted flyby of an outer satellite took place at 11 June 2004 at a minimum altitude of 2070 km over the lit side. Approach took place at 87° phase, departure around 93°. Complete rotations of Phoebe (9.3 h) were observed twice inbound and once outbound.

Iapetus 049IA: The sole targeted Iapetus flyby took place at 10 September 2007 at a closest-approach distance of 1615 km. The inbound trajectory allowed high phase observations and included a "Saturn system view from Iapetus", a stellar occultation and a cool ride over the giant equatorial ridge. Outbound imaging at low phase showed the bright trailing hemisphere at great detail. About 15 min after downlink start, a cosmic-ray hit triggered a switch and forced the S/C to go into safe mode. The S/C was recovered within a few hours, and the data downlink and a large orbit-trim maneuver were executed properly. However, all lower resolution outbound data was lost. More details and a brief history of the Iapetus flyby are described in [1].

References: [1] Denk, T. (2008), *Planetary Report* **28**, no.1, 10-16.

SATURNIAN MOON IAPETUS – GLOBAL ALBEDO ENIGMA AND CASSINI ISS OBSERVATIONS.
T. Denk[1], J.R. Spencer[2], Th. Roatsch[3], N. Schmedemann[1], and G.G. Galuba[1], [1]Freie Universität Berlin, Germany (Tilmann.Denk@gmx.de), [2]SwRI, Boulder, CO, [3]DLR (German Aerospace Center), Berlin, Germany.

Introduction: Iapetus, the outermost body of Saturn's regular moon system ($a = 3.56 \cdot 10^6$ km; P = 1904 h) and the third largest of all moons of Saturn (Ø = 1425 km x 1495 km) is most famous for its unique *global albedo dichotomy*. It was discovered by J.-D. Cassini almost 340 years ago [1] as the first ever recognised surface structure on a solid body ouside the Earth-moon system. Cassini did not try to explain the reason for this dichotomy, and it remained a mystery until the Cassini spacecraft observed Iapetus.

Voyager: Before Cassini's arrival at Saturn, Iapetus has been observed from the ground and by the Voyager spacecraft. Low resolution images (9 km/pxl or less) allowed a global characterization of the albedo dichotomy including the findings that the dark terrain faces precisely towards the apex of motion and that the polar regions are bright. The bright hemisphere was found to be heavily cratered and thus understood to be old [2]. A reinvestigation of Voyager images in the 1990s revealed an oblate spheroid shape, large basins, a similar crater size-frequency in parts of the dark terrain as in the adjacent bright area, and giant mountains near the equator on the anti-Saturn hemisphere [3].

Cassini imaging: Cassini imaging of Iapetus during one targeted (on 10 Sep 2007) and several more distant flybys mainly in the first years of the mission revealed an alien and often unique landscape [4,5]. The data show numerous impact craters on the bright and dark terrain, very complex and sharp boundaries between the dark and bright material with no "gray shading", equator-facing dark and pole-facing bright crater walls, additional huge impact basins, small bright-ejecta or bright-rim craters within the dark terrain, only minor endogenic geologic features, and a giant ridge which spans across half of Iapetus' circumference exactly along the equator with mountains up to ~15 km tall. A *global color dichotomy* was discovered besides the albedo dichotomy; it is presumably formed by dust from retrograde irregular moons [5]. Major parts of the surface have been mapped at a scale of 1:3,000,000 [6]. Neither precisely at the center of the trailing side (at 425 m/pxl resolution) nor elsewhere, a black crystalline monolith with dimensions 1:4:9 was found.

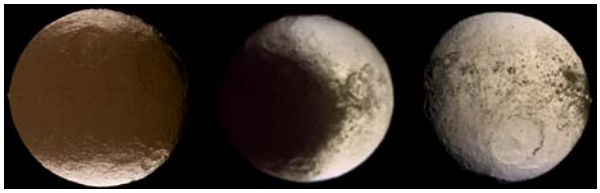

The extreme global albedo dichotomy, where the trailing side and poles were found to be more than 10x brighter than the leading side, has been characterized in great detail. For example, the small bright-ray craters [5] as well as Cassini RADAR data [7] suggest a very thin dark blanket in the order of decimeters on an otherwise bright, icy surface.

Albedo dichotomy enigma: Various attempts to explain the global albedo dichotomy have been published since the mid-1970s. Especially the deposition of exogenic dark material on the leading side, originating from outer retrograde moon Phoebe, was a leading hypothesis, but it could not explain the global shape, sharpness, and complexity of the transition between Iapetus' bright and dark terrain. Mainly with Cassini spectrometer (CIRS) and imaging (ISS) data, all these characteristics and the asymmetry's large amplitude are now plausibly explained by runaway global thermal migration of water ice, triggered by the deposition of dark material on the leading hemisphere [8]. This mechanism is unique to Iapetus among the Saturnian satellites for many reasons: (1) Size (mass) of Iapetus and (2) distance to the sun (=> right temperature; sublimed water molecules can migrate globally, but do not escape at substantial rates); (3) slow and synchronous rotation (=> temperature issue again, and there is a leading and a trailing side); (4) Iapetus orbits outside of the magnetosphere (=> very fine-grained dust from outside is not disturbed); (5) Iapetus is the outermost of the regular moons (=> it is the first obstacle for dust from outside); (6) the impact gardening rate on the surface is "about right" (=> preventing the whole surface from getting dark); (7) Hyperion and Titan, the moons next to Iapetus, either do not rotate synchronously or have a thick atmosphere (=> can not form a comparable surface dichotomy); (8) Saturn has retrograde outer moons (which deliver refractory dusty material). The combination of these circumstances makes the albedo dichotomy a unique feature on Iapetus in the solar system.

References: [1] Cassini, J.D. (1677) *Philos. Trans.* **12**, 831-833. [2] Morrison, D. *et al.* (1986) in *Satellites*, Univ. Ariz. press, 764-801. [3] Denk, T. *et al.* (2000) *LPSC XXXI*, abstract #1596. [4] Porco, C.C. *et al.* (2005) *Science* **307**, 1237-1242. [5] Denk, T. *et al.* (2010) *Science* **327**, 435-439. [6] Roatsch, Th. *et al.* (2009) *Plan.Spa.Sci.* **57**, 83-92. [7] Ostro, S. *et al.* (2006) *Icarus* **183**, 479-490. [8] Spencer, J.R., Denk, T. (2010) *Science* **327**, 432-435.

Negative Pickup Ions at Icy Moons: Rhea and Europa R. T. Desai[1,2], A. J. Coates[1,2], . . , . . Jones , S. P. Gary[3,4], H. Wei[5], L. Regoli[1,2,6] and M. Volwerk[7], [1]Mullard Space Science Laboratory, University College London, UK ravindra.desai.14@ucl.ac.uk, [2]Centre for Planetary Sciences at UCL/Birkbeck, London, UK, [3]Los Alamos National Laboratory, Los Alamos, New Mexico, USA, [4]Space Science Institute, Boulder, Colorado, USA, [5]Institute of Geophysics and Planetary Physics, University of California Los Angeles, USA, [6]Max Planck Institute for Solar System Research, Göttingen, Germany, [7]Space Research Institute, Austrian Academy of Sciences, Graz, Austria

Introduction:

The negatively charged ions observed outflowing from the Saturnian satellite Rhea and inferred at the Jovian satellite Europa were unexpected and intriguing in their differences. In this study we analyse these negatively charged pickup ions to better understand what they are telling us about their source environments.

Rhea is Saturn's largest icy moon with a radius of *~764km* and orbits within Saturn's inner magnetosphere at just under $9R_S$. An ethereal oxygen and carbon-dioxide atmosphere was discovered around the moon when Cassini plasma instruments observed positive and negative ions outflowing from the moon and also an extended neutral exosphere [1]. A subsequent more distant encounter however only observed positively charged pickup ions, thus indicating high loss rates of negative ions in Saturn's magnetosphere. Here we examine the roles played by positively and negatively charged pickup ions at this icy world. Using an updated model of Cassini's Electron Spectrometer response function, we are for the first time able to calculate the outward flux of negatively charged pickup ions and, using test particle simulations, trace these particles back to Rhea's exobase to better understand their production and loss mechanisms.

Europa is the smallest of the Galilean satellites with a radius of *~1561km* and orbits at $\sim 9.4R_J$. During several encounters Galileo observed strong Ion Cyclotron Wave activity indicating the pickup of a range of species including O_2, SO_2, *Na, K,* and *Cl [2]*. At the Chlorine gyrofrequency waves were observed at both left and right hand polarisations indicating the pickup of both positively and negatively charged Chlorine ions. We present the results of a self-consistent hybrid simulation study of both positively and negatively charged ions generating Ion Cyclotron Waves in the Europan plasma environment. Using simulated scaling of wave energy we are able to place upper limits on the positive and negative Chlorine pickup ions observed outflowing from the moon.

We also refer to further negative ion detections in planetary environments including the negatively charged ions and aerosols observed in Titan's ionosphere [3], the negatively charged water group ions and ice grains observed in the plumes of Enceladus [5,6], as well as those at Comets Halley and 67P/Churyumov-Gerasimenko [7,8].

References:

[1] Teolis, B. D., Jones, G. H., Miles, P. F., et al. (2010), Science, 330, 1813. [2] Volwerk, M., Kivelson, M. G., & Khurana, K. K. (2001), Journ. Geophys. Res., 106, 26033. [3] Coates, A. J., Crary, F. J., Lewis, G. R., et al. (2007), Geophys. Res. Lett., , 34, L22103. [4] Coates, A. J., Jones, G. H., Lewis, G. R., et al. (2010), Icarus, 206, 618. [5] Jones, G. H., Arridge, C. S., Coates, A. J., et al. (2009), Geophys. Res. Lett., 36, L16204. [6] Chaizy, P., Reme, H., Sauvaud, J. A., et al. (1991), Nature, 349, 393. [7] Burch, J. L., Cravens, T. E., Llera, K., et al. (2015), Geophys. Res. Lett., 42, 5125.

VARIATIONS IN THE SPECTRAL PROPERTIES OF ENCELADUS' PLUME IN SPACE AND TIME

Deepak Dhingra and Matthew M. Hedman, Department of Physics, University of Idaho, 875 Perimeter Dr. MS 0903, Moscow ID 83844. Email: deepdpes@gmail.com; mhedman@uidaho.edu.

Introduction: The Cassini spacecraft has obtained an immense amount of information about Encealdus' geological activity, and there is still much to be learned from detailed studies of the various Cassini data sets. In particular, the Visible and Infrared Mapping Spectrometer (VIMS) [1] has obtained hundreds of plume spectra covering the wavelength range between 0.35 and 5 microns. These spectra can provide important constraints on the physical and compositional properties of the plume's particles. This information in turn can provide important insights into the geological processes taking place beneath Enceladus' surface.

Near-Infrared Character of Plume Water-ice Particles: The plume spectra have all been obtained at high phase angles (> 140°), and so the observed signal is mostly from the light diffracted around the tiny ice grains in the plume. In this situation, absorption bands are suppressed. Indeed, the only obvious feature in the plume spectra is the fundamental water-ice absorption band around 3 microns. Outside of this band, the spectral slopes provide constraints on the shape of the particle size distribution between 1 and 5 microns, and the overall brightness provides information about the total particle mass flux. The VIMS spectra have already been used to estimate the distribution of particle launch velocities and to document variations in the plume activity with orbital phase [2,3].

Diversity of the 3-micron Band and New Insights: Examination of the 3-micron ice band [4, 5, 6] suggests that the plume particles consist predominantly of crystalline ice (constrained by the band minimum position being longwards of 2.85 microns). The shape of the 3-micron band also exhibits quite a bit of diversity. The band shape variations have been noted *within a single observation* at different altitudes as well as across eruptions along the individual tiger stripe fractures. The latter could reflect differences in the sub-surface environments connected to these fissures.

The band shape variations have also been observed *across different observations* collected at different times (temporal variations) suggesting that the environment of eruption is likely modulated as Enceladus goes around Saturn, leading to differences in the spectral character of the plume particles. The large brightness variations in the plume with respect to the orbital phase have already been documented [3,7] and so changes in the plume particle properties are not unreasonable. Some of the observed variations could potentially be due to non-icy material in the plume, such as water vapor and solid contaminants.

The near infrared spectra of the plume particles, as inferred from the VIMS observations, therefore hold a wealth of information about the workings of the Enceladus' plume.

References: [1] Brown, R. H., et al. (2004) *Space Sci. Rev.*, **115**, 111 [2] Hedman, M.M. et al. (2009) *ApJ*, **693**, 1749-1762. [3] Hedman, M.M. et al. (2013) *Nature*, **500**, 182-184. [4] Dhingra D. et al. (2015) *46th LPSC*, Abst# 1648 [5] Dhingra D. et al., (2015) *DPS Meeting*, Abstract# 411.01 [6] Dhingra D. et al., (2016) *47th LPSC*, Abstract# 2638 [7] Nimmo, F. et al., (2014), *AJ*, **148**, 46

.

FREEZING OF METHANOL-WATER MIXTURES AT HIGH PRESSURE IN A SUBSURFACE OCEAN

A. Dougherty, R. Chumsky, and D. Morris, Department of Physics, Lafayette College, Easton, PA 18042 USA. doughera@lafayette.edu

Introduction: Enceladus is a surprisingly active world. The observations of water-rich plumes [1, 2, 3, 4, 5] reveal either the presence of a liquid reservoir or highly active melting. The composition of the plumes suggests a liquid reservoir [5, 6], and the measured libration is consistent with a global subsurface ocean, rather than a localized reservoir [7].

Any subsurface ocean would likely contain impurities, such as ammonia[8] and methanol, that act as powerful antifreeze compounds. Small amounts of methanol may have been detected on the surface of Enceladus [9], as well as in the plume [3]. In addition to being a powerful antifreeze, methanol could also play a role in the formation of methane hydrates [10].

Experiment: In this work, we consider the freezing behavior of methanol-water solutions at low temperatures and moderate pressures such as might be encountered in the icy moons of the outer solar system. We report measurements of the liquidus and eutectic points for 30 wt.% and 80 wt.% methanol-water solution at pressures ranging from 5 to 400 MPa, using simultaneous measurements of pressure, volume, and temperature, coupled with optical images of the sample.

The phase diagram for methanol-water solutions at atmospheric pressure is shown in Fig. 1.

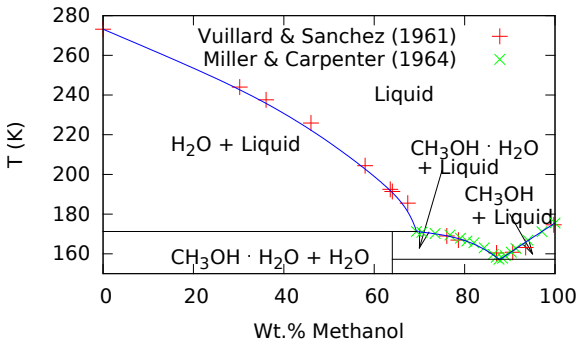

Figure 1: Atmospheric pressure phase diagram for methanol-water solutions, adapted from Kargel [11]. Data are from Vuillard & Sanchez [12] and Miller & Carpenter [13].

Approximately 1 mL of sample was loaded into a pressure cell made from a stainless steel block with four ports. Two opposing ports contain plugs that have sapphire windows for the imaging system. The third port contains a plug with a silicon diode thermometer, and the fourth connects the cell to the pressure system. A fiber optic light illuminates the sample, and an inverted periscope is used to obtain images. The pressure system includes a transducer that responds approximately linearly to changes in volume of the sample. The pressure cell is insulated, and temperature can be controlled between 200 and 300 K. Cooling below 200 K is done with liquid nitrogen.

For these investigations, we studied two samples, one with a concentration of 30 wt.% methanol in water, and a second with a concentration of 80 wt.%. The higher concentration was chosen to avoid experimental complications due to the expansion of Ice-Ih as it freezes.

Results: The transition temperatures are shown in Fig. 2. The phase boundaries for pure water [14] and methanol [15] are included for comparison. The eutectic point for the methanol-water solution appears to increase with pressure, similar to the behavior of the freezing point of pure methanol. Conversely, the liquidus point appears to decrease with pressure in the Ice-Ih regime, similar to the behavior of pure water.

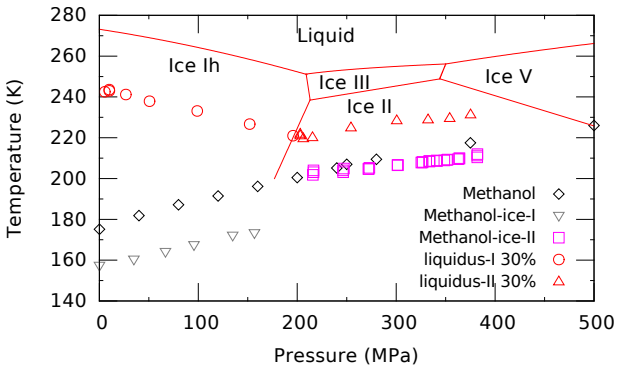

Figure 2: Transition temperatures as a function of pressure for methanol-water mixtures. The freezing temperatures for pure methanol are shown as diamonds. The eutectic temperatures are shown as inverted triangles and boxes in the Ice-Ih and Ice-II regimes, while the liquidus temperatures for 30 wt.% solutions are shown as circles and triangles.

References: [1] M. Dougherty, et al. (2006) *Science* 311 (5766):1406. [2] C. Porco, et al. (2006) *Science* 311 (5766):1393. [3] J. H. Waite, Jr., et al. (2009) *Nature* 460 (7259):1164. [4] C. J. Hansen, et al. (2011) *Geophys Res Lett* 38:L11202. [5] H.-W. Hsu, et al. (2015) *Nature* 519 (7542):207. [6] F. Postberg, et al. (2011) *Nature* 474 (7353):620. [7] P. C. Thomas, et al. (2016) *Icarus* 264:37. [8] D. Hogenboom, et al. (1997) *Icarus* 128 (1):171. [9] R. Hodyss, et al. (2009) *Geophys Res Lett* 36:L17103. [10] G. McLaurin, et al. (2014) *Angewandte Chemie-International Edition* 53 (39):10429. [11] J. S. Kargel (1992) *Icarus* 100:556. [12] G. Vuillard, et al. (1961) *Bull Soc Chim France* 1877–1880. [13] G. A. Miller, et al. (1964) *J Chem & Eng Data* 9 (3):371. [14] W. Wagner, et al. (2011) *J Phys and Chem Ref Data* 40 (4). [15] A. Wurflinger, et al. (1977) *J Phys Chem Solids* 38:811.

THE HISTORY OF THE ENCELADUS DISCOVERY. M. K. Dougherty[1], B. J. Buratti[2], P. K. Seidelmann[3] and J. R. Spencer[4], [1]Imperial College London, SW7 2AZ, UK, m.dougherty@imperial.ac.uk, [2]Jet Propulsion Laboratory, Pasadena, CA, 91109, bonnie.j.buratti@jpl.nasa.gov, [3]University of Virginia, Charlottesville, VA, 22911, pks6n@virginia.edu, [4]Southwest Research Institute, Boulder,CO, 80302, spencer@boulder.swri.edu

Introduction: Enceladus, the sixth largest moon of Saturn, was first discovered by William Herschel in 1789 [1]. Our understanding of the moon improved little after this initial discovery until the Voyager spacecraft flybys in the early 1980's. During the Voyager 2 flyby in August 1981, the first detailed observations of the surface were made revealing relatively few craters, numerous smooth areas as well as some extensive linear cracks. The smooth, very reflective surface of Enceladus which is dominated by water ice pointed to some type of resurfacing taking place [2]. At about the same time, the extensive diffuse E ring, discovered in 1966 [3] which extends between the orbits of Mimas and Titan, was found in groundbased observations during the 1980 ring plane crossing to peak in density near the orbit of Enceladus [4]. These discoveries, coupled with the expected short lifetime of E-ring particles [5] led to the suspicion that Enceladus might be the source of this E ring, perhaps even as a result of geyser-like activity [6].

In early 2005, the Cassini spacecraft made 2 distant flybys of Enceladus (a month apart), at 1265km and 500km from the surface. Observations from the magnetometer instrument showed draping of the Saturn magnetic field lines upstream of Enceladus, as well as an increase in ion cyclotron wave activity in the vicinity of the moon, driven by water group ions [7]. Based on these observations the magnetometer team made the case to the Cassini Project that there was potentially an atmosphere at Enceladus made up of water group ions which was holding off the Saturn field lines from the Enceladus surface and requested the third flyby, due to take place four months later, be lowered to fly much closer to the Enceladus surface to investigate this possibility. This was agreed and the third Cassini Enceladus flybys took place in July 2005 at a flyby altitude of 173km. On this flyby multiple Cassini instruments obtained definitive evidence for active ejection of water vapor and ice particles from Enceladus' south pole. A series of geologically youthful fractures, dubbed tiger stripes, centered on Enceladus' south pole [8] were found to be sources of endogenic thermal emission [9]. Magnetic field [7] and mass spectroscopy [10] confirmed that a water vapour plume was emanating from cracks (tiger stripes) close to the south pole of the moon, where internal heat was also leaking out from the interior. Cassini's dust detector found an associated cloud of ice particles [11]. This discovery led to a focus on Enceladus in the Cassini extended missions, confirmation of a liquid water ocean beneath its surface, organic material and dust within the plume, modulation of plume activity by Saturn's tides, as well as confirmation that Enceladus is the source of the E ring at Saturn.

References: [1] Herschel, W. (1790). *Philosophical Transactions of the Royal Society of London, 80*, 1–20. [2] Verbiscer, A.; French, R.; Showalter, M.; Helfenstein, P. (2007), *Science, 315*, 5813. [3] Feibelman, W. A. (1967), *Nature, 214*, 793-794. [4] W.A.Baum et al. (1981) *Icarus,47*, 84-96. [5] Jurac, S., McGrath, M. A., et al. (2002), *Geophys. Res. Lett., 29*, 215-1, [6] Haft, P. K., Siscoe, G. L., Eviatar, A. (1983), *Icarus, 56*, 426-438. [7] Dougherty, M. K.; Khurana, K. K.; et al. (2006), *Science, 311*, 1406–9. [8] Porco, C. C.; Helfenstein, P.; et al. (2006), *Science, 311*, 1393–1401. [9] Spencer, J. R.; Pearl, J. C et al. (2006), *Science, 311*, 1401–5. [10] Waite, J. H. et al. (2006), *Science, 311*, 1416-1418. [11] Spahn, F. et al. (2006), *Science, 311*, 1416-1418.

Development of an Extraterrestrial Organic Analyzer (EOA) for Highly Sensitive Organic Detection on a Kinetic Penetrator. Z. Duca[1], G. Tan[1], T. Cantrell[1], M. Van Enige[1], M. Dorn[1], M. Cato[1], P. Putman[2], J. Kim[3], R. A. Mathies[4], and A. Stockton[1†*]. [1]Georgia Institute of Technology, GA, USA, [2]Sierra Lobo, OH, USA, [3]Texas Tech University, TX, USA, [4]University of California, Berkeley, CA, USA ([*]zduca4@gatech.edu, [†]astockto@gatech.edu).

Introduction: Quantitative, compositional, and chiral analysis of small organic molecules *in situ* provides important information for studying planetary formation and evolution, and, more excitingly, also can provide signatures of past or present life. EOA, with microchip capillary electrophoresis (µCE) and laser-induced fluorescence (LIF) detection, is the only technique currently ready for space flight that has the resolution, selectivity, and sensitivity to provide these analyses. Through both in-lab [1,2] and field [3] testing, µCE-LIF has demonstrated the capability to provide highly sensitive (sub parts-per-trillion, or pptr) automated quantitative compositional chiral analysis of multiple organic compound classes [4], including polycyclic aromatic hydrocarbons (PAHs) [5], amino acids [6], aldehydes and ketones [7], carboxylic acids [8], thiols [9], and amines [10]. Lander or fly-by missions have largely been the focus for the development of µCE-LIF, as proposed in the Mars Organic Analyzer (MOA) and the Enceladus Organic Analyzer.

Here, we show the continued development of the microfluidic and LIF subsystems for a kinetic impactor mission. Preliminary results have shown promising sustainability of microdevices during a 50000g impact, indicating that µCE-LIF is a valid *in situ* technique for this extreme planetary mission format.

Instrument Development: Programmable microfluidic architechtures enable automated, complex microfluidic manipulation on-chip, including mixing, dilutions, fluorescent derivatization, and transfer [11]. Recently, we have shown that microdevices retain functionality of their pneumatically-actuated monolithic membrane microvalves after 10+ years in storage [12].

However, the survival of these microvalves during a high g impact is not proven. The pneumatic microvalves use a compressible fluid for actuation, which could be succeptible to bursting at sudden high pressures induced upon impact. Hydraulically-actuated microvalves that use incompressibile fluids to control valve acuation may not experience these issues. Early tests show that these hydraulic valves function properly and can replace the pneumatic valves for high impact or high pressure (e.g. deep ocean) missions.

The precision optics of LIF can be succeptable to high impact collisions and has never been developed for these high g conditions. Proper permanent alignment of components is essential for absolute sensitivity, and optical stack placement and material bonding properties must be optimized. Recent modeling data has shown that in order to reduce internal mechanical stress ideal placement of the optical components is directly in the center of the microdevice (Figure 1). By placing proper support underneath the structure, the mechanical strength of the microdevice is not exceeded. Indium bump bonding will be used in the optical stack to permenantly and precisely weld non-glass/glass connections. Glass/glass conections will be made using a Schott Glass bonding technique to create a continuous glass construction, avoiding any possible optical interferences.

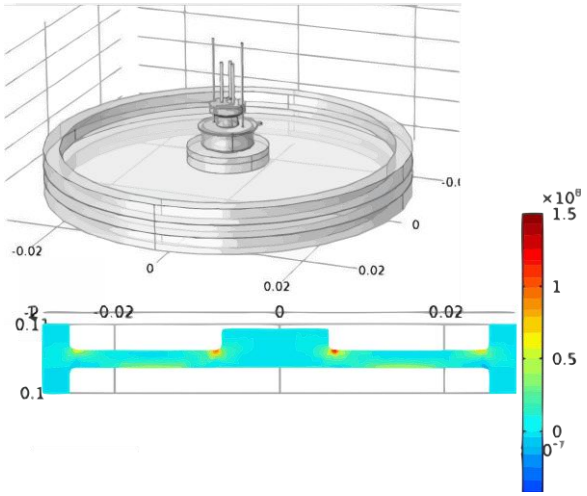

Figure 1: Structural (top) and stress (bottom) model of a centered optical stack without support structures.

Summary and Conclusions: This work shows the low-TRL development of EOA's LIF and microfluidic subsystems for future planetary impact penetrator missions. With correct structural decisions and optimizations, EOA can survive a 50,000g impact, making it the only current optical instrument with this capability.

References:

[1] Skelley, A. et al. (2005) *PNAS U.S.A., 102,* 1041 - 1046. [2] Benhabib, M. et al. (2010) *Anal. Chem., 82,* 2372-2379. [3] Skelley, A. et al. (2007) *JGR., 111,* G04S11. [4] Kim, J. et al. (2013) *Anal. Chem., 85,* 7682-7688. [5] Stockton, A. et al. (2009) *Anal. Chem., 81,* 790-7906. [6] Chiesl, T. et al. (2009) *Anal. Chem., 81,* 2537-2544. [7] Stockton, A. et al. (2010) *Electrophoresis, 31,* 3642-3649. [8] Stockton, A. et al. (2011) *Astrobiology, 11,* 519-528 [9] Mora, M. et al. (2013) *Electrophoresis, 34,* 309-216. [10] Cable, M. et al. (2013) *Anal. Chem., 85,* 1124-1131. [11] Kim, J. et al. (2016) *Lab Chip. 16,* 812-819. [12] Duca, Z. et al. (2015) EPSC, Abstract #416.

KINETIC PROCESSES IN THE ENCELADUS VENTS. A. R. Dzhanoev[1], J. Schmidt[2] and F. Spahn[1], [1]University of Potsdam, Karl-Liebknecht-Str. 24/25, Building 28, 14476 Potsdam-Golm, Germany (janoev@yahoo.com), [2]University of Oulu, Finland.

Abstract: We study the possibility of dust aggregation and fragmentation processes when icy grains are transported to space by water vapor streams in the subsurface vents of Saturn's active moon Enceladus [1]. Depending on their shape the dust aggregates, or non-spherical dust grains, can establish higher equilibrium charges than a spherical grain of the same mass when exposed to equivalent charging conditions. This indicates that dust charging models with spherical grains lead to a net charge underestimation. This effect in combination with small particle effect [2], [3] might be important if one likes to verify if dust charging can account for the misfit between ion and electron densities inferred from data taken by the Cassini-Langmuir probe in the E ring and in the Enceladus plume [5]. Furthermore, an increased charge-to-mass ratio, and a reduced bulk density for dust in Saturn's inner magnetosphere will affect the dynamics of these grains in the E ring region. This will modify the size-dependent lifetimes of particles, which ultimately determine the steady state size- distribution of E ring grains.

References:

[1] Schmidt. J. et al. (2008) *Nature,* 451, 685.

[2] Dzhanoev A. R., Schmidt J. et al. (2016) *A&A, acceped* (arXiv:1603.08565).

[3] Dzhanoev A. R., Spahn F. et al. (2015) *PRB,* 92, 125430 (arXiv:1605.00637).

[4] Dzhanoev A. R., et al. (2014) *EPSC Abstracts*, 9, #755.

[5] Shafiq M., J. et al. (2011) *Planetary & Space Sci.*, 59, 17.

A fly-through mission strategy targeting peptide as a signature of chemical evolution and possible life in Enceladus plumes

Kosuke Fujishima[1], Szymon Dziomba[2], Wataru Takahagi[3,4], Takazo Shibuya[4], Yoshinori Takano[4] Mohamed Guerrouache[2], Benjamin Carbonnier[2], Ken Takai[4], Lynn Rothschild[5] and Hajime Yano[6]

[1] Earth-Life Science Institute, Tokyo Institiute of Technology, Tokyo 152-8550 Japan
[2] University Paris-East, UPEC, ICMPE UMR7182, Thiais 94320, France
[3] Graduate School of Media and Governance, Keio University, Fujisawa-shi 252-0882 Japan
[4] Japan Agency for Marine-Earth Science and Technology (JAMSTEC), Yokosuka 237-0061, Japan
[5] NASA Ames Research Center, Moffett Field, CA 94035, USA
[6] Institute of Space and Astronautical Science (ISAS), Japan Aerospace Exploration Agency (JAXA), Sagamihara 252-5210 Japan

Abstract: *In situ* detection of organic molecules in the extraterrestrial environment provides a key step towards better understanding the variety and the distribution of building blocks of life and it may ultimately lead to finding extraterrestrial life within the Solar System. Here we present combined results of two separate experiments that enable us to realize such *in situ* life signature detection from the deep habitats of the "Ocean World": a hydrothermal reactor experiment simulating complex organic synthesis and a simulated fly-through capture experiment of organic-bearing microparticles using silica aerogels, followed by subsequent analysis. Both experiments employ peptide as a plausible organics existing in Encleadus plume particles produced in its subsurface ocean.

Recent laboratory hydrothermal experiments and a theoretical model on silica saturation indicated an ongoing hydrothermal reactions in subsurface Enceladus ocean [1]. Given the porous chondritic origin of the core, it is likely that organic compounds originated by radiation chemistry such as amino acid precursorscould have been provided, leached, and altered through widespread water–rock interactions. By using the same laboratory experimental setup from the latest water-rock interaction study [2], we performed amino acid polymerization experiments for 144 days and monitored the organic complexity changing over time. So far over 3,000 peaks up to the size of > 600 MW were observed through the analysis of capillary electrophoresis time-of-flight mass spectrometry (CE-TOF-MS) with an indication of amino acid derivatives and short peptides.

Generally abiotic polymerization of enantiomeric amino acids results in forming stereoisomeric peptides with identical molecular weight and formula [3] as opposed to homochiral biopolymers. Assuming Enceladus plume partciles may contain a mixture of stereoisomeric peptides, we were able to distinguish 16 of the 17 stereoisomeric tripeptides as a test sample using capillary electrophoresis (CE) under optimized conditions. We further conducted Enceladus plume fly-through capture experiment by accelerating peptides soaked in rock particles up to a speed of 5.7 km/s and capturing with originally developed hydrophobic silica aerogels [4]. Direct peptide extraction with acetonitrile-water followed by CE analysis led to detection of only but two stereoisomeric acidic peptide peaks, presenting the first run-through hypervelocuty impact sample analysis targeting peptides as key moelcule to to understand the ongoing astrobiology on Enceladus.

Reference

[1] Hsu HW et al. (2015) *Nature*, 519(7542):207-210.
[2] Sekine et al. (2015) *Nat Commun*, 6:8604.
[3] Danger G et al. (2012) *Chem Soc Rev*, 41(16):5416-5429.
[4] Tabata M et al. *Origins Life Evol B* 2015, 45(1-2):225-22.

FORMATION MECHANISMS OF CHANNELS ON TITAN. A. E. Gilliam[1] and A. Lerman[1], [1]Department of Earth and Planetary Sciences, Northwestern University, Evanston IL, 60208-3130 (ashley@earth.northwestern.edu).

Introduction: Titan, the largest moon of Saturn, is the only satellite in the solar system with a significant atmosphere, harboring a suite of hydrocarbons that display a meteorological cycle similar to the hydrological cycle on Earth. Dendritic networks of sinuous valleys on the surface of Titan were first observed by the Cassini-Huygens mission, where Synthetic Aperture Radar (SAR) images revealed drainage networks with branching morphologies on the order of 100 km in length [1]. These observations were supported in greater detail by the Huygens Probe Descent Imager and Spectral Radiometer (DISR) [2][3][4], and suggested formation by fluvial erosion into the water-ice bedrock. Additional support that the valleys were formed by flowing liquid is the paucity of impact craters on Titan's surface [4][5][6][7], indicative of rapid burial or removal of surface topography. Additionally, at the landing site, the DISR imaged Earth-like rounded cobbles 0.3-15 cm in diameter [2] composed of water ice, indicating that they had undergone abrasion during fluvial transport.

In this study we address fluvial erosion processes on Titan. Specifically, we examine the possibilities of channel formation by dissolution of ice by a concentrated solution of ammonium sulfate, and by mechanical erosion by flow of liquid ammonia and liquid ethane. Each of these processes might have functioned over a certain range of temperatures during the cooling history of Titan.

Observations of Streams on Titan: In this study we examine 27 different fluvial features as identified in VIMS, ISS, and RADAR data, chosen based on their geographic diversity and resolution – or our confidence in their classification as a fluvial feature. These valleys represent an array of morphologic features and range in size from tens of kilometers to over a thousand kilometers long, and up to ten kilometers wide. The majority of these features are dendritic in nature, forming tree-shaped networks with many contributing branches that converge into larger receiving streams, up to seventh in channel order, indicative of an origin from rainfall [2][4][8][9].

In order to calculate the relative rates of stream incision into the water-ice bedrock on Titan, the channel dimensions must be known. Measurements of channel slope were made directly from Cassini RADAR SAR-topo and altimetry data, and depth from an empirical relationship between channel depth and width as outlined in [10].

Mechanical Erosion: To calculate the rates of liquid stream incision into water ice bedrock on Titan, we build on a previous model of terrestrial water erosion by saltation of bedrock particles [11], and analyze the effect of bed-load transport on the lowering rate using the equations of bed-load transport rate developed by Einstein (1942) [12] and Chanson (1999) [13]. These models apply to channels of fixed width that are being deepened by erosion and abrasion of rock/ice by bed load, and assume that all bed load motion is by saltation of spherical grains of uniform size.

Results: We find that chemical erosion of Titan's channels could be completed in 280 to 1100 years, much shorter than the period of about 84,000 years that a concentrated $(NH_4)_2SO_4$-H_2O solution could exist as a liquid on the Titan surface. Mechanical erosion of Titan's channels is generally a much slower process, on the order of 10^2 to 10^5 years to completion, and is also slower than mechanical erosion of a model river on Earth, averaging 10^3 to 10^4 years. The erosional sequence of the channels on Titan may have started after the formation of water-ice on the surface by the process of chemical dissolution by $(NH_4)_2SO4$-H_2O, overlapping**,** or followed by**,** a period of mechanical erosion by liquid NH_3. A final stage on the cooling surface of Titan might have been characterized by liquid C_2H_6 as an agent of mechanical erosion.

References: [1] Elachi C. et al. (2004) *Space Sci. Rev. 115,* 71-110. [2] Tomasko M. G. et al. (2005) *Nature 438,* 765-778. [3] Soderblom L. A. et al. (2007) *Planet. Space Sci. 55,* 2015-2024. [4] Jaumann R. et al. (2009) *Titan from Cassini-Huygens,* 75-140. [5] Porco C. C. et al. (2005) *Nature 434,* 159-168. [6] Elachi C. et al. (2005) *Science 308,* 970-974. [7] Wood C. A. et al. (2010) *Icarus 206,* 334-344. [8] Lorenz R. D. et al. (2008) *Planet. Space Sci. 56,* 1132-1144. [9] Perron J. T. et al. (2006) *J. Geophys. Res. 111,* E11001. [10] William G. P. (1988) *Flood Geomorphology,* 321-334. [11] Sklar L. S. and Dietrich W. E. (2004) *Water Resour. Res. 40,* W06301. [12] Einstein H. A. (1942) *American Society of Civil Engineers 107,* 561-574. [13] Chanson H. (1999) *The Hydraulics of Open Channel Flow: An Introduction.*

THE GEOCHEMISTRY OF ENCELADUS' OCEAN TOWARD THE END OF THE CASSINI MISSION.

C. R. Glein[1], M. Y. Zolotov[2], S. D. Vance[3], E. L. Shock[2,4], and F. Postberg[5,6]. [1]Southwest Research Institute (cglein@swri.edu), [2]School of Earth and Space Exploration, Arizona State University, [3]Jet Propulsion Laboratory, California Institute of Technology, [4]Department of Chemistry and Biochemistry, Arizona State University, [5]Institut für Geowissenschaften, Universität Heidelberg, [6]Institut für Raumfahrtsysteme, Universität Stuttgart.

Introduction: Enceladus has put on a great performance. By erupting gases and solids in a cryovolcanic plume that emanates from an ice-covered ocean, we are able to obtain constraints that allow us to assemble the geochemical story of this world. Here, we focus on the chemistry of the subsurface ocean, and associated geochemical processes.

Observations: Plume compositionl constraints are provided by the Ion and Neutral Mass Spectrometer (INMS), the Ultraviolet Imaging Spectrograph (UVIS), and the Cosmic Dust Analyzer (CDA). INMS and UVIS measured the gaseous component of the plume, while CDA characterized plume particles. All three instruments showed that H_2O is the dominant constituent. INMS determined that CO_2, CH_4, NH_3, and possibly H_2 are key minor constituents [1,2]. Numerous trace organic species were also detected [1,2]. UVIS has helped to constrain the abundances of CO, N_2, and H_2 [3,4]. CDA data showed that Enceladus' salty ocean is a source of the plume, and the dominant salts are NaCl and $NaHCO_3$ or Na_2CO_3 [5,6]. Potassium is a minor species, and sulfates were not observed. In addition, CDA detected organic mass fragments [7] complementary to those observed by INMS [1,2]. Recent CDA observations indicate that SiO_2 nanoparticles are sourced from Enceladus' plume [8].

Ocean chemistry: Initial chemical models of ocean water on Enceladus [9-11] are generally consistent with the observational constraints and with each other. The most striking similarity between Enceladus' ocean and terrestrial seawater (as a reference) is the dominance of NaCl, which stems from its high solubility, which allows efficient extraction from rocky sources. However, Enceladus' ocean may be less concentrated in NaCl than terrestrial seawater because of the much greater abundance of water relative to rock on Enceladus. Enceladus' ocean also appears to differ from terrestrial seawater in being relatively rich in dissolved inorganic carbon, and apparently poor in $MgSO_4$. This may imply that Enceladus accreted abundant CO_2 or CO as in many comets; and its ocean may be relatively reduced if significant amounts of oxidants (H_2O_2, O_2) were not accreted, or produced and delivered to the water-rock system over time.

Enceladus' ocean has an alkaline pH. There is not yet a reconciliation between estimated pH values of ~9 [5,8] or ~11 [9,11], depending on assumptions in interpreting CDA or INMS data. Nevertheless, it is encouraging that there is general agreement because it is not simple to estimate the pH of a liquid water body from measurements in space. Minerals play a key role in regulating the activities ≈ concentrations of SiO_2 and CO_2, which affect the pH via fluid speciation. For example, the low pH endmember would be consistent with fluid buffering by an ocean floor mineral assemblage of quartz-talc-magnesite-dolomite (high activities of SiO_2 and CO_2), while the high pH endmember can be reproduced by a model assemblage of chrysotile-talc-calcite-dolomite.

Geochemical processes: Four processes have emerged as plausible "forces of geochemistry" on Enceladus: (1) aqueous alteration of ultramafic rocks [9,11], (2) hydrothermal (>0°C) mass transfer [8], (3) formation of gas hydrates (clathrates) [e.g., 12], and (4) organic compound transformations [13]. These processes may have been active during the history of Enceladus, and today if there are sources of thermal or chemical disequilibria that have not been dissipated or are replenished by a geophysically active interior.

Aqueous alteration of ultramafic rocks would produce an alkaline pH and abundant H_2 that may be present in the plume [2]. In low CO_2 cases, the formation of serpentine (serpentinization) would lead to a pH of ~11-12. The pH would not be as high (~8-9) in high CO_2 cases because of carbonation reactions [10]. The latter scenario would be more consistent with a hydrothermal model of nanosilica formation [8]. However, a high pH ocean would be rich in dissolved Si, which could facilitate alternative mechanisms of forming SiO_2 nanoparticles [14]. If hydrothermal fluids are present today, they may provide volatile species (e.g., CH_4) that can be outgassed or sequestered into clathrates [15]. In addition to CH_4, there are other more complex but less abundant organic compounds inside Enceladus, which may be dissolved in ocean water, or present as oil droplets or suspended particulates [2,7]. Hypothesized sources of these organic compounds include leached primordial species, thermally processed organic materials, abiotic (e.g., Fischer-Tropsch-type) synthesis, and biological carbon fixation.

References: [1] Waite J. H. et al. (2009) *Nature*, 460, 487. [2] Waite J. H. et al. (2015) *AGU Fall Meeting*, P11D-02. [3] Hansen C. J. et al. (2008) *Nature,* 456, 477. [4] Hansen C. J. et al. (2011) *Geophys. Res. Lett.,* 38, L11202. [5] Postberg F. et al. (2009) *Nature*, 459, 1098. [6] Postberg F. et al. (2011) *Nature*, 474, 620. [7] Postberg F. et al. (2015) *AGU Fall Meeting*, P11D-03. [8] Hsu H-W. et al. (2015) *Nature*, 519, 207. [9] Zolotov M. Y. (2007) *Geophys. Res. Lett.,* 34, L23203. [10] Zolotov M. Y. (2012) *Icarus*, 220, 713. [11] Glein C. R. et al. (2015) *Geochim. Cosmochim. Acta*, 162, 202. [12] Kieffer S. W. et al. (2006) *Science*, 314, 1764. [13] McKay C. P. et al. (2012) *Planet. Space Sci.*, 71, 73. [14] Zolotov M. Y. and Postberg F. (2014) *LPSC*, 45, 2496. [15] Bouquet A. et al. (2015) *GRL*, 42, 1334.

Cassini VIMS Spectra of the Thermal Emission from the Hottest Spots Along Enceladus South Pole Fissures.
J. D. Goguen[1], B. J. Buratti[1], and the Cassini VIMS Team, [1]Mail Stop 183-401, Jet Propulsion Laboratory, California Institute of Technology, Pasadena, CA 91109 (Jay.D.Goguen@jpl.nasa.gov)

Introduction: The discovery of thermal emission from the tiger stripe fissures at the S. pole of Enceladus is a major highlight of the Cassini mission. Both VIMS (Visible and Infrared Mapping Spectrometer) and CIRS (Composite InfraRed Spectrometer) detect the thermal 'blackbody' spectrum emitted from the warm fissure areas. The VIMS instrument is uniquely suited to measuring the hottest active locations because VIMS covers the 3 to 5 micron wavelength range where the rising edge of the Planck function for these T~200 K areas dominates the emission spectrum. At longer wavelengths, the spectrum is more complicated because contributions from small hot areas and larger cooler areas combine to form the broad emission spectrum that is detected by the CIRS instrument at wavelengths >6.7 microns. We present an overview of the VIMS measurements of the hottest fissure thermal emission and put these data within the context of the larger picture of these Ocean World fissure eruption characteristics as reported from other instruments.

VIMS Data Set: Most of the south pole fissure region has not been directly illuminated by sunlight since the sub-solar point moved into the northern hemisphere in 2009, thereby eliminating the background of reflected sunlight at VIMS wavelengths and making the fissure thermal emission readily measureable. Since then, VIMS has measured spectra of at least 11 hot spots along the fissures. Most of these measurements were acquired in ride-along mode with CIRS as the prime instrument. During at least 2 encounters, VIMS and CIRS acquired simultaneous or near-simultaneous spectra of the same fissure location. VIMS spectra include multiple hot spots along Damascus, Baghdad, Cairo, and a likely hot spot on Alexandria.

Results: During a 74 km altitude flyover rev 164, VIMS acquired the highest spatial resolution spectrum of a hot spot along Baghdad with a pixel footprint of 214 x 38 m [1]. Analysis of this spectrum led to the conclusions that: 1) this VIMS spectrum was measuring the warm T=197±20 K ice walls within the top 40 m depth of a 9 m wide fissure; 2) the exponential increase in the vapor pressure of ice with increasing T means that narrower and hotter fissures are unstable and the fissure will widen and cool to T~200 K on a timescale of ~month; and 3) the measured fissure T and width is consistent with the trend of T and width for a series of fissure models published in [2].

All of the VIMS spectra examined to date are consistent with this scenario of a self-regulating fissure maximum T~200 K with brighter VIMS emissions corresponding to fissures up to ~20 m wide. Emission from the warm fissure interior walls dominate the VIMS spectra with <15% contributed by conductive heating of the adjacent terrain.

CIRS spectra report slightly cooler T's due to CIRS increased sensitivity to lower T emission at longer wavelengths and averaging over contributions from both the hottest and cooler areas [3]. Combined analysis of the CIRS and VIMS spectra spanning 3 to 500 micron wavelengths promises to reveal the distribution of [T, area] near the fissures that cannot be spatially resolved. This [T, area] distribution holds the key to understanding how heat is transferred to the surface within a few 100 m of the fissures.

The VIMS-detected emission is concentrated in localized hot spots along the fissures and does not seem to be distributed continuously along them. CIRS spectra indicate a much more continuous distribution of the emission along the fissure length. Jets locations also are distributed alon the fissure length and it appears that the VIMS-detected hot spots in general correlate with jet locations [4], but not all of the jet locations have been seen as VIMS hot spots.

References:

[1] Goguen, J.D., *et al.* (2013). The Temperature and Width of an Active Fissure on Enceladus Measured with *Cassini* VIMS during the 14 April 2012 South Pole Flyover. *Icarus* **226**,1128-1137.

[2] Ingersoll, A.P., and A.A. Pankine (2010). Subsurface heat transfer on Enceladus: Conditions under which melting occurs. *Icarus* **206,** 594–607.

[3] Spencer, J.R. et al., 2011. Observations of thermal emission from the South Pole of Enceladus in August 2010. Paper presented at the EPSC-DPS Joint Meeting held at Nantes, France, October 2011, p. 1630. <http://meetings.copernicus.org/epsc- dps2011>.

[4] Porco, C.C. D. DiNino, F. Nimmo (2014). How the geysers, tidal stresses, and thermal emission across the south polar terrain of Enceladus are related. *Astron. J.* **148**:45.

Acknowledgement: This research was conducted at the Jet Propulsion laboratory, California Institute of Technolgy, Pasadena, CA.

PLUME VENTS AND DYNAMICS: A CHAPTER PREVIEW. D. B. Goldstein[1], M. Hedman[2], M. Manga[3], M. Perry[4], C. Porco[5], J. Schmidt[6], B. Teolis[7], [1]Dept. Aerospace Engineering, The University of Texas at Austin, Austin TX, 78712, david@ices.utexas.edu [2]Dept. of Physics, University of Idaho, 875 Perimeter Drive., MS 0903, Moscow, ID 83844, mhedman@uidaho.edu, [3]Dept. of Earth and Planetary Sci., UC Berkeley, Berkeley CA 94720, manga@seismo.berkeley.edu, [4]Johns Hopkins University Applied Physics Lab, mark.perry@jhuapl.edu, [5]UC Berkeley, CA 94720 and CICLOPS, Space Science Institude, Boulder, CO 80301, carolyn@ciclops.org, [6]University of Oulu, Dep. Of Physics, PL 3000, FI-90014 Oulu, Finland, jurgen.a.schmidt@oulu.fi [7]Space Science Division, Southwest Research Institute, San Antonio, TX, 78230, bteolis@swri.edu.

Introduction: The individual geysers of largely water vapor and icy particulates forming the broader plume over the south pole of Enceladus constitue a unique phenomenon and opportunity. That flow of material, moderated by several physical processes along its passage from a presumed liquid source all the way out to Cassini's orbit and beyond, provides a remarkable way to access information from deep within the moon. The chapter on *Plume Vents and Dynamics* will examine the observations of the plume and surface vent region and explore the mechanisms which lead from the subsurface vapor and particulate source to the observed properties.

Jet, Plume and Vent Observations. The evidence of vent/the plume structure and mechanisms will be presented in terms of the following Cassini instrument observations:

a) Images of scattered sunlight from jet/plume particulates obtained by ISS,

b) Thermal images of the vent regions obtained via CIRS,

c) Images of the Tiger Stripes and vent region obtained by ISS,

d) INMS profiles of molecules, atoms and ions along Cassini's path through the plume,

e) CDA profiles of particulates during Cassini's traverse through the plume,

f) UVS solar/stellar occultation profiles of the plume, and

g) VIMS measures of the particle velocity distributions.

Images of the jets/plume from different views, images of the TS region from ISS and with thermal overlays, and INMS, CDA and UVS-occultation profiles will all be included.

Interpretations, Mechanisms and Models. There are many jet vents, generally aligned along the Tiger Stripes, which presumably have a distribution of lengths and widths, directions, opening angles, mass flow rates, flow speeds, and particulate or vapor species mass fractions. The particle size distribution, including the distribution with altitude, as well as the salinity distribution are key indicators of venting processes to be discussed. We examine different jetting scenarios concentrating on vent distributions and strengths using both triangulations from the imagery and INMS, CDA and UVS higher altitude profiles. An overlay of source locations atop an ISS image of the South Polar region is expected.

The discussion of eruption mechanisms must begin below the surface and describe how vapor and particles travel up through the near-surface conduit, pass through the surface vent, and expand into the vacuum of space. Discussions of vapor/particulate interaction with icy side walls, including the effects of phase change, heat conduction within the surrounding solid, energy flux to space, gas-dynamic expansion and progressive rarefaction will be provided. We will explore what ultimately produces the jets/plume. And we examine what limits them – conduit/vent constrictions and tortuosity, flow mass/momentum/energy exchange with sidewalls, vents closing off due to condensation, and orbital variation. We expect to produce schematic drawings of the relevant physics in the near-vent regions and in regions further afield. There have been several computational simulations of the physics involving both solid ice as well as gas/particulate flows – these will be summarized and contrasted.

Resolved Controversies and Open Questions. It is now clear that the source of vapor and particulates surrounding Enceladus' orbit around Saturn are many generally discrete geysers ejected from the Enceladus SPT, probably originating from a salty liquid water source. But it was not always understood as such. After briefly reviewing earlier alternate interpretations, we highlight some of the key pending questions concerning vent and plume dynamics such as: By what mechanism is the plume tidally throttled? How do new geysers start up to replace those being clogged by condensates? How deep is the liquid interface? How large are the vents in terms of length and width? What are the implications of the geyser and vent dynamics for the search for evidence for life below the icy surface?

HIGH RESOLUTION OBSERVATIONS OF ENCELADUS' SOUTH POLE USING CASSINI/CIRS. N. Gorius[1], J. Spencer[2], C. Howett[2], S. Albright[3], D. Jennings[4], T. Hurford[4], P. Romani[4], M. Segura[5], and A. Verbiscer[6], [1]The Catholic University of America, Washington DC 20064 (nicolas.gorius@nasa.gov), [2]Southwest Research Institute, Boulder CO 80302, [3]the Hammers Company, Greenbelt MD 20770, [4]NASA Goddard Space Flight Center, Greenbelt MD 20771, [5]University of Maryland, College Park MD 20742, , [6]University of Virginia, Charlottesville VA 22904.

Introduction: During two low passes over the south polar region of Enceladus, the Composite Infrared Spectrometer (CIRS) on Cassini spacecraft [1] was configured to record high spatial resolution measurement while scanning over the tiger stripes. CIRS has three focal planes FP1 (17-1000 µm, single detector 3.9 mrad), FP3 (9-17 µm, linear array of 10 detectors with FOV 0.273 mrad) and FP4 (7-9 µm, linear array of 10 detectors with FOV 0.273 mrad).

We will report the results derived from these two observations but also a comprehensive list on how we used our spectrometer as a thermal imager.

E18: On April 14th 2012, the Cassini spacecraft flew at 74 km above the surface of Enceladus with a relative speed of about 7.5km/s. Because of this low altitude and the short duration of the flyby (~ 1min), it was impossible to realize one of our normal thermal maps, which would require minimum smear and integration of about 5 seconds per interferogram. Instead by using the longest scan duration permitted by CIRS, and by using a constant inertial pointing, we were able to measure the variations of thermal flux while crossing Baghdad Sulci at several locations during a single interferogram scan. In this configuration our temporal resolution is without processing about 22.5 ms or 170 m along track. The detectors of FP3 and FP4 were used in a pair mode, resulting in resolution of 40m across track.

However due to some limitations relative to the instrument electronics and the flight software capability, we had to develop a specific inversion technic using wavelet decompositions and a pursuit algorithm in order to inverse this time variant system.

Our analysis suggests strong variations of the emission along and across track, and identifies the location of several distinct sources. The location and intensity of the strongest source is compatible with the result from VIMS [2]

E21: On October 28th 2015, the Cassini spacecraft flew at an even lower altitude of 48 km at 8.5 km/s. In preparation for this flyby, we modified CIRS flight software to bypass the instrument digital filter and increase our temporal resolution to about 5 ms or 42 m along track.

During this activity, the spacecraft was inertially pointed in order to cross several tigers stripes and probe some of the most active regions. The detectors arrays of FP3 and FP4 were used again in pair mode, leading to 26 m spatial resolution across track. In this configuration, this is the observation of the tiger stripes with the highest spatial resolution.

During this scan, all detectors were able to measure thermal flux variations while crossing Cairo, Baghdad and Damascus. These measurements are showing important variations along and across track over distance less than 100 m.

Supplemental in-flight tests of CIRS - using Iapetus and the internal blackbody - were designed and will be used to enable an absolute flux calibration.

References:

[1] F.M. Flasar et al. (2004), *Space Science Rev.* **115** 169–297. [2] Goguen et al (2013), *Icarus 226, 1128-1137*

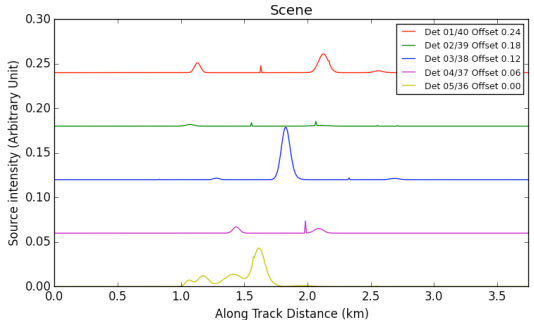

Figure 1 *Spatial distribution of the sources after inversion of E18, as seen by the 5 pairs of detectors.*

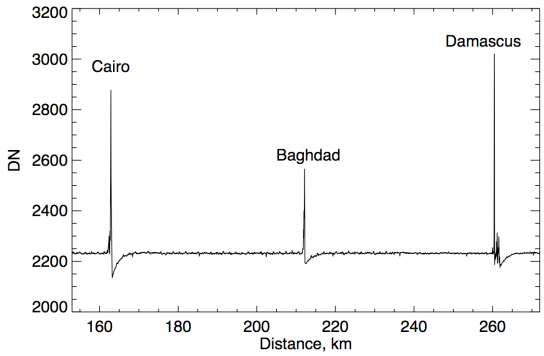

Figure 2 *Raw interferogram from CIRS FP3 acquired during E21 flyby.*

MODELING OF LOW ALTITUDE DYNAMICS OF GRAINS IN ENCELADUS JETS. M. Guzman[1], C.P. McKay[1], D. Hurley[2], R. Lorenz[2], R. Gold[2]. [1]NASA Ames Research Center, Moffett Field, California 94035, [2]John Hopkins University Applied Physics Laboratory, 11100 John Hopkins Rd, Laurel, MD 20723.

Introduction: Enceladus is of high interest due to its ejection of gaseous and particulate matter into space. Cassini mission data indicates that plume material derives from a subsurface liquid water reservoir containing organic carbon, biologically available nitrogen, redox energy sources, and inorganic salts. No other world has such well-studied indications of habitable conditions [1]. The particulate mass, or grains, are of particular interest to astrobiologists. At low altitudes, >99% of the particulate mass is salt-rich, or 0.5-2% sodium and potassium salts by mass [2].

Modeling of these salt-rich grains, which contain information on the habitability and potential evidence of life, is the subject of this research. Modeling of the grain dynamics at low altitudes is already present in the literature [e.g. 3, 4]. This research focuses on the behavior of those particles which are salt-rich and which do not achieve escape velocity and fall back to the Enceladus surface at low altitudes [5].

Background: Important assumptions and constraints on the jet modeling are defined by existing Cassini results. We consider the structure of individual jets, the dynamics of the grains and gas, the total particulate surface flux, the particle size and velocity distributions, and the composition of grains.

We use the set of ~100 point jets erupting from the tiger stripes identified by the Cassini Imaging Science Subsystem (ISS) [6], although we acknowledge that further modeling should consider an inter-geyser component of mass flux along the tiger stripes. For total particulate surface mass flux we use the ~5kg/s estimate from in-situ Cosmic Dust Analyzer (CDA) measurements [7].

Computational modeling:

Single jet model. We model an individual jet composed of regularly-emitted grain particles with a coupled size and velocity distribution. The simulation emits N particles per time interval from a vent source. The particle class in the simulation allows variance in particle size, initial velocity and angle of ejection. The gas is not modeled explicitly but its acceleration of the grain particles at the vent is considered in order to determine the initial speed of the grains at the vent [4,7]. In this way the velocity range of the particles is coupled to the radius size of the particle group. We use the acceleration of the particles by a gas in the vent column to approximate exit velocity distributions, then treat the particles ballistically after they exit the vent. Particles with radius >0.6um are treated as salt-rich particles [2].

Multiple jet model. The single jet model is multiplied for each of the 100 jets identified by [6] and assigned a source location. An example of a tiger stripe configuration composed of multiple single jet simulations is shown in Figure 1 (right). Particles from each separate source are shown in a different color. The mix of colors shows the amount of overlap expected at altitude where individual sources are no longer distinct. This modulation is calibrated to existing Cassini infrared data.

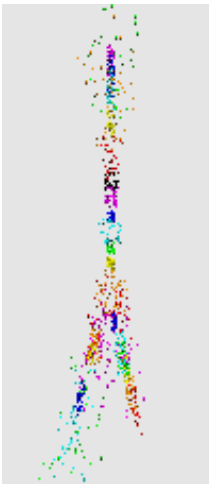

Figure 1: A VPython simulation of the multiple jet model. Particle color is linked to individual source on stripe.

Results: We will present the escape rate of grains as a function of grain size. The single jet approach will determine particle density, velocity distribution, size distribution and maximum particle size, all as a function of altitude. High altitude model results will be compared to Cassini in situ measurements [2, 5]. Low altitude model results will be compared to Cassini remote sensing data.

Conclusions: Material from the plume provides insight in a search for biomolecular evidence of life on Enceladus. Understanding the dynamics of low altitude grains is critical not only for astrobiology mission requirements but also for spacecraft design and hazard requirements. In addition, the model links measurements to the eruption parameters, which provides important information about the subsurface source of the grains.

References: [1] McKay C.P. et al. (2014) *Astrobiology*, *14*. [2] Postberg P. et al. (2011) *Nature, 474*, 620-622. [3] Yeoh S.K. et al. (2015) *Icarus, 253*, 205-222. [4] Degruyter W. and M. Manga (2011) *Geophy. Res. Letters, 38*. [5] Kempf S. et al. (2010) *Icarus, 206*, 446-457. [6] Porco C. et al. (2014) *The Astronomical Journal, 248*. [7] Schmidt J. et al. (2008) *Science, 451*, 685-688.

THE ROLE OF ENCELADUS' GAS JETS IN DIURNAL VARIABILITY OF PARTICLE FLUX. C. J. Hansen[1] , L. Esposito[2], G. Portyankina[2], K.-M. Aye[2], A. Hendrix[1], [1]Planetary Science Institute, Tucson, AZ (cjhansen@psi.edu), [2]LASP, University of Colorado, Boulder, CO.

Introduction: The Cassini Ultraviolet Imaging Spectrograph (UVIS) has observed a total of 6 occultations of stars (including one of the sun) by Enceladus' plume from 2005 to 2011 [1]. Supersonic gas jets were identified in the 2007 zeta Orionis occultation [2]. These supersonic collimated jets are imbedded in the overall expulsion of gas at escape velocity along the tiger stripe fissures that cross Enceladus' south pole. The gas flux can be calculated [1] and source rates are observed to vary just 15% in over 6 years, representing a steady output of ~200 kg/sec. In contrast, the brightness of the particle jets, a proxy for the amount of material streaming out, varies with orbital longitude [3], implicating tidal stresses. More particles are ejected from Enceladus at apokrone than perikrone by about a factor of 3. This is not inconsistent with the steady gas flux, which has not been measured at apokrone; rather, the combined dataset shows that material erupts from Enceladus steadily, but the rate is modulated diurnally.

2016 epsilon Orionis Occultation: In order to investigate whether gas flow increases dramatically at apokrone an occultation observation was inserted into the Cassini tour on March 11, 2016 on orbit 233. Enceladus was at a mean anomaly of 208 at the time of the occultation, not right at 180, but closer than previous occultations observed at mean anomalies of 98, 117 and 236. The star crossed diagonally behind the plume, and disappeared behind the limb, similar to the 2005 gamma Orionis occultation (other occultations have cut through the plume ~horizontally).

Using the same methodology as previously employed the column density for the plume as a whole has been determined to be 1.5 x 10^{16} cm^{-2}. Calculating gas flux in the same way as previously gives a rate for this occultation of 250 kg/sec. This value is 20% higher than the average 210 kg/sec, but only 15% higher than the occultations at a mean anomaly of 236; i.e. higher than the others but not by a factor of 2 or 3. We thus conclude that the overall expulsion of gas from the south pole of Enceladus does not change dramatically with orbital position.

Jets: The line of sight to the star crossed over the Baghdad I gas jet, with ingress behind the limb occurring just short of Cairo, as shown in Figure 1. The jet data, in contrast to the integrated plume, look significantly different in this dataset. The column density looking through the jet is higher than observed in previous occultations. The collimation of the jet is more pronounced and from that we derive a mach number of 8-12, compared to a previous value for this jet of 6. The amount of gas in this jet relative to the combined contribution from the rest of the tiger stripes is also larger, with the Baghdad I gas jet contributing ~8% of the total molecules seen, compared to other orbital longitudes when its contribution is just 2%.

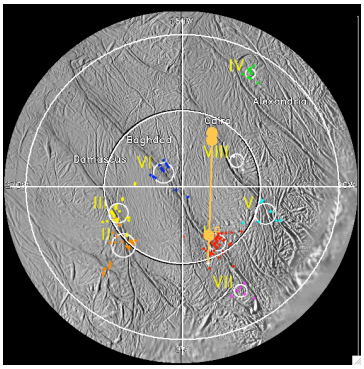

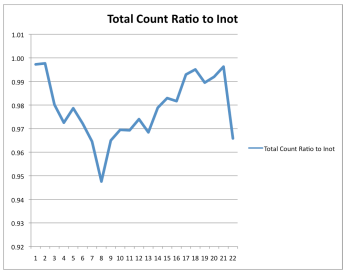

Figure 1. The top panel shows the groundtrack of a perpendicular dropped from the line-of-sight ray to the star, to the surface, with ingress at the Cairo fissure. The lower panel shows the ratio of the star signal to the average star signal as a function of time. The pronounced dip is crossing the Baghdad I jet and there is less gas between the fissures.

To summarize, the higher velocity of the jet and increased contribution to the overall gas flux implicates the jets as the primary contributors to the increased particle flux observed at perikrone.

References:

[1] Hansen, C. J. et al. (2006) *Science, 311,* 1422–1425. [2] Hansen, C. J. et al. (2008) *Nature, 456,* 477-479. [3] Hedman, M. M. et al. (2013) *Nature, 500,* 182–184.

MODELLING OCEAN DISSIPATION IN A VARIABLE THICKNESS OCEAN ON ENCELADUS Hamish C. F. C. Hay[1] and Isamu Matsuyama[1], [1]Lunar and Planetary Laboratory, University of Arizona, Tucson, AZ 85721, United States (hhay@lpl.arizona.edu).

Introduction: Radiogenic heating and tidal dissipation are the primary ongoing thermal contributors to icy satellite interiors. Tidal dissipation may provide the means to form and support global subsurface oceans over geological time, such as that confirmed in Enceladus through gravity [1, 2] and forced libration measurements [3]. Enceladus also remains unique among the icy satellites because its subsurface ocean is thickest beneath the active South Polar Terrain (SPT) and comparatively thinner elsewhere.

By considering the effects of tidal dissipation in the solid and liquid regions of icy satellites such as Enceladus, we hope to provide constraints on their current thermal and interior structures, as well as how the satellite's interior, rotation and orbit has evolved over time. Here we investigate how varying ocean thickness as a function of latitude affects both the time averaged and surface averaged ocean dissipation using a numerical model developed in [4].

Tidal Dissipation: Tyler [5] and Matsuyama [6] developed an analytical formalism to model dissipation in icy satellite global surface oceans. This work was limited by the need to decompose the solution into spherical harmonic components and ignoring non-linear effects. Numerically, most non-linear effects are trivial to solve for. Having developed a numerical model [4] that incorporates non-linear dissipative bottom drag, as well as testing it against results from both [6] and [7] (fig. 1), we now move to exploring how spatial ocean thickness variations alter ocean dissipation.

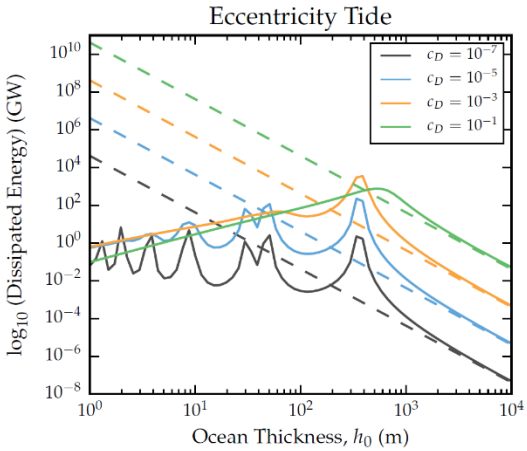

Figure 1. Comparison of numerical (solid lines) and scaling law (dashed lines) results developed by [7] for ocean dissipation under bottom drag on Enceladus, assuming a global surface ocean of constant thickness. Results are in excellent agreement away from resonant ocean configurations (from [4]).

Numerical Model: The numerical model, Ocean Dissipation in Icy Satellites (ODIS), is based on that developed by [8] and described in [4]. We use a two dimensional finite difference computational fluid dynamics code to solve the Laplace Tidal Equations over a fixed latitude-longitude grid.

Several adjustments had to be made to the original code in ODIS. Most obviously, the ocean thickness used in the calculations is no longer a numerical constant, but varies over the model domain. Modifications also had to be made to the fundamental equations under integration: the continuity and momentum equations [4]. These modifications include additional terms that introduce the effects of variable ocean thickness to the rest of the code by no longer making the assumption that the ocean thickness is constant.

Methodology: Simulations will be run to find average ocean surface dissipation over the orbital period for the eccentricity tide. We explore a variety of ocean geometries that vary the transition from thin to thick ocean under the SPT, as well as varying the ratio of thin to thick oceans. The maximum ocean thickness investigated under the SPT is 40 km, consistent with the gravity modelling of [2], which is likely beyond the shallow-water limit. There is very little constraint on the ocean thickness away from the SPT, but we consider thicknesses of up to 1 km. We also vary the latitude at which the ocean transition region begins to identify possible effects the transition may have on gravity-wave resonances in the system [5, 6]. All simulations assume a global surface ocean and employ bottom drag, and neglect the effects of ocean-loading and self-attraction.

Conclusions: The asymmetry in Enceladus' ocean thickness likely leads to enhanced regions of dissipation, especially at the boundary between thin and thick oceans. This ocean tidal heating could be significant in both a time and surface averaged sense. For this reason, ocean dissipation in an ocean of variable thickness is investigated for Enceladus for the first time.

Acknowledgements: This work was funded by the NASA Earth and Space Science Fellowship (NESSF) and the NASA Habitable Worlds program.

References: [1] Iess, L. et al. (2014). *Science*, *344*, 78–80. [2] McKinnon, W.B. (2015). *Geophysical Research Letters*, *42*, 2137–2143. [3] Thomas, P. C. et al. (2016). *Icarus*, *264*, 37-47. [4] Hay, H. and Matsuyama, I. (2016) *LPSC LXXVIII, poster #1234*. [5] Tyler, R. (2011) *Icarus*, *211*, 770-779. [6] Matsuyama, I. (2014) *Icarus*, *242*, 11–18. [7] Chen, E. M. A. et al. (2014) *Icarus*, *299*, 11-30. [8] Sears, W. D. (1995). *Icarus*, *113*, 39-56.

INTERIOR OF ENCELADUS. D. Hemingway[1,2], L. Iess[3], R. Tajeddine[4], and G. Tobie[5], [1]Miller Institute for Basic Research in Science and [2]Department of Earth & Planetary Science, University of California Berkeley, 177 McCone Hall, Berkeley, CA, 94720 (djheming@berkeley.edu), [3]Dipartimento di Ingegneria Meccanica e Aerospaziale, Università La Sapienza, Rome, Italy, [4]Cornell Center for Astrophysics and Planetary Science, Cornell University, Ithaca, NY, [5]Laboratoire de Planétologie et Géodynamique de Nantes, Université de Nantes, France.

Introduction: Constraining the internal structure of Enceladus is essential for understanding its origin and evolution [1], and for making sense of the salt-rich water ice geysers issuing from the surprisingly active south polar region—an indication of a potentially habitable internal liquid water reservoir [2–3]. Recent *Cassini* observations, in particular the gravity and libration measurements discussed below [4–5], have confirmed that Enceladus is differentiated, with a global subsurface liquid ocean lying between the icy crust and a (~2400 kg/m^3) rocky core (Fig. 1).

Shape and Gravity: Enceladus' quadrupole gravity field and the degree-3 zonal harmonic, J_3, were determined via radio tracking of the *Cassini* spacecraft during three close (<100 km altitude) flybys [4]. The observed J_2/C_{22} ratio is 3.51 ±0.08 (2σ), indicating a modest, but statistically significant departure from the expectation for a relaxed hydrostatic body, which would be ~3.24 in the case of Enceladus [6–7]. For the shape, which was determined based on analysis of limb profiles [8–9], the corresponding ratio is considerably larger, at 4.20 ±0.43 (2σ). The substantially non-hydrostatic shape accompanied by only a modestly non-hydrostatic gravity field suggests compensation.

An admittance analysis [4,7] yields self-consistent results when a moment of inertia factor of C/MR^2 ~0.33 is assumed, and indicates a mean compensation depth of 30–40 km. The most straightforward interpretation is that lateral variations in the thickness of the icy shell (e.g., due to tidal heating) are responsible for the observed non-hydrostatic topography, and that this topography is supported isostatically in a subsurface liquid layer, accounting for the small non-hydrostatic gravity.

Physical Librations: Like any tidally-elongated satellite, Enceladus experiences diurnally oscillating torques associated with its slightly eccentric orbit (ε=0.0047), leading to a small forced physical libration over its orbital period of 1.37 days. A network of optical control points was established and tracked through seven years of *Cassini* ISS (Imaging Science Subsystem) data to determine that this physical libration has an amplitude of 0.120° ±0.014° (2σ) [5]. In contrast, the physical libration amplitude expected for a homogeneous Enceladus is just 0.032°, more than 10σ smaller than the measured value [5]. A differentiated

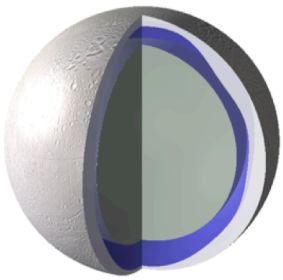

Figure 1: Three-layer interior model of Enceladus: rocky core, global liquid water ocean, icy shell.

Enceladus with a rocky core that is in contact with the ice shell would experience a similarly small physical libration in the range 0.032°–0.034°. Only when the ice shell is physically decoupled from the core—that is, when a global subsurface ocean is present—can the surface of Enceladus exhibit physical librations that match the observed amplitude.

Ice Shell and Internal Ocean: The gravity and libration results suggest a 10–30 km mean thickness global subsurface ocean beneath a 20–40 km mean thickness ice shell, that is perhaps considerably thinner at the south pole. The high heat flux and concentration of geologic activity at the south pole may be consistent with a locally thin, strongly tidally-heated ice shell, possibly resulting from earlier melting events [10–11]. A persistent subsurface liquid layer is favored by several models and, in spite of efficient cooling [12], can be kept from freezing if the orbital eccentricity is typically larger than the present-day value, or given the higher tidal heating rates associated with resonance locking [13]. The ice shell rigidity is high enough to support the ridges that cover much of the surface, but the shell appears to be weak at larger scales [4], likely owing to the extensive tectonic activity.

References: [1] G. Schubert et al. (2007) *Icarus 188*, 345–355. [2] C. C. Porco et al. (2006) *Science 311*(5766), 1393–1401. [3] F. Postberg et al. (2009) *Nature 459*, 1098-1101. [4] L. Iess et al. (2014) *Science 344*(6179), 78–80. [5] P. C. Thomas et al. (2016) *Icarus 264*, 37–47. [6] P. Tricarico (2014) *Astrophys. J., 782,* 99. [7] W. B. Mckinnon (2015) *Geophys. Res. Lett. 42*. [8] P. C. Thomas (2010) *Icarus, 208*, 395–401. [9] F. Nimmo, B. G. Bills, and P. C. Thomas (2011) *J. Geophys. Res., 116*, E11001. [10] G. Tobie, O. Cadek, and C. Sotin (2008) *Icarus, 196*, 642–652. [11] M. Běhounková et al. (2012) *Icarus, 219*, 655–664. [12] J. H. Roberts and F. Nimmo (2008) *Icarus, 194*, 675–689. [13] J. Fuller, J. Luan, and E. Quataert (2016) *Mon. Not. R. Astron. Soc., 458*, 3867–3879.

SURFACE COMPOSITION OF ICY MOONS. A.R. Hendrix[1], R.N. Clark[1], D. Cruikshank[2], B.J. Buratti[3], C.J.A. Howett[4], F. Scipioni[5] [1]Planetary Science Institute, Tucson, AZ (arh@psi.edu), [2]NASA Ames Research Center, [3]JPL/Caltech, [4]Southwest Research Institute, Boulder, [5]Lunar and Planetary Laboratory.

Introduction: Saturn's icy moons host a diverse array of surface compositions, controlled by exogenic processes, thermal and seasonal variations and radiolytic modifications.

In understanding the surface compositions of the icy moons of Saturn, we consider their environments: the orbits of the inner mid-sized moons (Mimas, Enceladus, Tethys, Dione, Rhea) result in important E-ring grain bombardment, affecting the composition of the uppermost layers of the icy regolith, along with charged particle bombardment that can drive chemical modifications within the regolith. In the outer part of the Saturn system, material from Phoebe's giant ring is significant at Iapetus, as well as at Hyperion.

Inner System Moons: Mimas, Enceladus, Tethys, Dione and Rhea all orbit within the broad, tenuous E-ring, which has a profound effect on their surface compositions. Their surface compositions are primarily water ice (e.g. [1] [2]), and water ice grain sizes maps have been produced (e.g. [3] [4] [5]) The dominance of water ice leads to relatively high albedos – but all of these moons exhibit a red slope in the UV-visible region, not characteristic of pure water ice. The strength of the UV-visible slope increases with distance from Enceladus (e.g. [6]) and thus may be related to E-ring grain deposition. The spectral signature has been related to nanophase hematite [7] and to organic tholins (e.g. [8] [9]). Similarly, radar albedos are found to decrease in the order Enceladus/Tethys, Rhea, Dione, indicative of increasing amounts of non-ice species, postulated to include include ammonia, silicates, metallic oxides, and organics [10].

An absorption band in the UV, centered near 260 nm, has been attributed to ozone [8] and has also been suggested to be due to an organic species [11].

The signature of CO_2 is present in dark terrains of Dione and Rhea [3] [4] [7], consistent with regions of magnetospheric bombardment on Dione [3]. In addition, Dione shows evidence on its trailing hemisphere for dark material derived from an unknown exogenic source [7].

Ammonia (or ammonia hydrate) is present in small amounts (~1%) on the surface of Enceladus as measured using near-IR [13] [14] and UV spectroscopy [9] and appears to be present on the Tethys leading hemisphere as well [11] [14]. It is likely that the NH_3, which is present in the Enceladus plume [15], is continually deposited onto the surfaces of these bodies.

The 26.7° obliquity of the Saturn system results seasonal variations due to photochemical processes (affecting the uppermost layers of the regolith only); in particular, UVIS data suggest the presence of H_2O_2 (a darkening agent) on the summer hemispheres of Mimas [16]; this effect may also been seen at Tethys.

Outer System Moons: In the outer part of the Saturnian system, the role of organic materials is important. Clark et al. [7] showed evidence for trace organics in the dark material of Iapetus, and Cruikshank et al. [17] showed that small IR spectral features are due to C-H stretching modes of aromatic hydrocarbons (probably indicating the presence of polycyclic aromatic hydrocarbons (PAHs)), as well as weaker signatures of aliphatic hydrocarbons, due to continual bombardment of Iapetus by material from Phoebe's interior, originating in the Kuiper Belt. Hendrix et al. [18] used UV data to demonstrate that Iapetus PAH signatures are likely present there as well.

The slow rotation of Iapetus, at its phase-locked distant orbit from Saturn, contributes to the important process of thermal migration [19] [20], which affects the composition of the dark material by volatile depletion.

References: [1] McCord, T. B. et al. (1971) Astrophys. J. 165, 413–424 [2] Cruikshank, D. et al. (2005) Icarus 175, 268–283 [3] Stephan, K. et al. (2010) Icarus 206 631–652 [4] Stephan, K. et al. (2012) Planet. Space Sci. 61, 142-160 [5] Scipioni, F. et al. (2015) 46th *LPSC, abs. # 1919* [6] Filacchione, G. et al. (2012) Icarus 220 1064–1096 [7] Clark, R. N. et al. (2008) Icarus 193 (2008) 372–386 [8] Noll, K. et al. (1997) Nature 388, 45-47. [9] Hendrix, A. R. et al. (2010) Icarus 206 608–617 [10] Ostro, S. J. et al. (2006) Icarus 183 479–490 [11] Hendrix, A. R. et al. (2015) *AGU abstract* [12] Emery, J. et al. (2005) A&A 435, 353–362 [13] Verbiscer, A. et al. (2006) Icarus 182, 211–223. [14] Verbiscer, A. et al. (2008) Sci. Solar System Ices, LPI. Abstract #9064 [15] Waite, J. H. et al. (2009) Nature 460, 487–490. [16] Hendrix, A. R. et al. (2012) Icarus 220 922–931 [17] Cruikshank, D. et al. (2014) Icarus 233:306–315. [18] Hendrix et al. (2016) Met. & Planet. Sci. 51, 105–115 [19] Spencer, J. & T. Denk, (2010) Science 327, 432 [20] Denk, T. et al. (2010) Science 327, 435

ENCELADUS AND THE OTHER MOONS OF SATURN AS OBSERVED BY CASSINI UVIS. A.R. Hendrix[1], C.J. Hansen[1], L.W. Esposito[2], E. Royer[2], T. Cassidy[2], D.E. Shemansky[3], G.Holsclaw[2] [1]Planetary Science Institute, Tucson, AZ, arh@psi.edu, [2]LASP/Univ. Colorado, [3]Space Environment Technologies.

Introduction: Throughout the Cassini mission, the Ultraviolet Imaging Spectrograph (UVIS) [1] has provided important results for studying both the plume and the surfaces of Enceladus and the other satellites. Plume results are the focus of Hansen et al. [2]. Surface measurements are complementary to longer wavelengths as the UVIS sensing depth is shallower; furthermore ice, organics and minerals exhibit unique spectral characteristics in this spectral regime. As such the UVIS data establish chemical processes (e.g. photolysis), physical processes (e.g E-ring grain bombardment/emplacement), and weathering effects via both mapping and spectroscopic techniques.

At Mimas, UVIS data indicate a unique seasonal variation wherein hydrogen peroxide (H_2O_2) is produced via photolysis in the summer hemisphere, lowering the far-UV albedo [3]; the effect may also be present at Tethys as well. At Phoebe, UVIS data have been used to demonstrate the varying presence of water ice across the surface [8], and at Iapetus UVIS data have been used to show that both Phoebe and Hyperion are richer in water ice than Iapetus' dark terrain. Spectra of the lowest latitudes of the Iapetus dark terrain display the diagnostic UV water ice absorption feature; water ice amounts increase within the dark material away from the apex (at 90◦ W longitude, the center of the dark leading hemisphere), consistent with thermal segregation of water ice. The water ice in the darkest, warmest low latitude regions is not expected to be stable and may be a sign of ongoing or recent emplacement of the dark material from the exogenic Phoebe ring.

At Enceladus, UVIS measurements have been utilized to detect the presence of a small amount of NH_3 [4], consistent with ammonia hydrate detections at infrared wavelengths [5] [6]. In this presentation, we focus on the varying UV signatures due to plume fallout (e.g. [10] [11]) as compared to regions where E-ring grain deposition dominates.

References: [1] Esposito, L. W. (2004) Space Sci. Rev. 115, 299–361 [2] Hansen, C. J. et al. (2016) *this meeting* [3] Hendrix, A. R. et al. (2012) Icarus 220 922–931 [4] Hendrix, A. R. et al. (2010) Icarus 206 608–617 [5] Emery, J. et al. (2005) A&A 435, 353–362 [6] Verbiscer, A. et al. (2006) Icarus 182, 211–223. [8] Hendrix, A. R. and C. J. Hansen (2008) Icarus 193 (2008) 323–333 [9] Hendrix, A. R. and C. J. Hansen (2008) Icarus 193 (2008) 344–351 [10] Kempf, S., U. Beckmann, S. Schmidt, 2010. *Icarus 206,* 446.

[11] Schenk, P., D. Hamilton, R. Johnson, W. McKinnon, C. Paranicas, J. Schmidt, M. Showalter, 2010. *Icarus 211*, 740.

Ring/Magnetosphere Interactions with Satellite Surfaces. C.J.A. Howett[1], A.R. Hendrix[2], C. Paranicas[3], J.R. Spencer[1], P.M. Schenk[4] and A.J. Verbiscer[5].[1]Southwest Research Institute, 1050 Walnut Street, Boulder, Colorado, 80302, USA, [2] Planetary Science Institute, Tuscon, Arizona, USA [3]The Johns Hopkins University Applied Physics Laboratory, Laurel, Maryland, USA, [4]Lunar and Planetary Institute, Houston, Texas, USA [5]University of Virginia, Charlottesville, Virginia, USA.

Introduction: The surfaces of Saturn's icy satellites are affected by their interactions with both Saturn's rings and magnetosphere. Active Enceladus continuously replenishes Saturn's E-ring [1], whose particles in turn strike Enceladus' neighbouring satellite surfaces [2]. All of the icy satellites move through Saturn's magnetosphere, although those most affected are closest to Saturn, where the plasma density is highest.

Magnetospheric Interactions: Global maps of Saturn's five inner midsized icy satellites, made with Cassini ISS data, show some intriguing patterns. Specifically Mimas and Tethys have lens shaped color anomalies that appear dark in the IR/UV color ratio maps at low latitudes on their leading hemispheres [3] (Fig. 1).

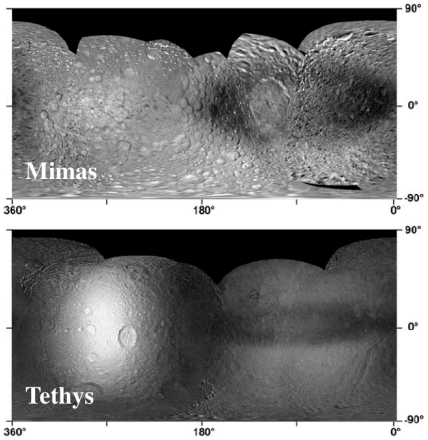

Figure 1- Cassini ISS global mosaics of IR/UV color ratio, of Mimas and Tethys [3]

Shortly after this discovery another surprising one was made: both of these lenses were spatially correlated with thermal anomalies [4, 5]. Data from Cassini CIRS showed the color anomaly region is cooler during the day, and warmer at night, than its surroundings (Fig. 2). An additional thermal anomaly also exists on Dione [6] but it is much weaker and a lens is not present in the Cassini ISS color ratio maps. Finally, this surface anomaly is not seen in the far-UV by Cassini UVIS on any of the satellites [7]. The lens regions may be altered by the high-energy electrons from Saturn's magnetosphere which preferentially bombard this region [8].

Ring Interactions: Satellites closest to Enceladus are bombarded by the highest E-ring flux. Results from the Hubble Space Telescope show a clear correlation

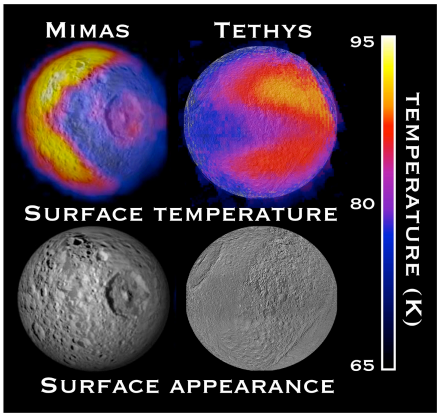

Figure 2 – Surface temperatures of Mimas and Tethys

between the reflectance and texture of a satellite and the flux of the bright E-ring grains that bombard it (Fig. 3): the surfaces of satellites closest to Enceladus have the highest visible albedo and the narrowest opposition effects. Strong leading/trailing albedo and color (Fig. 1) asymmetries seen on Tethys, Dione, and Rhea are also likely related to hemispheric differences in E-ring bombardment [2,7], perhaps in combination with cold plasma bombardment on the trailing hemispheres.

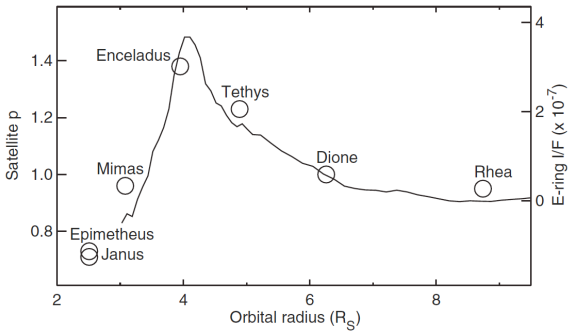

Figure 3 – Mean visual geometric albedo for Saturn's mid-sized icy satellites, compared to E-ring albedo [2]

References: [1] Pang et al. (1984), JGR 89, 9459-9470. [2] Verbiscer A.J. et al (2007), Science 315, 815. [3] Schenk et al. (2011), Icarus 211, 740-757. [4] Howett et al. (2011), Icarus 216, 221-226. [5] Howett et al. (2012), Icarus 221, 1084-1088. [6] Howett et al. (2014), Icarus 214, 239-247. [7] Hendrix et al. (2012), Icarus 220, 922-931. [8] Paranicas et al. (2014), Icarus 234, 155-161.

LINKING TIDAL VOLCANIC ACTIVITY TO SUBSURFACE VOLATILE SOURCES ON ENCELADUS.
T. A. Hurford[1], J. N. Spitale[2], A. R. Rhoden[3], and M. M. Hedman[4], [1]NASA Goddard Space Flight Center, Greenbelt, MD 20771, [2]Planetary Science Institute, Tucson, AZ 85719, [3]Arizona State University, School of Earth and Space Exploration, Tempe, AZ 85287, [4]University of Idaho, Moscow, ID 83844.

Introduction: Enceladus is a small (radius 250 km) moon that orbits Saturn between the moons Mimas and Tethys with a period of 1.37 days. This proximity to Saturn means that tidal dissipation should have quickly circularized the orbit. However, a 2:1 mean motion resonance with the moon Dione, which orbits just beyond Tethys, excites the orbital eccentricity to the observed value of 0.0047, which in turn produces periodic tidal stress on the surface.

In 2005, Cassini detected the eruption of material from warm regions, which correlated with the large Tiger Stripe fractures near the south pole of Enceladus [1,2]. While no temporal variation had been reported, a 2007 analysis of tidal stress postulated that the eruptive activity might be linked to tidal tension across these fractures and predicted that activity should vary on the orbital timescale such that greatest activity should be observed near apocenter [3]. Indeed, in 2013, results from analysis of Cassini's Visual and Infrared Mapping Spectrometer (VIMS) data confirmed the orbital variability of the erupting material and qualitatively confirmed the predictions of variable activity from 2007 [4,5].

Eruption Modeling and Depth of Volatile Reservoirs: Building off the simple models linking tensile stress on the Tiger Stripes with eruption activity [3,6,7], models were developed to fit activity seen in Cassini's Imaging Sub System (ISS) [8]. These models used shear, a phase lag in tidal response, or a physical libration to fit the observations. The latter two mechanisms were invoked in order to explain the delay in eruption activity since the Tiger Stripes start to experience tension quite quickly after pericenter passage whereas the peak eruption output is later in the orbit.

The simple model linking the fraction of the Tiger Stripes in tension with the eruptive activity was useful to predict variable activity and that pericenter would be the most quiescent period within the orbit. However, it may be too simplified to reproduce finer variations within the orbital activity. For example, when the fraction of fractures experiencing tension rises, the tensile stresses on the surface are small or only slightly tensile. Thus, just beneath the surface the fracture would still be in compression and not likely to vent material.

By adding overburden stress to the tidal model, the tensile stress acting on the fractures can be analyzed at various depths. The overburden stress is linear with depth and works to compress the fracture, delaying activity in the orbit until tensile stresses are larger. This naturally causes a lag in the orbital time at which fractures experience net tensile stress, potentially delaying the time of eruptive activity.

Conclusions: Adding the depth of a volatile reservoir to models of tidal activity can naturally delay the timing of fracture failure, as seen in VIMS and ISS eruption activity on Enceladus. If tensile failure is directly linked to tidal activity then a phase lag may still be required. At the greatest depths of tensile failure, peaks in the timing of failure are still before apocenter passage and not quite consistent with observations. Coulomb failure at greater depths might best match activity and does not require any additional phase lags or physical librations.

Tensile failure of the fracture system can only tap "shallow" sources. The maximum depth at which tensile failure can tap a volatile reservoir is about 1km. This may prove problematic for the production and release of salt enriched ice grains. If the ice shell is 10-40 km thick [9,10], then the water table is approximately 1-4km below the surface and if salty ice grains are formed at a chamber of exposed sea water [11], then fractures must be able to fail in tension at this depth to allow the release of these types of grains through tensile failure.

Coulomb failure can reach to deeper water table depths. In general, Coulomb failure acts to depths three times greater then tension. These failures can also facilitate release of volatiles closer to apocenter, without invoking any other mechanism (i.e. lags in response or physical libration). The ability to tap a liquid source at great depth may also account for variations in fracture temperatures seen on the surface. For example, the warmer branch of Baghdad sulcus can be active to significantly deeper depths.

References: [1] Porco C.C. et al. (2006) *Science* 311, 1394-1401. [2] Spencer J.R. et al. (2006) *Science* 311, 1401-1405. [3] Hurford T.A. et al. (2007) *Nature* 447, 292-294. [4] Hedman M.M. et al. (2013) *Nature* 500, 182-184. [5] Spencer J.R. (2013) *Nature* 500, 155-156. [6] Hurford T.A. et al. (2009) *Icarus* 203, 541-552. [7] Hurford T.A. et al. (2012) *Icarus* 220, 896-903. [8] Nimmo F. et al. (2014) Astro. J. 148, 46. [9] Iess L. et al. (2014) *Science* 344, 78-80. [10] Thomas, P. et al. (2016) Icarus, 264, 37-47. [11] Postberg F. et al. (2011) *Nature* 474, 620-622.

LOCAL ENHANCEMENTS IN THE ENCELADUS PLUME. D. M. Hurley[1] and M. E. Perry[2], [1]Johns Hopkins University Applied Physics Laboratory, 11100 Johns Hopkins Rd., Laurel, MD 20723 (Dana.Hurley@jhuapl.edu).

Introduction: The jets and plumes of Enceladus emit vapor and grains into the space environment above the south polar region of Enceladus. The contents and the plume provide insight into the subsurface ocean on Enceladus, which may host life. The dynamics of the emitted material stem from the conditions in the fissures and vents, which can be modulated by external and internal drivers. This study combines modeling and data analysis to increase the understanding of the spatial distribution of vapor and granular material at altitude.

Data: Cassini INMS data provide spatially resolved in situ measures of mass 44 u and mass 28 u species, presumably vapor CO_2 and CO. Although the mass 18 u data is not spatially resolved, the Cassini INMS data provides an overall measure of the water vapor sampled during a flyby. We use data from the low altitude, southern hemisphere flybys to provide a set of crosscutting samples of the plume [1]. Data from 3 parallel, nearly co-planar, passes provide an interesting way to investigate time variability in plume density. Additional data from the 50 km altitude E21 pass are also presented. The data from different masses provide the information on the dynamics of the vapor at the point of release from the surface.

Model: The Monte Carlo model tracks particles emitted from a prescribed spatial and velocity distributions from the point of release near the surface through eventual loss from the Enceladus system [2]. The code steps through the equation of motion under gravity in time using an RK-4 solver and provides the location and velocity of each particle at each time step. These data can be binned to produce density for comparison with in situ measurements, line of sight column density for comparison with remote sensing observation, and can factor in velocity information for field of view considerations.

Of particular interest is the relative contribution of material emitted along the length of the Tiger Stripes (curtain emissions) and those from more concentrated sources (jets) [3]. The model incorporates both possible sources for easy comparison to the data.

Results: The model output along the Cassini trajectory of E17 is shown in Figure 1 compared to the INMS 44 u observations. The model run using only emission along the Tiger stripes is show by the gray dashed line. The model run using only discrete sources is shown with the blue dashed line. The combination of the two models, red line, provides the best overall agreement with the observations. Deviations from the observations show fine scale structure in the source rate that has not been reproduced in the model.

Conclusions: The model demonstrates the distribution of vapor species at altitude. The dynamics of the fluid flow in the nozzle is set by the dominant species, water vapor. Minor species move along with the flow and are released with the same bulk velocity as water. However, as the flow transitions to a collisionless paradigm, the species differentiate because the random velocities are mass dependent, leading to higher collimation of the high mass species.

Comparison to INMS data show that a constant source rate of vapor emitted along the length of the Tiger Stripes cannot explain the observations. Additional, more significant sources are required in certain locations and certain times to reproduce the data.

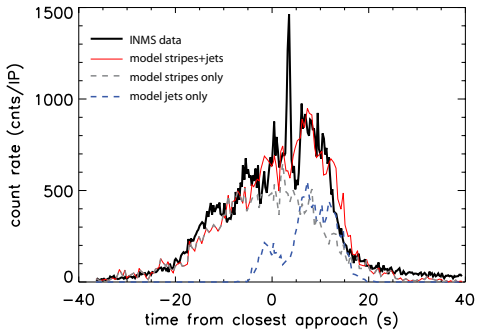

Figure 1. The model output compared to Cassini INMS data from E17, 44 u. The combination of emission along the stripes and emission from discrete jets is needed to reproduce the observations.

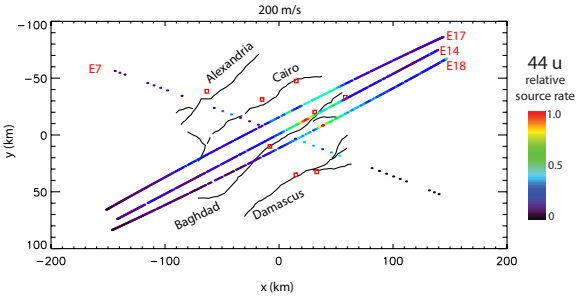

Figure 2. Ratios of the measured 44 u count rate and the modeled density, assuming only emissions along the stripes, reveals where additional sources are needed to reproduce the data.

References: [1] Perry M. E. et al (2015) *Icarus, 257,* 139-162. [2] Hurley D. M. et al (2015) *J. Geophys. Res., 120,* 1763-1773. [3] Porco C. et al (2014) *Astron. J., 148,* 45.

DECADAL TIMESCALE VARIABILITY OF THE ENCELADUS PLUMES INFERRED FROM CASSINI IMAGES. Andrew P. Ingersoll and Shawn P. Ewald, [1]Caltech mail 150-21, Pasadena, CA 91125, api@gps.caltech.edu, [2]Caltech mail 150-21, Pasadena, CA 91125, spe@gps.caltech.edu.

Decadal Variability: We have analyzed images from the ISS instrument and find that the plume's mass decreased by a factor of two from 2005 to 2015 [1]. This decadal variation is superposed but separate from the orbital variation discovered by Hedman et al. [2] using VIMS images, in which the plumes are brighter at apocenter (mean anomaly = 180°) by factors of 4-5 than they are at pericenter (mean anomaly = 0°). Our unit of mass is slab density—the total mass of particles in a horizontal slab per unit thickness of the slab. The decadal variation is seen also in equivalent width, which is closely related to brightness and is used by Hedman et al. [2].

Comparison with VIMS: Qualitatively, our ISS results agree with the VIMS results, but the reported VIMS equivalent widths are about 60% of the ISS equivalent widths taken at the same time. This difference arises because the VIMS field of view is too narrow to separate the downward-sloping wings of the plume from the negative curvature of the E ring background.

Vertical Profile: Slab density vs. altitude in the 25-200 km range is best described as a power law whose negative exponent is greatest in magnitude at apocenter, indicating a slower launch speed there than at pericenter.

Variation with Position in Orbit: A secondary maximum in slab density occurs at mean anomaly ~60°, which is before the main maximum at 180 ± 10°. We find no significant phase lag in the maximum, in contrast to the results of Nimmo et al. [3].

Eleven-year Orbital Cycle: The decadal trend is in phase with the orbital eccentricity itself, which varies by ±2.2% of its average value with an 11-year period. Because eccentricity is important in producing the tidal stresses that regulate plume activity (Hurford et al. [4]) it is tempting to associate decadal variations with variations in eccentricity. However, the eccentricity is small, about 4.8%, and the variations of eccentricity are a small fraction of that. Whether these variations are large enough to produce factor-of-two variations in slab density is an open question. This question is relevant to other questions about Enceladus, such as: What keeps the cracks from freezing shut due to vapor deposition on the walls [5]? How deep is the evaporating liquid, and what keeps it from freezing over [6]? Where is the tidal heat generated? Are eruptions of liquid onto the moon's surface possible?

Refernces: [1] Ingersoll A. P. and Ewald S. P. (2016) *Icarus,* submitted and under revision. [2] Hedman M. M. et al. (2013) *Nature 500,* 182-184. [3] Nimmo F. et al. (2014) *Astron. J. 148:46* (14 pp). [4] Hurford T. A. et al. (2007) *Nature 447*, 292–294. [5] Nakajima M. and Ingersoll A. P. (2016) *Icarus,* in press, doi: 10.1016/j.icarus.2016.02.027. [6] Ingersoll A. P. and Nakajima M. (2016) *Icarus,* in press, doi: 10.1016/j.icarus.2015.12.040.

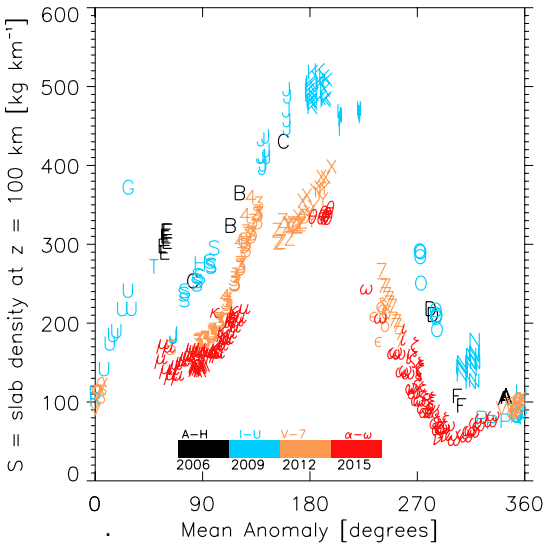

Figure 1. Plume mass vs. position in the orbit labeled by year of observation. The ordinate is slab density—the mass of particles in a horizontal slab one km thick 100 km above the South Pole. The abscissa is mean anomaly—time from pericenter divided by the orbit period expressed as an angle. Colors and shading give the time of observation in 3-year intervals centered on the years 2006, 2009, 2012, and 2015. In addition to the factor of 4-5 variation with mean anomaly, the graph shows a 2-fold decline in slab density from 2005 to 2015. From Ingersoll and Ewald [1].

SATURN'S DIFFUSE E RING AND ITS CONNECTION WITH ENCELADUS. S. Kempf[1], T. Hill[2], N. Krupp[3], M. Horanyi[1], J. Schmidt[4], T. Smith[5], and R. Srama[6], [1]Physics Dep. & LASP, Univ. of Colorado Boulder, USA, [2]Physics & Astronomy Dep., Rice University, USA, [3]MPI for Solar System Research, Göttingen, Germany, [4]Astronomy & Space Physics, Univ. of Oulu, Oulu, Finland [5]APL, Johns Hopkins Univ., USA, [6]IRS, Univ. Stuttgart, Germany.

Introduction: Saturn's E ring is the second largest planetary ring in the solar system, encompassing the icy satellites of Mimas (r_M = 3.07R_S), Enceladus (r_E = 3.95R_S), Tethys (r_T = 4.88R_S), Dione (r_D = 6.25R_S), Rhea (r_R = 8.73R^S), and Titan (r_R = 20.25R_S). Enceladus was proposed early on as the dominant source of ring particles [1], since the edge-on brightness profile peaks near the moon's mean orbital distance. We now know that the cryo-volcanoes at the moon's south-polar terrain are the main sources for the E ring particles [2]. Many features such as the ring's blue color and the local ring structure can be explained by the dynamics of the plume particle ejection [3][4].

Before the discovery of the Enceladus plumes in 2005, the mechanism for replenishing the E ring with ring particles was attributed to the ejecta particles produced by collisions of interplanetary particles [5] or by impact of the ring particles [6] with the moon's surface. In principle all ring moons contribute via the so-called impactor ejecta mechanism to the ring particle population, the extent of which is a focus of ongoing research [7][8]. However, there is now consensus that the primary source of ring particles are ice particles ejected by the Enceladus plume into an orbit around Saturn [8]. The fact that the particles emerge from localized sources at the Enceladus southpole terrain [9] has interesting consequences for the ring's fine structure. Spikes in the ring's vertical density profile observed by Cassini CDA as well as the long sinuous brightness structures dubbed tendrils observed by Cassini ISS can be associated with the strongest dust jets on Enceladus [4][3].

A surprising finding by the Cassini was that the E ring extends out to Titan's orbit [10]. Numerical simulations of ring particle evolution show that particles < 500 nm released at Enceladus can migrate far beyond Rhea's orbit [7]. However, measurements by Cassini CDA indicate the presence of larger particles at the outer parts of the E ring, which suggests that those particles cannot originate from Enceladus [7].

The ring particle composition is water ice with traces of sodium salts [11] and nano-silica inclusions, which act as nucleation seeds for the plume particles formed in the water vapor ascending through the fractures within the Enceladus surface [12]. After the ice

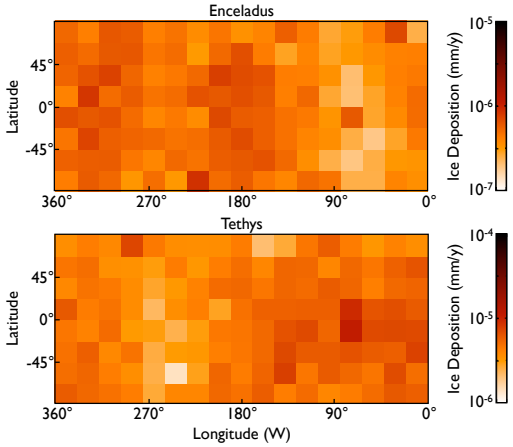

Fig. 1 Mass deposition rate of E ring particles on Enceladus (top) and Tethys (bottom) [14]. Saturn is at 0◦ longitude (W) and the moons' orbital motion is at 90◦ longitude (W).

mantels get removed by plasma sputtering, the silica inclusions form hypervelocity dust streams that are observed by Cassini CDA [13].

A fraction of ring particles are deposited on the surfaces of the moons embedded in the ring. Numerical simulations of the ring particle dynamics allow us to estimate where, and to what extent, E ring material is deposited (Fig. 1) [14].

References

[1] Baum et al. (1984). *Planetary Rings*, CNES.
[2] Spahn, F., et al. (2006) *Planet. Space Sci.*, *54*.
[3] Mitchell, C., Porco, C., & Weiss, J. (2015) *AJ*, *149*.
[4] Kempf, S., Beckmann, U., & Schmidt, J. (2010) *Icarus*, *206*.
[5] Horanyi, M., Burns, J, & Hamilton, D (1992) *Icarus*, *97*.
[6] Hamilton, D., & Burns, J. (1994) *Science*, *264*.
[7] Horanyi, M. et al. (2008). *GRL*, *35*.
[8] Spahn, F. et al. (2006). *Science*, *311*.
[9] Spitale, J., & Porco, C. (2007) *Nature*, *449*.
[10] Srama, R. et al. (2006). *Planet. Space Sci.*, *54*.
[11] Postberg, F. et al. (2009). *Nature*, *459*.
[12] Hsu, H.-W. et al. (2015) *Nature*, *519*.
[13] Kempf, S. et al. (2005) *Nature*, *433*.
[14] Kempf, S. et al. (2013). AGU Fall Meeting.

IMPACT CRATER DISTRIBUTIONS FOR GEOLOGICAL TERRAINS ON ENCELADUS. M. J. Kinczyk[1], G. W. Patterson[1], G. C. Collins[2], R. T. Pappalardo[3], and T. L. Becker[4]. [1]The Johns Hopkins Applied Physics Laboratory, Laurel, MD 20723, [2]Wheaton College Norton, MA 02766, [3]NASA Jet Propulsion Laboratory, Pasadena, CA 91109, [4]United States Geological Survey, Astrogeology Team, Flagstaff, AZ 86001.

Introduction: The geological history of Enceladus appears remarkably complex for a moon with a mean radius of ~250 km. Evidence of tectonic activity and episodic partial resurfacing is apparent in image data returned by the Voyager and Cassini spacecraft [1,2]. A fundamental method for deciphering these complex geological relationships is through measuring the distribution of craters across the surface of the satellite.

Background: Crater counts on Enceladus indicate a wide range of surface ages [3-6] suggesting a long history of geological activity. Crater density measurements for portions of the trailing hemisphere indicate variations with latitude and a relative deficiency of craters at diameters ≤2 km and ≥6 km for cratered plains compared to other icy Saturnian satellites [7]. It was concluded that these observations were the result of a combination of viscous relaxation and subsequent burial of large craters, and burial of small craters, by south polar plume and possibly E-ring material.

Analysis: Crater distributions for this work have been compiled from a 100 m/pixel controlled global mosaic of Enceladus produced as part of an effort to map the global geology of the satellite at a scale of 1:2M [8]. Sample regions of ancient cratered plains and younger leading and trailing hemisphere terrains were chosen for preliminary analysis. Their locations and corresponding cumulative size-frequency distributions are shown in **Figs. 1** & **2**. A method similar to [7] has been adopted for making measurements (e.g., non-impact related craters, such as pit craters, are excluded from analysis; image stretching is used to accentuate crater depressions in regions where crater rims are difficult to discern). All craters ≥0.5 km in diameter are counted in this analysis and crater distributions measured here are for diameters <10 km.

Results: The measured distributions of the two cratered plains sample regions are essentially equivalent for crater diameters >1.1 km. At smaller crater diameters, a falloff in the distribution for CP_2 with respect to CP_1 is observed. The falloff for CP_2 appears consistent with the previous observation of small crater burial by south polar plume particles [7]. This could indicate that a lack of falloff for CP_1 is related to its distance from the plume source. When comparing our sampled cratered plains regions to a model of plume particle deposition [9], it is clear that particle accumulation is less likely to occur in the CP_1 region. Additional work to map variations in the crater size frequency distribution of cratered plains material across Enceladus will provide additional insight into this phenomenon.

The measured distributions of the leading and trailing hemisphere terrains differ significantly for crater diameters of ~1-3 km. The deficiency of craters in this size range for the leading hemisphere terrain, compared to the trailing, could be indicative of a resurfacing event affecting the region. However, a bias resulting from limited viewing geometries for images of the leading hemisphere may also be present. Further investigation will be necessary to confirm this finding.

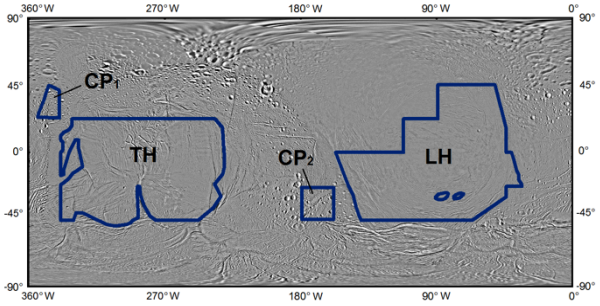

Figure 1. Count locations for the leading (LH) and trailing (TH) hemispheres and portions of cratered plains units (CP_1 and CP_2) in the northern and southern hemisphere.

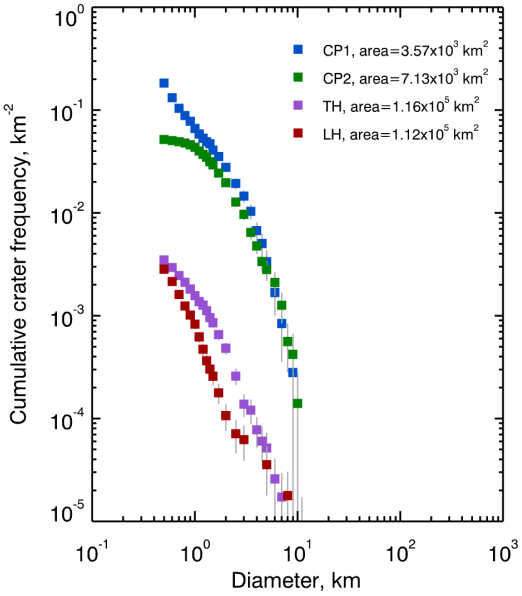

Figure 2. Cumulative size-frequency distributions for measured geologic terrains on Enceladus.

References: [1] Spencer et al. (2009) *Saturn from Cassini-Huygens,* 683–724. [2] Squyres et al. (1983) *Icarus, 53,* 319–331. [3] Plescia and Boyce (1983) *Nature, 301,* 666–670. [4] Lissauer et al. (1988) *JGR, 93,* 13776–13804. [5] Kargel and Pozio (1996) *Icarus, 119,* 385–404. [6] Porco et al. (2006) *Science, 311,* 1393–1401. [7] Kirchoff and Schenk (2009) *Icarus, 202,* 656–668. [8] Becker et al. (2016) *LPS XLVII,* Abstract #2342. [9] Kempf et al. (2010) *Icarus, 206,* 446–457.

CRATERING HISTORIES IN THE SATURNIAN SYSTEM. M. R. Kirchoff[1], E. B. Bierhaus[2], L. Dones[1], S. J. Robbins[1], K. N. Singer[1], R. J. Wagner[3], K. J. Zahnle[4]. [1]Southwest Research Institute, Boulder, CO. [2]Lockheed Martin Space Systems Company, Denver, CO. [3]Institute of Planetary Research, German Aerospace Center (DLR), Berlin, Germany. [4]NASA Ames Research Center, Moffett Field, CA. Email: kirchoff@boulder.swri.edu.

Introduction: A vital tool to constraining the evolution of the mid-sized saturnian satellites is their impact cratering histories. Images from the *Cassini* Imaging Science Subsystem (ISS) have resulted in a great leap in our knowledge of these histories. It has provided new insights into the crater populations, impact rates, and surface ages. We review the progress on each of these and discuss remaining issues.

Crater Populations: Four broad populations may form craters on Saturn's moons [e.g., 1]: (1) outer Solar System small bodies ("comets"); (2) planetocentric impactors from satellite collisions and primary crater ejecta that escape the moon; (3) secondary impactors from primary crater ejecta; and (4) captured inner Solar System small bodies ("asteroids"). Analyses of crater size-frequency distributions (SFDs), along with dynamical models and astronomical observations of small body populations, have helped to improve constraints on the contributions of these populations.

Comets are likely the main source for craters with diameter, (D) $\gtrsim$20 km. This is suggested by the shallow crater SFDs [e.g., 2], apex-antapex asymmetries [e.g., 3] (although reduced compared to predictions [4]), and the great extent of crater rays [e.g., 5].

Meanwhile, craters D$\lesssim$20 km may be partially composed by planetocentric impactors in addition to heliocentric impactors to potentially explain that no significant apex-antapex asymmetry has been observed so far [e.g., 3]. Some small craters on Dione, Tethys, and Rhea are also likely secondaries implied by steeper crater SFDs and model predictions [e.g., 6, 7].

Neukum et al. [e.g., 8] argue the similarity of satellite crater SFDs to the lunar production function supports asteroids captured by Saturn as the main source for all craters. However, dynamical corroboration has not been presented.

Remaining Issues: Does crater degradation or saturation possibly obscure the apex-antapex asymmetry for small craters? What is the contribution of sesquinaries [e.g., 6] and captured asteroids? How can Pluto/Charon data help further constrain the contribution of all populations [e.g., 9]?

Impact Rates: The first rates for cometary fluxes were computed by Shoemaker and Wolfe [10] extrapolating from rates observed at Earth. After *Voyager*, Zahnle et al. [11] determined current (since ~4 Ga) impact rates using crater SFDs, along with astronomical observations and dynamical models of small body populations. These rates were updated using *Cassini* data in [1]. Di Sisto and Zanardi [12] also computed current impact rates using a dynamical model of Centaurs constrained by *Cassini* data. Even though uncertainties are still large on these impact rates, *Cassini* data have helped to considerably improve our estimates.

Remaining Issues: How can outer Solar System impact rates be further improved? How do we incorporate the Late Heavy Bombardment into the rates [e.g., 13]?

Surface Ages: *Cassini* ISS imaging has vastly increased the surface area and diameter range over which crater SFDs can be observed on the mid-sized saturnian satellites. This, along with the improved knowledge of crater populations and impact rates, has provided significant new constraints on the surface ages.

The densely cratered plains on all satellites appear to be old with crater retention *model* ages of >3.5 Ga [e.g., 2, 14]. The only satellites that seem to have large areas of younger terrains (excluding basins) are Dione and Enceladus [e.g., 15–18]. The ridge terrains of Enceladus are suggested to vary in age from 0.7-2.0 Ga. For Dione, a ridged terrain is observed on the trailing hemisphere and is likely at least 2.5 Ga old, while a smooth terrain is found on the leading hemisphere that could be as young as ~1.7 Ga.

Studying the viscous relaxation of impact craters also plays an important role in understanding the surface ages of Saturn's moons. It can alter interpretation of crater SFDs [e.g., 16], help constrain ages of large basins [e.g., 19], and provide clues on surface modifications and defining different terrains [e.g., 20].

Remaining Issues: Have subtle resurfacing events been missed? What sources of error are not accounted for in computing crater retention model ages? How do crater SFDs compare among different researchers and what do similarities and differences mean?

References: [1] L. Dones et al., in *Saturn from Cassini-Huygens*, 613, 2009. [2] M. R. Kirchoff & P. Schenk, *Icarus 206*, 485, 2010. [3] N. Hirata, *JGRP 121*, 111, 2016. [4] K. Zahnle et al., *Icarus 153*, 111, 2001. [5] R. J. Wagner et al., *42nd LPSC*, Abst. #2249, 2011. [6] E. B. Bierhaus et al., *Icarus 218*, 602, 2012. [7] S. J. Robbins et al., *46th LPSC*, Abst. #1654, 2015. [8] G. Neukum et al., *EPSC*, Abst. #610, 2006. [9] K. N. Singer et al., *47th LPSC*, Abst. #2310, 2016. [10] E. M. Shoemaker & R. F. Wolfe, *LPSC XII*, 1, 1981. [11] K. Zahnle et al., *Icarus163*, 263, 2003. [12] R. P. Di Sisto & M. Zanardi, *A&A 553*, A79, 2013. [13] S. Charnoz et al., *Icarus 199*, 413, 2009. [14] R. J. Wagner et al., *LPSC XXXIX*, Abst. #1930, 2008. [15] M. R. Kirchoff & P. Schenk, *Icarus 256*, 78, 2015. [16] M. R. Kirchoff & P. Schenk, *Icarus 202*, 656, 2009. [17] C. C. Porco et al., *Science 311*, 1393, 2006. [18] R. Wagner et al., *LPSC XXXVII*, Abst. #1805, 2006. [19] G. Robuchon et al., *Icarus 214*, 82, 2011. [20] M. T. Bland et al., *GRL 39*, L17204, 2012.

SUSTAINED ERUPTIONS ON ENCELADUS EXPLAINED BY TURBULENT DISSIPATION IN TIGER STRIPES. Edwin S. Kite[1], Allan M. Rubin[2]. [1]University of Chicago (kite@uchicago.edu), [2]Princeton University.

Summary: Enceladus geysers apparently draw water from a subsurface ocean, but the sustainability of conduits linking ocean and surface is not understood. "Tiger stripes" sourcing the geysers should be clamped shut by tidal stresses for much of the 1.3 day orbit, and liquid-water conduits should freeze over quickly, so eruptions should be intermittent. However, observations show sustained geysering. A simple model of tiger stripes as tidally-flexed slots that puncture the ice shell can simultaneously explain: persistence of the eruptions through the tidal cycle; observed phase lag of eruptions relative to tidal stress; maintenance of fissure eruptions over geological timescales; and Enceladus' power output. Delay associated with flushing and refilling of $O(1)$ m-wide slots with ocean water generates a phase lag, while tidally pumped in-slot flow leads to heating and mechanical disruption that staves off slot freeze-out. Details, including citations to very useful papers omitted here due to space limits, are in Kite & Rubin, *PNAS* 113, 3972-3975, 2016.

Background: Each of Enceladus' eruptive fissures is flanked by <1 km-wide belts of endogenic thermal emission (10^4 W/m for ~500 km total fissure length). The tiger stripe region is tectonically resurfaced, suggesting an underlying mechanism accounting for both volcanism and resurfacing. Plume composition and gravity suggest that the geysers are sourced from a salty ocean. A continuous connection between ocean and surface is a simple explanation for these observations, but leads to a severe energy-balance problem. The water table within a conduit would be ~3.5 km below the surface (from isostasy), with liquid water below the water table, and vapor-plus-droplets above. Condensation of vapor on fissure walls releases heat that is transported to the surface thermal-emission belts by conduction (Fig. 1). Because this vapor comes from the water table there is strong evaporitic cooling of the water table. Freezing at the water table could release latent heat but would swiftly clog fissures with ice. This energy deficit has driven consideration of shear-heating, intermittent eruptions, and heat-engine hypotheses. The observed long-term steadiness of ice and gas geysering is modulated (for ice) by fivefold tidal variability. Peak activity anomalously lags peak tidal extension. Surprisingly, eruptions continue at Enceladus' periapse.

Simple slot model: Fissures are modeled as slots open to an ocean at the bottom. Subject to tidal stress, the water table initially falls, water is drawn into slots from the ocean (which is modeled as a constant-pressure bath), and slots widen. Wider slots allow stronger eruptions. Later in the tidal cycle, the water table rises, water is flushed from slots to the ocean, slots narrow, and eruptions diminish (but never cease). W>5 m slots oscillate in phase with σ_n, W<1 m slots lag σ_n by $\pi/2$ rad, and resonant slots (W ~ 1 m, tidal quality factor ~ 1) lag σ_n by ~ 1 radian. Net liquid flow feeding the eruptions is negligible compared to tidally-oscillating flow. Turbulent liquid water flow into and out of slots generates heat. Water temperature is homogenized by turbulent mixing. Aperture variations and vertical pumping help to disrupt ice forming at the water table. A long-lived slot must satisfy the heat demands of evaporitic cooling at the water table plus re-melting of ice inflow driven by the pressure gradient between the ice and the water in the slot. Turbulent dissipation can balance this demand for W=1-3 m, corresponding to phase lags of 0.5-1 rad, as observed. Eruptions are then strongly tidally-variable but sustained over the tidal cycle. W <1 m slots freeze shut, and W>5 m slots would narrow. Near-surface apertures ~10 m wide are suggested by modeling of high-temperature emission, consistent with near-surface vent flaring. Rectification by choke points, condensation on slot walls, and ballistic fall-back, could plausibly amplify the <2-fold slot-width variations in our model to the 5-fold observed plume variations. In summary, turbulent dissipation of tidal flows could plausibly explain the inter-annual-to-decadal sustainability of liquid-water-containing tiger stripes. At the conference, we will describe how a coupling between long-lived slots and the ice shell drives a 10^6 yr geologic cycle that buffers Enceladus' power to ~8 GW.

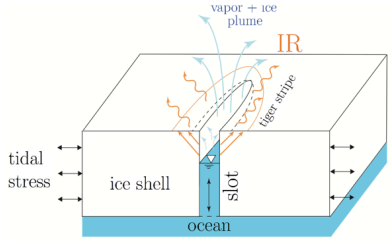

Fig. 1. Geysers vary on tidal timescales due to flexing of geyser source fissures by tidal stresses. Flexing also drives vertical flow in slots beneath source fissures, generating heat. Heat maintains slots against freeze-out despite strong evaporitic cooling at the water table, which provides heat for warm surface material.

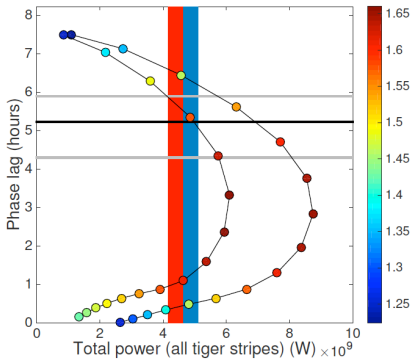

Fig. 2. Turbulent dissipation that matches the observed phase lag of Enceladus relative to a fiducial model of interior structure (gray lines bracket acceptable range) also matches observed Enceladus power (vertical lines). Thin black curves show power for two plausible slot geometries. Colored dots show fractional change in aperture. Aperture is sampled at 0.25 m intervals up to 5 m (lowermost dots). Best fit W are 1.25-2 m.

Tectonic dichotomy of icy satellites of Saturn. G. G. Kochemasov, IGEM of the Russian Academy of Sciences; 35 Staromonetny, 119017 Moscow, kochem.36@mail.ru.

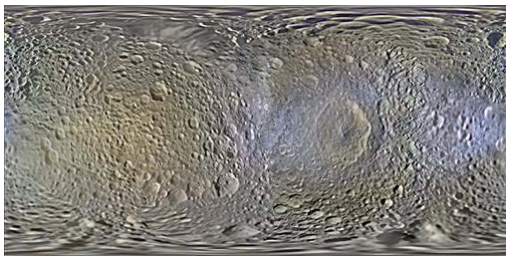
1

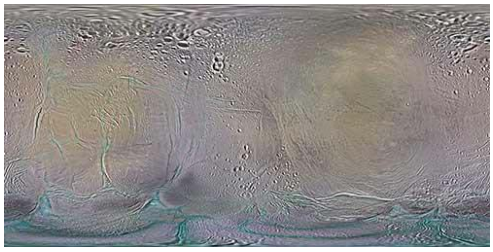
2

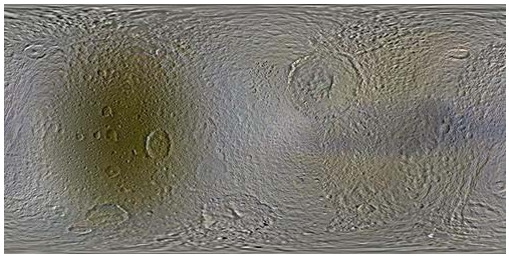
3

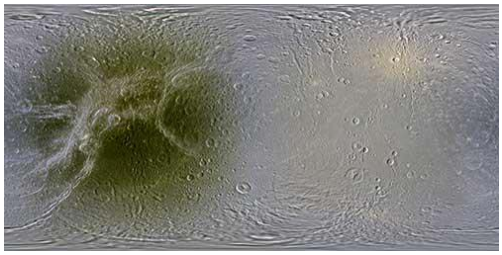
4

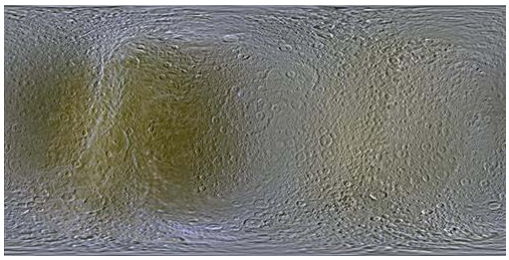
5

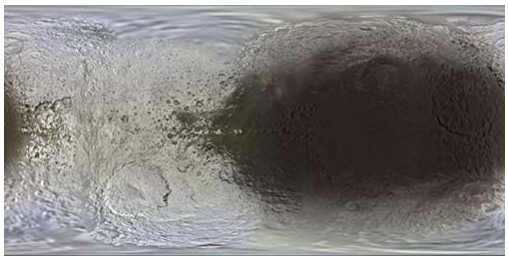
6

	Color maps of:	Radius, km:	Orbital period, days
-	**1 - Mimas, PIA18437**	**197**	**0.94**
	2 – Enceladus, PIA18435	**251**	**1.37**
	3 – Tethys, PIA18439	**524**	**1.89**
	4 - Diona, PIA18434	**559**	**2.74**
	5 – Rhea, PIA18438	**765**	**4.52**
	6 – Iapetus, PIA18436	**718**	**79.33**

Images credit: NASA/JPL-Caltech/Space Science Institute/Lunar and Planeetary Institutte

Global color mosaics of Saturn's moons (**Figs. 1-6**) were produced from images taken by NASA's Cassini spacecraft during the first ten years exploring the Saturn system. The most obvious feature on the maps is the difference in color and brightness between the two hemispheres. According to authors of the images, the darker colors on the trailing hemispheres (on the left side of the images) are thought to be due to alteration by magnetospheric particles and radiation striking those surfaces. The lighter-colored leading hemispheres are coated with icy dust from Saturn's E-ring formed of tiny particles ejected from Enceladus' South Pole. These satellites are all, supposedly, being painted by material erupted by neighboring Enceladus. Some corrections are however necessary for these explanations. The first theorem of the wave planetology [1, 2] states: "Cosmic bodies are dichotomous". This is due to warping action of the fundamental wave affecting moving in keplerian orbits with periodically changing acceleration celestial bodies. All cosmic explorations of numerous bodies show that a two-face appearance or dichotomy really is their typical trait. Normally, the subsided relatively smoothed hemisphere opposes the uplifted rugged one. The best-studied examples are Earth, Mars, and Moon. Thus, the painting action of Enceladus is an additional action superimposed on already existing tectonic dichotomy - a ubiquitous morphologic feature. It is true that the source of tiny icy particles is Enceladus; that is why it is less color dichotomous (whitened) than other icy satellites (Figs. 1-6). Uplifted cracked and fissured (rugged) hemispheres often are darker because some lighter (but darker under decomposition-soot) substance is coming up. This is not the case for Iapetus and probably for Enceladus degassing light toned material.

Uplifted hemispheres are more rugged, cracked, and cratered than the opposite pressed-in hemispheres. Normally pressing – diminishing radius is a reason for forming denser formations in these tectonic blocks (preserving angular momentum considerations; look at Earth and Mars). In the saturnian satellites cases darker substance could be less dense than water ice or presents very thin dark veneers originating from decomposition of material extracted from satellite depths due to very deep cracks (Diona and Rhea). In much more wave warped Iapetus [3] the darker and presumably denser material (tholins?) already fills hemispheric depression. Thus, tectonic (geomorphologic) dichotomy is basically more regular, stable and universal than color and brightness characteristics. **Ref: [1]** Kochemasov, G.G., 1998. Tectonic dichotomy, sectoring and granulation of Earth and other celestial bodies. Proceedings of the International Symposium on New Concepts in Global Tectonics, "NCGT-98 TSUKUBA", Geological Survey of Japan, Tsukuba, Nov 20-23, 1998,144-147. **[2]** Kochemasov, G.G., 1999. Theorems of wave planetary tectonics. Geophys. Res. Abstr., v.1, no. 3, p. 700. **[3]** Thomas, P.C., Veverka, J., Helfenstein, P., Porco, C. et al., 2006. Shapes of the saturnian icy satellites. Lunar and planetary Science Conference XXXVII, Houston, USA, Abstract 1639 pd. CD-ROM.

TOWARDS SIMULATION-BASED MISSION SUPPORT FOR SUBSURFACE EXPLORATION OF THE ICY MOONS

J. Kowalski[1], K. Schüller[1], A. Zimmermann[1], [1]Aachen Institute for Advanced Study in Computational Engineering Science, RWTH Aachen University, Schinkelstr. 2, 52062 Aachen, Germany, kowalski@aices.rwth-aachen.de

Introduction: Direct exploration of the Icy Moons of our Solar System implies landing on its icy surface. Advanced mission scenarios suggest to deploy a robotic exploration probe in order to migrate into the subsurface aiming for data collection and sampling of subglacial liquid [1]. Since water ice melts at a moderate temperature many of the robotic concepts are inspired by the idea of melting their way through the ice. This approach means that while migrating into the ground the probe is surrounded by convecting melt water and experiences a complex thermal state. In order to (autonomously) control the probe while making optimal use of the collected sensor data, it is crucial to have a solid understanding of the probes' ambient environment during a melting scenario.

In our contribution, we will address this objective and present an integrated computational model for an exploration probe migrating through ice and its ambient cryospheric state. When we first started this project, we had a particular application in mind, namely modeling the dynamic behavior of the robotic exploration probe IceMole [2,3]. Though the IceMole still inspires much of our work, we now reached a level of generality that allows us also to study related processes such as self-burrying meteorites. Instead of the robotic probe one can hence also think of any generic heat source.

Observation scale: Existing computational models for studying the Icy Moons often act on very large spatial and time scales and address objectives such as the evolution of our Solar System. These are hence macro-scale models. Other studies investigate micro-scale processes, e.g. when studying details about the ice structure. In our project, we are most interested in time scales in the order of hours to months and spatial scale that range from the submilimeter scale (melt film in the vicinity of the probe) to tens or hundreds of meters (length of the melting channel). It is important to us to consider both transient heat and mass transport, phase-change processes, as well as natural or forced convection in the melt. We distuinguish two modules:

Modeling the ambient cryo-state: Currently our model is capable of computing phase-change processes that are fully coupled to the convecting liquid melt. We compute the temperature distribution in the ice, convection and temperature distribution in the melt, as well as the evolving location of the solid-liquid phase interface. Our algorithm relies on a fixed-grid, weak interface approach and implements the enthalphy-porosity method. First results realize simplified 2d and 3d geometries and have been computed with an OpenFoam implementation. The implementation can be used both on a desktop PC or parallelized on a compute cluster. It has been tested with analytical reference solutions and with experimental data, both of which showed very nice agreements.

Modeling the heat source migration: The objective of the second module is to determine the trajectory of a rigid heat source in a migrating state. Here, our current approach updates position and attitude through minimizing an appropriately chosen energy functional. The exact form of the energy functional depends on the design of the probe.

In this presentation, we will describe the current state of both modules, discuss scope and validity of their underlying assumptions and current implementation, and show various test cases. We will introduce two collaborations in the context of the Enceladus Explorer Initiative, during which our model will be applied in the near future, namely

1. re-analysis of laboratory and field experiments of the IceMole team at FH Aachen University of Applied Sciences, Germany,
2. optimal control of melting probes together with the CAUSE (Cognitive Autonomous Subsurface Exploration) team at University of Bremen.

Finally, we will sketch next steps such as quantifying the error of simplified models [4], and future development areas on our way towards a fully capable tool for simulation-based mission support.

Acknowledgements: As part of the Enceladus Explorer Initiative, the project is supported by the Federal Ministry of Economics and Technology, Germany, on the basis of a decision by the German Bundestag (FKZ: 50NA 1502).

References: [1] Konstantinidis K. et al. (2015), *Acta Astronaut., 106*, 63–89. [2] Kowalski J. et al. (2016), *Cold Reg. Sci. Technol., 123*, 53-70. [3] Dachwald B. et al. (2014), *Ann. Glaciol., 55(65)*, 14-22. [4] Schüller K. et al. (2016) *Int. J. Heat Mass, 92*, 884-892.

Life on Icy Worlds? Emergence vs. Panspermia. P. E. Laine[1], [1]Department of Computer Science and Information Systems, University of Jyväskylä, Finland.

Introduction: The icy moons present some of the promising examples of extended habitable locations in our Solar System. Some of them seem to have liquid water that is in contact with the rocky mantle, enabling them to deliver elements for life. They also may have temperature gradient, potential hydrothermal vents for free energy source for possible chemolithotrophic organisms. How all this fits in to our knowledge about the origin of life? Where are the caps and challenges in each model for life on the icy moons?

If there is life on one or more of the icy moons in our Solar System (e.g. Enceladus and Europa), how could it have got in there? Did it emerged independently there, or was it delivered from somewhere else? Endogenous theories of the origin of life often depend on the environment where life could have emerged. One theory favor hydrothermal vents, another dry volcanic surfaces, and third ices. Icy moons could have two such environments: hydrothermal vents and ice. Panspermia is a theory that life originated from somewhere else, Earth as one obvious place of origin. All these theories have caps and challenges in them. Organic molecules have limited stability in high temperatures. On the other hand, chemical reactions are very slow in ice. If life came from somewhere else, how it survived its journey through the space, and how did it get itself to the potential ocean under thick ice shell? In this paper, pros and cons of these theories are presented.

CONTRAINING THE VISCOSITY OF ENCELADUS'S ICE SHELL THROUGH THE CRATER ISLANDS. E. J. Leonard[1], A. Yin[1] and R. T. Pappalardo[2]. [1]University of California Los Angeles, Earth, Planetary and Space Science, erinleonard@ucla.edu, [2]Jet Propulsion Laboratory, California Institute of Technology, Pasadena, CA

Introduction: Enceladus has a complicated geological history, dominated by partial resurfacing episodes [1]. The South Polar Terrain (SPT) is the youngest form of these resurfacing episodes, as it is currently active, however there is also evidence for past partial resurfacing in the Leading and Trailing Hemisphere [2]. In the southeastern region of the Leading Hemisphere (around 30° S, 90° W), there are relic fragments of an ancient cratered terrain encircled by a ridge-forming matrix. These "crater islands" exhibit evidence of rotation around vertical axes, from which we may estimate the viscosity of the ice at the time of block rotation.

Ice viscosity is used for assessing heat flux. Estimates for the heat flux outside of the SPT range from 110-270 mW/m^2 based on observations such as ridge height and crater relaxation [3-5]. Thus, by constraining the ice shell viscosity, we will provide constraints on other properties of the ice-shell.

Methods: In order to constrain the ice viscosity, we first estimate the rotation angle of the crater islands. We estimate this angle by measuring the deflection in the surrounding ridges (Figure 1). The rotation angle is related to the strain by:

$$\cot\alpha' = \cot\alpha - \gamma \qquad \text{(Equation 1)}$$

where α' is the rotation angle and γ is the strain. We then get the strain rate by dividing the strain by the time of formation. Finally, we estimate the viscosity using:

$$\mu = \frac{\tau}{\dot{\gamma}} \qquad \text{(Equation 2)}$$

where μ is the viscosity of the ice-matrix, τ is the stress and γ is the strain rate.

Preliminary Results: Our initial estimate of the rotation angle is based on the angle of the deflected ridges with respect to the overall sub-horizontal trend. We use 10 Ma, the youngest potentail age for the Leading Hemisphere terrain [1], for the time of formation. The stress (τ), we assume to be diurnal due to the relatively short formation time, though we plan on investigating nonsynchronous rotation (NSR) as a possible source as well in the future. The diurnal stresses on Enceladus have a predicted maximum of 100 kPa [6,7]. As such we took τ to range from 10-100 kPa, resulting in the viscosity range 10^{17}-10^{18} Pa s (Table 1).

Implications and Future Work: The brittle-ductile transition is likely to occur when the ice viscosity is 10^{13}-10^{17} Pa s [8]. As such, the initial rough estimate of the viscosity indicates ductile ice at or close to the surface. Having such a low viscosity, ductile ice at the surface implies a high heat flow in this region at the time of formation.

In order to improve our initial viscosity estimate, we will evaluate our stress mechanism by considering NSR as well as diurnal and plausibility of each based on stress orientations provided by the SatStressGUI [9] and contraints based on the Maxwell Time [e.g., 8]. We will also create a detailed map of the cratered island region and the surrounding area in order to analyze potential internal deformation of the blocks which would effect our strain estimate. Overall, we will refine our viscosity analysis with the goal of constraining the conditions under which the crater islands formed and the implications for Enceladus's geologic history.

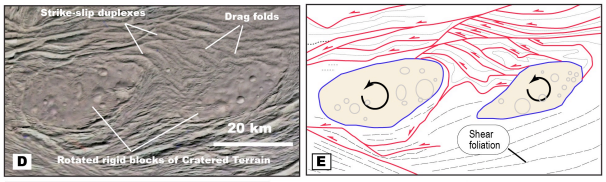

Figure 1: Crater islands image (left) and a rough geological map (right).

Table 1: Correnspond values for each quantity calculated to get the ice viscosity from Equations 1 and 2.

Quantity	Value
α', angle of rotation	30°
γ, strain	1.7
t, time	10 Ma or 10^{14} s
$\dot{\gamma}$, strain rate	10^{-14} s^{-1}
τ, stress	10-100 kPa
μ, viscosity	10^{17}-10^{18} Pa s

References: [1] Spencer, J.R. and Nimmo, F. (2013) *Annu. Rev. Earth Planet Sci., 41,* 693–717. [2] Crow-Willard, E. and Pappalardo, R.T. (2015) *JGR., 120,* 928-950. [3] Giese et al., B.R. (2008) *Geophys. Res. Lett., 35.* [4] Bland, M., et al. (2007) *Icarus, 192,* 92-105. [5] Bland, M., et al. (2012) *Geophys. Res. Lett., 39.* [6] Hurford, T. et al. (2007) *Nature, 447,* 292-94. [7] Smith-Konter and Pappalardo (2008) *Icarus, 198,* 435-51. [8] Bland, M. et al. (2015) *Icarus, 260,* 232-45. [9] Patthoff, D.A, et al. (2015) *AGU, 96.*

FUTURE EXPLORATION OF ENCELADUS AND SATURN'S ICY MOONS. J. I. Lunine[1], G. Tobie[2], G. Mitri[2], F. Tosi[3] and A. Coustenis[4], [1]Dept. of Astronomy, Cornell Univ., Ithaca, NY,14853, [2] Laboratoire de Planétologie et Géodynamique de Nantes, Université de Nantes, Nantes, France, [3]INAF-IAPS, Istituto di Astrofisica e Planetologia Spaziali, Area di Ricerca di Tor Vergata, Via del Fosso del Cavaliere, 100, I-00133 Rome, Italy, [4]LESIA, Observatoire de Paris, CNRS, UPMC Univ Paris 06, Univ. Paris-Diderot, Meudon 92195, France.

Introduction: The final flythrough of the plume of Enceladus by the Cassini Orbiter on October 21, 2015 marked the end of Cassini's *in situ* investigations of this remarkable small moon of Saturn. Over a decade of flybys and seven flythroughs of the plume, Cassini has determined that Enceladus has a global ocean [1,2], organics [3], salty water [4], and a possible hydrothermal system at the ocean's base [5]. This makes Enceladus a key target for future exploration.

Near-term exploration proposals: A proposal in 2011 from the Jet Propulsion Laboratory with international collaborations to fly a Discovery-class Saturn orbiter repeatedly past Enceladus and Titan, called Journey to Enceladus and Titan (JET), would have carried a Rosetta-spare mass spectrometer, a near-infrared mapping spectrometer, and conducted experiments in gravity mapping of the two bodies [6]. The intent was to provide an astrobiological assessment of both Saturn moons, together with Titan mapping and geophysical objectives. The spacecraft power supply was the Advanced Sterling Radioisotopic Generators, or ASRG's, then under development but with a currently uncertain future. The proposal was not selected.

In 2015 a revised JPL Discovery proposal, again with international collaboration, refocused the objectives on those that could be accomplished entirely with mass spectrometry. This concept, called Enceladus Life Finder (ELF), was to fly a solar-powered spacecraft into Saturn orbit and to make multiple deep flythroughs of the Enceladus plume [7]. The payload consisted of one mass spectrometer to study the gaseous species in the plume, while a second would analyze ice grains features, both with an exceptional mass range, sensitivity and substantial resolution improvement over Cassini. In addition to assessing the habitability of the ocean by determining key parameters such as redox state, pH and temperature of the ocean, ELF would conduct three tests looking for biological activity in the ocean. The mission was not selected for Phase A in the 2015 Discovery round.

A sample return concept involving a flythrough of the plume and capture of material for return to the Earth has been developed at JPL; called Life Investigation for Enceladus (LIFE) the mission would also sample and analyze the plume in situ [8]. The concept was too ambitious for Discovery but potentially might be a New Frontiers-class mission. The TSSM mission to Titan and Enceladus was studied by ESA and NASA as a flagship and large (L-)class mission in 2008-2009, but was not selected [9].

Parallel efforts in Europe to continue the exploration of Enceladus led to a mission proposal for an L-class mission in 2013 [10] and several M-class concepts possibly in conjunction with Titan exploration. In 2016, the 'Explorer of Enceladus and Titan' (E^2T) mission was proposed in response to the M5 ESA call to assess the evolution and habitability of these Saturnian icy moons using a solar electric powered spacecraft in orbit around Saturn, performing multiple flythroughs of Enceladus' plume. The E^2T mission payload consists of two time-of-flight mass spectrometers and a high resolution IR Camera.

Roadmap: The plethora of mission concepts for future exploration of Enceladus and the interest by NASA and ESA in the "Ocean Worlds" (planetary bodies with water or other-type oceans), requires a strategy to be developed against which proposals can be fielded. One such strategy has recently been published [11]. It features a roadmap that progresses from plume flythrough missions, to plume sample return, and on to more ambitious missions that might land near fractures or even attempt to enter the ocean. Progression to more ambitious missions depends on the results of their predecessors. With current launch vehicles, a possible Enceladus plume flythrough mission that might be completed and approved through a New Frontiers' opportunity in 2016/2017 would not arrive until after 2030. This makes the search for life in the Saturn system a multi-generational effort.

Other icy moons of Saturn: The entire Saturn satellite system exhibits a diversity of processes and properties unrivalled by the other giant planets. While proposals for future missions have focused on Titan and Enceladus, it is tempting to speculate that a mission to one or both of these bodies would also carry out investigations of some of the other moons.

References: [1] McKinnon W.B. (2015) *GRL 42*, doi:10.1002/2015GL063384. [2] Thomas P.C. et al. (2016) *Icarus 264,* 37–47. [3] Waite J.H. (2009) *Nature 460,* 487–490. [4] Postberg F. et al. (2011) *Nature 474,* 620–622. [5] Hsu H.-W. et al. (2015) *Nature 519*, 207–210. [6] Sotin, C. et al. (2011) *LPSC 42*, 1326. [7] Lunine, J.I. et al. (2015). *LPSC 46*, 1525. [8] Tsou, P. et al. (2014). *Astrobiology 12*, 730-742. [9] Reh, K. (2008) report, jpld-48442 [10] Tobie, G. et al. (2014) *Planet. Space Sci. 104*, 59-77. [11] Sherwood, B. (2016). *Acta Astron. 126*, 52-58.

HISTORY OF TECTONIC DISRUPTION ON ENCELADUS, DIONE, AND RHEA. E. S. Martin[1], D. A. Patthoff[2], and T. R. Watters[1]. [1]Center for Earth and Planetary Studies, National Air & Space Museum, Smithsonian Institution, Washington, DC 20560 (martines@si.edu), [2]Planetary Science Institute (apatthoff@psi.edu).

Introduction: Enceladus is one of the most heavily tectonized bodies in the Saturnian system; however its long-term tectonic history of deformation is not well described. The source of the small moon's observed ongoing geologic activity, focused in the south polar terrains (SPT), can not be understood without a more complete picture of the fracture history preserved on the surface.

To elucidate Enceladus's tectonic history, we create detailed fracture maps and model the early- and late-stage tectonic environments on Enceladus. Similar work will be completed for Dione and Rhea, both have late- and early-stage fracture populations. This comparative planetalogical approach will enhance results from Enceladus by exploring bodies where tectonic activity ceased before terrains were tectonically resurfaced. Differences in orbital distances (Enceladus ~4 R_s, Dione ~6 R_s, and Rhea ~9 R_s) and eccentricity (Enceladus 0.0047, Dione 0.0022, Rhea 0.00125) contribute to varied levels of tectonic complexity on each satellite. There are likely other factors that have enabled Enceladus's ongoing activity. We present preliminary global, fracture maps of Enceladus, Dione, and Rhea as well as preliminary tidal stress models to begin to elucidate and compare their early- and late-stage tectonic histories.

Enceladus: Enceladus's cratered plains on the Saturn- and anti-Saturn hemispheres have preserved a record of cratering in contrast to the paucity of craters in the tectonized leading and trailing hemisphere terrains (LHT and THT) [1, 2]. Stratigraphically, the cratered terrains preserve a record of tectonism pre- and post-dating cratering. Pre-cratering tectonism is characterized by troughs and ridges, and troughs are further distinguished between as those that fit into parallel sets (grouped) and those that don't (ungrouped) [3].

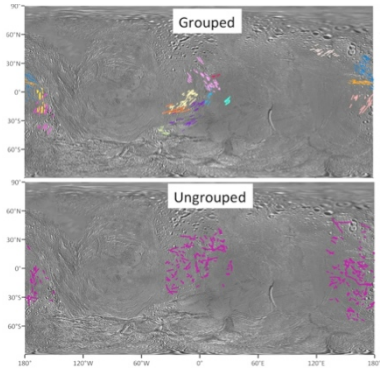

Figure 1: The distribution of ancient fractures on Enceladus.

Post-cratering activity is preserved as fractures called pit chains [4]. Preliminary stress modeling using SatStressGUI [5] suggest that grouped troughs and pit chains may have formed due to nonsynchronous rotation (NSR), whereas the randomly orientated ungrouped troughs suggest ice shell thickening [3, 6].

Dione: Preliminary mapping of Dione's wispy terrains of its trailing hemisphere do not show the same diversity of fracture types as described on Enceladus [7]. Dione's wispy terrains are primarily normal fault scarps and graben. Preliminary tidal stress modeling results from SatStressGUI suggest that the wispy terrains formed due to NSR. A secondary population of fracturing appears older and not associated with the wispy terrains [e.g. 8]. Ongoing mapping and modeling will further elucidate their formation mechanism(s).

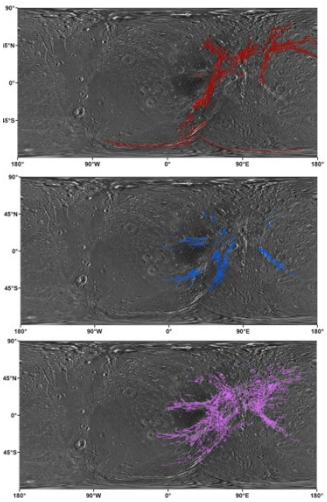

Figure 2: Twin scarps, scarps, and linea make up Dione's wispy terrains.

Rhea: Similar to Dione, Rhea has two populations of fractures: younger wispy terrains also on its trailing hemisphere [9] and other older younger than other fractures elsewhere on Rhea. Mapping and tidal stress modeling of Rhea is ongoing.

Discussion: Preliminary observations of Enceladus suggest punctuated episodes of tectonic activity. The two populations of fractures on Dione and Rhea may also preserve a similar kind of varied stress history within the fracture patterns expressed on their surface. Similarities and differences of the preserved fracture histories on these bodies will inform the complex tectonic history and geologic activity on Enceladus.

References: [1] Kirchoff, M. R. & Schenk, P. (2009) *Icarus, 202,* 656-668. [2] Sims, D. W. et al., (2014) *GRL, 41,* 3774-3778. [3] Martin, E. S. (2015) *46th LPSC,* Abstract #1620. [4] Michaud R. L. et al., (2008) *39th LPSC,* Abs. #1678. [5] Patthoff D. A. et al., (2015). *Eos, Trans. AGU* 96, Fall Meet. Suppl., Abs. P31C-2079. [6] Martin, E. S. & Kattenhorn, S. A. (2014) *45th LPSC*, Abs. #1083. [7] Nahm, A. L. & Kattenhorn, S. A. (2015) *Icarus, 258*, 67-81. [8] Hammond, N. P. et al., (2013) *Icarus, 223,* 418-422. [9] Stevenson, D. J. (1982) *Nature, 298*, 142-144.

COMPOSITION OF ENCELADUS: ORIGIN AND EVOLUTION. William B. McKinnon[1], J. H. Waite, Jr.[2], O. Mousis[3], J. I. Lunine[4] and M. Yu Zolotov[5], Department of Earth and Planetary Sciences and McDonnell Center for the Space Sciences, Washington University in St. Louis, Saint Louis, MO 63130 (mckinnon@wustl.edu), [2]Southwest Research Institute, San Antonio, TX 78228, [3]Aix Marseille Université, CNRS, LAM UMR 7326, 13388, Marseille, France, [4]Department of Astronomy and Carl Sagan Institute, Cornell University, Ithaca, NY, 14853, [5]School of Earth and Space Exploration, Arizona State University, Tempe, AZ 85287.

Introduction: Enceladus is a remarkable world. We infer from Cassini mass spectrometry of plume gas, ice and silica grain analyses, and gravity and libration measurements the existence of an internal ocean in contact with a rock core that *may* be undergoing hydrothermal activity [1-7]. Such active hydrothermal conditions provide a habitable environment and have been implicated as a region where early life emerged on Earth [e.g., 8]. In this talk we put these compositional analyses and structural inferences into the context of origin and internal evolution models (including those of Titan), and by doing so constrain these models where practical, with the ultimate goals of 1) assessing Enceladus' habitability and 2) suggesting future measurements that may resolve these issues.

Overview of Origins: The saturnian regular icy satellites, as a whole, almost certainly formed in a circumplanetary accretion disk (CPD) that surrounded the growing gas giant at the end of its formation [9]. Proto-Saturn would have been sufficiently massive to have opened a gap in the solar nebula (SN) [10]. Accretion of gas and entrained particles ("pebbles") then proceeded through streamers, which coalesced and formed a prograde-rotating CPD [e.g., 11,12].

Early in this phase, temperature and pressure conditions in the CPD may have been high enough to induce gas phase chemistry (e.g., CH_4 to CO [13]) and devolatilize solids captured from the solar nebula. As the SN dissipates, however, the CPD progressively attenuates and cools, enough so that gas phase chemistry is kinetically inhibited and that the compositions of captured solids captured remain largely unaltered [9].

The D/H ratio in H_2O measured in Enceladus' plumes by INMS is relevant here: D/H is close to the value inferred for Oort Cloud comets (~2.9×10^{-4} [1]; cf. [14]), precluding the possibility that Enceladus' building blocks condensed in an initially warm and dense saturnian subnebula [15]. In the latter, the D/H ratio acquired by the water ice accreted by Enceladus should be close to the much lower, protosolar value [15]. By inference then, Enceladus largely accreted from rock, ices, and organic matter directly inherited from the solar nebula by the saturnian CPD.

Composition: Carbonaceous chondrites are the most primitive chondrite class, so it is often assumed that they are most representative of outer solar system "rock." CI chondrites contain the fullest complement of elements at solar abundance levels (except H, C, O, N, and noble gases) [16], and are the class typically associated with outer planet satellite composition [e.g., 17,18]. CIs are the most aqueously altered chondrites, however, and it is not clear if icy moons accreted CI-type material or their anhydrous precursors (perhaps both). Comet-like abundances in plume vapor [1] suggest a substantial fraction of organic H-C-O-N-rich cometary material, which would make the bulk composition of Enceladus even closer to solar composition than CI chondrites. On the other hand, evidence from Stardust samples [19] and recent dynamical models [20] argue for some degree of mixing across the solar nebula, so that even inner solar system materials may have ended up incorporated into Enceladus.

Evolution: Minor species that have been securely identified, at the percent level or less, in plume vapor are CO_2, CH_4, and NH_3; higher hydrocarbons are also present [1,2; cf. 22]. Salts (principally NaCl and Na carbonate/bicarbonate) have been detected in E-ring and plume ice grains [2]. The presence of all of these in the plume is consistent with a model of an sodic, alkaline ocean with Na^+, Cl^-, and CO_3^{-2} as the major solutes [6,18]. This, and specifically the possible detection of native H_2 [23], are consistent with an actively serpentinizing core [5,6]. A principal question, then, is whether ongoing serpentinization (here taken to generically mean aqueous alteration of Fe-bearing ultramafic minerals) is consistent with a 4.5 billion year old Enceladus, or whether such "serpentinization" is more consistent with a cosmogonically much younger satellite, such as two recent studies have proposed [24,25].

References: [1] Waite J.H. (2009) *Nature 460,* 487–490. [2] Postberg F. et al. (2011) *Nature 474,* 620–622. [3] Iess L. et al. (2014) *Science 344*, 78–80. [4] McKinnon W.B. (2015) *GRL 42*, doi:10.1002/2015GL063384. [5] Hsu H.-W. et al. (2015) *Nature 519*, 207–210. [6] Glein C.R. et al. (2015) *GCA 162* (2015) 202–219. [7] Thomas P.C. et al. (2016) *Icarus 264,* 37–47. [8] Sullivan W.T. and Baross J.A. (2007) *Planets and Life: The Emerging Science of Astrobiology*, CUP. [9] Peale S.J. and Canup R.M. (2015) in *Treatise on Geophysics*, Elsevier, 559-604. [10] Morbidelli A. and Crida A. (2007) *Icarus 191*, 158-171. [11] Ayliffe B.A. and Bate M.R. (2009) *MNRAS 397*, 657–665. [12] Tanigawa T. et al. (2014) *ApJ 784*, 109. [13] Prinn R.G and Fegley B. (1981) *ApJ 249*, 308-317. [14] Altwegg K. et al. (2015) *Science 620*, 1261952. [15] Kavelaars J. J. et al. (2011) ApJL 734, L30. [16] Lodders K. (2003) *ApJ 591*, 1220–1247. [17] McKinnon W.B. and Zolensky M.E. (2003) *Astrobiol. 3*, 879–897. [18] Zolotov M. Yu. (2007) *GRL 34*, L23203. [19] Brownlee D. (2014) *AREPS 42*, 179–205. [20] Walsh K. et al. (2012) *MAPS* 1–7. [21] Waite J.H. et al. (2011) EPSC/DPS abs. #61. [22] Postberg F. et al. (2008) *Icarus 193*, 438-454; [23] Glein C.R. et al. (2016) *47th LPSC*, abs. #2885. [24] Charnoz S. et al. (2011) *Icarus 216*, 535–550. [25] Cuk M. et al. (2016) *ApJ 820*, 97.

WHY IS ENCELADUS ACTIVE WHEREAS MIMAS IS NOT? M. Neveu[1] and A. R. Rhoden[1], [1]School of Earth & Space Exploration, Arizona State University, Tempe, AZ 85287, USA. Email: mneveu@asu.edu.

Context: Thermal models struggle to sustain an ocean on Enceladus, even with tidal heating [1-5]. In contrast, Mimas, Saturn's innermost mid-sized moon, is surprisingly geologically inactive, although likely differentiated [6]. An ocean on Mimas would lie below warm ice, subject to tidal dissipation at a rate 30 times higher than on Enceladus [7]. Strong tides would drive surface activity and circularize Mimas' orbit, regardless of dissipation inside Saturn [7-9]. Yet, Mimas' orbit is four times as eccentric as Enceladus', and not in an eccentricity-type resonance with other moons. Previous studies suggested that Enceladus' lower surface area:volume ratio and higher density (i.e. more abundant radionuclides) may have warmed it enough for tidal dissipation to produce heat and melt, whereas Mimas may never have been warm enough to be sufficiently tidally heated [10-12]. However, none of these studies explicitly modeled tidal dissipation.

Model: We model the thermal evolution of Mimas and Enceladus from formation to the present. We use the 1-D code *IcyDwarf* [13,14] to model partial or full ice-rock differentiation, ammonia antifreeze, parameterized convective heat transfer both in the shell and due to hydrothermal flow, and radiogenic, gravitational, and chemical heating. We have added viscoelastic tidal heating [15-17], as well as porosity (model simplified from [18]) and its effects on thermal conductivity [19,20]. Between simulations, we vary the time of accretion (short- and long-lived radionuclide content), initial temperatures, porosities, and structure (homogeneous or rocky core + icy shell), as well as tidal dissipation models (elastic, Maxwell, Burgers, or Andrade).

Results and discussion: Successful evolution scenarios must yield differentiated moons [6], an extant ocean on Enceladus, but no dissipative interior on Mimas (which likely precludes ocean emplacement or persistence). We have yet to find a set of realistic conditions that satisfies all criteria. Melting is favored in insulating interiors (undifferentiated and/or porous). Ocean sustainability hinges on tidal dissipation, but is also favored by undifferentiated crust and hydrothermal circulation, which efficiently transports heat from the radiogenic core into the hydrosphere. Unlike previous findings [10-12], most sets of initial conditions that yield an ocean on Enceladus also yield one on Mimas, for which the positive tidal feedback on ocean persistence is stronger. This highlights the need to explicitly model tidal effects on thermal evolution.

Our simulations produce an extant ocean on Enceladus if (1) it retains an insulating crust (Fig. 1); or (2) with Andrade-like dissipation, which yields an ice thickness of 50 km, or 25 km if dissipation is ten times higher as suggested by [17]. In scenario (1), Mimas has no ocean, but remains undifferentiated. In scenario (2), Mimas also has an ocean.

Ongoing work: Because differentiation requires ice softening, conducive to runaway dissipation, a scenario in which Mimas accretes rock before ice could explain its present state [21]. It would then never heat up enough for tidal feedbacks to take place, whereas Enceladus would. We are now testing such scenarios.

References: [1] Roberts J. H. and Nimmo F. (2008) *Icarus, 194,* 675–689. [2] Shoji D. et al. (2014) *Icarus, 235,* 75–85. [3] Roberts J. H. (2015) *Icarus, 258,* 54–66. [4] Travis B. J. and Schubert G. (2015) *Icarus, 250,* 32–42. [5] Malamud U. and Prialnik D. (2016) *Icarus, 268,* 1–11. [6] Tajeddine R. et al. (2014) *Science, 346,* 322–324. [7] Meyer J. and Wisdom J. (2008) Icarus 193, 213–223. [8] Goldreich P. and Soter S. (1966) *Icarus, 5,* 375–389. [9] Lainey V. et al. (2012) *ApJ, 752,* 14. [10] Schubert G. et al. (2007) *Icarus, 188,* 345–355. [11] Malamud U. and Prialnik D. (2013) *Icarus, 225,* 763–774. [12] Czechowski L. and Witek P. (2015) *Acta Geophys, 63,* 900–921. [13] Desch S. J. et al. (2009) *Icarus, 202,* 694–714. [14] Neveu M. et al. (2015) *JGR, 120,* 123–154. [15] Henning W. G. et al. (2009) *ApJ, 707,* 1000. [16] Shoji D. et al. (2013) *Icarus, 226,* 10–19. [17] McCarthy C. and Cooper R. F. (2016) *EPSL, 443,* 185–194. [18] Neumann W. et al. (2014) *A&A, 567,* A120. [19] Shoshany Y. et al. (2002) Icarus, 157, 219–227. [20] Krause M. et al. (2011) *42nd LPSC,* 2696. [21] Charnoz S. et al. (2011) *Icarus, 216,* 535–550.

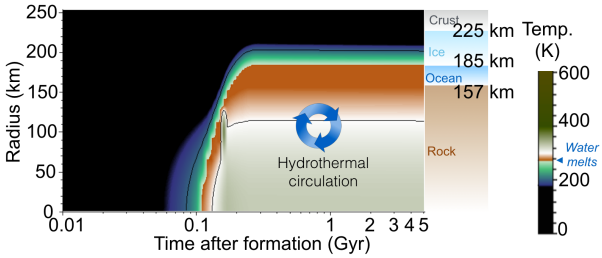

Fig. 1: Thermal evolution of Enceladus for accretion 7 Myr after Ca-Al-rich inclusions, with initial temperature 100 K and 20% initial porosity. Tidal dissipation follows the Andrade model. Maxwell dissipation yields a thinner ocean and thicker crust.

GEOPHYSICS AND TIDAL-THERMAL EVOLUTION OF ENCELADUS. F. Nimmo[1], A. Barr-Mlinar[2], W.B. McKinnon[3], M. Behounkova[4] [1]Dept. Earth and Planetary Sciences, University of California Santa Cruz, 1156 High St, Santa Cruz, CA 95064, USA (fnimmo@es.ucsc.edu); [2]Planetary Sciences Institute, Tucson, AZ, USA [3]Dept. Earth and Planetary Sciences, Washington University, St Louis MO, USA [4]Dept. Geophysics, Charles University in Prague, 180 00 Praha 8, Czech Republic.

For a small body like Enceladus, the main source of energy driving activity comes from its orbit via tidal dissipation. Because the rate of dissipation depends on the internal structure, and the internal structure is affected by tidal heating, the thermal and orbital history are tightly coupled [1].

In this talk, I will first briefly summarize our understanding of the current internal structure of Enceladus. I will then go on to discuss its long-term thermal-orbital evolution, focusing on two key questions. The first is how to explain the observed surface heat flux of up to 16 GW [2]. The second is how to explain the presumed persistence of a global subsurface ocean [3]. Both ultimately depend on understanding how tidal dissipation operates.

Because Enceladus is in an orbital resonance, its eccentricity may grow or decrease depending on the relative rates of tidal dissipation in Enceladus and Saturn. If the eccentricity is in equilibrium, the dissipation rate depends only on dissipation in Saturn and is 1.1 GW for the conventional Q of Saturn of 18,000 [4]. This dissipation rate is much less than the observed heat flow. There are three possible explanations: 1) The long-term dissipation rate is 1.1 GW but Enceladus is unusually dissipative at present (e.g. as a result of periodic thermal-orbital behaviour [5]). 2) The long-term dissipation rate is 1.1 GW but Enceladus is currently releasing accumulated heat at an unusually high rate (e.g. due to convective turnover [6]). 3) The long-term dissipation rate is much greater than 1.1 GW (Saturn is more dissipative). The first two options imply that we are seeing Enceladus at a special time; the third does not.

Astrometric evidence suggests that Saturn may indeed be more dissipative than the conventional estimate [7], at least at the frequencies characteristic of the present-day satellite orbits. Until recently it was assumed that such high dissipation drives rapid orbital migration and implies ages for the inner satellites much less than the age of the solar system. However, recent work [8] suggests that Saturn's Q is a very strong function of frequency, and that the satellite outwards evolution rate is controlled by the evolution timescale of Saturn itself. In this formulation, high present-day dissipation is compatible with an ancient age for the inner satellites.

Because of the high surface area:volume ratio of Enceladus, it is difficult to maintain a global ocean for billions of years [9]. A long-lived ocean is assumed because if the ocean freezes entirely, dissipation is reduced and it is hard to re-melt the ice. Tidal heating in the shell at a rate of 1.1 GW is insufficient to prolong the ocean life-time. Tidal dissipation in the ocean itself would help, but is likely a very minor contribution [10]. Tidal heating in the silicate interior is the most effective way of maintaining the ocean, but it is not yet clear whether such heating is plausible [11]. Higher rates of tidal heating (as suggested above) make the long-term survival of an ocean much more likely.

References: [1] Ojakangas and Stevenson, *Icarus* 66, 341-358, 1986. [2] Howett et al. *JGR* 116, E03003, 2011. [3] Thomas et al., *Icarus* 264, 37-37, 2016. [4] Meyer and Wisdom, *Icarus* 188, 535-539, 2007. [5] Shoji et al., *Icarus* 235, 75-85, 2014. [6] O'Neill and Nimmo, *Nature Geosci.* 3, 88-91, 2010. [7] Lainey et al. *Astrophys. J.* 752, 14, 2012. [8] Fuller et al., *MNRAS* 458, 3867-3879, 2016. [9] Roberts and Nimmo, *Icarus* 216, 426-439, 2011. [10] Chen et al., *Icarus* 229, 11-30, 2014. [11] Roberts, *Icarus* 258, 54-66, 2015.

The near-surface electron radiation environment of Saturn's moon Mimas. T. A. Nordheim[1], K.P. Hand[1], C. Paranicas[2], C. J. A. Howett[3], A. R. Hendrix[4], G.H. Jones[5,6] and A. J. Coates[5,6], [1]Jet Propulsion Laboratory, California Institute of Technology. [2]Applied Physics Laboratory, John Hopkins University, [3]Southwest Research Institute, [4]Planetary Science Institute, [5]Mullard Space Science Laboratory, University College London, [6]Centre for Planetary Sciences at UCL/Birkbeck

Introduction: Saturn's inner mid-size moons are exposed to a number of external weathering processes, including charged particle bombardment and UV photolysis, as well as deposition of E ring grains and interplanetary dust. While optical remote sensing observations by several instruments onboard the Cassini spacecraft have revealed a number of weathering patterns across the surfaces of these moons [1][2][3][4][5], it is currently not entirely clear which external process is responsible for which observed weathering pattern. Here we focus on Saturn's moon Mimas and model the effect of energetic electron bombardment across its surface. Our results are discussed in the context of previously reported Cassini remote sensing observations of Mimas.

Method: To model the access of energetic electrons to different surface locations we used a guiding center, bounce-averaged approach which has previously been employed for the Jovian [6][7] and Saturnian moons [8]. The electron spectrum at the orbit of Mimas was implemented according to the fit functions provided by [8], which are based on averaged measurements from the Cassini Magnetospheric Imaging Instrument (MIMI) Low Energy Magnetospheric Measurement System (LEMMS) at a narrow corridor near the orbit of Mimas (~3.08 Rs) during the period 2004-2013. We populate the energetic electron spectrum from 10 keV to 10 MeV, assuming that the electron flux above 10 MeV is negligible due to macrosignature formation.

The interaction of electrons with the surface of Mimas was implemented using the PLANETOCOSMICS code [9], which is based on the Geant4 toolkit [10]. The simulation geometry was constructed as a flat slab of material consisting of H_2O with a density of 1 g/cm^3. For each primary particle simulated, the energy deposited by all primary and secondary particle interactions within the surface geometry layer was recorded at 1 µm depth intervals.

Results: We predict a lens-shaped electron energy deposition pattern which extends down to ~cm depths at low latitudes near the center of the leading hemisphere. These results are consistent with previous remote sensing observations of a lens-shaped color anomaly[4] as well as a thermal inertia anomaly at this location [2][3][5]. At the trailing hemisphere, we predict a similar lens-shaped electron energy deposition pattern, which to date has not been observed by the Cassini optical remote sensing instruments. We suggest that no corresponding lens-shaped weathering pattern has been observed on the trailing hemisphere due the comparatively short range of lower energy (<1 MeV) electrons into surface ice, as well as competing effects from cold plasma bombardment.

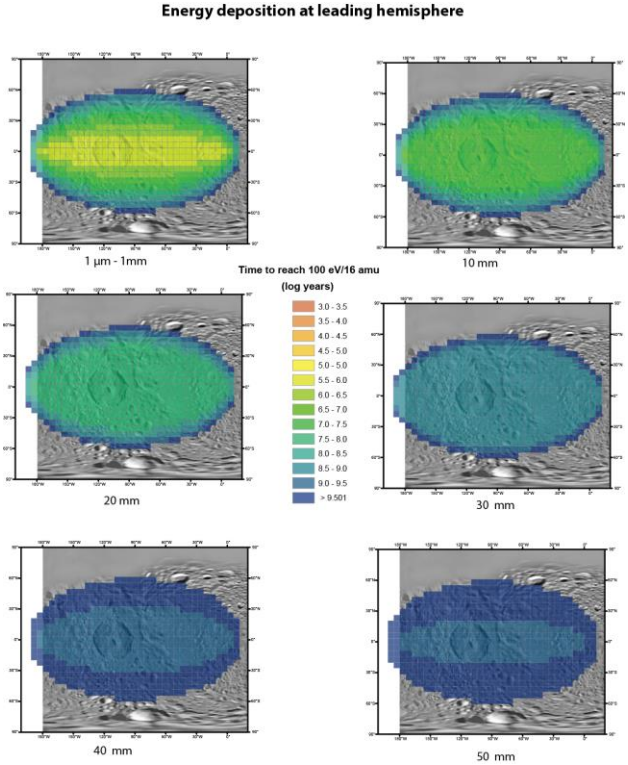

Figure 1 - Energy deposition maps at different depths at the leading hemisphere of Mimas. The energetic electron dose is given in terms of years to reach a significant dose of 100 eV/ 16 amu, which is equal to a dose of 6.03 x 10^{10} Rad.

References: [1] Hendrix, A.R. et al (2012) *Icarus 220*, 922–931. [2] Howett, C.J.A. et al. (2011) *Icarus 216*, 221–226. [3] Howett, C.J.A. et al. (2012) *Icarus 221*, 1084–1088. [4] Schenk, P. et al. (2011) *Icarus 211*, 740–757. [5] Filacchione, G. Et al (2016) *Icarus 271*, 292–313. [6] Patterson, G.W. et al. (2012) *Icarus 220*, 286–290. [7] Paranicas, C. et al. (2001) *Geophys. Res. Lett. 28*, 673–676. [8] Paranicas, C. et al. (2014) *Icarus 234*, 155–161. [9] Desorgher, L. et al. (2005) *Int. J. Mod. Phys. A 20*, 6802–6804. [10] Agostinelli, S. et al. (2003) *Nucl. Instruments Methods Phys. Res. Sect. A 506*, 250–303.

LANDSLIDE PHENOMENA ON SATURN'S ICY MOON: RHEA. R.Parekh, S.Vijayan and B.Sivaraman, Physical Research Laboratory,India. rutuparekh02@gmail.com; vijayan@prl.res.in

Introduction: Rhea, the second largest satellite of Saturn has undergone the geological activity at larger scale for longer period of time[1]. Airless moon of Saturn shows numerous stratigraphic features which were analysed earlier from Voyager mission [1,2,3]. The geological landform includes presence of lineaments, scarps, grabens, ridges, fault lines, grooves [4] etc. Through the treasure of high resolution data provided by Cassini mission on multiple flybys of Rhea starting from 2005, it is possible to sneak into this icy moon in more efficient way. Landslide is one of the most common geological activities seen on the surface of the earth till day. However, this phenomenon is already observed at large scale on other planets like Mars [5, 6], Moon [7], Venus [8] and few icy satellites like Iapetus [10], Io [11] and Rhea [10]. The presence of mass wasting on these planets shows some activity similar to the surface of earth. Additionaly, mass wasting on one of the youngest crater called Inktomi[9] shows that the surface of Rhea was active till few years back.

Imaging datasets: To study the landslide phenomena image was downloaded from USGS Pilot site. Cassini Narrow Angle Camera (NAC) and Wide Angle Camera (WAC) provide images which resolution varies from 10 m/pixel to ~800 m/pixel depending upon the area of study.

Observations: Located at leading hemisphere of Rhea, Nishanu crater (9°S,129°W) shows many unusual geological features at its current condition. The elliptical shape central uplift and absence of ejects blanket on ~117 km diameter crater shows that formation of this crater took place long back. The post impact large landslide at inner crater wall altered the crater rim at its north east direction (Fig.1) and small scale avalanche scare is quite prominent in the eastern direction of the landslide which seems to be affected the rim of another unknown crater nearby. On planetary bodies chemical and physical weathering process plays vital role in the reformation of existing surface structure. According to [9] on icy bodies due to friction within the rock, the surface ice melts which makes the floor slippery enough to form landslides. This could be one of the mechanisms for landslide at current location on Rhea however; further laboratory evidences can give more insight about avalanche. The landslide mechanism other than Moon, Mars and Earth is least explored in detailed because of limited high resolution image data. To generate productive results author will derive observation regarding volume and frictional coefficient (H/L). For, Mars and Earth H/L give inverse trend with increase in landslides length studied by [6,12,13,14], for Iapetus it is independent of this relation and for Rhea similar study carried out by [10] but only for two sites.

Discussion: Add onto this, on the basis of age difference between Nishanu crater and landslide, it is possible to have deep understanding regarding formation of mass wasting; whether it is a result of impact effect or any weathering process. If any physical weathering process is associated with it then what are the feasible driving factor behind it, and how it formed. The idea will be taken further by mapping the landslide locations on Rhea through which it will be possible to get the understanding of surface composition and its structure.

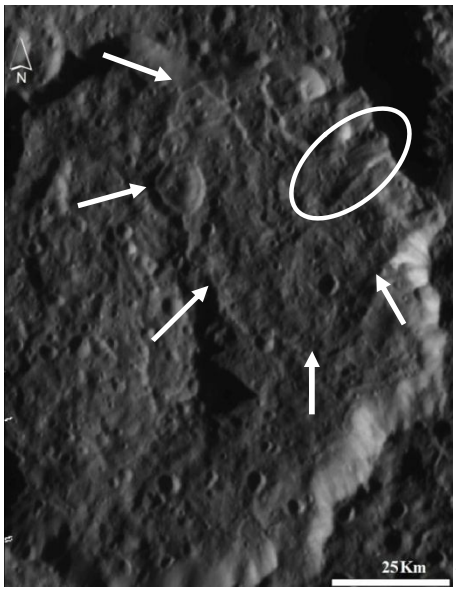

Figure 1 Part of Nishanu crater acquired from ISS NAC with product id N1665994776, The image resolution is approx. 257m/pixel. The arrows indicate area of landslide and avalanche scarps highlighted in white circle.

Reference:[1]Palencia J.B. (1985), *NASA-TM 87563* ,585-587.[2] Smith et al. (1981), *Science 212*, 163-191.[3] Moore J. M. et al. (1985), *JGR 90 (suppl.)*, C785-C795.[4] Thomas P. G. (1987), *Icarus 74*, 554-567.[5]Lucchita B.K. (1979), *JGR 84*,8097-8113.[6]Quantin C. et al. (2004), *PSI 52*,1011-1022.[7] Howard K.A. (1973), *Science 180*,1052-1055.[8]Malin M.C.(1992), *JGR 97*,16337-16352.[9]Melosh J.H.(2011), *Uni. Press Cambridge*,340-344.[10]Singer K. et al. (2012),*Nature Geosci. 5*, 574-578. [11]Schenk P.M. (1998), *Science 279*, 1514-1517. [12]McEwen A.S (1989), *Mars. Geology 17*,1111-1114.[13]Harrison K.P. & Grimm R.E.(2003), *Icarus163*,347-362.[14]Collins G.S. et al.(2003),*JGR 108*,2473-2486.

THE GEOLOGICAL HISTORY AND TECTONICS OF ENCELADUS. G. W. Patterson[1], G. C. Collins[2], P. Helfenstein[3], S. A. Kattenhorn[4], R. T. Pappalardo[5], P. Schenk[6], [1]Johns Hopkins Univ. Applied Physics Lab., Laurel, MD (Wes.Patterson@jhuapl.edu), [2] Wheaton College, Norton, MA, [3]Cornell Univ., Ithaca, NY, [4]University of Alaska Anchorage, Anchorage, AK, [5]Jet Propulsion Laboratory, Pasadena, CA, [6]Lunar and Planetary Institute, Houston, TX.

Introduction: Image data of Enceladus shows clear evidence of tectonic activity and episodic partial resurfacing [1-3]; suggesting a geological history that is remarkably complex for a moon with a mean radius of ~250 km. The key to understanding that history is buried in and, to some extent, obscured by: 1) the complex geological relationships between the SPT and other recognized geological provinces on Enceladus, 2) the distribution and density of observed craters on the surface, and 3) the distribution, orientations, and cross-cutting relationships of tectonic features across the surface of Enceladus.

Geological provinces: Most notable among the recognized geological provinces on Enceladus is the South Polar Terrain (SPT). It harbors active plumes containing water vapor, dust, and other materials erupting from fractures, referred to as tiger stripes, and is bound by a circumpolar chain of south-facing scarps and confined mountain chains [4,5]. Fissure-style venting [6] and discrete geyser eruptions [7] have been observed for both the tiger stripes and associated fractures. Analyses of this region have revolutionized our understanding of the evolution of icy satellite surfaces [e.g., 8-11]. However, Enceladus' south polar terrain tells only the most recent part of the story of this unique icy body. Distinct geological provinces on the leading and trailing hemispheres of Enceladus that share characteristics with the SPT have also been recognized [cf. 3,12]. Analyses of these provinces, and their relationship to each other, have provided insight into the thermal evolution of the satellite [13,14], the potential for reorientation of its spin-pole axis [8,9], and the potential for variability in the rheological and mechanical properties of its icy shell [10,15].

Crater morphology/distribution: Crater morphologies observed on Enceladus are generally consistent with those observed for other icy Saturnian and Galilean satellites [16,17] and viscous relaxation and/or infilling of craters on Enceladus is apparent [18,19]. Analyses of the latitude dependent distribution of relaxed and buried craters on Enceladus has provided important insight into the thermal evolution of its ice shell and into the role of in-falling SPT plume and E-ring material in the crater modification process.

Tectonics: Enceladus exhibits a variety of tectonic landforms [20], including: isolated straight troughs and pit chains; deep, steep-sided depressions called chasmata; a diversity of morphologies of curvilinear ridges; sets of closely spaced parallel ridges and troughs, sometimes defining tabular bands; and double-ridged tiger stripes at the south pole. The distribution and cross-cutting relationships of tectonic features on Enceladus have been used to define distinct regions of the satellite's surface [1,3,4,11]. An analysis of the orientations of observed fracture patterns within the SPT suggest the formation of at least some tectonic features is consistent with a temporally varying global stress field caused by nonsynchronous rotation of a floating ice shell [11].

Summary: The geological history of Enceladus appears to be divided into distinct episodes of locally-focused activity. The conclusions drawn from analyses of the recognized geological provinces of Enceladus, the morphologies and distributions of craters, and the distributions and orientations of tectonic structures each provide a piece to the puzzle that represents the geological history of Enceladus' surface. Understanding that history requires integrating these insights, and others not highlighted here, into a self-consistent picture of the surface evolution of this unusual moon.

References: [1] Smith et al. (1982) Science 215, 504–537. [2] Squyres et al. (1983) Icarus 53, 319–331. [3] Spencer et al. (2009) *in* Saturn from Cassini–Huygens, 683–724, Springer, New York. [4] Porco, et al. (2006) Science 311, 1393–1401. [5] Spencer et al. (2006) Science 311, 1401–1405. [6] Spitale et al. (2015), Nat, 521, 57. [7] Porco et al. (2014) AJ, 148, 45. [8] Nimmo and Pappalardo (2006) Nature 441, 614–616. [9] Collins and Goodman (2007) Icarus 189, 72–82. [10] Barr (2008) J. Geophys. Res. 113, E07009. [11] Patthoff and Kattenhorn (2011) Geophys. Res. Lett., 38, L18201. [12] Crow-Willard and Pappalardo (2015) J. Geophys. Res. 10.1002/2015JE004818. [13] Bland et al. (2007) Icarus 192, 92–105. [14] Giese et al. (2008) Geophys. Res. Lett. 35, L24204. [15] O'Neill and Nimmo (2010) Nature Geosci. 3, 88-91. [16] Schenk et al. (2004) *in* Jupiter, 427-456, Cambridge University Press, Cambridge, U.K. [17] Jaumann et al. (2009) *in* Saturn from Cassini–Huygens, pp. 637–681, Springer, New York. [18] Bray et al. (2007) LPSC XXXVIII, #1873. [19] Kirchoff and Schenk (2009) Icarus 202, 656-668. [20] Nahm and Kattenhorn (2015) Icarus 258, 67-81.

RIDGES OF ENCELADUS: PRESERVING ANCIENT AND RECENT TECTONICS BEYOND THE SOUTH POLAR TERRAIN. D.A. Patthoff[1,2], R.T. Pappalardo[2], A. Maue[3], E.S. Martin[4], H.T. Chilton[5], P.C., Thomas[6]. [1]Planetary Science Institute, (apatthoff@pis.edu), [2]Jet Propulsion Laboratory, [3]Boston University, [4]National Air and Space Museum, [5]Georgia Institute of Technology, [6]Cornell University.

Introduction: The surface of Enceladus has a diverse array of geologic terrains that includes ancient cratered regions, young ridges, and numerous fractures. Here we focus on the numerous ridges that are observed in the terrains outside of the active south polar terrain (SPT). North of ~55° S latitude, Enceladus can be broadly divided into the the young tectonic terrains that dominate the leading and trailing hemispheres and the older Saturnian and anti-Saturnian cratered terrains [1]. Here we explore the geometries, morphologies, relative ages, and potential formation mechanisms for ridges observed outside the SPT.

Ridge types: *Leading hemisphere*. In their geological map, [1] divided the leading hemisphere into 3 sub-terrains: northern and southern regions, surrounded by a curvilinear terrain. Each region contains different types of ridges. In the northern portion of the leading hemisphere terrain are two ridge types, one smaller in amplitude and wavelength, and a second larger amplitude set (Fig. 1). The smaller ridges have a spacing of 1–2 km, are ~10s m high, and 1–20 km long. The larger ridges are ~600 m high, 15–35 km long, show a lens-like shape in map view, and in cross-section are broad with flank slopes of 6–30°. The southern leading hemisphere terrain is dominated by ridges that are similar in size and shape to the smaller ridges to the north; however, this region lacks a larger ridge set. The raised topography suggest these ridges likely formed as a result of a compressional stress event.

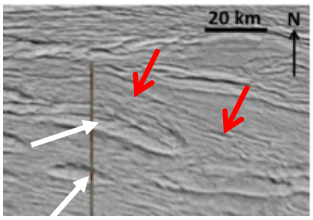

Fig 1. Leading hemisphere northern ridge terrain. Large (white arrows) and small ridges (red arrows) are visible. Vertical line shows the location of a limb profile. Image comprised of image N160436392.

Trailing hemisphere. The trailing hemisphere is dominated by a striated plains unit which is composed of small amplitude (10s m), roughly N-S oriented ridges and troughs [2]. These ridges appear very similar to the "ropey terrain" of the south polar terrain in their morphology and the geometry of their intersections with other ridges. However, they do not appear to be associated with any tiger-stripe-like structures or jetting activity. The second ridge type, the "dorsa," stand up to ~1 km above a region of the trailing hemisphere that is slightly depressed. The dorsa are ~2.5 km wide, and in map view (Fig. 2) they can bifurcate in a branching manner with branches that intersect other dorsa at near right angles. They can reach lengths of ~50 km and heights of 600–800 m [3]. Our analyses show that they have gentle sloping flanks of ~20° and appear rounded to trapezoidal in cross section, and potentially accommodated ~10% shortening.

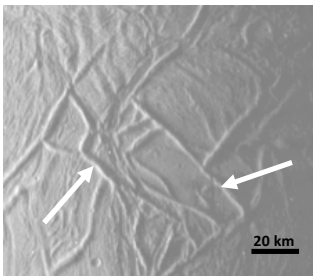

Fig 2. Saturn shine image illuminating the dorsa. Cylindrical projection of image N1675146616. White arrows show location of some dorsa.

Cratered terrains. Dispersed among the numerous craters of the region are ancient ridges. These ancient ridges are generally <10 km long and ~100 m high and linear (Fig. 3). Most ancient ridges are cut by other identifiable features including craters and fractures, suggesting they pre-date all other deformation [4, 5].

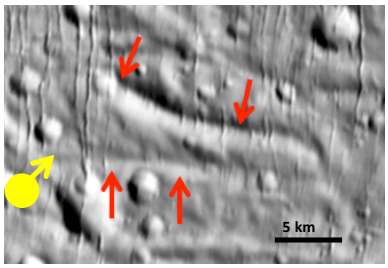

Fig 3. Cratered terrain. Red arrows point to ancient ridges. Image from Cassini ISS basemap [6].

Discussion: Distinct sets of ridges with unique morphologies and geometries are observed in each of Enceladus's major tectonic terrains. Ridges of any one type are almost exclusively observed in only one region, i.e. dorsa are observed only in the trailing hemisphere. This suggests potentially unique formation conditions for each type of ridge and different styles of tectonics for each terrain. The large difference in ages between the ridges within the cratered regions and those on the leading and trailing hemispheres suggests two major periods of compression separated by a long history of relative quiescence.

References: [1] Crow-Willard & Pappalardo (2015), *JGR* 10.1002/2015JE004818. [2] Bland, et al. (2007) *Icarus, 192*, 92-105. [3] Spencer et al. (2009) in *Saturn from Cassini-Huygens*, 683-724. [4] Michaud et al. (2008) 39th *LPSC,* abs 1391. [5] Martin et al (2015) 46th *LPSC*, abs 1620. [6] Roatsch et al. (2013) *Plant. Space Sci. 77*, 118-125.

ANY SMALL BODIES NEAR THE ENCELADUS ORBIT. N. I. Perov, Cultural and Educational Centre named after Valentina Tereshkova, ul. Chaikovskogo, 3, Yaroslavl, 150000, Russian Federation. E-mail: perov@yarplaneta.ru.

Introduction: As it is known, Enceladus is one of only three outer Solar system bodies (along with Jupiter's moon Io and Neptune's moon Triton) where active eruptions have been observed. Radius of Enceladus' gravity sphere action is equal to 488 km that is less in comparison with the radius of Enceladus (500 km). Here we use a) mass ratio of Enceladus (m_E) and Saturn (m_S) equals $m_E/m_S=1.900204\cdot10^{-7}$; b) semimajor axes ($a_E$) and eccentricity ($e_E$) of Enceladus orbit are equal to $a_E=236.8\cdot10^3$ km and $e_E=0.0047$ respectively [1]. Below the closed trajectories of hypothetical small bodies near the orbit of Enceladus are stated in the model of motion of particle with negligible small mass m_3 in the frame of the planar circular restricted three body problem [2], [3]. Let us, m_S and m_E are mass of main bodies, r_{SE} is a distance between these bodies, *and G* is the gravitational constant. We find the region of the point motion (m_3), – distance r_3, ($\boldsymbol{r_3}=\boldsymbol{r}_3(x_3,y_3)$) *in* respect of the system center mass, – and numerically investigate the region of the particle stability motion, using method of Runge-Kutta integrating, where *N* is the numbers of points in the figures. The regions of the particles stable motion, in the given model, will be considered as the regions of concentration of undiscovered bodies in this system.

Fundamental Equation: In accordance with works [2] and [3] we have the vectorial differential equation (1) of the particle m_3 motion in the uniformly rotating system

$$d^2\boldsymbol{r_3}/dt^2+Gm_S(\boldsymbol{r}_3-\boldsymbol{r}_S)/(|\boldsymbol{r}_3-\boldsymbol{r}_S|)^3 + Gm_E(\boldsymbol{r}_3-\boldsymbol{r}_E)/(|\boldsymbol{r}_3-\boldsymbol{r}_E|)^3)-2[d\boldsymbol{r}_3/dt, \boldsymbol{\Omega}]-\Omega^2\boldsymbol{r}_3 = 0. \quad (1)$$

Here, $\boldsymbol{r}_3$ is the radius-vector determined the position of considered point (m_3) in respect of the center mass of the system. $\boldsymbol{r}_S$ and $\boldsymbol{r}_E$ are radii – vectors in respect of the center mass of the system determined the positions of major bodies with mass m_S and m_E correspondingly. Ω is the angular velocity of uniformly rotation of the major bodies.

$$\boldsymbol{r}_S=-(m_E/(m_E+m_S))\boldsymbol{r}_{SE},\ \boldsymbol{r}_E=(m_S/(m_S+m_E))\boldsymbol{r}_{SE}, \quad (2)$$

$$\Omega=\sqrt{\frac{G(m_S+m_E)}{r_{SE}^3}}.$$

Examples: For the numerical experiments we put $G=6.672\cdot10^{-11}$ $m^3/(sec^2\cdot kg)$, $m_S=568.36\cdot10^{24}$ kg (mass of the Saturn), $m_E=1.08\cdot10^{20}$ kg is mass of Enceladus. In the process of the equation (1) solving we use the following units: m_S is the unit of mass, r_{SE} is the unit of length, the unit of time *t* is corresponded for the case $G=1$. Moreover, we put for all considered cases (except fig. 4) the following *initial* conditions: $x_S\neq0$, $dx_S/dt=0$, $y_S=0$, $dy_S/dt=0$, $x_E\neq0$, $dx_E/dt=0$, $y_E=0$, $dy_E/dt=0$, $x_3\neq0$, $dx_3/dt=0$, $y_3=0$, $dy_3/dt=0$. The results of the numerical experiments in intervals of time motion corresponded hundreds and thousands revolutions of major bodies are presented in Fig. 1 – 5.

Conclusions: a) For the curve (Fig.1) the velocity of m_3 equals zero only in initial moment of time but in the work [2] the corresponding curves are plotted, mainly, only for V≡0. b) Asteroid 2010 SO16 moves along the trajectory like presented in Fig. 1. and it approaches the Earth so, it may be supposed – there are undiscovered small bodies in the system "Saturn and Enceladus" moving along the curves presented in Fig. 1. c) Fig1. illustrates closed trajectories of any small bodies near Enceladus. d) Fig. 1. is not contradicted with the celestial mechanical model of the stable motion of dust matter near the points of Lagrange in the considered system).

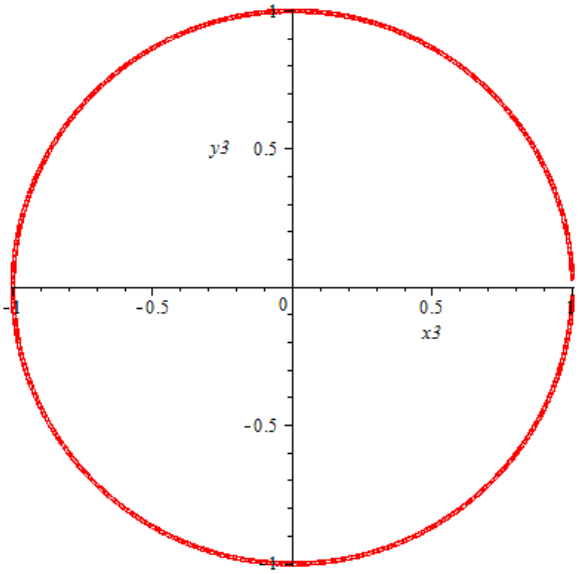

Fig.1. The trajectory of the small body m_3 in the system "Saturn ($m_S=1$) and Enceladus ($m_E=m_S/(5.26259259\cdot10^6)$)", in respect of the center mass of the system (m_S and m_E). $x_S=-1.900203734918\cdot10^{-7}$, $x_E=0.999999809996$. $x_{30}=-x_E-\varepsilon$. $\varepsilon=1\cdot10^{-3}$. Unit of length equals r_{SE}. Time τ of m_3 motion varies from $\tau_i=0$ to $\tau_f=10000$ units of time.

References: [1] http://archive.org/pdf1104.0036v. [2] Szebehely V. (1967) *Theory of Orbits. The Restricted Problem of Three Bodies.* Yale University. New Haven Connecticut. Academic Press New York and London. [3] Perov N. I. et. al. (2011) *Theoretical Methods of Localization in the Space–Time of Unknown Celestial Bodies,* Yaroslavl, YSPU, 208 pp.

THE VELOCITY OF WATER MOLECULES IN THE ENCELADUS PLUMES. Mark E. Perry[1], Benjamin D. Teolis[2], Dana M. Hurley[1], J. Hunter Waite, Jr.[2], Ralph L. McNutt, Jr.[1], [1]The Johns Hopkins University Applied Physics Laboratory, Laurel, MD. [2]Southwest Research Institute, San Antonio, TX.

During four Enceladus encounters between November 2009 and October 2015 (Table 1), the Cassini Ion and Neutral Mass Spectrometer (INMS) operated in its Open Source Neutral Beam (OSNB) mode. In the OSNB mode, INMS makes direct measurement of the velocities of the neutrals. Although the velocity data from OSNB measurements are coarse, they provide strong constraints on the speed distribution of H_2O molecules within and surrounding the plumes.

In the OSNB mode, the velocity of the neutrals measured by INMS are determined by the angle of the INMS boresight, which sets the direction of the molecules, and the INMS compensation velocity parameter (V_{COMP}), which sets the speed of the molecules. The vector addition of this velocity with Cassini's velocity provides the neutrals' velocity relative to Enceladus. During E8, E11, and E16, V_{COMP} was fixed, but Cassini rotated so that INMS scanned the velocity of neutrals. Cassini's rotation produced a single velocity scan, where the measured molecules had velocities that were radial from Enceladus with speeds increasing from 0 to 2 km/s. E21 operations were different: Cassini's attitude was fixed and V_{COMP} was scanned throughout the encounter to purposely sample the velocity distribution of the plume multiple times.

Flyby	Min alt	Location relative to plume
E8	1,600km	In a high-velocity jet
E11	2,300km	Slower, broader velocities
E16	100km	Far from south pole region
E21	49km	Deep in plume; multiple scans

Table 1. Enceladus encounters with OSNB measurements. Except for E21, Cassini rotated during each encounter and the compensation velocity (V_{COMP}) was fixed. During E21, pointing was fixed at 3° relative to Cassini's flight path and V_{COMP} was varied to obtain velocity scans.

For each OSNB measurement, INMS accepts molecules with a small range of speeds and a narrow range of angles. For H_2O at the velocities of the encounters with Enceladus, the speed resolution is ±300 to ±600 m/s and the angular resolution is ±2° to ±3° [1]. For E8, E11, and E16, the measurement ranges translate to an uncertainty in the speed of approximately ±0.3 km/s. The angular resolution of the measured molecules was sufficient to identify Enceladus as the source of the molecules. During E21, the velocity-space dependence of the neutral density is convolved with the spatial dependence as Cassini traveled through the plumes.

The H_2O neutrals measured during E8 had a Mach-4 distribution centered on 1.2 km/s with a width of ±300m/s, which corresponds to a temperature of 65K (Figure 1). The Mach-4 result is consistent with the width of dense, high-velocity jets as deduced from UVIS occultation data [2]. An interpretation of the OSNB velocities is that the H_2O source is one or more of the dense, high-velocity jets. Recent, improved ground calibration tests indicate that the distribution may be shifted to lower velocities, with the peak velocity closer to 1 km/s. This lower velocity meets the limit imposed by the ultimate velocity of adiabatic expansion, which is 1,004 km/s for H_2O molecules at their triple-point temperature.

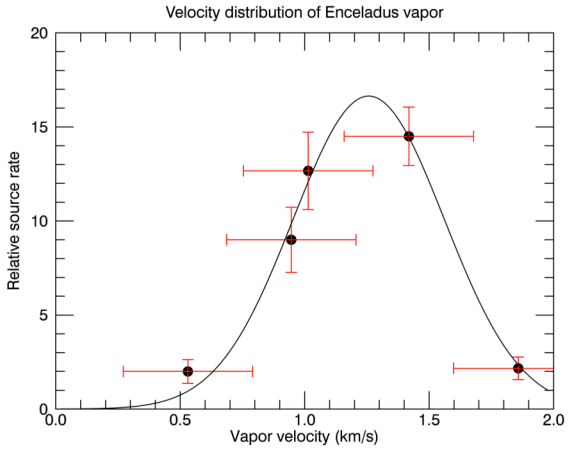

Fig. 1. A drifted Maxwellian distribution fit to the E8 OSNB measurements of neutral velocity. The distribution has a bulk velocity of 1.25±0.1 km/s and a width of ±300 m/s.

E11 showed a bulk velocity of 750 m/s with a width of ±430 m/s. This slower, broader distribution of velocities may represent the more-diffuse emissions that comprise most of the plume. Velocity measurements from E16, which was outside the plumes, shows velocities centered on 0 km/s, as expected when measuring the velocities of the neutral cloud orbiting Saturn at the distance of Enceladus.

Because E21 measurements simultaneously varied both angle and speed, interpretation depends on modeling, which is ongoing.

References: [1] Waite J. H. et al. (2004) *SSR, 114*, 113 [2] Hansen et al. (2011) *GRL, 38*, L11202..

INTERPLANETARY DUST FLUX TO SATURN'S ICY SATELLITES: A POTENTIAL SURFACE CONTAMINANT SOURCE? A. R. Poppe[1], [1]Space Sciences Laboratory, 7 Gauss Way, University of California at Berkeley, Berkeley, CA, 94720 (poppe@ssl.berkeley.edu)

Introduction: Despite their dominant water ice surface composition, many of Saturn's satellites are contaminated by various amounts of dark material. The most striking example of this is Iapetus, with its well-known global color and surface compositional dichotomy. Additionally, dark material is also found to contaminate the spectra of Hyperion, Rhea, and Dione [1,2]. Both interplanetary and Phoebe-originating dust grains have been invoked as sources of these contaminants (among others) [e.g., 3,4]; however, the exact balance between these two dust sources (and their potential variability at different satellites) has not been thoroughly quantified.

Recent work has modeled the deposition of dust grains ejected from the surface of Phoebe onto the surface of Iapetus via a series of numerical integrations [5]. This work found that grains > 10 μm were almost certain to strike Iapetus and additionally found that these grains struck Iapetus' leading hemisphere in a similar spatial pattern as seen in Iapetus' albedo. Importantly, grains that did not strike Iapetus were either (i) efficiently swept up by Titan (due to Titan's large cross section) or (ii) rapidly lost to Saturn or ejected from the system entirely due to perturbations by solar radiation pressure (mainly for the smallest sized grains). Thus, while the work of [5] can most plausibly explain the Iapetian surface dichotomy, it is not clear that Phoebe grains are also the dominant contaminant for the other inner icy satellites.

Here, we investigate the possibility that interplanetary dust grains (IDPs) may contribute to the contamination of Saturn's mid-sized icy satellites, especially those inside the orbit of Titan (i.e., Rhea, Dione, Tethys, Enceladus, and Mimas). In contrast to the Phoebe-originating dust which faces a significant dynamical barrier in the form of Titan, IDP fluxes penetrate directly into the entire Saturnian system on hyperbolic trajectories. Thus, to first order, these grains should have nearly equal access to all of Saturn's satellites.

Methodology: In order to quantify the magnitude, variability, and spatial distribution of interplanetary dust grain fluxes to the saturnian satellites, we have combined the results of a recent model of interplanetary dust grains fluxes in the outer solar system [6] with a planetary dynamics model that tracks the dust grain phase space distribution within a planetary system (i.e., Saturn). The IDP flux model suggests that the total dust flux to Saturn is a nearly co-equal mix of dust originating from Edgeworth-Kuiper Belt objects, Jupiter-family comets, and Oort Cloud comets, see **Figure 1**. The dust grain flux and velocity distribution at any point within the Saturnian system is then determined by applying Liouville's theorem (i.e., phase space densities are conserved along trajectories). Thus, we backwards integrate dust grain trajectories from a common starting point with a distribution of velocities (i.e., a satellite surface) out to the saturnian Hill radius and assign the appropriate IDP phase space density (as determined from the IDP model [6]) to each starting condition. By integrating the aggregated phase space distributions over all initial conditions, we calculate the flux and velocity distribution of IDP grains at each point in the saturnian system.

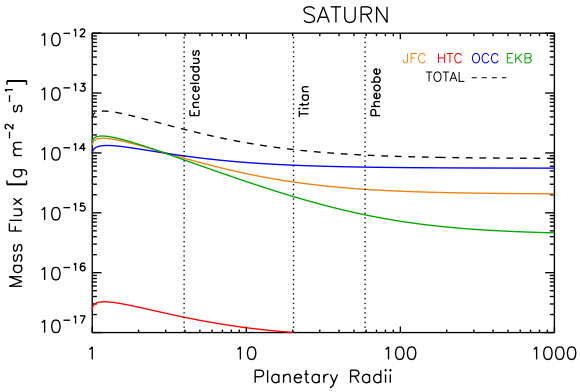

Figure 1: The interplanetary dust grain mass flux to Saturn as a function of distance from Saturn's cloud-tops [6].

Comparison to previous work: Our initial results suggest that IDP fluxes are (i) lower to Iapetus than those from Phoebe (consistent with Phoebe as the dominant contamination source at Iapetus [5]), (ii) approximately equal to Phoebe dust fluxes to Titan, and (iii) potentially the dominant source of exogenous dust flux (i.e., not from the E-ring) to the inner satellites. We will present the magnitude, spatial variation, and velocity distribution(s) of the IDP flux to each of Saturn's icy satellites and discuss the implications for surface contamination.

References: [1] Jaumann, R., et al. (2009), in *Saturn from Cassini-Huygens*, ch. 20 [2] Stephan, K., et al. (2012) *Plan. Space Sci.*, **61** [3] Soter, S. (1974), *IAU Colloquium*, **28**, Cornell Univ. [4] Clark, R. N., et al. (2008), *Icarus*, **193** [5] Tamayo, D., et al. (2012) *Icarus,* **215**, 260-278. [6] Poppe, A. R. (2016) *Icarus,* **264**, 369-386.

COMPARING UVIS OCCULTATIONS OF THE SUN AND STARS VIA JET MODELING. G. Portyankina[1], L. W. Esposito[1], C. J. Hansen[2], and K.-M. Aye[1], [1]LASP, 3665 Discovery Dr., Boulder, CO 80303, USA (Gan-na.Portyankina@lasp.colorado.edu), [2]Planetary Science Institute, Tucson, AZ, USA

UVIS observations: The Cassini's Ultraviolet Imaging Spectrograph (UVIS) observed occultations of several stars and the Sun by the water vapor jets of Enceladus. UVIS observed Enceladus jets occulting γOri in 2005, ζOri in 2007, the Sun in 2010, εOri and ζOri in 2011 [1], and εOri in 2016. These observations directly provide data about water vapor column densities along the line of sight (LoS) of the UVIS instrument. To be able to compare relative strengths of the jets between the occultations, one has to consider that each of these UVIS occultations is unique relative to the positions and attitudes of UVIS, Enceladus and occulted body.

Model: We use a 3D direct simulation Monte Carlo (DSMC) model for Enceladus jets to analyze UVIS jet observations [2]. The Monte Carlo model tracks test particles from their source at the surface into space. Jet sources can be placed along the tiger stripes to form extended curtains' sources or at particular locations, for example following [3]. At the end of the simulation run water vapor number density in the domain around Enceladus is calculated. It is converted to the water vapor column density along the LoS by considering the precise 3D geometry of the observation with the help of SPICE [4].

In the case of the isolated jets, each jet is represented by a curve with time of observation on the x-axis and test particle number density on the y-axis. To fit the model to UVIS data we should integrate all jets that are crossed by the LoS at each point of time during the observation. The relative strength of the jets can be modified by multiplying each of them by a coefficient to fit the observed UVIS curve.

RREF and fitting procedure: We developed a fitting procedure that varies jets' relative strengths to find the best fit of their cumulative contribution to the UVIS column density curve during each occultation. For each occultation a matrix J is created and analyzed. A contribution of each model jet is represented by a column of J. Because of observational geometry J-matrices differ between the occultations even if the exact same DSMC model was used. We compute the reduced row echelon form (RREF) of J, which gives us a sub-set of linearly independent jets and then we use this sub-set in the least-square fitting procedure. An example of the resulting fit is shown in Fig. 2.

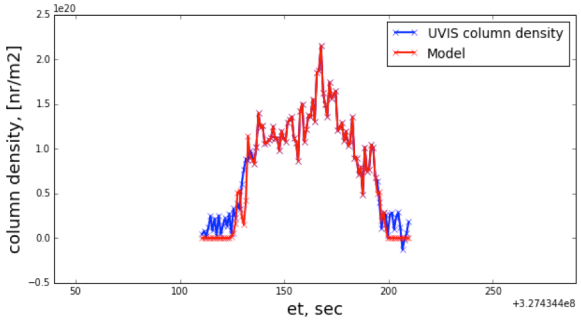

Figure 2: Comparison of water vapor column density derived from the UVIS solar occultation observation 2010 (blue curve) and best fit of 43 modelled jets (red curve).

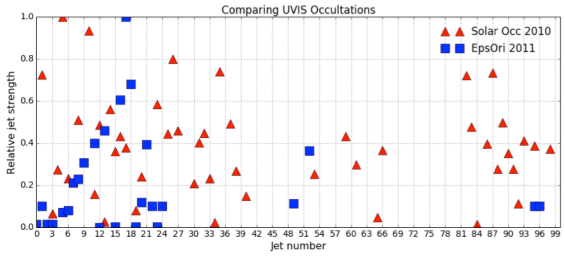

Figure 1: Relative strength of modeled jets resulting from the best fits of DSMC jet model to UVIS data of Solar Occultation 2010 and Epsilon Orionis 2011.

Selected results: The model run for the Solar Occultation in 2010 resulted in the sub-set of 72 linearly independent jets, 43 of which had non-zero contribution to the modeled cumulative water vapor number density after the fitting.

The εOri occultation 2011 was significantly shorter, hence providing fewer data points for the fit. The geometry of the observation was such that LoS was almost perpendicular to the Tiger stripes leading to multiple overlapping jets. The model run resulted in 26 linearly independent jets, and the fit to UVIS data reduced that to 25 non-zero jet contributions.

Fig. 1 shows the relative contributions of the jets for the two occultations. Jet numbers shown on x-axis are consistent with the list by Porco et al. [3]. Multiple jets from the Solar Occultation aren't present in the εOri occultation. This is because the stronger jets on the same LoS overlap them. However, the number of jets are repeatedly found in both observations showing their stability over a year.

References: [1] Hansen et al., 2011 GRL 38 [2] Portyankina et al, 2016, 47th LPSC [3] Porco et al. 2014 The Astronomical Journal 148, 45 [4] Acton, C.H., 1996 PSS 44, 65-70.

Plume and Surface Composition of Enceladus

F. Postberg[1], A.J. Coates[2], R.N. Clark[3], C. Dalle Ore[4], C. J. Hansen[3], M.M. Hedman[5], F. Scipioni[6], J.H. Waite[7]
[1]University of Heidelberg, Germany, e-mail: Frank.Postberg@geow.uni-heidelberg.de; [2]University College London, UK; [3]Planetary Science Institute, USA; [4]SETI Institute, Mountain View, USA; [5]University of Idaho, Moscow, USA; [6]Lunar and Planetary Institute, Houston, USA; [7]South-West Research Institute, San Antonio, USA

Cassini-Huygens' discovery of an active cryo-volcanic plume on Enceladus in 2005 is one of the most astonishing findings of the entire mission. Right from the start, the composition of the plume and its surface deposits was of highest interest. Analyzing this material, emitted from regions deep below Enceladus' surface, provides insights into the moon's internal geochemical and geophysical processes and, as it turned out, can be used to characterize the properties of a subsurface ocean. This review talk gives a general overview on the topic of plume and surface composition and displays a first impression on the respective chapter in the forthcoming book "Enceladus and the Icy Moons of Saturn".

The versatile instrumentation of the Cassini-Huygens spacecraft allows for many different compositional perspectives. The Visible and Infrared Mapping Spectrometer (VIMS) provides information on size, crystallinity and composition of ice grains both on Enceladus' surface, and in the plume. Utilizing stellar and solar occultations, the Ultraviolet Imaging Spectrograph (UVIS) measures chemical constituents in the plume vapour whereas reflectance spectra give hints of the composition of the moon's surface. The Ion and Neutral Mass Spectrometer (INMS) acquired in situ mass spectra of plume vapour during Cassini's frequent passages through the plume. The Cosmic Dust Analyser (CDA) acquired complementary in situ measurements on the chemical constitution of ice grains emitted by Enceladus into the plume and the E ring. The composition of charged atoms and molecules in the plume as well as in Saturn's magnetosphere has been constrained by two other in situ instruments: The Cassini Plasma Spectrometer (CAPS) and the Magnetospheric Imaging Instrument (MIMI).

We will try to cover the current knowledge on Enceladus' plume and surface composition from all these instruments. Over 95% of the ejected icy plume solid material falls back as fine 'snow', thereby covering, a substantial part of the Enceladian surface (Fig. 1) and may accumulate there over geological time-scales. As a consequence, there naturally is a large overlap when assessing plume and surface composition. Plume gases leave Enceladus with greater than escape velocity, populating the Saturn magnetosphere with an abundance of initially neutral species. Consequently, as outlined above, compositional measurements in the E ring and Saturn's magnetosphere, which help to understand Enceladus' plume and surface, will be covered as well. The goal is to combine all these different compositional aspects to one comprehensive and coherent perspective and, where this is not possible, to discuss divergent views and to highlight open issues.

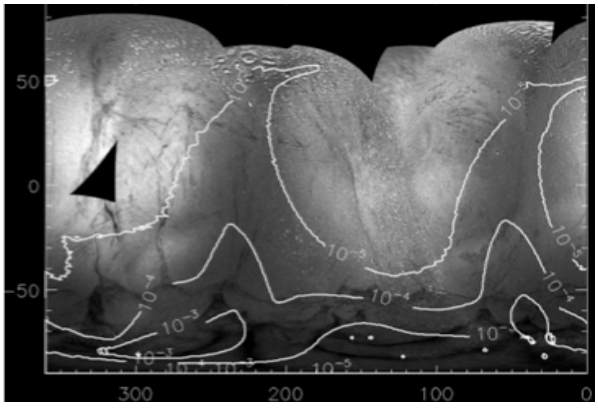

Fig. 1: IR/UV color ratio map of Enceladus with dark regions indicating plume fallout. Contours show the modeled plume deposition. Credits P.Schenk / J.Schmidt / S.Kempf.

Reexamining the role of tidal stress in Enceladus' tectonic history. A.R. Rhoden[1], [1]School of Earth and Space Exploration, ASU, Tempe, AZ 85287, Alyssa.Rhoden@asu.edu.

Introduction: Enceladus' librations and gravity field indicate a global subsurface ocean [1,2]. Hence, Enceladus likely possesses both characteristics thought to drive tidal-tectonic activity on Europa [3]: an ice-covered ocean and an eccentric orbit. There are several additional lines of evidence that tides play a dominant role in resurfacing Enceladus, including the heavily tectonized terrain at Enceladus' south pole (the SPT) that is reminiscent of Europa [4], the orientations of the Tiger Stripe Fractures (TSFs) that correlate with tidal stresses [5], older fracture sets in the SPT that imply rotation of the shell through a diurnal stress field [6], and daily variations in eruptive output from the TSFs [7]. However, several issues need to be reconciled to determine the role of tides and develop a self-consistent model of an ocean-bearing Enceladus.

Discussion: We need to consider implications of:

1) *Spatial variation.* Extensive tectonic resurfacing on Enceladus is largely restricted to the SPT [4]. Older tectonized terrains are located at the equator, near the leading and trailing points, and some fractures are observed in the crater-dominated north polar terrain (NPT) [8]. With a global ocean, what controls the spatial variation in fracture type and density?

2) *Low tidal stresses.* In an attempt to match the variability in eruptive output of the plumes, [9] calculated tidal stresses for many interior structure models; the best fits included either a global ocean under >60 km of ice or a regional sea. Neither of these interiors are compatible with the librations, which indicate a global ocean with an ice shell ~12km thick at the south pole and ~22km thick shell at the north pole [1]. Furthermore, the tidal stress magnitudes for these models peak at ~14 kPa. Europa's tidal stresses peak at ~100 kPa, and fracture modeling suggests failure at ≥50 kPa [10]. If SPT fractures form at <14 kPa, the lack of extensive NPT fracturing is even more problematic.

Global ocean models compatible with the librations can produce tidal stresses in the SPT that are comparable to Europa's but only if the ice shell viscosity is $\leq 10^{13}$ Pa*s [11]; stresses in the NPT are then similarly high. A large difference in ice shell viscosity, in addition to the small change in thickness, can reduce stresses in the NPT by a factor of 2-4, which implies that Enceladus' ice fails at a very precise threshold.

3) *High heat flow*. Craters in the NPT are extremely relaxed, indicating a high heat flow in the recent past [12]. Even a thick insulating regolith is insufficient to reproduce the observations. If the heat flow in the NPT is high, it is harder to justify invoking different thermal structures between the SPT and NPT.

4) *NSR predictions*. Older fracture sets in the SPT appear to show a systematic change in orientation with time, perhaps indicating NSR [6], although the results rely on several simplifying assumptions and an old prediction of the effects of NSR on fracture orientations [13]. More recent work that focused on an equatorial region of Europa showed that fracture orientations would only cycle through ~45° due to NSR, and may not change systematically depending on the failure criterion [14]. If applied to Enceladus' SPT, would NSR account for the fracture orientations? Furthermore, observations of plume activity suggest that new fractures near the TSFs are being activated while other portions are becoming dormant [15]. The orientation changes do not follow the pattern suggested by [6].

5) *Global-scale processes*. Structural mapping of the SPT suggests that the TSFs are more consistent with large-scale motion of the ice shell than with tidal stresses [16], a hypothesis supported by maps of strike-slip faults [17]. Finally, shape models reveal several large depressions that suggest polar wander may repeatedly reorient the shell [18]; past work concluded the shape instead favors a regional sea [19]. Because polar wander provides a potentially important alternative global modification process, reconciling these studies for an ocean-bearing Enceladus is warranted.

Conclusion: These complications force us to question whether diurnal tidal stresses are the dominant modification process on Enceladus. I will present possible unifying hypotheses and tests to determine the nature of fracturing on Enceladus.

References: [1] Thomas, P. et al. (2016) Icarus 264, 37-47. [2] McKinnon, W. (2015) GRL 42, 2137-2143. [3] Kattenhorn, S. & Hurford, T. (2009) In: Europa, 199-236. [4] Porco, C. et al. (2006) Science 311, 1393-1401. [5] Hurford, T. et al. (2009), Icarus 203, 541-552. [6] Patthoff, D. & Kattenhorn, S. (2011) GRL 38, L18201, 1-6. [7] Hedman, M. et al. (2013) Nature 500, 182-184. [8] Crow-Willard, E. & Pappalardo, R. (2015) JGR-Planets 120, 928-950. [9] Behounkova, M. (2015) Nat Geo 8, 601-604. [10] Rhoden, A. et al. (2010) Icarus 210, 770-784. [11] Rhoden, A. et al. (2015) AGU P21B-08. [12] Bland, M. et al. (2012) GRL 39, L17204, 1-5. [13] Greenberg, R. et al. (1998) Icarus 135, 64-78. [14] Rhoden, A. & Hurford, T. (2013) Icarus, 225, 841-859. [15] Spitale, J. et al. (2015) Nature 521, 57-69. [16] Yin, A. & Pappalardo, R. (2015) Icarus 240, 409-439. [17] Martin, E. (2016) GRL 43, 2456-2464. [18] Tajeddine, R. et al. (2015) AGU P21B-06, [19] Collins, G. & Goodman, J. (2007) Icarus 189, 72-82.

Implications of tidal stresses on global ocean models of mid-sized icy moons. A.R. Rhoden[1] W. Henning[2], T.A. Hurford[3], M. Bland[4], G. Collins[5], and R. Tajeddine[6]. [1]School of Earth and Space Exploration, ASU, Tempe, AZ 85287, Alyssa.Rhoden@asu.edu; [2]Department of Astronomy, University of Maryland – College Park, College Park, MD 20742; [3]NASA Goddard Space Flight Center, Code 693, Greenbelt, MD 20771; [4]USGS Astrogeology, Flagstaff, AZ 86001; [5]Physics and Astronomy Department, Wheaton College, Norton, MA 02766; [6]Centre for Astrophysics and Planetary Science, Cornell University, Ithaca, NY 14850.

Introduction: *Cassini* ISS observations have revealed a great deal of diversity among the surfaces of Saturn's mid-sized icy moons. Enceladus is currently, and dramatically, active. Tectonic activity is widespread on Dione and Rhea, while Tethys has limited tectonic activity, and Mimas has an ancient, heavily cratered surface, nearly devoid of fractures. The reason for the geologic diversity of the moons is unknown.

Eccentricity-driven tidal stresses have been invoked to explain activity on Enceladus [e.g. 1], especially due to the presence of subsurface liquid. This mechanism has not been seriously considered for the other icy moons because their eccentricities are low (with the exception of Mimas) and they were not expected to have oceans, which inhibits tidal response. However, more recent work has provided evidence for subsurface global oceans within Mimas [2], Enceladus [3,4], Dione [5,6], and Rhea [5,7], and some new models for the formation of the Saturnian satellites predict periods of past higher eccentricities [e.g. 8,9], which could have allowed for increased tidal activity. We compute tidal stresses on each of these moons for a variety of interior structure models and presumed eccentricities to determine which are most likely to have been tidally active in the past. We can then use the tectonic records of the moons to constrain possible interiors and histories.

We focus first on Mimas, which lacks widespread tectonic activity, and determine the conditions under which it could possess a global ocean and avoid both tidal activity and circularization of its eccentric orbit. We will then discuss tidal stresses on Enceladus in an attempt to address the hemispheric dichotomy in its tectonic activity. Finally, we will present calculations of tidal stress using a preliminary suite of interior models for Dione and Rhea and discuss the overarching implications for the presence of oceans within these worlds as well as their failure properties.

Methods: We use a 5-layer model, based on [10], to calculate tidal stresses on each moon for a suite of interior structure models. The models all include ice shells with both brittle and ductile layers overlying global oceans. To explore a large range of possible interior structures, we vary the whole ice shell thickness, the depth of the upper brittle ice layer, and the viscosities of the brittle and ductile ice layers. For Mimas and Enceladus, we further constrain our models to be consistent with the observed librations [2,3]. We compute global peak tidal stresses for each moon and interior model. For those models that can produce tidal stresses comparable to Europa's, we also create histograms of peak daily stresses at thousands of locations across the surface. We then compare our results across all four Saturnian moons and Europa.

Because Mimas is not currently in an eccentricity-pumping resonance and maintains an eccentricity twice that of Enceladus, we also compute circularization timescales and tidal heating rates for each interior model, following the approach of [11].

Results: Our results show that it is challenging to reconcile a global ocean within Mimas with its lack of tectonic activity and large present-day eccentricity. On Enceladus, the challenge lies in achieving high stresses in the south polar region, where tectonic activity is abundant, but low stresses in the north polar region, which displays limited fracturing. We were able to identify models for Dione that produce tidal stresses within the range of magnitudes on Europa; Rhea will be the subject of our future work. Given the similar magnitudes of stress involved and the high heat flows inferred for Dione and Enceladus, it seems more likely that some tidal-tectonic activity has occurred on Dione and Enceladus, perhaps even in the north polar region, and that Mimas does not possess a global ocean.

References: [1] Hurford, T. et al. (2009), Icarus 203, 541-552. [2] Tajedinne, R. et al. (2014) Science, 346, 322-324. [3] Thomas, P. et al. (2016) Icarus 264, 37-47. [4] McKinnon, W. (2015) GRL 42, 2137-2143. [5] Phillips, C. et al. (2012) AGU Fall Meeting, #P22B-03. [6] Hammond, N. et al. (2013) Icarus 223, 418-422. [7] White, O. et al. (2013) Icarus 223, 699-709. [8] Charnoz, S. et al. (2011) Icarus 216, 535–550. [9] Asphaug, E. & Reufer, A. (2013) Icarus 223, 544-565. [10] Jara-Orue, H. and Vermeersen, B. (2011) Icarus 215, 417-438. [11] Henning, W. & Hurford, T. (2014) Astrophys J., 789, 30.

Acknowledgements: This work was supported by NASA's Cassini Data Analysis Program.

CARTOGRAPHY OF THE MEDIUM-SIZED SATURNIAN SATELLITES BASED ON CASSINI-ISS IMAGES

Th. Roatsch[1], E. Kersten[1], K.-D. Matz[1], F. Scholten[1], R. Wagner[1], and C.C. Porco[2], [1]Institute of Planetary Research, DLR, Berlin, Germany (Thomas.Roatsch@dlr.de), [2]CICLOPS, Space Science Institute, Boulder, CO.

Introduction: The Cassini Imaging Science Subsystem (ISS) consists of two framing cameras. The narrow angle camera is a reflecting telescope with a focal length of 2000 mm and a field of view of 0.35 degrees. The wide angle camera is a refractor with a focal length of 200 mm and a field of view of 3.5 degrees. The stated objective of the ISS is to obtain global coverage for all medium-sized icy satellites with a resolution better than 1 km/pixel and high-resolution images of selected areas [1]. This goal was achieved with image sequences obtained during close flybys supplemented by images from greater distances to complete the coverage. The only exception so far is Mimas which will be imaged again during a close flyby in January 2017.

Basemaps: The processing of the Cassini images follows the typical processing chain for framing cameras: radiometric correction, geometric correction and map projection, and mosaicking [2]. Digital global mosaics that are also called basemaps were prepared in simple cylindrical projection, a special case of equirectangular projection. The prime meridian is in the center of the map. All basemaps were calculated using Cassini images. Voyager images were used to fill remaining gaps.

High-resolution atlases: High-resolution atlases were produced to conform to the design and standards of the USGS airbrush maps and photomosaics, established by Greeley and Batson [1990], widely used in planetary cartography. The selection of the atlas format depends on the resolution of the mosaics and the size of the satellites.

Three different formats were used for the generation of the atlases [3,4]:

- Synoptic format for making planetwide maps on a single sheet used for Phoebe
- Subdivision of the synoptic format for making planetwide maps with four quadrangles on three sheets, used for Mimas and Iapetus
- 15 quadrangles format for medium-sized bodies and high-resolution imaging, used for Enceladus, Tethys, Dione, and Rhea

Many new feature names were suggested by the Cassini Imaging Team and approved by the IAU. In naming the features on the Saturnian satellites, the Working Group for Planetary System Nomenclature within the International Astronomical Union (IAU) has expanded the mythological theme first used on the Jovian satellites. On the Saturnian satellites, however, the features bear names derived from the great epics and legends of the world [5,6]. All feature names were applied to the atlases. Fig. 1 shows a basemap of Enceladus with nomenclature. All maps and atlasses are available to the public through the Imaging Team's website [7]. The map tiles are also archived as standard products in the Planetary Data System (PDS) [8].

References: [1] Porco, C.C. (2004) *Space Science Review 115*, 363-497, [2] Roatsch, T. (2006) *Plan. Space Sciences 54*, 1137 -1145, [3] Roatsch et al., in: *M. Dougherty et al. (eds.), Saturn from Cassini-Huygens, Springer,* 761-778, [4] Roatsch et al. (2012) *Plan. Space Sciences 61,* 135-141, [5] Batson, R. (1984) Voyager 1 and 2 Atlas of Six Saturnian Satellites, http://history.nasa.gov/SP-474/sp474.htm, [6] http://planetarynames.wr.usgs.gov/, [7] http://ciclops.org/maps, [8] http://pds.jpl.nasa.gov/

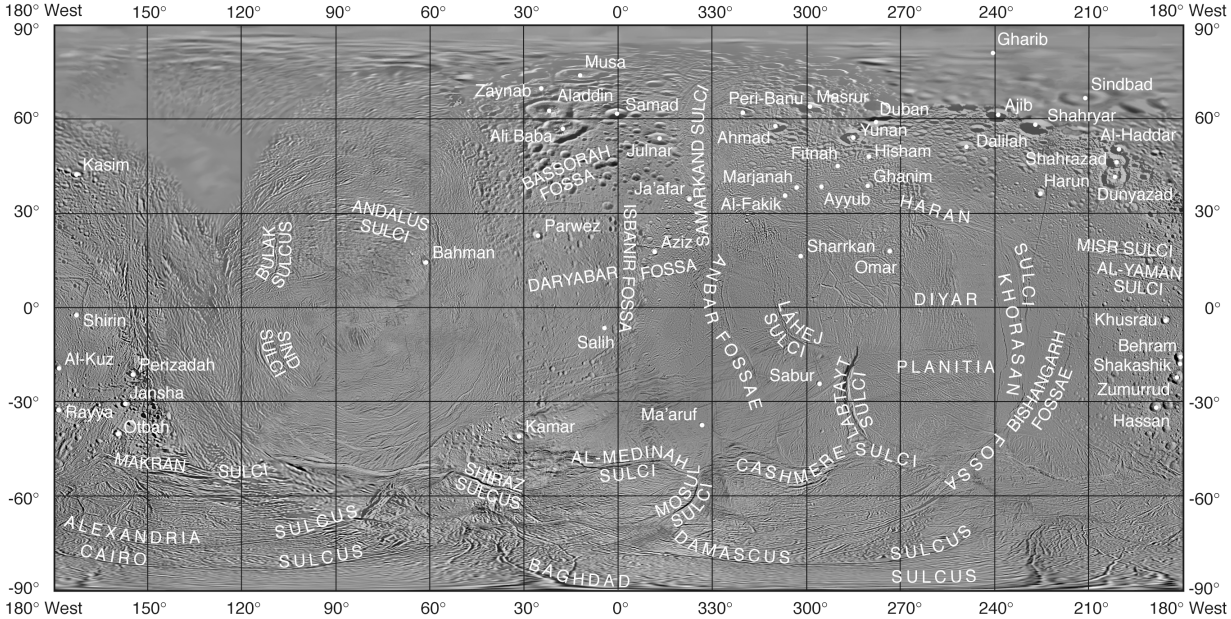

Figure 1: Global Cassini image basemap of Enceladus from 2010 with nomenclature.

IMPACT HEATING AND THE SOUTH POLAR THERMAL ANOMALY ON ENCELADUS. J. H. Roberts[1] and A. M. Stickle[1], [1]Johns Hopkins University Applied Physics Laboratory, 11100 Johns Hopkins Rd., Laurel, MD 20723, James.Roberts@jhuapl.edu

The south polar region on Enceladus is characterized by plume activity and a substantial thermal anomaly [1-3]. Tides are a probable energy source, however this heat tends to be lost faster than it is produced, resulting in the geologically rapid freezing of any global subsurface ocean [4,5] and severe reduction of subsequent tidal heating. Moreover, tidal heating is symmetric about the equator, and no corresponding thermal anomaly or activity is observed in the north. The presence of significant lateral variations in the mechanical properties of the ice shell can break this symmetry.

Here we examine the effects of a large impact on both the initial meltwater production and on softening of the surrounding ice by the shock heating. We model the subsequent tidal dissipation and thermal evolution of the ice shell in response to the impact heating.

We use the CTH hydrocode [6] in 2D to simulate a vertical impact into an ice shell and use the 5-phase ANEOS for ice [7] to compute the temperature change and melt production. We model thermal evolution of the ice shell using Citcom in 2D-axisymmetric geometry [8]. We compute the tidal heating using the propagator-matrix code TiRADE [4]. We read in the impact heating and initial tidal heating into Citcom, and allow the temperature to evolve, periodically updating the tidal heating based on the evolving viscosity structure.

In Figure 1, we show the temperature increase resulting from the vertical impact of a 5 km diameter icy projectile into a 40 km thick ice shell over an ocean at 20 km/s, scaled to create a crater the approximate size of the south polar terrain (SPT) [1]. Even though an ice shell this thin does not convect, the impact heat diffuses away in ~1 My. This result is broadly similar to that of earlier studies of a very slow collision with a co-orbital object [9]. However, the impact heating softens the ice and enhances the tidal heating locally; a more self-sustaining enhancement. Nevertheless, this thermal anomaly does not last for more than ~10 My (Figure 2); less if the ice shell is thicker and less dissipative. Unless such an impact occurred in the very recent past, the thermal effects would not be observable today. However, a projectile capable of creating a crater the size of the SPT also produces a significant amount of melt, which may drain into a subsurface ocean, and cause subsidence of the surface. The impact shown in Figure 1 generates approximately 200,000 km^3 of meltwater, down to about 30 km depth at the impact center. This corresponds to a reduction in elevation of ~3 km. Such an impact would melt though any ice shell thinner than 30 km, enabling transfer of material between the surface and an ocean. The resulting topography is more consistent with that observed for the south polar terrain and with gravity measurements [10] that suggest a south polar sea [11] or regional thickening of a global ocean.

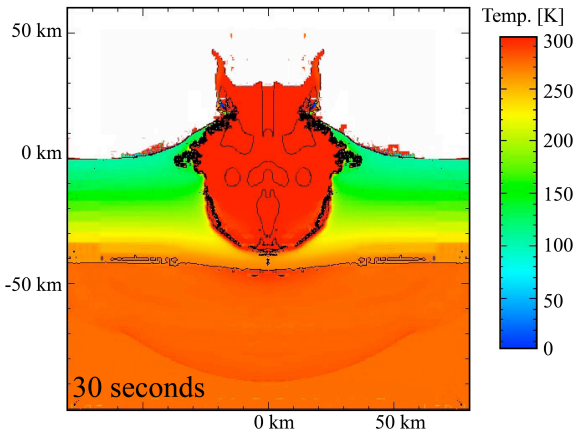

Figure 1: Temperature profile in and below the ice shell, 30 s after an SPT-forming impact.

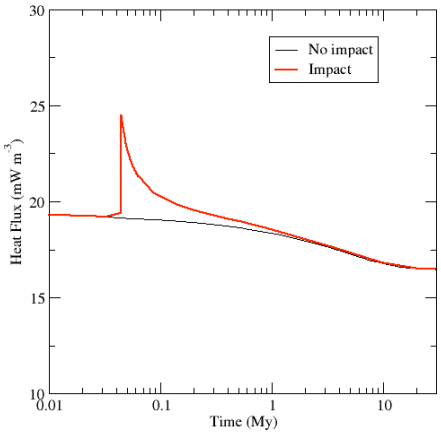

Figure 2: Heat flux out of Enceladus with and without an SPT-forming impact

References: [1] Thomas P. C. et al. (2007) *Icarus, 190*, 573-584. [2] Porco C. C. et al. (2006) *Science, 311*, 1393-1401. [3] Spencer J. R. et al. (2013) *DPS 45,* 403.03. [4] Roberts J. H. and Nimmo F. (2008) *Icarus, 194*, 675-689. [5] Tobie G. et al. (2008) *Icarus, 196*, 642-652. [6] McGlaun, J.M., et al. (1990), *Int. J. Impact Eng*., 10, 351-360. [7] Senft L. E. and Stewart S. T. (2008), *MAPS, 43*, 1993-2013. [8] Roberts J. H. and Zhong S. (2004), *JGR, 109*, E06013. [9] Peale S. J. and Greenberg R. (2007) *AGU Fall Meet. 2007*, P12B-02. [10] Iess L. et al. (2014) *Science, 344*, 78-80. [11] Collins G. C. and Goodman J. C., *Icarus, 189*, 72–82.

FAR-ULTRAVIOLET PHOTOMETRIC MODELING OF THE ICY SATELLITES OF SATURN. E. M. Royer[1] and A. R. Hendrix[2], [1]LASP, University of Colorado, Boulder, CO (Emilie.royer@lasp.colorado.edu), [2]Planetary Science Institute (PSI), Tucson, AZ

Introduction: We present here an analysis of ultraviolet disk-integrated phase curves of the five inner moons of Saturn: Mimas, Enceladus, Tethys, Dione and Rhea. Orbiting inside the E-ring, these icy moons experience weathering processes such as E-ring grain bombardment and cold plasma ions, neutrals and energetic particles impact on their surfaces.

The Cassini UltraViolet Imaging Spectrograph (UVIS) instrument, operating at FUV wavelengths, from 118 to 190nm, probes the uppermost layers of the regolith and is uniquely suited to studying these exogenic processes, leading to a better understanding of the surfaces' evolution and the saturnian environment [1]. We display here (Fig. 1) phase curves at 180 nm for the leading and trailing hemispheres as well as for the Saturn and anti-Saturn hemispheres of each satellites.

Methods: Our data set covers a wide range of phase angles, from 6.8 to 163.9 degrees for Tethys for example. Our analysis is completed by using a Hapke model [2] to retrieve the photometric parameters of these surfaces, such as the single scattering parameters, the opposition effect parameters (where possible) and information on the roughness. The model is based on the presence of a shadow-hiding opposition effect (SHOE) and does not include coherent backsctattering. The single scattering function is modelized by a double Henyey-Greenstein function.

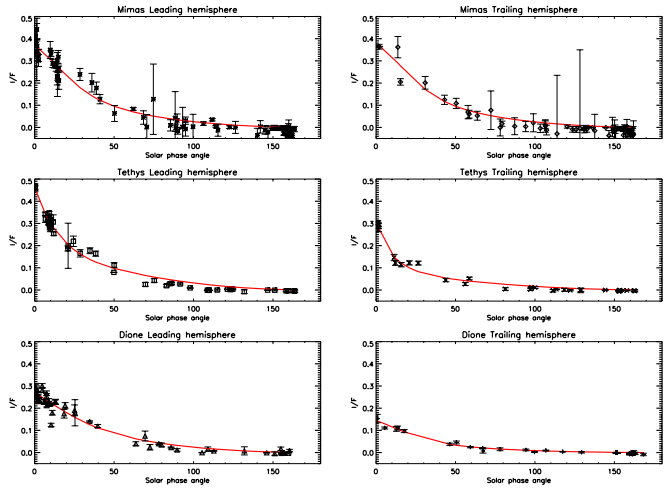

Figure 1: Hapke best fit of the leading and trailing hemispheres at 180 nm of Mimas, Tethys and Dione.

Results: Photometric properties of the surfaces of icy satellites are affected by exogenic processes, and this can be particularly important in the ultraviolet regime. The icy moons of Saturn analyzed here are all located in the E ring and their leading hemisphere (except for Mimas) is predominantly affected by E-ring grain bombardment, which is expected to decrease with the distance from Enceladus, as the E-ring density diminishes [3]. We found Tethys to have a brighter leading hemisphere than Dione in the FUV, consistent with this hypothesis. Comparisons of photometric properties of these surfaces will bring key answers about the dynamics of the E-ring grains and their weathering effects on the icy surfaces [4,5,6].

References: [1] Esposito, L. W. et al. (2004) Space Sci. Rev. 115, 299-361. [2] Hapke B. (2012) Cambridge University Press. [3] Porco, C. C. et al. (2006) Science 311, 1393-1401. [3] [4] Hamilton, D. P. and Burns, J. A. (1994) Science 267, 550-553. [5] Buratti, B. J. (1990) Icarus 87, 339-357. [6] Royer and Hendrix (2014) Icarus 242, 158-171

ACCRETION OF SATURN'S ICE-RICH MOONS FROM MASSIVE RINGS. J. Salmon[1] and R. M. Canup[1], [1]Southwest Research Institute, Planetary Science Directorate, 1050 Walnut Street - Suite 300, Boulder, CO, 80302, USA (julien@boulder.swri.edu)

Introduction: The origins of Saturn's inner satellites and its ice-rich rings are challenging to explain. Simulations of the viscous evolution of Saturn's rings show that the total ring mass asymptotically approaches its current mass over the age of the Solar System, implying that the ring's initial mass is unconstrained [1]. A recent ring formation model predicts a primordial ice ring that was vastly more massive than the current rings, which would have spawned the inner moons out to ice-rich Tethys as it spread [2]. If a massive ring was initially a mixture of rock and ice and tidal evolution was very rapid (a tidal dissipation factor for Saturn $Q \sim 10^3$), all the satellites out to Rhea may have formed from ring material as it spread beyond the Roche limit [3]. A low Q value is inferred from recent observations [4], but its applicability to primordial Saturn is unknown. Further, if one begins with a rock-ice ring, an extremely efficient process is needed to preferentially remove rock to explain the current nearly pure ice rings. Ideas for how this might occur have been proposed [3], but remain uncertain.

We consider Saturn's inner moons as two groups, based on the mass of rock in each object: 1) Mimas, Enceladus and Thetys, and 2) Dione and Rhea. The total rock content of group (1) may be compatible with ice-rich moons that acquired their rock from a secondary source, e.g. during the Late Heavy Bombardment [5]. Group (2) has much more rock than can be explained by such secondary contamination processes.

We here model the formation of moons as an ice-dominated massive ring viscously evolves, assuming a primordial Saturn with $Q \sim 10^4$. We focus on whether Mimas, Enceladus and Tethys (or their progenitors) could have formed in this manner.

Numerical setup: We use a numerical model adapted from studies of lunar origin [6,7]. The code couples a continuous ring model to the N-body code SyMBA [8], and includes viscous spreading (with a viscosity that includes the effects of the rings' self-gravity), tidal accretion criteria, disk-satellite interactions, tidal evolution [9], and satellite-satellite interactions. As the Roche-interior ring spreads beyond the Roche limit ($a_R \sim 2.24\ R_{Sat}$) material accretes into new moonlets that are added to the N-body code.

We consider initial ring masses 0.5 to 3×10^{-6} M_{Sat} [2], and a newly-formed Saturn whose physical radius is 1.3 to 1.5 times its current radius (R_{sat}) [10] to estimate its rotation rate and the co-rotation distance.

Results: The figure below shows the distribution of satellites obtained in our simulations after 10^9 years. Masses and orbital radii are generally comparable to those of Mimas, Enceladus, and Tethys. Direct ring torques drive a moon out only to $1.6a_R = 3.55\ R_{Sat}$, because for greater distances its strongest resonances fall outside the ring. However we find satellites evolve beyond this distance due to mutual interactions: if an outer moon captures an inner moon into a mean motion resonance and the inner moon has resonances in the rings, then both objects recede in a lock-step configuration. Moons as distant as Tethys then result even with traditional strength tides.

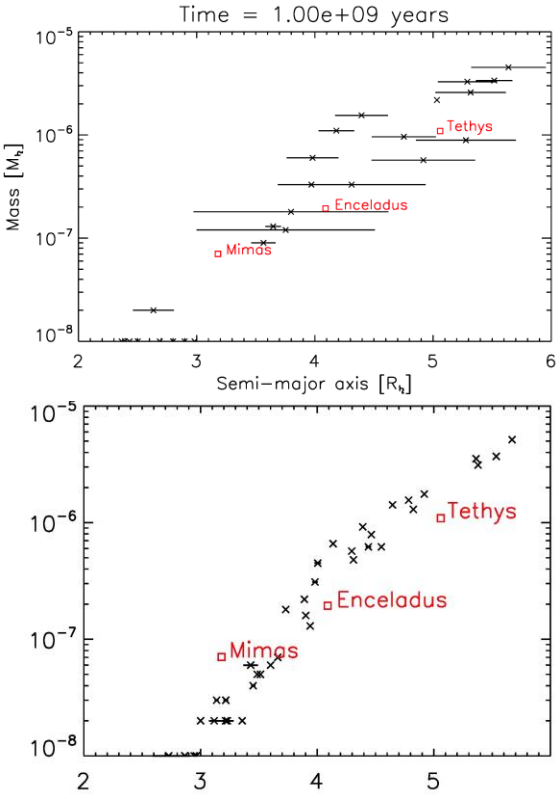

Mass vs. semi-major axis of satellites formed in our simualtions. Horizontal bars show peri/apocenter. (top) 12 simulations without tidal dissipation in the satellites (bottom) 12 simulations with satellite tides.

References: [1] Salmon, J. et al. (2010) *Icarus*, 209, 771. [2] Canup, R. (2010) *Nature*, 468, 943. [3] Charnoz, S. et al. (2011) *Icarus*, 216, 535. [4] Lainey, V. et al. (2014) *ApJ* 752, 14. [5] Canup, R. (2013) *LPSC XLIV*. [6] Salmon, J. and Canup, R. (2012) *ApJ*, 760, 83. [7] Salmon, J. and Canup, R. (2014) *Phil. Trans. R. Soc*. [8] Duncan, M. et al. (1998) *AJ, 116*, 2067. [9] Mignard, F. (1981) *Moon Plan.*, 24, 189. [10] Fortney, J. et al. (2007) *ApJ*, 659, 1661-1672.

Radiative sintering of ice grain regoliths: formation of the PacMan anomalies on the icy Saturnian moons.
M. J. Schaible[1], R. E. Johnson[2], L. V. Zhigilei[2]. [1]University of Virginia, Engineering Physics program, ms5vf@virginia.edu. [2]University of Virginia, Department of Materials Science and Engineering, rej@virginia.edu

Introduction: A unique space weathering phenomenon has been identified on several icy Saturnian moons. The Cassini mission revealed anomalous lens shaped regions in both optical and thermal wavelengths centered on the leading hemispheres and approximately symmetric about the equators [1-3]. In particular, the Cassini InfraRed Spectrometer (CIRS) measurements of thermal emission in the mid-IR showed that diurnal surface temperature variations were smaller inside the anomalous regions. The appearance of the CIRS images led to the anomalies becoming colloquially known as the 'PacMan' anomalies. The boundaies of the anomalous regions were shown to closely match the expected deposition profile of high energy (~ MeV) electrons moving opposite the rotation direction of the moons. Furthermore, simple estimates of the electron penetration depth were similar to the thermal skin depth [2]. These results provide strong evidence that the high energy electrons drive the discolorations and thermal inertia differences of the anomalous regions. However, the mechanisms by which the changes occur lack quantitative comparison with theoretical and experimental results.

Electron Irradiaiton Effects: Electron interactions with the grains can ionize and excite molecules, which, if near enough to an intergrain contact, can cause atoms or molecules to migrate into the contact region, thus increasing the contact volume or 'sintering' the grains. Sintering improves the thermal contact between grains, leading to increased effective thermal conductivity of the regolith.

Electron ionization events in the water ice regolith can sputter molecules from grain surfaces and induce bulk, surface, and grain boundary diffusion. By estimating the number of molecules which gain energy larger than a given diffusion activation energy per ionization event, *N*, and the approximate diffusion length of each mobilized molecules, *l*, an effective diffusion coefficient can be determined [4]. This can then be used with sintering equations previously developed for solid spheres in thermal equilibrium [5] to estimate the time scale of grain sintering due to the energetic electrons. A plot of the sintering timescale at Mimas versus the ratio of the contact to grain radius, R_{con}/r_g, is shown in Figure 1 where a grain size of 5um and a regolith porosity of 50% were assumed. The electron energy distribution measured in the vicinity of each of the moons was used in the calculations. Comparing the sintering timescale to the regolith formation timescale due to E-ring grain deposition and meteorite bombardment of the surfaces indicates that only certain regolith properties result in stable thermal anomalies. For Mimas and Tethys the regolith grains must be ≤ ~5um, the porosity ~50%. Furthermore, low activation energies are required which suggest that the regolith grains are highly irregular.

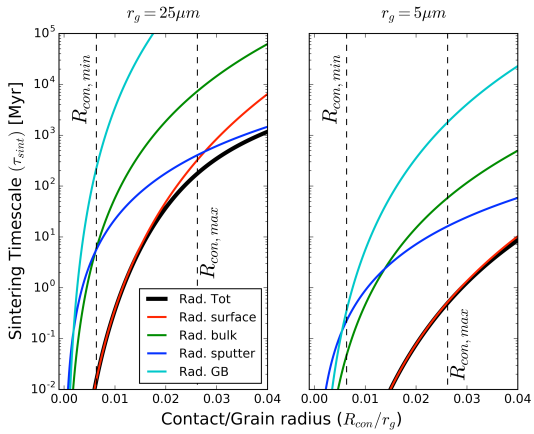

Figure 1: Sintering timescales at 80 K determined from sintering equations. The vertical dashed lines represent the limits of Rcon/rg calculated for Mimas using φ = 0.5 and kg = 6.5W/m/K.

Modeling of Grain Sintering: In order to properly constrain the electron induced sintering rates, accurate estimates of the average number of molecules excited and diffusion length of each molecule are needed. Due to the difficulty of such measurements, molecular dynamics (MD) simulations of excited electrons in water ice were used to simulate an electron ionization event. Electron effects were investigated for several different water ice polymorphs to determine the effects of molecular ordering on *N* and *l*. Different excitation energies and the effect of free surfaces on the ejection of molecules were considered.

References: [1] Schenk. P. et al. (2011) *Icarus, 211,*740-757. [2] Howett C. J. A. et al. (2011) *Icarus, 216,* 221-226. [3] Howett C. J. A. et al. (2012) *Icarus,* 221, 1084-1088. [4] Myers S. M. (1980) *Nuc. Inst. Meth., 168, 265-274*. [5] Swinkels F. and M. Ashby (1981) Acta. Metal., 29, 259-281

GLOBAL COLOR AND CARTOGRAPHIC MAPPING OF SATURN'S MIDSIZE ICY MOONS. P. Schenk[1]. [1]Lunar & Planetary Institute, Houston, TX (schenk@lpi.usra.edu)

Cassini mapping of Saturn's icy moons is now complete to 250-400 m/pixel for Mimas, Tethys, Dione, and Rhea and Iapetus (except gaps there), and to ~100 m/pixel for Enceladus. Simultaneous mapping mosaics acquired during the numerous encounters with these moons included color imaging at resolutions similar to that of the clear-filter images or (more commonly) in summation mode. Initial analyses of these data have already produces significant discoveries, including high-energy electron bombardment coincident with thermal pac-man features, and ring deposits on Rhea [1, 2]. With the completion of targeted and untargeted icy moon flybys during 2015, the priority for the remainder of the mission will be north polar gap coverage, though these will rarely exceed 1 km is resolution. Here we highlight the global color mosaics, which are available for download to the public [http://lpi.usra.edu/icy_moons/]

Map Production: The production of these basemaps involved the manual selection of several thousand tiepoints per moon, used to make a bundle-adjustment to the camera vectors for each image. Images used include all clear and color filters typically down to 5 km resolution (and sometimes down to 10). The most commonly used filters were IR3 (0.94), Green (0.56) and UV3 (0.33 microns). Only polarized filter images have not been included to date though plans are set to begin integrating those later this year. The images were then mosaicked in a two-step process involving formation of an albedo map and then placing mosaics within this first map.

Color Features: The icy moons, especially Enceladus, proved to be much more colorful than suggested by Voyager analyses, largely because of Cassini's NIR capabilities. Voyager observed a cryptic darkening along the equatorial zone of Tethys. Cassini color mapping revealed this to be a prominent lens–shaped color anomaly on both Tethys and Mimas [1], and subsequent IR mapping by CIRS [2] revealed a coincident thermal anomaly indicating a difference in thermal inertia. These features are likely due to surface microstructure alterations triggered by high-energy electrons bombardment [5]. Global color patterns are related to magnetospheric implantation /alteration and E-ring dust populated by Enceladus.

Local color features include recent fracture scarps and fresher crater rims. Cassini observed rayed craters for the first time, many of which have distinct color signatures, including the prominent Inktomi rayed crater system on Rhea. The fresh 400-km basin Odysseus reveals a bluish fracture system within its central pit. One of the biggest surprises from Cassini is evidence for surface alteration due to (extinct) rings around moons. On Rhea, Blue Pearls, or IR-dark patches, formed on high-standing topography along the equator [5].

On Enceladus, the global color pattern is dominated by plume fallout [1] but locally geologic units can be identified with distinct color signatures, including funiscular terrain. The tiger stripes have UV-bright color patterns but fresh fracture walls also have similar color signatures Analysis of these data sets should provide much further insight in the geology of these complex worlds.

REFERENCES: [1] Schenk, P. et al. (2011) *Icarus*, 211, 740. [2] Howett, C. et al. (2011), *Icarus*, 216, 221.

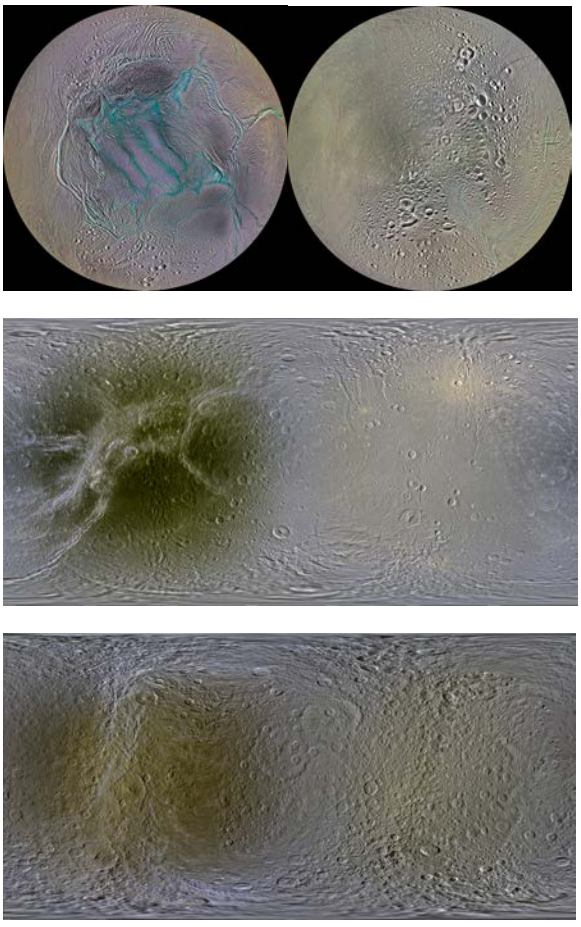

Figure 1. Basemaps of the icy Saturnian moons, in three colors (UV3, Grn, IR3). Top to bottom: Orthographic projections of Encleadus basemap showing south and north polar regions; Simple cylindrical maps of Dione; and Rhea.

"NOT SO BORING AS WE WERE LED TO BELIEVE": GEOLOGY OF SATURN'S OTHER MIDSIZE ICY MOONS. P. Schenk[1] J. Moore[2], O. White[2], P. Byrne[3]. [1]Lunar & Planetary Institute, Houston, TX (schenk@lpi.usra.edu); [2]NASA Ames Research Center Moffett Field, CA; [3] North Carolina State University, Raleigh, NC 27695

INTRODUCTION: Enceladus would not be so interesting were it not for it's sibling ice satellites, Mimas, Tethys, Dione, Rhea, and Iapetus. These moons interact gravitationally (except Iapetus) and with their environment, including material discharged by Enceladus. Pre-arrival expectations for Cassini in 2004 were governed by Voyager's uneven mapping in 1980/81 at ~30 to ≥1 km/pixel (except the cratered north of Rhea). Geology of these moons was inferred to be dominated by cratering, with evidence for modest relaxation and fracturing, and enigmatic areas of smooth material [e.g., 1]. Cassini mapping of these moons is now complete to 250-400 m/pixel (except gaps on Iapetus), and, with color and spectroscopy into the NIR and far-IR, reveal worlds of surprising diversity and complexity, and planetary processes previously unknown.

Endogenic processes: Global mapping reveals complex tectonic systems on all these worlds, including ancient fractures on Mimas, extensive arcuate fractures across Tethys including possibly recently active red streaks [2], and surprisingly pristine hemispheric-scale extensional fractures on Dione and Rhea. The origins of these systems remain enigmatic, but late freezing may play a role. Smooth (though cratered) plains on Tethys and Dione are suggestive of resurfacing, possibly by water- or ammonia-rich volcanism. Two walled depressions on Dione constitute the only candidates for volcanic vents. Ridges on Dione remain the most plausible candidate for compression [3], and washboard terrain on Dione may be the best analog to terrains on Enceladus. Evidence for landform degradation is limited by resolution but is most prominently expressed as landslides on Iapetus, Tethys and Rhea [4]. The lack of similar such features on rocky Vesta suggests that the weakness of icy materials make them susceptible to this process.

Elevated past heat flow levels are indicated by relaxation of large craters on Tethys, Dione and Rhea [5]. Relaxation on Tethys and Dione is spatial heterogenous and prolonged over their geologic history. Evidence for higher past heat flows is also betrayed by the global topography of these bodies. Relief on the 5 inner moons have 1-sigma of +/- 5 km, in contrast to Iapetus (+/- 15 km), indicating that the rugged basin-induced relief of the inner moons was effectively erased by a global heat pulse prior to the observed cratering record.

Exogenic Processes: Voyager observed a cryptic darkening along the equatorial zone of Tethys. Cassini color mapping revealed this to be a prominent lens–shaped color anomaly on both Tethys and Mimas [5], and subsequent IR mapping by CIRS [6] revealed a coincident thermal anomaly indicating a difference in thermal inertia. These features are likely due to surface microstructure alterations triggered by high-energy electrons bombardment [5]. Global color patterns are induced by magnetospheric implantation /alteration and E-ring dust accumulation populated by Enceladus.

Local color features include recent fracture scarps and fresher crater rims. Most impact craters are dominated by prominent central peaks. Cassini observed rayed craters for the first time, including the prominent Inktomi rayed crater system on Rhea, where secondaries and self-secondaries are well observed. The fresh 400-km basin Odysseus reveals a bluish fracture system within its central pit.

One of the biggest surprises from Cassini is evidence for surface alteration due to (extinct) rings around moons. On Rhea, Blue Pearls, or IR-dark patches, formed on high-standing topography along the equator [5]. On Iapetus, the prominent but discontinuous equatorial ridge rising up to 20 high [7] was proposed to be accumulated ring deposits [8], a hypothesis given weight by the lack of a tectonic mechanism and the spatial similarity to the staccato Blue Pearls on Rhea, the difference being the likely presence of much more mass in the Iapetus ring system, and by the discovery of an apparent ring around the centaur Chariklo [9].

SUMMARY: The icy moons of Saturn have turned out to be unexpectedly complex geologically and reveal many of the complex processes within the Saturn system. While many questions remain, prolonged elevated heat levels and endogenic activity and exogenic surface alterations due to charged particles and ring redeposition indicate that the Uranian satellites and such moons in general should be equally complex, as suggested by the complexity of Pluto's large moon Charon [10].

REFERENCES: [1] Moore, J. et al. (2004) *Icarus*, 171, 421. [2] Schenk, P. et al. (2015) *EOS*, P21B-02. [3] Giese, B. et al. (2007), *G.R.L.*, 34, 0314674. [4] Singer, K. et al., (2012), *Nat. Geosc.*, 5, 574. [5] White, O. et al. (2013), *Icarus*, 223, 699; White, O. et al. (2016) to be submitted. [5] Schenk, P. et al. (2011) *Icarus*, 211, 740. [6] Howett, C. et al. (2011), *Icarus*, 216, 221. [7] Porco, C., et al. (2005), *Science*, 307, 5713. [8] Ip, W. (2006), *G.R.L.,* 33, L16203. [9] Braga-Ribas, F., et al. (2014), *Nature*, 508, 7494. [10] Moore, J. et al. (2015) *Science*, 351, 1284.

SPECTRAL ANALYSIS OF ENCELADUS' SURFACE. F. Scipioni[1], P. Schenk[1], R. Clark[2], F. Tosi[3], J.-Ph. Combe[4], C. Dalle Ore[5]. [1]Lunar and Planetary Institute, 3600 Bay Area Blvd. 77058 Houston, Texas, United States, scipioni@lpi.usra.edu; [2]PSI, Tucson, AZ; [3]INAF-IAPS, Rome, Italy; [4]Bear Fight Institute, Winthrop, WA; [5]Seti Institute, Mountain View, CA.

Introduction: Enceladus' surface is composed primarily by pure water ice. The Cassini spacecraft has observed present-day geologic activity at the moon's South Polar region, related with the formation and feeding of Saturn's E-ring. Plumes of micron-sized particles, composed of water ice and other contaminants (CO_2, NH_3, CH_4), erupt from four terrain's fractures named Tiger Stripes. Some of this material, however, falls back on Enceladus' surface to form deposits that extend to the North at 40° W and 220° W and whose highest concentration is at the South Pole (Figure 1 TOP panel, from [1]).

Data analysis: In this work we analysed Cassini-VIMS-IR data to identify E-ring deposits across Enceladus' surface through the variation in band depth of the main water-ice spectral features located at 1.25, 1.50, and 2.02 μm, and of the hight of the reection peak at 3.60 μm. Since plumes deposits on the surface undergo darkening processes for less time than surrounding terrains, they are supposed to appear brighter and the water-ice absorption bands should be deeper. To characterize the global variation of water-ice band depths across Enceladus, we divided the surface into a 1°x1° grid and then averaged the band depths and peak values inside each square cell (Figure 2).

Results: The position of the plumes's deposits predicted by theoretical models [1] correspond very closely with ISS color patterns on the surface [2] (Figure 1 BOTTOM panel). This pattern also has a relatively good match with water ice band depths' maps on the trailing hemisphere, but they diverge significantly on the leading side (Figure 2).

The space weathering processes acting on Enceladus's surface have the further effect to ionize and brake up water ice molecules, resulting in the formation of particles smaller than one micron. When the incoming light hits the surface, Rayleigh scattering is induced by these kind of ice particles, which translate in peculiar effects on the IR spectrum. We mapped the spectral indicators for sub-micron particles and we compared the results with the plumes deposits models. Again, a good overlap is observed on the trailing hemisphere only.

Finally, we investigated the variation of the depth of the water ice absorption bands with the phase angle. In the visible range, some terrains surrounding the Tiger Stripes show a decrease in albedo when the phase angle drops below 10°.

This peculiarity is not observed in the near infrared, since the depth of the water ice features remains quite constant at different ranges of phase angles.

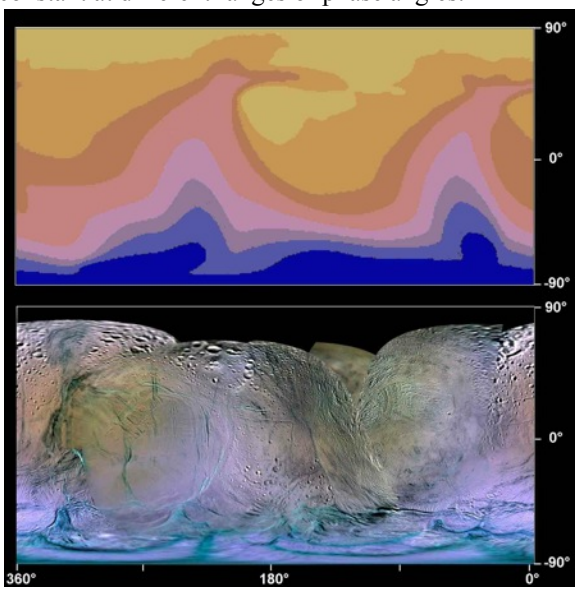

Figure 1: TOP – Plumes dpeosits on Enceladus surface as modeled by [1]. BOTTOM - RGB color map, in simple cylindrical projection, produced by combining three ISS filters: IR3 (0.930 μm), GRN (0.586 μm) and UV3 (0.338 μm) [2].

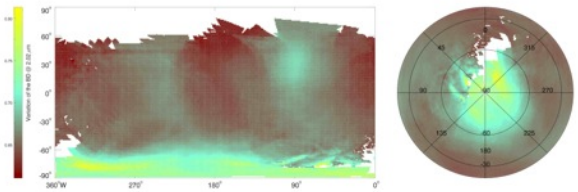

Figure 2: Global variation of the dept of the water ice absorption band located at 2.02 μm, across Enceladus's surface.

References: [1] Kempf et al. (2010) *Icarus*, 206, 446. [2] Schenk et al. (2011) *Icarus*, 211, 740.

USING HARTLEY BAND TO DETECT THE OZONE PRECURSOR ON ICY SATELLITES. B. Sivaraman[1], S. Pavithraa[2], J. –I. Lo[3], B. N. Raja Sekhar[4], B. –M. Cheng[3] and N. J. Mason[5], [1]Physical Research Laboratory, Ahmedabad, India-380009. Email: bhala@prl.res.in. [2]National Chiao Tung University, Hsinchu-30076, Taiwan. [3]National Synchrotron Radiation Research Center, Hsinchu-30076, Taiwan. [4]Bhabha Atomic Research Center, Mumbai-400085, India. [5]The Open University, Milton Keynes, MK7 6AA, United Kingdom.

Introduction: Ozone, as a biomarker, is of interest to astronomers and planetary scientists. Since the finding of ozone on icy satellites [1], the abiological synthesis of ozone from oxygen ices and simple oxygen bearing molecular ices, such as CO / CO_2 / SO_2 /and N_xO_y has been the focus of laboratory based simulations [2-5]. Ozone synthesized in laboratory based experiments was probed using infrared spectroscopic technique. The ν_3 (1040 cm^{-1}) band of ozone is intense enough for detecting ozone presence on icy analogs [2, 4, 5]. However, in real scenario due to band overlap from silica absorption infrared spectroscopic technique, used in laboratory simulations, cannot be applied to detect the presence of ozone elsewhere.

In fact, to-date Hartley band (220 nm – 310 nm) of ozone is widely used to detect the presence of ozone [1]. Recently the Vacuum UltraViolet (VUV), 110 nm – 190 nm, photoabsorption spectra of pure solid ozone revealed the absence of Hartley band while ozone concentrations are low [3]. This could be one reason for the weak absorption in the Hartley band in Iapetus while it was intense in Rhea and Dione. Yet, due to strong absorption of other simple molecular ices, such as H_2O / CO_2 etc., in the VUV region unambiguous identification of ozone could not be made. Therefore, Hartley band is the only wavelength that is available to-date for the identification of ozone elsewhere, which demands sufficient ozone concentration. It is surprising to note that there was only two experiments to-date that had reported the Hartley band of pure solid ozone synthesized from O_2 / CO_2 ices under astrochemical conditions [3, 5]. Though the ozone synthesizers are considered simple molecular species the chemical complexity and different range of temperatures that prevails on icy bodies, indeed, demands more investigation. This is important especially when there could be absorption, from another molecule like SO_2, at similar wavelength.

Here, we propose using the Hartley band in identifying the ozone precursor molecule on the icy satellites based on a series of experiments carried out on simple ozone precursor ice analogs.

Experimental methodology: Experiments were carried out in the VUV beamline at NSRRC, Taiwan, where beamline end station was an ultrahigh vacuum chamber that houses the tip of a 10 K cold head where a Lithium Fluoride (LiF) window was mounted to form the molecular ice analogs [3]. Temperature commensurate to the icy satellite conditions were maintained using the heater and cooler combination at the LiF substrate. Molecules were deposited at 10 K and were then irradiated using VUV photons in the range from 8 – 11 eV, and for about one to few hours, depending on the molecule. After irradiation, spectra were recorded both in the VUV and at UltraViolet (UV) wavelengths covering the entire range from 110 -320 nm.

Results and Discussion: Upon irradiation of O_2, CO, CO_2, CO_2+H_2O, SO_2, NO, N_2O and NO_2 ices and subsequent recording of spectra strong absorption in the Hartley band was observed (Figure 1). This confirms the presence of ozone in the icy analogues. After irradiation, spectra were also recorded as a function of temperature until the sublimation of majority of ozone molecules observed by the reducing intensity of Hartley band.

Depending on the icy analogue the peak of the observed Hartley band was found to vary from 255 – 270 nm (Figure 1). Therefore, the implication of this experimental data could lead to the identification of ozone precursor molecules on icy satellites by observing the Hartley band, where many of the icy satellites are known to harbour a variety of ozone precursors, simple oxygen bearing molecules.

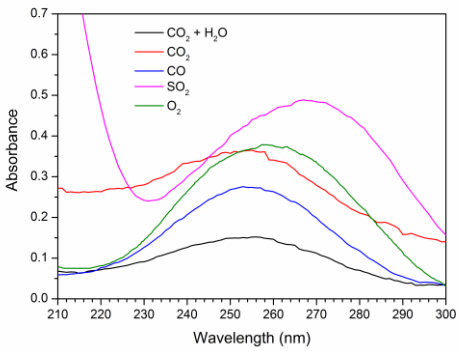

Figure1: Hartley band observed after in-situ ozone synthesis in different ozone precursor molecular ices.

References: [1] Noll K. S. et al. (1997) *Nature, 388,* 45. [2] Sivaraman B. et al. (2007) ApJ, 669, 1414 [3] Sivaraman B. et al. (2014) *Chem Phys Lett, 603,* 33. [4] Sivaraman B. et. al. (2008) *Chem Phys Lett, 460,* 108. [5] Jones B. M. et al. (2014) *ApJ, 781,* 85.

ENCELADUS AND ITS INFLUENCE ON SATURN'S MAGNETOSPHERE. H. T. Smith[1], F. Crary[2], M. Dougherty[3], M. Perry[1], E. Roussos[4], S Simon[5] and R. Tokar[6], [1]Johns Hopkins University Applied Physics Laboratory, 11101 Johns Hopkins Road, Laurel, MD 20723, [2]Laboratory for Atmospheric and Space Physics, 1234 Innovation Drive, Boulder, CO 80303, [3] Huxley Building Room 6M54, Imperial College London, London SW7 2AZ, United Kingdom [4]Max Planck Institute for Solar System Research, Justus-von-Liebig-Weg 3, 37077 Göttingen, Germany, [5]Georgia Institute of Technology, 311 Ferst Drive, Atlanta, GA 30332-0340, [6]Planetary Science Institute, 1700 East Fort Lowell, Suite 106, Tucson, AZ 85719.

Abstract: The discovery and study of active water plumes[1][2] emanating from the southern pole of the Enceladus has provided key information for understanding particle sources and dynamics in Saturn's magnetosphere. Prior to 2004, knowledge of the Saturnian system was limited to Earth based observations and only three in-situ flybys. The subsequent arrival of the Cassini spacecraft rapidly changed what we know about the influence of this moon on the Saturnian system causing dramatic revisions to our understanding of the physical processes occurring in Saturn's magnetosphere. The very dense, relatively unprotected atmosphere of the large moon Titan, which was once believed to be a dominant source of plasma [3][4][5][6] has taken a back seat to its much smaller cousin, Enceladus. This relatively small moon serves as the primary source of particles in the magnetosphere [7][8] and thus has a significant impact on both the near Enceladus environment as well as the entire magnetosphere. We present an overview of the current understanding of Enceladus' impact on Saturn's magnetosphere with respect to neutral and charged particles, magnetic fields and dynamics.

References:

[1]Dougherty, M. K. et al. (2006), *Science*, Volume 311, Issue 5766, pp. 1406-1409.

[2]Porco, C. C. et. al (2006), *Science*, Vol 311, 5766, pp. 1393-1401.

[3]Barbosa, D.D. (1987), *Icarus*. 72, 53-61.

[4]Ip, W., (1997), *Icarus* 97, 42-47.

[5]Richardson, J.D., and Sittler, E.C., Jr. (1990), *JGR* 95, 12,019-12,031.

[6]Eviatar, A. (1984), *JGR 89*, 3821-3828.

[7]Jurac, S. and Richardson, J.D. (2005), *JGR 110*, A9, A09220.

[8]Johnson, R. E. et. al (2006), *ApJ Letters*, 644:L137-L139.

OBSERVATIONS OF ACTIVE THERMAL EMISSION FROM ENCELADUS BY THE CASSINI COMPOSITE INFRARED SPECTROMETER. J. R. Spencer[1], C. J. A. Howett[1], A. J. Verbiscer[2], T. A. Hurford[3], N. J. P. Gorius[4], J. C. Pearl[3], M. Segura[3], [1] Southwest Research Institute, 1050 Walnut St. Suite 300, Boulder CO 80302, [2]Dept. of Astronomy, University of Virginia, Charlottesville, VA 22904, [3]NASA-Goddard Space Flight Center, Greenbelt, MD 20771, [4]The Catholic University of America, Washington, DC 20064

Introduction: Key information about the activity on Enceladus has been provided by Cassini's Composite Infrared Spectrometer (CIRS), which contributed to the discovery of activity in 2005 [1], and has continued to obtain numerous observations of the endogenic and passive (re-radiated sunlight) thermal emission from Enceladus' tiger stripes and their surroundings throughout the mission. CIRS is a thermal IR Fourier transform spectrometer [2] which has three focal planes sensitive to different wavelength ranges: "FP1" 16 – 500 μm (20 – 600 cm^{-1}); "FP3" (9 – 17 μm, 600 – 1100 cm^{-1}); and "FP4" (7 – 9 μm, 1100 – 1500 cm^{-1}). FP1 consists of a single detector with 3.9 mrad IFOV, while FP3 and FP4 each have a linear array of 10 detectors with IFOV 0.29 mrad. FP1's broad long-wavelength coverage provides measurements of the total heat flow from the active south polar region, and passive surface temperatures, while FP3 and FP4's shorter wavelength coverage and higher spatial resolution allows mapping of the spatial and temperature distribution of high-temperature endogenic emission from the tiger stripes.

Heat Flow: CIRS's first detection of south polar thermal emission in 1995, with FP3, [2] provided an estimate of the heat flow from the south polar region, 4 – 8 GW, which was surprisingly high compared to expectations for steady-state tidal heating [3]. Subsequent low-resolution FP1 observations of the combined active and passive emission from the south polar region in 2008, combined with models of the passive emission, implied even higher heat flow, 13 – 19 GW [4]. However, combination of high-resolution FP3 and FP4 observations in 2008, with relatively high-resolution FP1 scans in 2010, implied that the tiger stripes themselves emit only about 4 GW [5]. The discrepancy with the earlier 13 – 19 GW estimate could be due either to limitations of the thermal model used to subtract the passive emission from the earlier estimate, and/or to the fact that there is significant emission from between the tiger stripes. The latter possibility is being addressed with recent FP1 observations of the tiger stripe and inter-stripe emission in late 2015 [6], which suggest that inter-stripe emission may be significant.

Temperatures: The highest temperatures recorded by CIRS, obtained from blackbody fits to the 7 – 9 μm FP4 observations from the brightest parts of the tiger stripes, imply peak temperatures along the tiger stripes of 190 – 200 K. This is comparable to the emission temperatures recorded by the Cassini VIMS instrument at shorter wavelengths (4 – 5 μm) of 197 +/- 20 K [7]. This temperature upper limit is likely controlled by sublimation cooling of the near-vent regions [8].

Spatial Distribution of Emission: Emission is strongly variable along the tiger stripes [4], with the brightest regions being near the Saturn-facing ends of Damascus and Baghdad Sulci, and the anti-Saturn end of Alexandria Sulcus. Strong spatial variability persists down to 100-meter scales [6]. Thermal emission also occurs along branch fractures near the ends of the main fractures, including some, in particular an active branch of Baghdad, that are quite inconspicuous in visible images. There is good correlation between the locations of thermal emission and the locations of plume activity [9,10]. The spatial distribution of emission can be explained to first order by the conductive heating of near-surface ice by warm vertical fractures [11, 12].

References:

[1], J. R. Spencer et al. (2006), *Science* **311** 1401 – 1405. [2] F.M. Flasar et al. (2004), *Space Science Rev*. **115** 169–297. [3] J. Meyer, J Wisdom (2007). *Icarus* **188**, 535-539. [4] C.J.A. Howett et al. (2011), *J. Geophys. Res*. **116**, CiteID E03003. [5] J. R. Spencer et al. (2013), *2013 EPSC meeting* EPSC2013-840. [6] J. R. Spencer et al. (2016) *Lunar Planet Sci. Conf. XXXVII,* Abstract #2860. [7] J. D. Goguen et al. (2013), *Icarus* **226**, 1128 – 1137. [8] R. R. Howell, J. D. Goguen, J. R. Spencer (2013), Division for Planetary Sciences Meeting 45, abstract 416.01. [9] C. Porco, D. DiNino, F. Nimmo (2014). *Astron. J.* **148**:45. [10] J. N. Spitale et al. (2015) *Nature* **521**, 57 – 60. [11] O. Abramov, J. R. Spencer (2009), *Icarus* **199**, 189 – 196. [12] A. P. Ingersoll, A. A. Pankine (2010), *Icarus* **206**, 594-607.

OBSERVING SURFACE-LEVEL ERUPTIVE VARIABILITY AT ENCELADUS' SOUTH POLE. J. N. Spitale[1], T. A. Hurford[2], A. R. Rhoden[3], and M. M. Hedman[4], [1]Planetary Science Institute, Tucson, AZ 85719, [2]NASA Goddard Space Flight Center, Greenbelt, MD 20771, [3]Johns Hopkins University Applied Physics Lab., Laurel, MD 20723, [4]University of Idaho, Moscow, ID 83844.

Introduction: Cassini observations of the south pole of Enceladus revealed large rifts in the crust that have been shown to be the sources of the observed jets of water vapor and icy particles [1, 2, 3] and which exhibit higher temperatures than the surrounding terrain [4, 5]. A physical mechanism in which temporal variations in tidal stress open and close the tiger stripe rifts was proposed [6], governing the timing of eruptions: during each orbit, every portion of each tiger stripe rift spends about half the time in tension, which allows the rift to open, exposing volatiles, and facilitating eruptions. Based on triangulation results [3], the tidal control hypothesis was tested by calculating the tidal stresses along the tiger stripes that were associated with each source region [7], finding that tensile and shear stresses should allow the observed jetting activity to occur.

The evidence is growing that the south-polar eruptions are indeed controlled by tidal stresses that vary as the satellite orbits Saturn. Using Cassini VIMS (Visual and Infrared Mapping Spectrometer) observations, it was shown [8] that the integrated brightness of the broad plume at altitude varies consistently over a factor of several during Enceladus' orbit.

Establishing a link between the geophysical processes driving the eruptive activity and the broad plume observed at altitude motivates an analysis of the local-scale emission from individual fractures at the surface of the body.

Curtains vs. Jets: Although curtains may sometimes be mistaken for discrete jets, it is clear that both eruptive styles are active on Enceladus [9]. Each style likely arises from different physical conditions within the fracture. The long curtain-style eruptions may reflect the broad sub-surface fracture geometry, in which case they should be strongly correlated with tidal stresses. Discrete jets may reflect local fracture conditions. For example, debris backfill and scouring would likely obfuscate any correlation with tidal forcing, as debris might prevent the fracture from completely closing under compression, while a scoured channel would be too localized to close under regional diurnal stress. Discrete jets may also be geographically correlated with fracture junctions [10]; in that case, even if strongly tidally controlled, such jets could be activated by multiple stress states, corresponding to the multiple fracture orientations in the vicinity of the junction.

Observational Limitations: The relationship between tidal stress and surface-level eruptive activity has yet to be established. Observational difficulties include: 1) too few curtain-based activity maps [9] are currently available, resulting in poor statistics when considering the fractures individually; 2) large regions of the fracture system typically cannot be mapped in a given observation, yielding large uncertainties in the total amount of active fracture at any given time; 3) most of the fracture system is apparently active at any given time [9], and the time variation is a relatively small effect.

Observations of Variability: Additional curtain-based activity maps are in progress in order to improve the counting statistics. Moreover, we have identified three discrete jets -- all located near fracture junctions -- that may have been captured turning on during Cassini imaging sequences.

References:

[1] Porco C.C. et al. (2006) *Science* 311, 1394-1401. [2] Hansen et al. (2006) *Science* 311, 1422-1425. [3] Spitale, J. N. and Porco, C. C. (2007) *Nature* 449, 695-697. [4] Spencer J.R. et al. (2006) *Science* 311, 1401-1405. [5] Howett, C. J. A. et al. (2011) Geophys. Res. 116 E03003. [6] Hurford T.A. et al. (2007) *Nature* 447, 292-294. [7] Hurford T.A. et al. (2012) *Icarus* 220, 896-903. [8] Hedman M.M. et al. (2013) *Nature* 500, 182-184.[9] Spitale J. N. et al. (2015) *Nature* 521, 57-60. [10] Helfenstein, P. and Porco, C. C. (2015) *AJ* 150, 96-129.

SPECTRAL AND GEOLOGICAL PROPERTIES OF TETHYS. K. Stephan[1], R. Wagner[1], R. Jaumann[1,2], R.N. Clark[3], D.P. Cruikshank[4], C. Dalle Ore[4], R.H. Brown[5], B. Giese[1], T. Roatsch[1], G. Filacchione[6], D. Matson[7], K. Baines[8], N. Krupp[9], F. Capaccioni[6], B.J. Buratti[7] and P.D. Nicholson[10], [1]DLR, Institute of Planetary Research, Berlin, Germany, [2]FU Berlin, Germany, [3]U.S.G.S., Denver, USA, [4]NASA Ames, Moffett Field, USA, [5]UoA, Tucson, USA, [6]INAF-IASF, Rome, Italy, [7]JPL, Pasadena, USA, [8]SSEC, Madison, USA, [9]MPS, Göttingen, Germany, [10]Cornell Univ., Ithaca, USA. (Katrin.Stephan@dlr.de).

Introduction: In order to further our understanding of the Satutnian system we performed an analysis of the spectral surface properties of Tethys based on CASSINI VIMS data [1,2] in context of the surface geology as well as topography based on simultaneously acquired Cassini ISS images. The spectral analysis follows the analyses previously done for Dione and Rhea as described in detail in [3,4]. The main focus lies on mapping the distribution of the major surface compounds H_2O including its physical properties as well as a surface darkening agent.

Global spectral properties: The available VIMS data set enabled us to generate global maps of Tethys' surface displaying unique hemispherical spectral differences characteristics as well as regional maps covering geologically most interesting surface features like Tethys' prominent graben system Ithaca Chasma. Despite the spectral dominance of H_2O ice on Tethys' surface distinct spectral variations could be detected, which are surprisingly very different from what was expected from the visible albedo derived from Voyager and Cassini camera data [5,6]. The abundance of H_2O ice is qualitatively expressed by the depth of the ice absorptions at 1.5 and 2µm and usually follows the visible surface albedo as seen on many other satellites. Thus, on Dione and Rhea [3,4], H_2O ice absorptions are weakest on the trailing hemisphere due to magnetospheric 'dust' impacting and darkening the surface. Although on Tethys', the weakest absorptions could be also measured on the trailing hemisphere, the detailed mapping shows a more complex pattern. Two relatively narrow N/S trending bands characterized by deep H_2O ice absorptions separate the Saturn-facing and the anti-Saturnian hemisphere. With respect to the discrepancy between the global trends in the band depth and the visible albedo, the observed variations are interpreted to be caused by particle sizes rather the abundance of H_2O. The oval shaped dark albedo unit observed by Cassini ISS in the equatorial region of Tethys' leading hemisphere [6], which could be related to magnetispheric 'dust' impacting the surface, may only be indicated in the VIMS data by slightly surpressed H_2O ice absorptions compared to their surrounding regions. In contrast, the variations in the spectral slope from the visible to the ultra-violet wavelength range i.e from 0.5 to 0.35µm again are similar to the variations observed by Cassini ISS [6] as well as observed on Rhea [4]. The spectral slope is steepest (i.e. the effect of an ultra-violet absorber other than H_2O ice is strongest) on the leading as well on the trailing hemisphere.

Regional spectral properties: It is interesting that the largest impact crater *Odysseus* (33°N/129°W) in included in one band of deeper H_2O absorptions described above, whereas the geologically older and fourth largest impact crater *Penelope* (11°S/249°W) is different from the other 'icy' band. Although, the uppermost surface layer in the vicinity of Odysseus is expected to be strongly affected by space weathering processes, deeper H_2O ice band depths might be taken as ghosts of the genuine spectral properties of this impact basin.

In contrast to the prominent graben systems on Dione and Rhea [3,4] with a relatively high H_2O ice abundance exposed on steep walls, no spectral properties could be exclusively associated with Tethys' extended graben system *Ithaca Chasma*. Although, a slight increase in depth of the H_2O ice absorptions could be observed in the vicinity of Ithaca Chasma, the graben system rather largely separates weaker H_2O absorptions in the neighboring the trailing hemisphere from deeper ones in the leading hemisphere including the graben system itself. Changes of the spectral slope toward the ultra-violet wavelength range appears to be more independent of the geological Local variations, i.e. local deepening of H_2O ice ab-sorptions, are mostly related to several probably *fresh impact craters* and to locations where topographic slope is high like crater walls. In constract to Dione and Rhea [3,4], however, only a few such fresh impact craters could be observed.

References: [1] Brown, R.H. et al. (2004) Space Sci. Rev., 115(1-4), 111-168. [2] Stephan, K. et al., (2016) Icarus, 274, 1-22. [3] Stephan, K., et al. (2010) Icarus, 206(2), 631-652. [4] Stephan, K. et al. (2012) *PSS*, doi:10.1016/j.pss.2011.07.019. [5] Buratti, B. & Veverka, J. (1984) *Icarus*, 58(2), 254-264. [6] Schenk, P. et al. (2011) *Icarus*, 211(1), 740-757.

MODELING AN EXOGENIC ORIGIN FOR THE EQUATORIAL RIDGE ON IAPETUS. A. M. Stickle[1] and J. H. Roberts[1], [1]Johns Hopkins University Applied Physics Laboratory, 11100 Johns Hopkins Rd, Laurel, MD, USA, 20723 (angela.stickle@jhuapl.edu).

Introduction: A ridge aligned with the equator of Iapetus [1] exists very nearly along the equator and extends for more than 110° in longitude, roughly 1400 km, though some portions of the ridge are broken into segments [1]. The ridge is also characterized by extreme topographic relief, with parts of the feature rising as much as 20 km above the surrounding terrains. Earlier observations by the Voyager spacecraft revealed mountains on the anti-Saturn side of Iapetus with as much as 25-km in relief, extending from 180°W-220°W [2] which may be a continuation of this ridge.

Ridge Formation Models: Most models for the formation of this enigmatic ridge are endogenic, generally requiring the formation of a fast-spinning Iapetus with an oblate shape due to the rotation speed [1, 3-9]. If Iapetus cooled rapidly enough, this shape would freeze, leaving behind the oblate body seen today. Further despinning processes could then generate the ridge. Though abundant, many of these models require specific scenarios and have constraining parameters.

An exogenic formation mechanism has also been proposed, that the ridge represents the remains of an early ring system around Iapetus that collapsed onto the surface [10]. Thus far, none of the exogenic models [10-12] have conclusively identified the origin of the ridge.

Here, we investigate an exogenic origin for the ridge, derived from a disk of debris around Iapetus, without invoking any specific model for the generation of the debris disk. Assuming there is a collapsing debris disk encircling the moon, then, we ask the question of whether it is possible to generate a ridge of the size and shape as observed on Iapetus today.

Methods: We simulate the impact of the collapsing debris using the CTH hydrocode developed by Sandia National Laboratories [13]. We assumed the impact speed to be 400 m/s, representative of the speed a decaying debris disk would impact the surface of Iapetus [10]. Projectile sizes ranged from 1-m to 1-km in diameter, and impacted at angles of 1°, 3° and 10°. We assumed water ice as the composition for both the target and the projectile. To determine if impacts from a decaying ring could generate a ridge, we tracked crater size and morphology, surface temperature, and material location following each impact.

Discussion: Assuming water ice for both projectile and target material, pi-scaling calculations suggest that extremely oblique impact angles are needed to add to ridge topography. These extreme impact angles reduce the cratering efficiency, adding material rather than eroding it during crater formation (Fig. 1 A, B); further, material is likely to be excavated at low angles, enhancing downrange accumulation. Multiple impacts from debris pieces will heighten this effect (Fig. 1 C,D). Because infalling debris is predicted to impact at extremely low angles, both of these effects might have contributed to ridge formation on Iapetus.

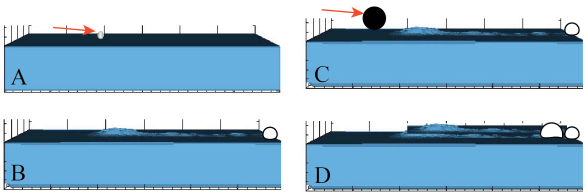

Fig. 1: Schematic of ridge building process from grazing impacts into the surface of Iapetus. Multiple, low-angle impacts can build topography on the surface over time.

Infalling material will also deliver heat to the surface of Iapetus, which can lead to a weakening of the moon's surface and near subsurface material, thus potentially reducing the ability of the moon to support ridge topography. The extreme grazing angles of the impacts modeled here decouple much of the projectile energy, however, and impact heating of the surface is not significant. Where present, heating is localized in the shallow subsurface. Thus, the surface retains strength enough to maintain loading from the buildup of ridge topography

These models suggest that, if present, a collapsing disk of debris should have been able to build topography to create a ridge around Iapetus. Continuing work examining multiple impacts and projectile shape and size effects is ongoing to further contstrain what a debris generated ridge may look like in more detail.

References: [1] Porco, C. C. et al. (2005), *Science*, *307*(5713), 1237–1242; [2] Denk, Tet al. (2010) *LPSC XXXI,* Abstract #1596; [3] Castillo-Rogez et al. (2007) *Icarus*, 179-202; [4] Czechowski and Leliwa-Kopystyński (2008) *Adv. Space Res.* 61-69; [5] Dombard and Cheng (2008) *LPSC XXXIX* Abstract #2262; [6] Robuchon et al. (2010) *Icarus,* 959-971; [7] Beuthe, M. (2009) *AGU Fall Meet. Abs.* p. 9; [8] Dombard et al. (2010) *AGU Fall Meet. Abs.*; [9] Singer and McKinnon (2011) *Icarus, 216*(1), 198-211; [10] Ip, W. H. (2006), *Geophys. Res. Lett.*, *33*(16), L16203; [11] Levison et al. (2011) *Icarus, 214*(2), 773-778; [12] Dombard et al. (2012) *J. Geophys. Res., 117*(E3); [13] McGlaun, J. M., et al. *(1990),* Int. J. Imp. Engr. *10*(1-4), 351–360.

Titan and Enceladus Relationship-Titan as Planet and Enceladus Water Related to Titan

James T. Struck A French American Museum

Of Chicago, NASA

Titan has a diameter of 3200 miles larger than Mercury at 3032 miles. Enceladus was seen spouting water in 2005 from its southern pole. A Titan and Enceladus relationship can be argued for where Titan can be seen as a planet in relationship to Enceladus. Enceladus can be seen as giving off water in relation to Saturn and Titan's Gravitation.

Titan as a planet might seem radical, but the size of Titan is larger than Mercury so that by itself is enough reason to use planet language.

Titan and Saturn can be seen as applying pressure to Enceladus. Gravitation from Titan and Saturn can be seen as pressuring the moon Enceladus.

Enceladus water can be seen as related to Titan's mass and gravitation effect.

True Polar Wander of Enceladus From Topographic Data. Radwan Tajeddine[1,*], Krista M. Soderlund[2], Peter C. Thomas[1], Paul Helfenstein[1], Matthew M. Hedman[3], Joseph A. Burns[4], Paul M. Schenk[5].

[1]Center for Astrophysics and Planetary Science, Cornell University, Ithaca, NY 14853, USA
[2]Institute for Geophysics, John A. & Katherine G. Jackson School of Geosciences, The University of Texas at Austin, J. J. Pickle Research Campus Building 196 (ROC), 10100 Burnet Road (R2200), Austin, Texas 78758-4445, USA
[3]Department of Physics, University of Idaho, Moscow, ID 83844-0903, USA
[4]College of Engineering, Cornell University, Ithaca, NY 14853, USA
[5]Lunar and Planetary Institute, Houston, TX 77058, USA
*Corresponding author: Tajeddine@astro.cornell.edu

Abstract: Apart from the relative motion of lithospheric plates, the Earth as a whole moves with respect to its rotation pole, as shown by paleomagnetic, astrometric and geodetic measurements [1]. Such so-called *true polar wander* (TPW) occurs because our planet's moments of inertia change temporally owing to internal thermal convection and to the redistribution of surficial mass during ice ages. Thus, to conserve angular momentum while losing rotational energy, Earth's axis of maximum moment of inertia aligns with its spin axis. Theoreticians suspect similar reorientations of other celestial bodies but supporting evidence is fragmentary, at best [2]. Here we report the discovery of a global series of topographic lows on Saturn's satellite Enceladus indicating that this synchronously locked moon has undergone reorientation by ~55°. We use improved topographic data from spherical harmonic expansion of Cassini limb [3,4,5] and stereogrammetric [5,6,7] measurements to characterize regional topography over the surface of Enceladus. We identify a group of nearly antipodal basins orthogonal to a topographic basin chain tracing a non-equatorial circumglobal belt across Enceladus' surface (Figure 1). We argue that the belt and the antipodal regions are fossil remnants of old equator and poles, respectively. We place the former north and south poles respectively at (79°W, 35°N) and (259°W, -35°N), The topographic lows are proposed to arise from isostasic compensation [7,8] with their pattern reflecting variations in internal dynamics of the ice shell. Our hypothesis is consistent with a variety of geological features visible in Cassini images [9].

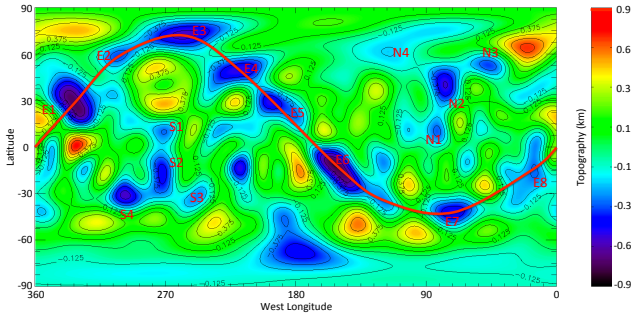

Figure 1. Topographic map of Enceladus based on degree l=4 to l=16 in spherical harmonics.

References:

[1] Mitrovica, J.X. & Wahr, *Annual Review of Earth and Planetary Sciences*, **39**, 577-616 (2011).
[2] Matsuyama, I. *et al. Annual Review of Earth and Planetary Sciences*, **42**, 605-634 (2014).
[3] Thomas, P.C. et al. *Icarus*, **190**, 573-584 (2007).
[4] Thomas, P.C. *Icarus*, **208**, 395-401 (2010).
[5] Thomas, P.C. et al. *Icarus*, **264**, 37-47 (2016).
[6] Edwards, K. *Photogrammetric Engineering and Remote Sensing*, **53**, 1219-1222 (1987).
[7] Schenk, P.M. & McKinnon, W. B. *Geophys. Res, Let.*, **36**, Issue 16, CiteID L16202 (2009).
[8] Besserer, J. et al. *J. Geophys. Res. Planets*, **118**, 908-915 (2013).
[9] Crow-Willard, E.N. & Pappalardo, R.T. *J. Geophys. Res.*, **120**, 928-950 (2015).

Abiotic peptide synthesis under Enceladus alkaline hydrothermal condition. W. Takahagi[1,2,3], T. Shibuya[3], Y. Takano[4], K. Seo[2,5], K. Adachi[2,5], K. Fujishima[6], M. Tomita[2,5] & K. Takai[3], [1]Graduate School of Media and Govenance, Keio University (5322 Endo, Fujisawa-shi, Kanagawa 252-0882, Japan, watarut@sfc.keio.ac.jp), [2]Institute for Advanced Biosciences, Keio University, [3]Department of Subsurface Geobiological Analysis and Research, Japan Agency for Marine-Earth Science and Technology (2-15 Natsushima-Cho, Yokosuka, 237-0061, Japan, [4]Department of Biochemistry, Japan Agency for Marine-Earth Science and Technology (2-15 Natsushima-Cho, Yokosuka, 237-0061, Japan), [5]Department of Environment and Information Studies, Keio University (5322 Endo, Fujisawa-shi, Kanagawa 252-0882, Japan), [6]Earth-Life Science Institute, Tokyo Institute of Technology (2-12-1-IE-1 Ookayama, Meguro-ku, Tokyo, 152-8550, Japan).

Enceladus is one of the moons of Saturn, and it has been known to harbor interior ocean beneath the icy crust [1]. The mass spectrometry data obtained by *Cassini* spacecraft indicates the presence of salty, and most likely alkaline ocean containing various organic compounds. While geochemical and other radiation related processes for *in situ* production of organics remain elusive, carbonaceous chondrites, consisting the main body of Enceladus are known to be enriched with organic matters potentially including the building blocks of life (e.g., organic molecules including amino acids and their precursors) [2]. Assuming such abiotic amino acids existing in the Enceladus alkaline seawater, we hypothesized that water-rock interaction [3] may contribute to condensation of localized amino acids leading to a peptide formation. In order to verify this hypothesis, we have developed an Enceladus hydrothermal reactor based on the chemical constraints obtained through previous experimental and theoretical studies based on the Cassini flyby data. We subjected six different amino acids to a thermal fluctuation system simulating the periodic tidal heating of the interior chondritic core. Total, eight sea water samples were obtained over the time course of 147 days. Analysis was performed using Capillary Electrophoresis Time-of-Flight Mass Spectrometry (CE-TOF/MS) and as a result, we observed peaks of over 4000 molecules larger than the mass of a single amino acid. We have so far confirmed the presense of prebiotic marker Sarcosine and candidate peaks for dipeptides. The pH monitoring and H_2 and CO_2 Gas Chromatography (GC) data clearly indicated the occurrence of serpentinization / carbonation reaction. These data also indicate that H_2 was consumed as chemical energy to synthesis organic compounds under simulated condition of Enceladus alkaline seawater. These results suggest the interaction between amino acids, aqueous alteration reaction and thermal cycling processes for the role of abiotic peptide formation under alkaline hydrothermal condition.

References: [1] Hsu H.W., Postberg F., Sekine Y., Shibuya T., Kempf S., Horanyi1 M., Juhasz A., Altobelli N., Suzuki K., Masaki Y., *et al*. Ongoing hydrothermal activities within Enceladus, *Nature* 2015;**519**(7542)207. [2] Postberg F., Kempf S., Schmidt J., *et al*. Sodium salts in E-ring ice grains from an ocean below the surface of Enceladus, *Nature* 2009;**459**(7250)1098-1101. [3] Sekine Y., Shibuya T., Postberg F., *et al*. High-temperature water–rock interactions and hydrothermal environments in the chondrite-like core of Enceladus, *Nature Communications* 2015;**6**(8604).

ICY MOONS ATMOSPHERES / EXOSPHERES FROM MAGNETOSPHERIC INTERACTIONS.

Ben Teolis[1], Robert Tokar[2], *et al*
[1]Space Science Division, Southwest Research Institute, San Antonio, TX, 78230, bteolis@swri.edu
[2]Planetary Science Institute, 1700 E. Fort Lowell, Suite 106, Tucson, AZ, 85719, rltokar@psi.edu

Introduction: A major milestone of Cassini's extended tour of Saturn's icy moons has been the discovery of exospheres around Rhea and Dione [1-3], produced by magnetospheric radiolysis and sputtering of the surfaces, and held in place by the moon's gravity. The exospheres have similar density, and chemical composition; consisting of carbon dioxide and molecular oxygen, suggesting similar exospheric mechanisms at both bodies. Over multiple close flybys at different dates and over locations, Cassini CAPS and INMS measurements have led to a remarkably detailed new understanding [4] of these icy satellite exospheres; revealing that (1) the exospheres stick to the cold night side and polar surfaces, (2) the gas diffuses into the regolith, and (3) the exospheres are seasonal.

Background & Objectives: Exospheres at Saturn's icy moons had long been predicted [5, 6], first on the basis of laboratory studies confirming radiolytic O_2 to be a major component of the material sputtered from ion and electron irradiated water ice [7], and then from the discovery by the Hubble Space Telescope of O_2 exospheres at the irradiated Galilean icy moons Ganymede and Europa [8, 9] (and now recently, at Callisto [10]). However exospheres at the Saturnian satellites proved more difficult to detect than anticipated, with several unsuccessful attempts at exospheric detection at Rhea [11] by way of UVIS occultation and MIMI energetic neutral atom data. The explanation was later provided by Cassini CAPS and INMS on several close Rhea and Dione flybys, which showed that the exospheric densities are much lower – by two orders of magnitude - than anticipated on the basis of known sputtering and radiolysis yields from laboratory water ice [12], suggesting the a possible refractory surface lag layer built up by preferential sputtering of H_2O [4]. Another surprise came from Cassini's magnetometer, which measured magnetic field perturbations at Rhea [13] and Dione [3] too intense to be explained by exospheres of the low density found by CAPS and INMS [4]. At Rhea the apparent inconsistently was resolved by two new fundamental discoveries in the plasma physics of moon-magnetosphere interactions: (1) the formation of Alfven wings from the plasma wake [13, 14], and (2) a field-aligned thermoelectric current system formed due to plasma absorption by the moon [15]. Analysis of the Dione results is ongoing but, in addition to possible similar current systems as seen at Rhea, another possibility is that the magnetometer detected episodic cryovolcanic activity, though this remains unconfirmed.

The presence of CO_2 in almost equal amounts to O_2 at both Rhea and Dione was not expected, and suggests significant carbon-bearing molecular constituents in the surface material; a finding at odds with VIMS IR spectra indicating a surface of almost pure H_2O. Together with the observation of surface sputtering far below expectations, such a high carbon content suggests a possible refractory lag layer built up by preferential sputtering of the H_2O [4], possibly only nanometers thick (too thin for detectability by VIMS). The presence of a lag layer raises the possibility that micrometeorite impacts – which may a major source of carbon to the surface material - may expose fresh ice from below the lag layer, and possibly control the surface sputtering rate, and the O_2 source, to the exosphere. These fundamental discoveries, resulting from only a handful of Cassini icy satellite flybys, may have major implications for the exospheric source rates and compositions at other solar system icy objects, and augers well for the science potential for future spacecraft missions to such objects.

The chapter on *Icy Moon Atmospheres / Exospheres From Magnetospheric Interactions* will explore the mechanisms of exospheric generation, mantinance and loss at Saturn's icy satellites, the observations by the Cassini spacecraft in the Saturn system, the new physics and understanding revealed by these data, the implications of these observations for the Saturn satellites (and, more generally, icy satellites throughout the solar system), and conclusions and outstanding questions.

References

[1] B.D. Teolis et al, Science, 330 (2010) 1813.
[2] R.L. Tokar et al, JGR, 39 (2012) L03105.
[3] S. Simon, et al, JGR, 38 (2011) L15102.
[4] B.D. Teolis, J.H. Waite, Icarus, 272 (2016) 277.
[5] E.C. Sittler, et al, JGR, 109 (2004) A01214.
[6] J. Saur, D.F. Strobel, ApJ, 620 (2005) L115.
[7] W.L. Brown, et al, NIM, 198 (1982) 1-8.
[8] D.T. Hall, et al, ApJ, 499 (1998) 475-481.
[9] D.T. Hall, et al, Nature, 373 (1995) 677-679.
[10] N.J. Cunningham, et al, Icarus, 254 (2015) 178.
[11] G.H. Jones, et al, Science, 319 (2007) 1380.
[12] B.D. Teolis, J.H. Waite, LPSC, Woodlands, Tx, USA (2012).
[13] S. Simon, et al, JG, 117 (2012) A07211.
[14] K.K. Khurana, et al, AGU (2014), abstract # P43B-3986
[15] B.D. Teolis, et al, JGR, 119 (2014) 8881.

SYSTEMATICS OF THE INNER SMALL SATELLITES OF SATURN. P. C. Thomas[1], M. S. Tiscareno[2], P. Helfenstein[1] [1]Cornell University, [2]SETI Institute

Introduction

More than a decade of encounters of the Cassini spacecraft with the small satellites of Saturn shows objects having distinct morphologies occupying distinct dynamical settings[1]. The prime scientific challenge in the study of these objects is determining how these morphologies restrict the evolutionary development of objects in the different dynamical niches and thus help in constraining the broader history of the Saturn system.

The distinguishing features include: Satellites in the main ring system have equatorial ridges [2]. The coorbitals are by far the most massive, have the highest (and nearly identical) mean densities, and have the most asteroid-like appearances. The three resolved satellites in diffuse rings or ring arcs have the lowest inferred mean densities and appear to be equilibrium ellipsoids, unique among small solar system objects. Libration zone satellites have deep coverings of debris subject to long distance downslope motion.

Distinguishing forms

In interpretation of an object's history, the presence of a surface with evidence of different phases or processes is important, as is the presence of a surface indicating an equilibrium of processes without evidence of discrete events. The equatorial ridges of ring-related satellites, Pan, Daphnis, and Atlas suggest at least a two-stage history, the latter involving addition of ring materials at low latitudes. Prometheus, the inner F-ring shepherd, shows evidence of stripping (by impact?) of an outer mantle of material from about half the satellite's area exposing a core of perhaps 2/3 the satellite's volume. The putative exposed core is heavily cratered, so any exfoliation occurred relatively early in the satellite's history. Janus and Epimetheus have the most asteroid-like appearances among the small inner satellites, namely surfaces accumulating craters with local debris accumulation, basically showing one style of surface history.

The most remarkable surfaces are the smooth ellipsoids of the ring-arc related moons, Aegaeon, Methone, and Pallene. Methone and Pallene are sufficiently well resolved to show they have equilibrium shapes consistent with mean densities of 310 and 250 kgm^{-3}, respectively. Aegaeon is consistent with a mean density of 540 kgm^{-3}[1]. These objects are apparently shaped by surface processes and materials that are effectively fluid on modest geological time scales. This unique arrangement, occurring within ring arc materials, suggests recently active interchange of materials, but limits on their ages and fluxes are not well established.

The libration satellites have deep coverings subject to long-range downslope motion. In at least the case of Helene, the covering is being eroded and is not in an equilibrium with local deposition. The source and reason for apparent discrete nature of the deposition is not yet clear.

Photometry and colors

The small satellite albedos increase and colors become bluer [3] progressively from Atlas to the Trojans showing the influence of E-ring particles that originate from Enceladus [4]. The differences are likely caused by water ice with minimal contaminants that are distinct from those in the darker components of regoliths of outer satellites such as Iapetus, Phoebe or Hyperion [3,5]. However, surface resolved albedo and color variegations also exist in relation to local geology, such as downslope transport [6].

Dynamics and possible ages

Consensus on the dynamical history of the small and mid-size satellites of Saturn is currently in flux. Longtime suspicions that Saturn's rings are only ~100 Myr old have recently intensified as the rings appear less massive than previously thought [7] and because the pollution of the rings' pristine water ice by interplanetary dust is faster than previously thought [8]. Also, the orbital evolution of moon orbits due to Saturn's internal friction may be faster than previously thought [9]; this result has led some to conclude that the moons also cannot be more than 100 Myr old [10]. Formation from young massive rings, rather than from the protosatellite disk, was previously discussed for the small moons [11] and should be revisited in light of these new results.

Hyperion

Hyperion is distinguished from the inner small satellites by its size, sponge-like morphology, but not its mean density. Its dynamical and surface history is likely very distinct from that of the inner small objects.

References: [1]Thomas, P.C., et al. (2013) Icarus 226, 999-1019. [2] Charnoz, S. et al. (2007) Science 318, 1622. [3] Buratti et al. (2010) Icarus 206, 524–536. [4] Verbiscer et al. (2007) Science 315, 815, [5] Filacchione et al. (2010) Icarus 206, 507–523, [6] Morrison et al. (2010) BAAS 42, p.955. [7] Hedman, M.M., Nicholson, P.D. (2016) ArXiv e-prints arXiv:1601.07955. [8] Kempf, S., et al. (2015) EPSC 2015, EPSC2015-411 10. [9] Lainey, V., et al. (2015) ArXiv e-prints, October 2015. [10] Cuk, M., Dones, L., Nesvorny, D. (2016) The Astrophysical Journal 820, 97. [11] Charnoz, S., Salmon, J., Crida, A. (2010) Nature 465, 752-754.

Orbits and rotation states of Enceladus and other moons of Saturn

Matthew S. Tiscareno, SETI Institute, Mountain View CA 94086, USA (matt@seti.org)

While Enceladus rotates once per orbit, so that it always keeps the same face towards Saturn, its non-spherical shape and non-circular orbit together give rise to a wobble (a "libration") upon that base rotation state. The rotational libration has been measured with an amplitude of $0.120^\circ \pm 0.014^\circ$, which is large enough to demonstrate that the core of Enceladus cannot be rigidly connected to the surface [1]. This proves that its subsurface water, already inferred to exist via geyser activity [2] and to be at least regional in scope via gravity measurements [3], in fact extends globally [1].

We will describe the method we used to carry out this measurement and will review the method's previous applications to Janus and Epimetheus [4] and Mimas [5], as well as the prospects for applying it to other moons of Saturn.

We will also review the orbit of Enceladus and the other moons of Saturn, identifying resonances and other effects that shape their current behavior. For example, not only is Enceladus in a 2:1 inner Lindblad resonance with Dione, the two nearby 2:1 corotation resonances (eccentricity-type and inclination-type) are in a near-resonant state and also significantly affect the orbital behavior of Enceladus.

Consensus on the dynamical history of the small and mid-size moons of Saturn is currently in flux. Although origins scenarios are easier to construct when set near the beginning of solar system history, longtime suspicions that Saturn's rings are only $\sim$100 Myr old have recently intensified due to realizations that the rings are less massive than previously thought [6] and that the pollution of the rings' pristine water ice by interplanetary dust is faster than previously thought [7]. The simultaneous realization that orbital evolution of moon orbits due to Saturn's internal friction is faster than previously thought [8] has led some to conclude that even the mid-sized moons (e.g., Enceladus) cannot be more than 100 Myr old [9]. Genesis from a young massive ring, rather than from the protosatellite disk, was previously discussed for the small [10] and mid-sized [11] moons and should be revisited in light of these new results.

References

[1] P. C. Thomas, R. Tajeddine, M. S. Tiscareno, J. A. Burns, J. Joseph, T. J. Loredo, P. Helfenstein, and C. Porco. Enceladus's measured physical libration requires a global subsurface ocean. *Icarus*, 264:37–47, January 2016. doi: 10.1016/j.icarus.2015.08.037.

[2] H.-W. Hsu, F. Postberg, Y. Sekine, T. Shibuya, S. Kempf, M. Horányi, A. Juhász, N. Altobelli, K. Suzuki, Y. Masaki, T. Kuwatani, S. Tachibana, S.-I. Sirono, G. Moragas-Klostermeyer, and R. Srama. Ongoing hydrothermal activities within Enceladus. *Nature*, 519:207–210, March 2015. doi: 10.1038/nature14262.

[3] L. Iess, D. J. Stevenson, M. Parisi, D. Hemingway, R. A. Jacobson, J. I. Lunine, F. Nimmo, J. W. Armstrong, S. W. Asmar, M. Ducci, and P. Tortora. The gravity field and interior structure of Enceladus. *Science*, 344:78–80, April 2014. doi: 10.1126/science.1250551.

[4] M. S. Tiscareno, P. C. Thomas, and J. A. Burns. The rotation of Janus and Epimetheus. *Icarus*, 204:254–261, November 2009. doi: 10.1016/j.icarus.2009.06.023.

[5] R. Tajeddine, N. Rambaux, V. Lainey, S. Charnoz, A. Richard, A. Rivoldini, and B. Noyelles. Constraints on Mimas' interior from Cassini ISS libration measurements. *Science*, 346:322–324, October 2014. doi: 10.1126/science.1255299.

[6] M. M. Hedman and P. D. Nicholson. The B-ring's surface mass density from hidden density waves: Less than meets the eye? *Icarus*, 2016. in press (arXiv:1601.07955).

[7] S. Kempf, M. Horanyi, R. Srama, and N. Altobelli. Exogenous dust delivery into the Saturnian system and the age of Saturn's rings. *European Planetary Science Congress Abstracts*, 10:411, October 2015.

[8] V. Lainey, R. A. Jacobson, R. Tajeddine, N. J. Cooper, C. Murray, V. Robert, G. Tobie, T. Guillot, S. Mathis, F. Remus, J. Desmars, J.-E. Arlot, J.-P. De Cuyper, V. Dehant, D. Pascu, W. Thuillot, C. Le Poncin-Lafitte, and J.-P. Zahn. New constraints on Saturn's interior from Cassini astrometric data. 2015. arXiv:1510.05870.

[9] M. Ćuk, L. Dones, and D. Nesvorný. Dynamical Evidence for a Late Formation of Saturn's Moons. *Astrophys. J.*, 820:97, April 2016. doi: 10.3847/0004-637X/820/2/97.

[10] S. Charnoz, J. Salmon, and A. Crida. The recent formation of Saturn's moonlets from viscous spreading of the main rings. *Nature*, 465:752–754, June 2010. doi: 10.1038/nature09096.

[11] A. Crida and S. Charnoz. Formation of Regular Satellites from Ancient Massive Rings in the Solar System. *Science*, 338:1196, November 2012. doi: 10.1126/science.1226477.

OPTICAL REMOTE SENSING AND SURFACE PROPERTIES OF SATURN'S ICY MOONS. A. J. Verbiscer[1], P. Helfenstein[2], B. J. Buratti[3], and E. M. Royer[4], [1]University of Virginia (P.O. Box 400325, Charlottesville VA 22904-4325, verbiscer@virginia.edu), [2]Cornell University, [3]Jet Propulsion Laboratory, [4]University of Colorado.

Introduction: Much of our understanding of the surface physical properties of the icy satellites comes from optical remote sensing, thermal infrared data, and radar. Among the regolith properties that can be characterized are the textural properties, state of compaction, grain sizes, composition, and thermophysical properties such as albedo and thermal inertia. The spectrophotometric behavior of the surfaces of Saturn's satellites provides a record of the processes that have shaped their regolith formation and evolution. Here we examine the known photometric properties of the satellites and their terrains from the far-UV to the near-infrared and how they depend on geological setting and placement in the saturnian system.

Albedo Variations: The albedos on the satellites as a whole, vary strongly both with position in the saturnian system and hemispherically between the leading and trailing hemispheres [1-8]. However, the most extreme differences occur on regional and local scales of terrains and individual features. Most dramatically, on Iapetus thermal segregation of ices [9] and dark contaminants has resulted in albedos that vary by a factor of ten. There and elsewhere, albedo contrasts are often also associated with impact cratering, where dark streamers and downslope accumulations of dark materials are conspicuous. On the brightest satellites, like Enceladus, albedo and color contrasts occur along scarps and medial troughs of fractures, where exposures of solid ice or large grained particles are present.

Opposition Effect: In general, the opposition effects of the saturnian satellites are typically very narrow (less than a couple degrees in angular width), but they vary from obect to object. Those of the small inner satellites differ from those of the nearby larger satellites and rings. For Janus and Epimetheus, the opposition effect at 555 nm is broader and more intense than for Tethys, Enceladus, Mimas, Dione, and Rhea [1, 6].

Wavelength Dependence: The phase curve behavior of the icy satellite regoliths can exhibit both a direct and an indirect dependence on spectral wavelength. Average particle albedos vary primarily as a function of wavelength and composition. Other scattering properties, such as the contribution of multiply scattered light, the strength of the opposition effect and the detailed shape of the average particle phase function can vary indirectly with wavelength and more directly on the wavelength-dependent albedo.

Effects of Ring Interactions: The photometric properties of Saturn's icy satellites depend strongly on their distance relative to Saturn. Strong systematic variations are seen from those embedded in the E-ring and magnetosphere to those outward from Titan which interact with Phoebe ring particles. With the exception of the non-synchronous satellites and Mimas in the far-UV, the icy moons all exhibit leading-trailing hemisphere asymmetries in albedo and scattering properties.

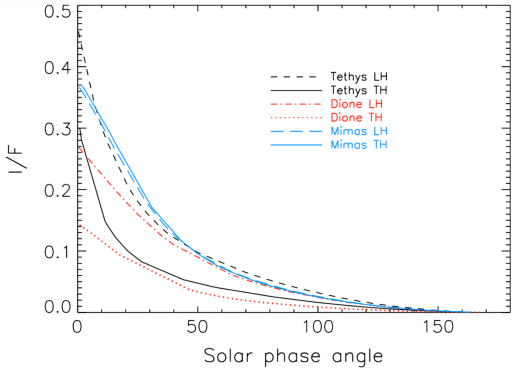

Fig. 1 Disk-integrated solar phase curves of the leading (LH) and trailing (TH) hemispheres of Tethys, Dione, and Mimas at 180 nm [2] highlight the differences in scattering properties of the surface particles on these satellites embedded within Saturn's E ring.

Singe Particle Phase Function and Roughness: All of Saturn's icy moons are moderately to strongly backscattering in the UV, visible, and near-infrared. Although the high visible albedos and thus large multiple scattering effects can interfere with the analysis of macroscopic roughness, the lower albedos in the far-UV and within the water ice absorption bands in the near-infrared make it possible to assess the textural characteristics of regolith and constituent grains on Saturn's icy moons.

References: [1] Verbiscer A. J. et al. (2007) *Science, 315*, 815. [2] Royer E. M. and Hendrix A. R. (2014) *Icarus, 242,* 158–171. [3] Ciarniello M. et al. (2011) *Icarus, 214,* 541–555. [4] Pitman, K. et al. (2010) *Icarus, 206*, 537–560. [5] Buratti, B. J. et al. (2010) *Icarus 206,* 524–536. [6] Verbiscer, A. J. et al. (2005) *BAAS 37*, 702. [7] Blackburn, D. G. et al. (2010) *Icarus 209*, 738-744. [8] Hendrix, A. R. and Hansen, C. J. (2008) *Icarus 193*, 344-351. [9] Spencer, J. R. and Denk, T. (2010) *Science 327*, 432. [10] French, R. G. et al. (2007) *PASP 119*, 623–642.

CRATER RELAXATION ACROSS RHEA, IAPETUS, DIONE, AND TETHYS, AND RELATION TO PAST HEAT FLOW. O. L. White[1], P. M. Schenk[2], A. W. Bellagamba[3], A. M. Grimm[3], and A. J. Dombard[3]. [1]NASA Ames Research Center, Moffett Field, CA, 94035-1000 (oliver.l.white@nasa.gov), [2]Lunar and Planetary Institute, 3600 Bay Area Blvd., Houston, TX, 77058, [3]Dept. of Earth and Environmental Sciences, University of Illinois at Chicago, 845 W. Taylor St., Chicago, IL, 60607.

Introduction: We have used stereo- and photoclinometry-derived global digital elevation models of the surfaces of Rhea, Iapetus, Dione, and Tethys that we have generated from Cassini data, as well as shadow measurements, to obtain depth and diameter measurements for more than 500 craters on these four Saturnian satellites. Our stereo depth measurements for large basins on Rhea and Iapetus have been verified with limb profiles extracted from Cassini imagery. We perform relaxation simulations using the MSC.Marc finite element package [1] to determine what heat flow magnitudes and durations are necessary to achieve the morphologies of certain relaxed craters; in combination with crater age dating, we can assign a chronology to crater relaxation across the surfaces of these satellites, thereby inferring their thermal histories.

Rhea and Iapetus: Measurements have been obtained for 116 craters on Rhea and 97 on Iapetus. Craters on Rhea are unrelaxed, with the exception of impact basins with diameters exceeding 100 km. Our simulations and crater age-dating indicate that Rhea appears to have undergone an early period of global elevated heat flow reaching 20 to 30 mW m^{-2} that caused the relaxation of its largest impact basins [1]. A few highly relaxed impact craters appear crater-saturated and are therefore very ancient, and may represent a 'first generation' of large basins on Rhea that have mostly been obliterated via relaxation and later impacts. Rapid despinning and tidal interaction with Saturn and its other satellites may have played roles in promoting such early heating.

We have revised our initial assessment (espoused in [1]) that all impact craters on Iapetus are unrelaxed. We have since identified two impact basins (326 and 207 km in diameter) that appear to have relaxed morphologies, and which also appear very ancient – one is superposed by a younger basin, that is in turn superposed by another basin. While we maintain that the unrelaxed state of the majority of large impact basins on Iapetus indicates that it has not experienced heat flows above radiogenic levels since their formation (due to factors associated with the very isolated location of Iapetus in the Saturnian system), these two relaxed examples may have formed during a period of elevated heat flow soon after the formation of Iapetus, perhaps when interior heat flow due to accretion and short-lived radioisotopes was still sufficiently high to cause appreciable relaxation of impact basin topography.

Dione and Tethys: These satellites both present a more complex relaxation/heat flow story compared to Rhea. Whereas relaxation on Rhea affects large impact basins regardless of their location on its surface, relaxation on Dione and Tethys affects impact craters down to smaller diameters in select locations across their surfaces, implying that relaxation and heat flow have been more geographically variable than on Rhea. We have obtained measurements for 194 craters on Dione and 106 on Tethys. With the exception of a few large, relaxed impact craters in its northern hemisphere, relaxation on Dione appears to be mainly confined to its far southern latitudes and antipodal equatorial zones centered at ~90°E and 270°E. This distribution corresponds closely to areas exhibiting smooth plains with low impact crater spatial densities [2], implying that elevated heat flow contributing to crater relaxation in these regions may also be responsible for large-scale resurfacing. Tethys does not show a similarly well-defined dichotomy between unrelaxed and relaxed regions. However, our ability to gauge relaxation across the entire satellite is hindered by the relatively young Odysseus impact and its ejecta [3], which has likely eliminated many of the large craters in this region of Tethys. Odysseus itself has a depth/diameter that is consistent with it being somewhat relaxed, although it is uncertain if its morphology may be the result of anomalous impact conditions.

Relaxation is seen affecting craters down to smaller diameters on Dione and Tethys compared to Rhea. Our simulations show that higher heat flows are necessary to achieve the observed relaxation, always reaching >40 mW m^{-2} for craters with diameters of less than 200 km, and in some instances, more than 60 and even 100 mW m^{-2}. For a thermally conductive shell, such high heat flows would imply shell thicknesses of <20 km, in which case Europa-like maculae would be expected; alternatively, convection in the ice could drive a melt interface deeper, possibly negating the need for localized oceans forming underneath these craters [4].

References: [1] White O. L. et al. (2013) *Icarus*, *223*, 699-709. [2] Kirchoff M. R. and Schenk P. (2015) *Icarus*, *256*, 78-89. [3] Kirchoff M. R. and Schenk P. (2010) *Icarus*, *206*, 485-497. [4] Dombard A. J. et al. (2007) *39th DPS Annual Meeting*, abstract #11.05.

THE EFFECTS OF TEMPERATURE-DEPENDENT THERMAL PROPERTIES, COHESION, AND CRYSTALLINITY ON MODEL-PREDICTED TEMPERATURES OF ICY REGOLITH ON SATURN'S MOONS. Stephen E. Wood, Dept. of Earth & Space Sciences, Univ. of Washington, Seattle WA, sew2@uw.edu.

For regolith on cold airless bodies (non-cometary), the only significant mechanism of heat transfer is solid-phase conduction between particles. Radiative heat transfer, which dominates in the inner solar system, accounts for <10% of the total effective thermal conductivity (*eTC*) of regolith at T<200K (for sub-mm grains). The magnitude of *eTC* in this case is proportional to the relative size of each contact surface between particles (R_{con}/R_{part}), the number of contacts, the porosity, and *directly proportional* to the conductivity of the solid particle material (k_{sld}) [1,2]. Therefore, *eTC* is expected to have the same temperature-dependence as k_{sld} , as indicated by the author's model calculations [3,4,5] shown in Fig. 1, and by others [6].

The thermal conductivity of crystalline water ice ($k_{ice,Ih}$) is well known, with an estimated uncertainty of 5% for T=40–273K [7,8]. Like most crystalline minerals, as temperature *decreases* its thermal conductivity *increases*, and it does so at an increasing rate. For the range of surface temperatures found on Saturnian satellites (40–120K), $k_{ice,Ih}$ varies by a factor of 3 (Fig. 1). The conductivity of amorphous water ice ($k_{ice,LDA}$) is much lower, with a weaker T-dependence [8].

If the upper regolith is composed of crystalline water ice, due to the high values of $k_{ice,Ih}$, it is difficult to match the low thermal inertia values observed on most Saturnian satellites (≤30 $Jm^{-2}s^{-0.5}K^{-1}$) for particles larger than 100μm unless porosity (φ) is ≥75% [5,6] (Fig.1). However, such values are easily achieved with amorphous ice particles for R_{part}=50μm and φ=50% [5,6] (Fig.1). While φ>75% is certainly possible for micron-sized grains due to van der Waals cohesive forces, these same forces cause *eTC* to have an *inverse size dependence* [5,6,9], so at a given porosity the predicted thermal inertia for 1μm grains is 3 times greater than for 100μm grains (e.g. 90 $Jm^{-2}s^{-0.5}K^{-1}$ at φ=75%).

The T-dependence of *eTC* has a number of important consequences for analysis of remote-sensing data and for the behavior of subsurface temperatures. Due to the positive T-dependence for specific heat (Fig. 1-bm), the effective thermal inertia, $eTI=(eTC*\rho c)^{1/2}$, remains fairly constant, while the thermal diffusivity, $eTD=eTC/\rho c$, has a magnified T-dependence (Fig. 1-bl,tm). *eTI* controls the amplitude of surface temperature variations, while *eTD* determines the depth that thermal waves penetrate (z_{skin}). This means that, effectively, cold temperatures penetrate more deeply than warm temperatures. Defining

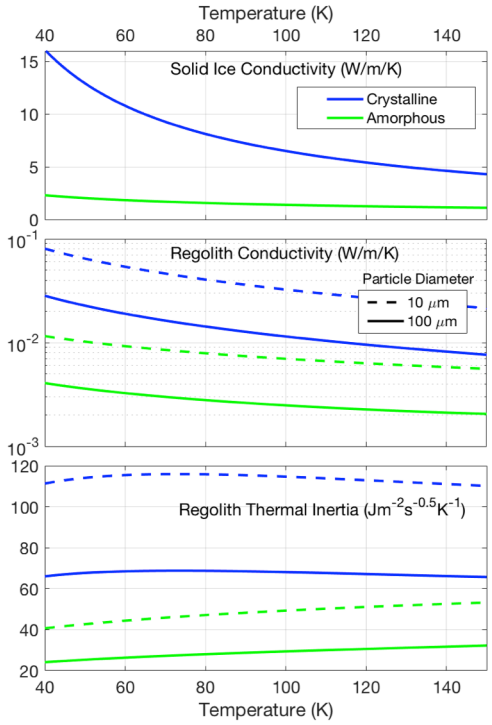

Fig. 1 - Temperature-dependence of solid ice conductivity (top) and model-calculated values of *eTC* (mid) and *eTI* (bottom) for particulate icy regolith on Mimas composed of non-spherical particles of crystalline (blue lines) or amorphous (green lines) water ice, for two different particle diameters – 10 um (thin lines) and 100 um (thick lines). Porosity = 50%.

$T_{z,1}$ as the temperature at a depth where periodic variations are dampled to <1K, a key result of the negative T-dependence of *eTC* is that $T_{z,1}$ can be significantly *colder* than the average surface temperature ($T_{s,avg}$) [4]. The same effect is responsible for the 45K difference ($T_{z,avg}$-$T_{s,avg}$) that was both predicted [10] and observed [11] on the Moon, though in that case $T_{z,1}$ is *warmer* because *eTC* increases with temperature due to the dominance of radiative heat transfer (prop. to T^3).

References: [1] Chan, C. K. & Tien, C. L. (1973), *J. Heat Transfer* 95, 302-308. [2] Batchelor, G. K., & O'Brien, R. W. (1977), *Proc. Royal Soc. London A*, 355, 313. [3] Wood, S.E. (2013) *LPSC 44, Abstract* 3077 (see E-poster). [4] Wood, S. E., Griffiths, S. G., & Eluszkiewicz, J. (2014), *LPI Contrib.1774*, 4075. [5] Wood, S.E. (2016), In preparation (preprint avail. on request). [6] Ferrari, C., & Lucas, A. (2016), *Astron. & Astrophys.*, *588*, A133. [7] Slack, G. A. (1980), *Phys. Rev. B*, 22, 3065. [8] Andersson, O., & Inaba, A. (2005), *Phys. Chem. Chem. Physics*, *7*(7), 1441-1449. [9] Watson, K. (1964), Ph.D. dissertation, Cal. Tech., Pasadena. [10] Linsky, J. L. (1966), *Icarus*, *5*(1), 606-634. [11] Keihm, S. J. *et al.* (1973), *EPSL*, *19*(3), 337-351.

A GLOBAL TECTONIC MAP AND TECTONIC HISTORY OF ENCELADUS. An Yin[1] and Robert T. Pappalardo[2], [1]Department of Earth, Planetary, and Space Sciences, University of California, Los Angeles, CA 90095-1567, USA (email: ayin54@gmail.com), [2]M/S 321-560, Jet Propulsion Laboratory, California Institute of Technology, Pasadena, CA 91109, USA (robert.pappalardo@jpl.nasa.gov).

Following the early work of Spencer et al. [1], Crow-Willard and Pappalardo [2], Nahm and Kattenhorn [3], and Yin and Pappalardo [4], we systematically correlate the morphology of first-order surface features to their geological, and in particular structural, origins across three tectonized terrains on Enceladus: the Leading Edge Terrain, the Trailing Edge Terrain, and the South Polar Terrain on Enceladus. This has resulted in a first-order global tectonic map of the icy satellite that characterizes the three tectonic provinces:

South Polar Terrain: The semi-squared shaped terrain is marked by paired compression/extension margins and right-/left-slip zones. Its interior is marked by five left-slip faults commonly referred to as the tiger-stripe fractures that terminate at hook-shaped compressional structures or Y-shaped transtensional structures. The development of the terrain can be explained by unidirectional flow of the terrain with internal deformation dominated by clockwise-rotation shear and related left-slip bookshelf faulting.

Leading Edge Terrain: Many relics of the Cratered Terrain behaving as rigid blocks with sizes of 5-30 m across are bounded by strike-slip ductile shear zones. Block rotations in this terrain mimic typical ductile shear-zone features exposed on Earth. Its margin to the Cratered Terrain is transitional and is marked by a right-slip transpressional shear zone in the Anti-Saturnian hemisphere and an extensional fault zone in the Sub-Saturnian hemisphere. There are no through-going brittle strike-slip fractures zones similar to the tiger-stripe fractures in the South Polar Terrain. We suggest that the development of the terrain was accomplished by mechanical fragmentation of the ice shell associated with a short and weak duration of the associated thermal event, which allowed the preservation of fragments of cratered ice shell.

Trailing Edge Terrain: Margins are marked by compressional mountain belts, extensional ridge-trough zones, and discrete strike-slip faults. The interior displays (1) a compressional domain characterized by high-relief ridges that are interpreted as folds and (2) an extensional domain expressed by low relief troughs that are interpreted as grabens. No through-going brittle strike-slip fractures zones similar to the tiger-stripe fractures in the South Polar Terrain. We suggest the duration of the thermal event associated with the tectonic deformation of the Trailing Edge Terrain was sufficiently long to allow nearly completely resurfacing across the terrain. The development of the terrain may have been associated with unidirectional translation of an internally deforming fragment of the ice shell, similar to the gravitational spreading process inferred for the development of the South Polar Terrain.

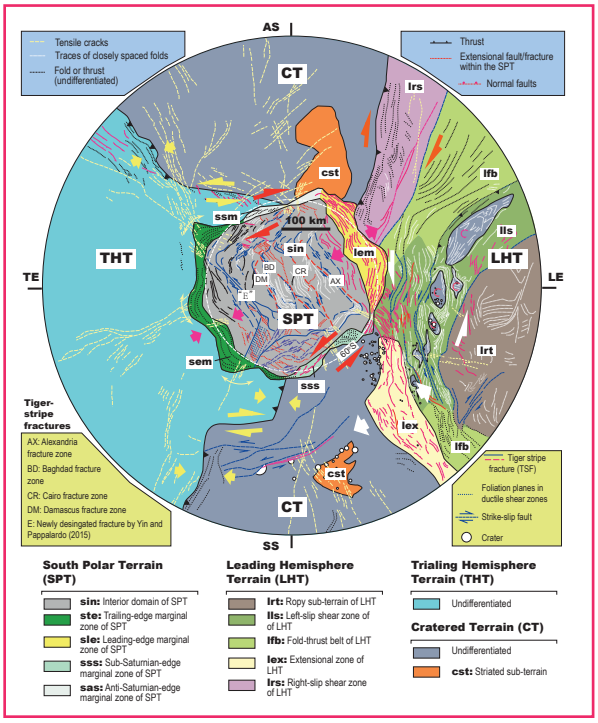

Figure 1. Simplified tectonic map of the southern hemisphere of Enceladus.

References: [1] Spencer, J. R. et al. (2009) Enceladus: An active cryovolcanic satellite, *in* Saturn from Cassini- Huygens, 683- 724. [2] Crow-Willard E. N. and Pappalardo R.T. (2015), *JGR*, 120, 928-950. [3] Nahm A.L. and Kattenhorn S.A. (2015) *Icarus,* 258, 67-81. [4] Yin, A., and Pappalardo, R.T. (2015), Icarus, 260, 409-439.